Probing Protein-Ligand Interactions *via* Solution Phase Hydrogen Exchange Mass Spectrometry

Stefan Theo Eßwein

The University of Edinburgh

Submitted in partial fulfilment of the degree of Doctor of Philosophy

February 2010

Declaration

This thesis is submitted in part fulfilment of the requirement of the degree of Doctor of Philosophy at the University of Edinburgh. Unless otherwise stated, the work is original and has not been previously submitted, in whole or in part, or any other University.

Stefan Eßwein, Edinburgh, February 2010

Acknowledgments

First of all, I owe my deepest gratitude to my supervisor Perdi for giving me the opportunity to do my postgraduate studies in her group and giving me the freedom to follow up my own ideas within my project.

Thanks to Dr. Hannah Florance for getting me started with my PhD project and for the AGr2 protein samples.

Further thanks to Dr. Holger Husi for advising me on HPLC related issues.

I owe a really big thanks to Prof. Paul Barlow for letting me use his lab and equipment for the protein expression work.

I am also indebted to Prof. Malcolm Walkinshaw and Dr. Martin Wear for the Cyclophilin A expression plasmid, the FKBP12 protein as for their help with the protein purification and Prof. Nick Turner for the ligands.

Dr. Phillip Camp really helped me out with the evaluation of my PLIMSTEX data.

Thanks to Dr. Andrew Herbert for kindly supporting me with factor H protein and fondaparinux.

A further great thanks to Dr. Dominic Campopiano for the groEL/ES expression plasmid and the opportunity to use his facilities.

I offer my regards to past and present members of the PBRG for their assistance and giving me a great time.

I further owe a big thank you to Diplom Chemikerin Isabell Pechtl for her help with the molecular biology work and for giving me a proper introduction to protein purification, as for the peptide structure optimisation.

Thanks to my project student Ms. Laura Baillie for doing the manual cyclophilin A SUPREX work.

Great thanks to Stewart Mains and David Paden for letting me use their workshop whenever I needed to and for assistance with general pump maintenance and equipment design.

I would like to show my gratitude to the Marie Curie Research Training network (contract: MEST-CT-2005-020744) and the University of Edinburgh for funding me and making all this possible.

Finally a big thanks to Diplomchemiker Lars Barzen for printing this thesis.

Abbreviations

'apo' protein	protein without ligand/cofactor
'holo' protein	protein with ligand/cofactor
A. calcoacet.	*Acinetobacter calcoaceticus*
C. elegans	*Caenorhabditis elegans*
E. coli	*Escherichia coli*
aa	amino acid
ADP	adenosine diphosphate
AGr2	anterior gradient 2
AMD	age related macular degeneration
APCI	atmospheric pressure chemical ionisation
API	atmospheric pressure ionisation
APS	ammonium persulfate
ATP	adenosine triphosphate
BLAST	basic local alignment search tool
BSA	bovine serum albumin
C3	complement component 3
CAD	collisionally activated dissociation
CaM	calmodulin
CCP	complement control proteins
CD	circular dichroism
CID	collision induced dissociation
CN	calcineurin
CR1	complement regulator 1

CRM	charge residue model
CsA	cyclosporin A
CypA	cyclophilin A
Da	dalton
DDD	dense deposit disease
DI	direct infusion
DNA	desoxyribonucleic acid
DSC	differential scanning calorimetry
DTT	dithiothreitol
EB	elution buffer
ECD	electron capture dissociation
EDTA	ethylenediaminetetraacetic acid
EI	electron impact ionisation
EM	electron multiplier
eq	equation
ER	endoplasmatic reticulum
ESI	electrospray ionisation
FA	formic acid
FAB	fast atom bombardment
fH	factor H
FID	free induction decay
FKBP	FK506-binding protein
FPX	fondaparinux
FT	fourier transformation

GDH	guanidinium hydrochloride
H_2O_{dd}	double distilled water
H-bond	hydrogen bond
HDX	hydrogen deuterium exchange
HEPES	4-(2-hydroxyethyl)-1-piperazineethanesulfonic acid
HHM	horse heart myoglobin
HIV-1	human immunodeficiency virus type 1
HPLC	high-performance liquid chromatography
HSQC	heteronuclear single quantum coherence
HUS	haemolytic uraemic syndrome
ICR	ion cyclotron resonance
ID	inner diameter
IEM	ion evaporation model
IL-2	interleukin-2
IM-MS	ion mobility mass spectrometry
IPTG	isopropyl β-*D*-1-thiogalactopyranoside
ITC	isothermal titration calorimetry
K_a	affinity constant
K_d	dissociation constant
LB	lysogeny broth
LC	liquid-chromatography
LEM	linear extrapolation method
MALDI	matrix assisted laser desorption ionisation
MCP	membrane control protein

MCP	microchannel plate
MPGN	membranoproliferative glomerulonephratitis
mRNA	messenger ribonucleic acid
MS	mass spectrometry/mass spectrometer
NF-AT	nuclear factor of activated T cells
NMR	nuclear magnetic resonance
NOE	nuclear overhauser effect
PLIMSTEX	**p**rotein-**li**gand **i**nteractions in solution by **MS**, **t**itration and HD **ex**change
PM	photomultiplier
PMSF	phenylmethylsulphonyl fluoride
PPIase	peptidyl-prolyl-*cis-trans* isomerase
QMA	quadrupole mass analyser
r	recombinant
RCA	regulators of complement activation
RT	room temperature
s/n	signal to noise
SDS-PAGE	sodium dodecyl sulfate polyacrylamide gel electrophoresis
SID	surface induced dissociation
SIMS	secondary ion mass spectrometry
SIMSTEX	**s**elf-association **i**nteractions using **MS**, self-**t**itration and HD **ex**change
SPR	surface plasmon resonance
SPROX	**s**tability of **p**roteins from **r**ates of **ox**idation
ss	stainless steel

SUPREX	**s**tability of **u**npurified **p**roteins from **r**ates of H/D **ex**hange
TEMED	tetramethylethylenediamine
TOF	time of flight
UV	ultraviolet
Vpr	viral protein R
WB	washing buffer

Abstract

Mass spectrometry is a versatile, sensitive and fast technique with which to probe biophysical properties in biological systems and one of the most important analytical tools in the multidisciplinary field of proteomics. The study of native-state proteins and their complexes in the gas-phase is well established and direct infusion electrospray ionisation mass spectrometry (DI-ESI-MS) techniques are becoming increasingly popular as a tool for screening and determining quantitative information on protein-protein and protein-ligand interactions. However, complexes retained by ESI-MS are not always representative of those in solution and care must be taken in interpreting purely gas-phase results. This thesis details modification and advancement of solution phase techniques devised by Gross *et al.* utilising ESI-MS and Fitzgerald *et al.* applying matrix assisted laser desorption ionisation (MALDI)-MS termed PLIMSTEX (**p**rotein-**l**igand **i**nteractions by **m**ass **s**pectrometry, **t**itration and hydrogen-deuterium-**ex**change)[1] and SUPREX (**S**tability of **u**npurified **p**roteins from **r**ates of H/D **ex**change)[2] to quantify these interactions with regards to high throughput analysis.

The first part of this thesis describes the different developmental stages of the devised HPLC-front ends and their optimisation with myoglobin and insulin. The successfully developed HPLC-front end in conjunction with PLIMSTEX and SUPREX and ESI-MS then gets tested with self expressed and purified cyclophilin A(CypA)-cyclosporin A (CsA) system, followed by a test screen with potential CypA binding ligands. Dissociation constants (K_d's) within one order of magnitude to reported values are determined.

In the third part of this thesis the application of the devised ESI-SUPREX methodology has been applied to anterior gradient 2 (AGr2) and the factor H complement control proteins module 19-20 (fH19-20) exhibiting binding potential to a tagged-hexapeptide and a synthetic pentasaccharide, respectively, resulting in thermodynamical data for these protein-ligand interactions. For the AGr2 system another dimension of investigation has been added by temperature controlling the devised ESI-SUPREX approach, revealing a phase transition in the protein at higher temperatures.

The final part of this thesis describes the application of the ESI-SUPREX methodology to probe folding properties of CypA in the presence of the self expressed and purified *E. coli* chaperonin groEL. Thereby the denaturing properties of groEL have been emphasised along with the stabilisation of a denatured CypA species.

Contents

Declaration i

Acknowledgments ii

Abbreviations iii

Abstract viii

Contents ix

List of Figures xv

List of Tables xvii

1 Introduction 1

1.1 Mass Spectrometry . . . 1
1.1.1 Ionisation . . . 2
1.1.2 Mass Analysers . . . 3
1.1.3 Detectors . . . 6
1.1.4 Liquid Chromatography ESI-Mass Spectrometry . . . 6
1.2 Protein Structure and Folding . . . 7
1.2.1 Protein Building Blocks . . . 8
1.2.2 Noncovalent Interactions . . . 8
Electrostatic Interactions . . . 8
Van der Waals Interactions . . . 9
Hydrogen Bonding . . . 9
1.2.3 Protein Structure . . . 10
Structure Elucidation Tools . . . 11
1.2.4 Protein Folding . . . 11
1.2.5 Protein Stability . . . 13
1.2.6 Protein-Ligand Interactions . . . 14
1.3 Hydrogen Deuterium Exchange . . . 16
1.3.1 HDX in Macromolecules . . . 17
1.3.2 HDX Models . . . 17
1.3.3 Mechanisms of Exchange . . . 19
1.4 Biological Systems . . . 20

1.4.1 The Peptidyl-Prolyl *cis-trans* Isomerase Family 20
Cyclophilin A 22
Cyclosporin A 23
FKBP12 24
FK506/Rapamycin 25
1.4.2 The GroEL/GroES *E.coli* Chaperon System 25
1.4.3 AGr2 28
1.4.4 The Complement System and Factor H 29
The Complement System 29
Factor H 29
1.5 PLIMSTEX 31
1.5.1 SIMSTEX 32
1.6 SUPREX 33
1.6.1 The SUPREX Protocol 33
1.6.2 Precision and Accuracy 35
1.6.3 Single Point SUPREX and SPROX 36

2 Experimental and Method Development 37
2.1 Bacterial Work 37
2.1.1 Preparation of Electrocompetent Cells 37
2.1.2 Chemical Transformation of Recombinant DNA 37
2.1.3 Transformation of Recombinant DNA *via* Electroporation . . 38
2.1.4 Isolation of Plasmid DNA (Minipreparation) 38
2.1.5 Isolation of Plasmid DNA (Maxipreparation) 39
2.1.6 Buffers and Media 40
LB-Medium 40
2x YT-Medium 40
Ampicilin/Carbenicillin Containing LB-Agar-Plates 40
2.2 Protein Expression and Purification 41
2.2.1 Cyclophilin A Expression and Purification 41
2.2.2 GroEL Expression and Purification 44
2.2.3 SDS-PAGE 47
2.2.4 Bradford Assay 48
2.3 Reagents and General Sample Preparation 49
2.3.1 Protein Sample Preparation 49
2.3.2 Ligand Preparation 49

2.3.3 MS-Sample Introduction 50
Electrospray 50
Nano-Electrospray 50
2.3.4 Direct Infusion 50
2.3.5 HDX Labeling Experiments 51
2.4 General Experimental Procedures 51
2.4.1 Buffer Exchange/Dialysis 51
2.4.2 Instrument Calibration 52
Platform II 52
QTOF Ultima/ QTOF 2 52
2.4.3 Instrumental Parameters 52
2.5 General Data Processing 53
MassLynx 53
Xcalibur 53
2.6 PLIMSTEX Method Development 54
2.6.1 PLIMSTEX Buffers and Sample Preparation 54
2.6.2 The Beginning; First Steps 55
First HDX Labeling Experiment 56
2.6.3 The Manual Approach 57
Flow Rates 58
HDX Labeling Experiment with the Manual Setup 59
Back Exchange Optimisation 60
CypA-CsA PLIMSTEX 60
2.6.4 The Automated Method 61
Hardware 61
Methodology 62
Automated Back Exchange Optimisation 64
2.6.5 PLIMSTEX Data Processing 65
2.6.6 PLIMSTEX Optimisation 65
Insulin 66
Insulin PLIMSTEX 66
2.7 SUPREX Method Development 67
2.7.1 SUPREX Buffers and Sample Preparation 67
2.7.2 Manual SUPREX 71
2.7.3 Automated SUPREX 71
Hardware 71

Software . . . 71
Methodology . . . 73
2.7.4 Temperature Dependent Automated SUPREX . . . 73
2.7.5 SUPREX Data Processing . . . 74
2.7.6 SUPREX Optimisation . . . 75
Myoglobin . . . 75
Myoglobin SUPREX Results . . . 75

3 SUPREX and PLIMSTEX of the Immunophilins 78
3.1 Introduction . . . 78
3.1.1 The Dissociation Constant . . . 81
3.2 Direct Infusion . . . 81
3.3 Labeling Experiments . . . 86
3.4 PLIMSTEX - Manual . . . 88
3.5 PLIMSTEX - Automated . . . 92
3.5.1 Bulk Incubation . . . 92
3.5.2 Individual Incubation . . . 95
3.6 Cyclophilin A Manual SUPREX . . . 96
3.7 SUPREX - Automated . . . 99
3.7.1 Apo Cyclophilin A . . . 99
3.7.2 Cyclophilin A-2.3 % MeOH . . . 100
3.7.3 Cyclophilin A-Cyclosporin A . . . 102
3.7.4 Cyclophilin A-KM184 . . . 103
3.7.5 Cyclophilin A-ES1234 . . . 104
3.8 Denaturant Effect on HD-Exchange Behavior . . . 105
3.9 Conclusion . . . 108

4 SUPREX of AGr2 and FH19-20 111
4.1 Introduction . . . 111
4.2 Direct Infusion . . . 113
4.3 Labeling Experiments . . . 115
4.4 SUPREX - Manual . . . 119
4.4.1 AGr2 SUPREX . . . 119
4.4.2 FH19-20 SUPREX . . . 121
4.5 SUPREX - Automated . . . 123
4.5.1 AGr2 SUPREX . . . 123
4.5.2 FH19-20 SUPREX . . . 130

4.6 Automated Temperature Dependent SUPREX of AGr2 133
4.7 Conclusion 135

5 SUPREX of CypA and GroEL 137
5.1 Introduction 137
5.2 Direct Infusion 138
5.3 Labeling Experiments 139
5.4 SUPREX - Automated 142
5.4.1 Apo GroEL 142
5.4.2 CypA-GroEL 143
5.4.3 CypA-CsA-GroEL 146
5.5 Conclusion 150

6 Summary 152

7 References 156

8 Appendix 1 178
8.1 Amino Acid Table 178
8.2 Thermodynamics 179
The Internal Energy and Enthalpy 179
Heat Capacities 179
Entropy, Free Enthalpy and Energy 180

9 Appendix 2 182
9.1 Bradford Assay for Cyclophilin A 182
9.2 Direct Infusion Chromatogram 182
9.3 HPLC-MS Elution Chromatogram 183
9.4 Manual PLIMSTEX CypA Mass Spectrum 183
9.5 LC Program for HDX Labeling 184
9.6 LC Program for Bulk PLIMSTEX 185
9.7 LC Program for Individual PLIMSTEX 186
9.8 The PLIMSTEX Modelling Procedure 188
9.9 Human Insulin Sequence 189
9.10 SUPREX LC Method Apo Sample List 190
9.11 SUPREX LC Method Holo Sample List (Even) 191
9.12 SUPREX LC Method Holo Sample List (Odd) 192
9.13 Automated SUPREX CypA Mass Spectrum 193

9.14 Derivation of SUPREX Equations . . . 193
9.15 HHM Sequence . . . 194
9.16 Automated Myoglobin SUPREX Curves . . . 195

10 Appendix 3 **197**
10.1 Cyclophilin A Sequence . . . 197
10.2 FKBP12 Sequence . . . 197
10.3 CypA Manual SUPREX Curves . . . 197
10.4 CypA-CsA Manual SUPREX Curves . . . 198
10.5 CypA-ES1234 Manual SUPREX Curves . . . 199
10.6 Apo CypA Automated SUPREX Curves . . . 200
10.7 CypA-36.88 % MeOH Automated SUPREX Curves . . . 201
10.8 CypA-CsA Automated SUPREX Curves . . . 202
10.9 CypA-KM184 Automated SUPREX Curves . . . 203
10.10CypA-ES1234 Automated SUPREX Curves . . . 205

11 Appendix 4 **206**
11.1 Anterior Gradient 2 Sequence . . . 206
11.2 FH19-20 Sequence . . . 206
11.3 Apo AGr2^{Nicholson} Manual SUPREX Curves . . . 206
11.4 AGr2^{Nicholson}-PTTIYY-Pen Manual SUPREX Curves . . . 207
11.5 Apo AGr2^{Florance} Automated SUPREX Curves . . . 208
11.6 Apo AGr2^{Nicholson} Automated SUPREX Curves . . . 209
11.7 AGr2^{Nicholson}-PTTIYY-Pen Automated SUPREX Curves . . . 210
11.8 AGr2^{Nicholson}-PATIAA-Pen Automated SUPREX Curves . . . 211
11.9 Apo FH19-20 Automated SUPREX Curves . . . 212
11.10FH19-20-Fondaparinux Automated SUPREX Curves . . . 213

12 Appendix 5 **215**
12.1 GroEL Sequence . . . 215
12.2 Automated Apo GroEL SUPREX Curves . . . 216
12.3 CypA-GroEL Automated SUPREX Curves for CypA . . . 217
12.4 CypA-GroEL Automated SUPREX Curves for GroEL . . . 218
12.5 CypA-CsA-GroEL Automated SUPREX Curves for CypA . . . 219
12.6 CypA-CsA-GroEL Automated SUPREX Curves for GroEL . . . 220

List of Figures

1.1 Components of a Mass Spectrometer 1
1.2 Schematic of the ESI Processes 3
1.3 Quadrupole Mass Analyser. 4
1.4 Protein Energy Landscape. 13
1.5 Types of Hydrogens in an Enzyme. 17
1.6 Amide Bond Exchange Rates. 19
1.7 HDX Mechanisms. 20
1.8 Possible Pathways Associated with Immunophilin Complexation. . . . 22
1.9 The CypA-CsA Binding Pocket. 24
1.10 Structures of Immunophilin Binding Ligands. 25
1.11 Protein Structures of GroEL/GroES. 27
1.12 GroEL/ES Folding Mechanism. 28
1.13 Complement Mechanism and FH Structure. 30
1.14 PLIMSTEX Protocol. 31
1.15 Sharp-Break PLIMSTEX and SIMSTEX Curves. 32
1.16 SUPREX Methodology and Curves. 35
2.1 Cation Exchange Chromatography for Cyclophilin A. 42
2.2 Gel Filtration Chromatography for Cyclophilin A. 43
2.3 Weak Anion Exchange Chromatography for GroEL. 45
2.4 Gel Filtration Chromatography for GroEL. 46
2.5 Strong Anion Exchange Chromatography for GroEL. 47
2.6 PLIMSTEX and SUPREX Sample Array. 55
2.7 First PLIMSTEX Setup. 56
2.8 First HPLC-HDX Labling Experiment. 57
2.9 Manual PLIMSTEX and SUPREX Setup. 58
2.10 Flow Rates for Manual PLIMSTEX and SUPREX. 59
2.11 CypA HPLC-HDX Labling and Back Exchange. 59
2.12 Manual CypA-CsA PLIMSTEX. 61
2.13 Autosampler Tubing. 62
2.14 HPLC Ice Box. 63
2.15 Automated PLIMSTEX Overview 64
2.16 Automated Back Exchange Optimisation. 65
2.17 Human Insulin Structure. 66
2.18 Insulin HDX Results. 68

2.19 Automated SUPREX Overview 72
2.20 Heated 48-Well Sample Tray. 74
2.21 Protein Structure of Myoglobin. 75
2.22 SUPREX Curves Myoglobin (10-180 min). 77
3.1 Direct Infusion Spectrum CypA-CsA. 83
3.2 Direct Infusion Spectrum CypA-KM184. 84
3.3 Direct Infusion Spectrum CypA-ES1234. 85
3.4 Direct Infusion Spectrum FKBP12-Rapamycin. 86
3.5 Automated CypA HDX Labeling. 87
3.6 Automated CypA HDX Labeling with the Denaturant. 88
3.7 Manual CypA PLIMSTEX Data. 89
3.8 Manual CypA PLIMSTEX Data 2. 90
3.9 Manual FKBP12 PLIMSTEX Data. 91
3.10 Automated PLIMSTEX CypA-CsA Bulk Incubation. 93
3.11 Automated FKBP12 PLIMSTEX Data. 95
3.12 Single Automated CypA-CsA PLIMSTEX. 96
3.13 Manual CypA-CsA SUPREX Data. 98
3.14 Automated Apo CypA SUPREX Data. 100
3.15 Automated CypA-2.3 % MeOH SUPREX Data. 101
3.16 Automated CypA-CsA SUPREX Data. 103
3.17 Automated CypA-KM184 SUPREX Data. 104
3.18 Automated CypA-ES1234 SUPREX Data. 105
3.19 Automated CypA SUPREX with Urea. 107
4.1 AGr2 Binding Hendeca-Tagged Hexa-Peptides. 112
4.2 Fondaparinux Structure. 113
4.3 Direct Infusion Spectrum of AGr2 and Ligands. 114
4.4 Direct Infusion Spectrum of FH19-20 and Fondaparinux. 115
4.5 Automated AGr2-Ligand HDX Labeling. 116
4.6 Automated AGr2 Temperature HDX Labeling. 117
4.7 Automated FH19-20-FPX HDX Labeling (129 aa). 118
4.8 Automated FH19-20-FPX HDX Labeling (131 aa). 119
4.9 Manual AGr2 SUPREX Data. 120
4.10 Manual FH19-20 SUPREX Data. 123
4.11 Automated Apo AGr2 SUPREX Data. 126
4.12 Automated AGr2-PTTIYY-Pen SUPREX Data. 127
4.13 Automated AGr2-PATIAA-Pen SUPREX Data. 128

4.14 Automated FH19-20-FPX SUPREX Data. 133
4.15 Automated Temperature Dependent AGr2 SUPREX. 134
5.1 Direct Infusion Spectrum Apo GroEL. 139
5.2 HDX Labeling of CypA-GroEL. 141
5.3 Automated SUPREX Apo GroEL. 143
5.4 Automated SUPREX of CypA with GroEL. 144
5.5 The GroEL-Cyclophilin A Interaction. 145
5.6 Automated SUPREX of GroEL with CypA. 145
5.7 Automated SUPREX of CypA with CsA and GroEL. 147
5.8 Automated SUPREX of GroEL with CypA and CsA. 148

List of Tables

1.1 Electrostatic Interactions. 9
2.1 Self Cast SDS-PAGE Gels. 48
2.2 Ligand Preparation. 50
2.3 GDH and Urea Stocks. 70
2.4 LC Method Programmes for SUPREX. 72
2.5 Myoglobin SUPREX Results. 77
3.1 Mass Spectrometry Solution Phase HDX Methods. 80
3.2 PPIase Dissociation Constants. 82
3.3 Manual CypA SUPREX Results. 99
3.4 Automated CypA SUPREX Results. 106
4.1 Manual SUPREX Results for AGr2 and FH19-20. 122
4.2 Automated AGr2 SUPREX Results. 130
4.3 Automated FH19-20 SUPREX Results. 132
5.1 Automated CypA-CsA-GroEL SUPREX Results. 149

1 Introduction

1.1 Mass Spectrometry

Mass spectrometry (MS) is a powerful technique for identifying unknown compounds, studying molecular structure, and probing fundamental molecular interactions. It is essentially a technique for "weighing" molecules based on the motion of an ion in an electric or magnetic field. The mass to charge ratio (m/z), often referred to as Thomson [3], describes the properties of observed ions where m is mass and z is the charge of the ion. The charge of a given molecule can be obtained, if some knowledge of the chemical nature is known and hence the mass calculated.

Most mass spectrometers consist of three regions: an ion source to generate analyte ions, a mass analyser which separates the ions; and a detector (Fig 1.1). However, as the field of MS rapidly expands into other disciplines, especially Life Sciences, changes and additions have been made to adapt the technique initially devised to analyse small molecules. Chromatographic front ends allow separation before analysis (Section 1.1.4). Ion mobility enables gas phase separation after ionisation and a variety of post acquisition methods aid a researcher's life today. As work presented in this thesis solely employs ESI-mass spectrometry in conjunction with high-performance liquid chromatography (HPLC) the relevant background to this is now discussed.

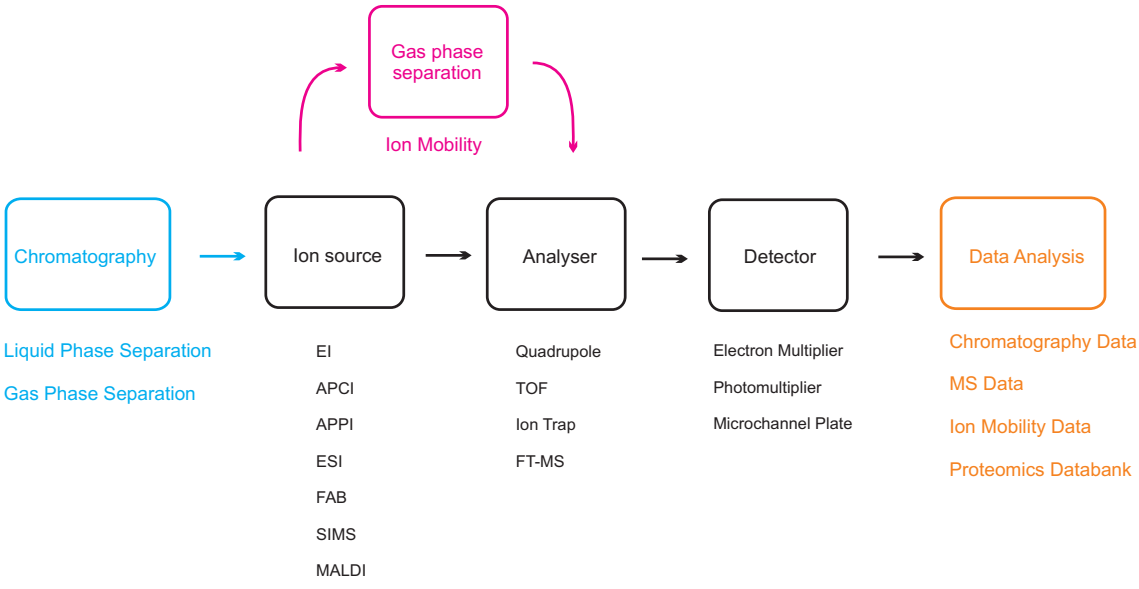

Figure 1.1: Components of a Mass Spectrometer (acronyms defined in glossary).

1.1.1 Ionisation

A variety of ionisation techniques (Fig. 1.1) are used in the field of MS to produce analyte ions, which ideally are selected based on the sample to be analysed. Electron impact (EI) and atmospheric pressure chemical ionisation (APCI) involve gas phase ionisation and hence require volatile analytes, whereas fast atom bombardment (FAB), secondary ion mass spectrometry (SIMS), ESI and MALDI are used to ionise condensed phase samples [4].
EI bombards the analyte with electrons to generate ions [5, 6]. This is useful for analysis of non-polar compounds but is often destructive to the analyte structure. FAB and SIMS use high energy atoms (about 5 keV) to sputter and ionise the sample in a single step by focusing a beam of rare gas neutrals (FAB) or ions (SIMS) on the liquid or solid sample. As there is no heating required, these sputter techniques are appropriate for thermally sensitive compounds [7, 8].
Atmospheric pressure ionisation (API) sources ionise the sample at atmospheric pressure and transfer the ions into the MS. This is used to ionise thermally labile samples such as peptides, proteins and polymers directly from the condensed phase *via* a liquid-chromatography (LC) system at a flow rate of a few hundred µL/min. The sample is introduced through a series of differentially pumped stages resulting in a large pressure difference between the ion source and the MS. In addition a drying gas is used to break up clusters that form as the solvent evaporates [4].
ESI-MS was introduced by Yamashita and Fenn in 1984 [9, 10] based on the work of Dole in 1968 [11] and since then has developed into a method of outstanding importance, particularly for new biochemical applications in the field of MS [12, 13, 14]. The liquid sample flows through a steel capillary tip, where a voltage of 3-6 kV is applied, resulting in a charge enrichment at the liquid surface and the formation of the Taylor cone, ultimately resulting in a jet of emitting droplets with a charge excess [15] (Fig. 1.2). Nebulising-/drying-gas and constant sample evaporation shrink the radius r of the droplet at constant charge q until electrostatic repulsion reaches the Rayleigh limit [16]:

$$q_{\mathrm{Ry}} = 8\pi(\varepsilon_0 \gamma r^3)^{\frac{1}{2}} \tag{1}$$

with ε_0 permittivity of vacuum. Equation 1 gives the conditions at which the charge q becomes equal to the surface tension γ, holding the droplet together. At a particular r the droplet becomes unstable and a 'coulombic explosion' releases smaller droplets. Further solvent evaporation leads to ion generation *via* one of two possible

mechanisms. The **charge residue model** (CRM) proposed by Dole *et al.* suggests solvent evaporation until a single analyte ion emerges [11] (Fig. 1.2b). *Per contra*, Iribarne and Thomson [17] proposed a mechanism coined the **ion evaporation model** (IEM) were q and γ become so high, that direct ion emission becomes possible and dominating for radii smaller 10 nm, as confirmed by Kebarle *et al.* [18] (Fig. 1.2b).

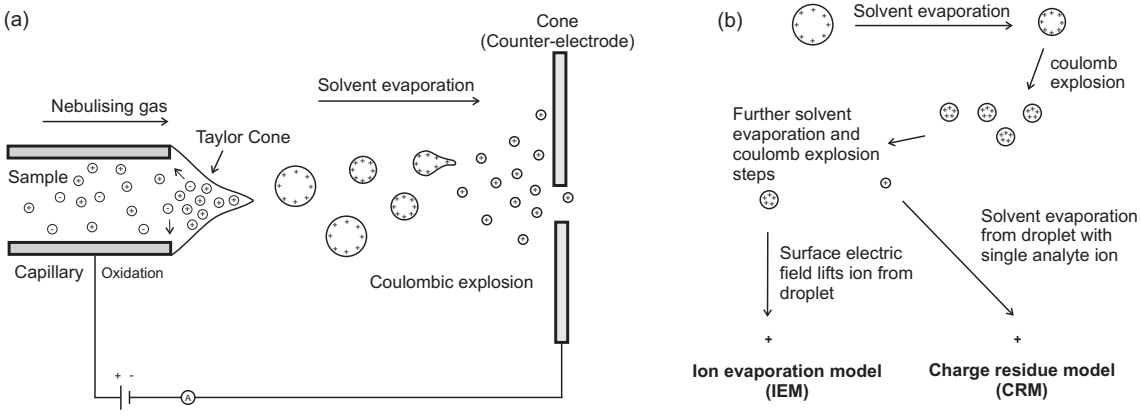

Figure 1.2: Schematic of involved processes during electrospray ionisation (a) (positive ionisation mode). (b) The two mechanisms discussed for ESI (adapted from [18, 19]).

MALDI is used to analyse large molecules up to 300 kDa employing pulsed laser techniques for ionisation [20]. Thereby the analyte is condensed in an ultraviolet (UV) light absorbing organic matrix such as α-cyano-4-hydroxycinnamic acid or trihydroxyacetophenone. The technique is often used for the analysis of synthetic and natural polymers, proteins, and peptides because mainly singly charged ions and few fragments are observed [4].

1.1.2 Mass Analysers

After ions are formed in the source region they are accelerated into the mass analyser by an electric field and separated according their m/z values. The quadrupole mass analyser (QMA) is the most common analyser used in MS comprising of multiples of two perfectly parallel rods as first described by Paul and Steinwedel [21]. Ions traveling through the QMA are subjected two potentials $\pm\Phi_0$:

$$\Phi_0 = +(U - V\cos\omega t) \qquad \text{and} \qquad -\Phi_0 = -(U - V\cos\omega t) \tag{2}$$

with ω the angular frequency, U the direct potential and V the amplitude of the RF voltage. To quantify the motion of an ion in the QAM an expression by Mathieu

can be used:

$$\frac{d^2u}{d\xi^2} + (a_u - 2q_u \cos 2\xi)u = 0 \tag{3}$$

where u stands for either x or y, ξ is a dimensionless parameter ($\xi = \omega t/2$), a_u is the ion stability with respect to the DC component (U) and q_u the ion stability for the RF component (V). So a_u and q_u can be expressed as:

$$a_u = a_x = -a_y = \frac{8zeU}{m\omega^2 r_0^2} \qquad \text{and} \qquad q_u = q_x = -q_y = \frac{4zeV}{m\omega^2 r_0^2} \tag{4}$$

As long as x and y remain less than r_0, an ion can travel *via* the QMA and scanning with a constant U/V ratio allows successive detection of different masses [4, 22].

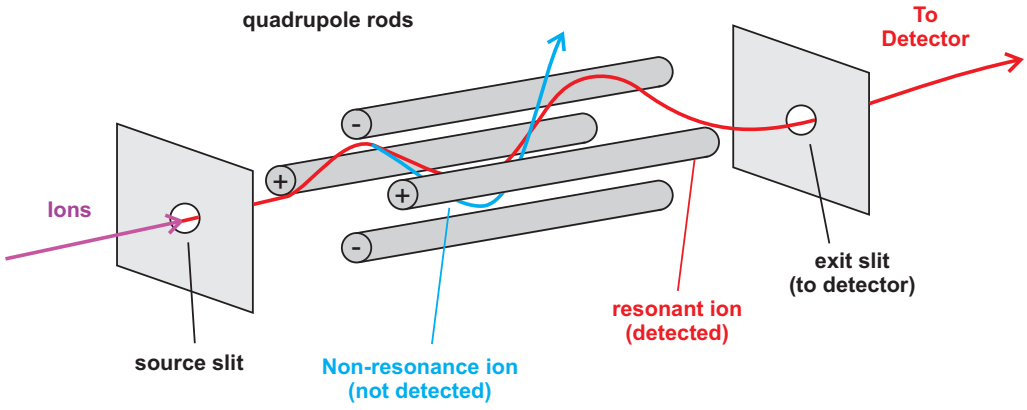

Figure 1.3: Quadrupole mass analyser. Ions generated in the source region travel through two sets of parallel rods before reaching the detector (adapted from [22]).

The time of flight (TOF) mass analyser separates ions in time as they traverse a flight tube. In the drift tube the ions are accelerated to high velocities by a potential V_s (Eq 5), flying the distance d (Eq 6) before reaching the detector. Mass to charge ratios (Eq 7) are calculated from the time ions take to travel through the flight tube with respect to the traveled distance [4].

$$E_{kin} = \frac{1}{2}mv^2 = qv^2 = zeV_s \tag{5}$$

with E_{kin} kinetic energy, m mass, v speed and q charge of an ion and e its elementary charge.

$$t = \frac{d}{v} \tag{6}$$

with t time.

$$t^2 = \frac{m}{z}\left(\frac{d^2}{2V_s e}\right) \tag{7}$$

The concept of the first TOF analyser was described by Stephens [23] in 1946 and in 1955 McLaren [24] published the design of a linear TOF-MS which became one of the first commercial instruments available. A disadvantage of the linear TOF-MS was its poor resolution, which improved dramatically with the invention of reflectron TOF analysers [25]. The reflectron is usually defined by a series of grids and ring electrodes, which create a retarding field acting as an ion mirror by reflecting the ions back through the flight tube. The TOF anaylser has become a popular tool largely due to its flexibility, low cost and theoretically no upper mass limit of detection [4].

The quadrupole ion trap was first reported by Paul and Steinwedel in the 1960' s and has been refined to provide a very sensitive and relatively inexpensive MS by Stafford *et al.* in 1984 [26, 27]. The sensitivity results from the efficiency of trapping and analysing ions produced in the source with the drawback of higher signal to noise (s/n) ratios, compared to other analysers. The quadrupole ion trap consists of a ring- and two endcap-electrodes to which a combination of RF and DC voltages are applied, creating an electric field trapping the ions in a potential energy well in the trap center. Mass spectra are acquired by scanning the RF and DC fields so that ions of increasing m/z values are ejected through a hole in one of the endcap-electrodes and strike the detector, followed by refilling the trap [4, 22].

Ion cyclotron resonance (ICR) MS offers high mass resolution and was first applied by Sommer [28]. The heart of the instrumentation is a superconducting magnet trapping ions in a circular orbit with a particular cyclotron frequency ω. An applied RF-voltage allows resonance absorption and excites ions of a particular mass, resulting in a larger orbit with a different ω. Measuring the changes in ω, the mass can be calculated.
In 1974 Marshall and Comisarov [29] implemented fourier transformation (FT) to the ICR technique. Thereby a short RF-pulse over a wide frequency range is applied to excite all trapped ions, producing a signal at the cyclotron frequency of each m/z-value for the present ion. Transforming this signal, which is similar to a free induction decay (FID) produced in an FT-NMR experiment, from the time domain

to the frequency domain resulting in a mass spectrum [30].

1.1.3 Detectors

There are three different types of detectors found in state of the art MS equipment: electron- and photo-multiplier and microchannel plates (MCP). In electron multipliers (EM) detection of primary ions triggers the emission of secondary particles (ions, electrons or neutrals), which are then responsible for amplification in a channeltron (horn shaped device comprising a series of dynodes), resulting in a measurable current. Electron multipliers are often found in quadrupole- and ion-trap instruments [4] (Section 1.1.2).
Photomultipliers (PM) work on the same principles as EM with the difference that the secondary particles collide with a phosphorescent screen, leading to photon emission and amplification in a photomultiplier tube.
The microchannel plate or array detector represents an array of thousands of individual EM fit on a plate enabling the detection of a large number of ions at the same time. Due to its quick response time <1 ns it is often coupled to TOF-MS instrumentation [4].

1.1.4 Liquid Chromatography ESI-Mass Spectrometry

Over the last few decades MS coupled separation techniques have become more and more sophisticated and the development of ESI-MS (Section 1.1.1) prompted a break through in these methods, allowing continuous ionisation/analysis ('on-line' LC-MS). The first on-line LC-ESI-MS experiment was conducted in 1984 by Alexandrov and co-workers [31] and since then HPLC-ESI-MS has become one of the major tools for separation coupled MS. Current development follows two major routes, (a) the reduction of scale, using smaller columns for improving the detection limits and (b) the reduction of time to satisfy the ever growing demands of high-throughput analysis [22].

Miniaturisation of LC-columns from mm to low µm inner diameters (ID) results in dramatic flow rate reductions from mL/min to low nL/min utilising 'nano-capillary-LC-systems' in conjunction with nano-ESI sources. This capillary/nano-scale HPLC-ESI-MS approach has had a massive impact on the amount of sample that is needed for analysis, especially in the field of proteomics when coupled with tandem mass spectrometry as reviewed by Heck *et al.* [32].

Traditionally, LC was not viewed as a fast methodology, however, the time consuming nature of chromatography has stimulated design of methods that improve the speed of separations, aiming for the minimal separation efficiency still leading to accurate results [33]. This is especially important for hydrogen deuterium exchange (HDX; Section 1.3) LC-MS experiments, where short run times are necessary to guarantee data accuracy. Increased flow rates and the use of capillary columns, monolithic columns, open tubular columns and small diameter packed capillaries further increase the speed of analysis [34]. Another approach to increase throughput utilises multiple HPLC columns [35], autosamplers [36] or high flow rate ionisation sources such as TurboIonSpray[1].

In conclusion, there is no 'best' methodology for a particular application rather a plethora of options to choose from, compromising between sample requirements and resources. Other liquid phase separation techniques such as capillary electrophoresis, capillary electrochromatography and microchips, or gaseous phase 'gas chromatography' can further be utilised in conjunction with API sources as reviewed in [37, 33, 38].

1.2 Protein Structure and Folding

Proteins are the major functional molecules enabling life on earth. They are involved in almost every metabolic process within our bodies and play a key role in the development of serious diseases, *e.g.* muscular dystrophy and Kreutzfeld-Jakob disease, due to either mutations in their primary sequence or their structural properties may be impaired, resulting in a loss of physiological activity [39]. Many types of cancers are attributed to mutations in 'guardian-proteins' (Section 1.4.3) such as p53, altering its structure and disabling apoptosis induction of malignant cells [40]. Therefore enzymes and receptors interacting with those proteins are usually drug targets to restore function or destroy cancer.
After the human genome revolution [41, 42] the field of proteomics started systematically characterising proteins in different biological compartments and their correlation with the available genomic data. The ultimate goal of protein science is to be capable of *de novo* protein structure- and activity-prediction and gain insight of how potential ligands will bind to an enzyme [43].

[1] Applied Biosystems - Foster City, USA

1.2.1 Protein Building Blocks

Proteins are macromolecules translated in the ribosomes from messenger ribonucleic acid (mRNA), transcripted from desoxyribonucleic acid (DNA) mainly comprising 20 'natural' occurring *L*-α-amino acids (aa; Appendix 8.1) along an unbranched polypeptide chain linked by an amide bond between the α-carbonyl- of one residue and an α-amino group of the next residue [44, 45]. This molecular arrangement infers amphoteric properties so that each aa can exist in either a neutral or zwitterionic state. In nature chirality is a major criterium for efficiency and during evolution, for no obvious reason, the *L*-form was chosen over the *D*-form. The planar double bond character of the amide bond rotationally restrains the polypeptide resulting in two possible configurations, *cis* and *trans*, where the *trans*-form is intrinsically energetically favored, probably due to lesser repulsion between non-bonded atoms. All naturally occurring peptide bonds in proteins exhibit the *trans* conformation with a few rare exceptions. If the following residue is proline, its cyclic side chain diminishes the repulsion between atoms and the intrinsic stability of the *cis* isomer is comparable to that of the *trans* isomer, however, still slightly favoring the *trans* conformation of the peptidyl-prolyl-bond (Section 1.4.1) [46, 43].

1.2.2 Noncovalent Interactions

To maintain the three-dimensional structure of proteins and nucleic acids, or to enable a molecule to bind specifically but transiently to another and form a complex, several types of non-covalent interactions are essential. The energy released in the formation of non-covalent bonds is 4-250 kJ/mol [47], less than the bond energies of single covalent bonds (*e.g.* C-H, 418 kJ/mol) [48]. Hence these weak bonds are often referred to as interactions, rather than bonds. Three fundamental non-covalent interactions can be distinguished: electrostatic- and van der Waals interactions and hydrogen bonding.

Electrostatic Interactions

Electrostatic interaction energies vary according to the nature of the charges and the permittivity ε of the medium. For two ions q_1, q_2 with net charges the energy V falls of with distance r as $1/\varepsilon r$ (Coulomb potential Eq 8). The permittivity ε ($\varepsilon = \varepsilon_r \cdot \varepsilon_0$) is also important, being about 80 in water and 2-4 in a protein. Functional groups on individual amino acids show specific ε, which are influenced by both the surrounding solvent and other functional groups within the protein [43].

$$V = \frac{q_1 q_2}{4\pi\varepsilon r}. \tag{8}$$

Table 1.1 provides an overview of other charged/non-charged or polarised species and their distance dependence along with typical energies of the interaction [47].

Table 1.1: Electrostatic interactions and distance dependence of potential energy (adapted from [47]).

Interaction	Distance dependence of potential energy	Typical energies (kJ/mol)
ion-ion	$1/r$	250
ion-dipole[a]	$1/r^2$	15
dipole[a] -dipole[a]	$1/r^3$	2
dipole[a] /dipole[b] -dipole[b]	$1/r^6$	0.6
London (dispersion)	$1/r^6$	2

[a] permanent dipole.

[b] induced dipole.

Van der Waals Interactions

The basis of non-polar, hydrophobic van der Waals, or dispersion forces is that the distribution of electronic charge around an atom changes with time creating transient dipoles. The interaction of these induced-dipoles is described as dispersion- or London-interaction and depends on the polarisibility α of the two molecules and the formation of instantaneous dipoles. The energy of the interaction can be written:

$$V = -\frac{C}{r^6} \qquad C = \frac{3}{2}\alpha_1\alpha_2\frac{I_1 I_2}{I_1 + I_2} \tag{9}$$

where I_1 and I_2 are the ionisation energies of the two molecules. Van der Waals interactions are smaller compared to electrostatic binding energies (Table 1.1) but when the surfaces of two large molecules come together a large number of atoms are in van der Waals contact, and the net effect, summed over many atom pairs, can be substantial [47, 43, 48].

Hydrogen Bonding

A particular important bond in biological systems is the hydrogen bond (H-bond). The hydrogen atom is formally bonded covalently to one of two electronegative atoms competing for the same proton, the donor. It also interacts favorably with the other,

the acceptor. Usually it is bonded to one of the atoms with a normal covalent bond length. The main component of the H-bond is an electrostatic interaction between the dipole of the covalent bond and the partially positively charged hydrogen atom and the partially negatively charged other atom. The small size and the substantial charge attributed to positively polarisation, lead to H-bond formation [44, 48].
In enzymes hydrogen bonding often involves the carbonyl- and the amino-group of the peptide backbone most often forming hydrogen bonds with bond lengths of 1.9-2.0 Å.
The energy of H-bonds have been variously estimated to be between 12 and 38 kJ/mol. Bonds of this strength are of particular importance, since they are stable enough to provide a significant binding contribution, but sufficiently weak to allow rapid dissociation [44, 43].

1.2.3 Protein Structure

The three dimensional structure of a protein is determined by its genetically encoded sequence [49] or its **primary structure**.
The polypeptide chains are found to be organised by hydrogen bonding of buried carbonyl oxygen atoms and an amino group into α-helices and β-sheets. This organisation is referred to as **secondary structure**. The α-helix was first described in 1951 by Linus Pauling and is an important structural element in biological macromolecules [50]. A carbonyl oxygen of residue n bonds with an amide bound hydrogen atom of residue $n+4$ resulting in 3.6 aa's in each turn of the cylindrical helix. About one-third of aa-residues in proteins are organised in helical structures, often exhibiting amphipathic character. One side has hydrophobic residues, allowing hydrophobic interactions, one side has hydrophilic properties enabling interactions with water. The second major element of structure are β-sheets, whereby the polypeptide chains are either aligned parallel or antiparallel. Individual strands vary in length between 5-10 aa-residues. α-helices and β-sheets are connected by loop regions of various lengths and irregular shape. Frequently recurring α and/or β substructures or folds are collectively termed motifs or supersecondary structures. One simple example is the β hairpin, comprising two antiparallel strands joined by a loop of three to five residues [50, 43].
The arrangement in space of all the atoms in a single polypeptide chain or in covalently linked chains is coined **tertiary structure**, whereas the overall organisation of subunits in oligomeric proteins is termed **quaternary structure** [43, 48].

Structure Elucidation Tools

Over the last few decades a set of biophysical methods has evolved which have enabled the determination of the tertiary structure of proteins.

The single most important technique in the investigation of enzymes has been **x-ray diffraction crystallography**, because it has provided the experimental basis of the present knowledge of the structure of proteins. X-rays are scattered when they strike an electron in a crystal, creating a unique diffraction pattern, which after fourier transformation, yields the electron density of the crystal. The degree of accuracy depends on the resolution, which can vary between 6.0-1.9 Å, the quality and the size of the crystal. The time frame for solving a novel crystal structure is from several months to years [43, 48].

As x-ray crystallography provides little information about the position of hydrogen atoms due to weak electron density of the H atom, **neutron diffraction** circumvents this issue. However, it is a time consuming approach with the need for special facilities [43, 48].

In recent years **NMR** has become one of the most important tools for protein structure determination. The principle is based on calculating the overall protein structure from short distance restrains (<5 Å) between natural abundance ^{1}H atoms in a one dimensional experiment. *Per contra*, multidimensional methods such as nuclear overhauser effect- (NOE) or heteronuclear single quantum coherence (HSQC) experiments with ^{13}C- and ^{15}N-labeled proteins provide further information for the structure determination of larger proteins [51].

1.2.4 Protein Folding

The major driving force for protein folding seems to be the burying and clustering of hydrophobic side chains (secondary structural elements) to minimise their contact with water. Also weak interactions such as H-bonds and van der Waals forces contribute to the process of protein folding [43, 48].
According to the first and second law of thermodynamics (Appendix 8.2), the total energy in a system and its surrounding being constant, and the total entropy increases of a system and its surrounding for spontaneous processes, the free energy change ΔG must be negative for a reaction to be spontaneous [52]. As protein folding can be assumed a spontaneous process under appropriate conditions, there

has to be an increase in entropy in the system or its surrounding. Polar molecules (aa-residues) in an aqueous phase interact with water molecules forming ionic or hydrogen-bonding interactions (Section 1.2.2). *Per contra*, water molecules in contact with non-polar, hydrophobic molecules (aa-residues) form a cage around it resulting in a decreased entropy compared to free water. In the process of two non-polar molecules (aa-residues) coming together more highly ordered water gets released, increasing the entropy of the water. This phenomenon, termed the hydrophobic effect, helps to compensate for the entropy losses inherent in the folding process [48].
In conclusion, protein folding is a complex procedure attributed to hydrophobicity, non-covalent interactions and heat release during the folding reaction resulting in a negative enthalpy change of the system, resulting in an overall negative free energy [43, 48, 53].

The energy landscape theory describes how the energy of a protein system changes with geometry of the individual residues [54]. The classical viewpoint established by Levintal was that an unbiased search through the plethora of conformations open for a denatured protein would take too long for a protein to fold, suggesting the existence of *pre*-defined pathway offering choices [43]. For proteins with random aa-sequences one would not assume such bias and expect the most stable structure to be the least 'frustrated' one [55]. The term frustration evolved from the spin-glass system emphasising the inability of a system to reach its energetic ground state [43]. Replacing and generalising the classical stepwise pathway with a series of intermediates, the energy landscape theory of protein folding involves the progressive organisation of an *ensemble* of partially folded structures on a free energy surface represented by a folding funnel (Fig. 1.4) [56]. The evolution of new techniques, *e.g.* nuclear magnetic resonance (NMR) dynamic spectroscopy has enabled observation of fast folding events supporting the basic validity of the theory [57].

The two axes of a two dimensional protein-energy landscape depict the energy-entropy balance associated with competing physical processes and the ruggedness of the funnel indicating frustration [58]. Local free energy minima represent transient kinetic traps, whereas the native state lies at the bottom of the funnel. Frauenfelder *et al.* emphasised that the physiologically active state is not just a lowest energy one but more a variety of states differing at least in side-chain orientation [59, 60]. The free energy of folding corresponds to the ordinate, whereas Q represents a fraction

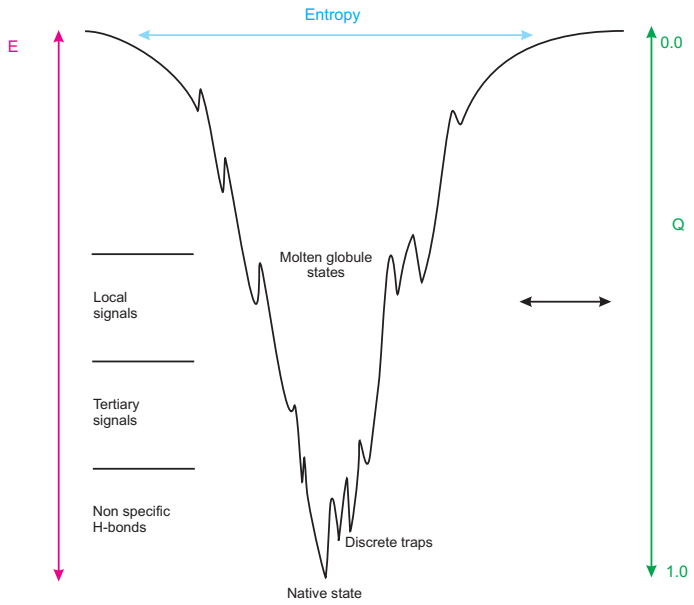

Figure 1.4: Protein energy landscape. E represents free energy and Q the fraction of native-like contacts, whereas entropy corresponds to the width of the folding funnel (adapted from [43]).

of native-like contacts. The width of the funnel represents the entropy (Fig. 1.4) [58]. A quantitative statistical approach to free energy landscapes can be found in [61].

1.2.5 Protein Stability

The stability of a protein is governed by the sum of its non-covalent interactions such as packing of the hydrophobic side chains and hydrogen bonding (Section 1.2.4) ranging from 20 to 63 kJ/mol [43]. Furthermore the interactions of individual water molecules have to be considered. So the gross thermodynamic properties of a protein in the native and unfolded state are determined by enthalpy/entropy changes in water and the protein in question (Section 1.2.4, Appendix 8.2).
Experimentally the free energy of protein folding is determined using thermal-/solvent-denaturation methods such as differential scanning calorimetry (DSC) or denaturation with a chaotropic agent. In the first instance the heat absorbance is measured as the protein is slowly heated through its melting transition. Denaturing agents such as urea or guanidinium hydrochloride (GDH) either solubilise all the constituent parts of the protein, from the amide backbone to the side chains or directly interact with groups of the protein [62]. To a first approximation, the transfer of protein backbone and side chains from water to the denaturant is proportional to its concentration as shown by Tanford *et al.* [63, 64]. As the denatured state

(D) is more exposed than the native state (N), it is preferentially stabilised by the denaturant and ΔG can be determined:

$$\Delta G_{D-N} = \Delta G_{D-N}^{H_2O} - m_{D-N}[\text{Denaturant}] \tag{10}$$

where m is a constant of proportionality named by Greene *et al.* [65] ($-\partial(\Delta G_{D-N})/\partial[\text{Denaturant}]$) containing information pertinent to the protein. The m-value strongly correlates with the surface exposure of the protein upon unfolding in a two-state unfolding event [66]. Low m-values may indicate a protein does not become highly unfolded during denaturation or the denaturation step occurs stepwise rather than in a single cooperative step [66, 43]. This observation is important for interpretation of findings in Chapters 3, 4 and 5.

1.2.6 Protein-Ligand Interactions

Over the last few decades a variety of methodologies have evolved to investigate non-covalent enzyme substrate interactions.
Utilising low sample volumes and radioactively labeled ligands, **equilibrium dialysis** with a semi permeable membrane directly yields concentrations of free and bound ligand.

In **equilibrium gel filtration** assays a gel filtration column is primed with a ligand, prior to application of the enzyme. As the protein travels through the column it drags any bound ligand with it at the same flow rate resulting in a ligand peak in the position of the protein and a trough in the position normally occupied by the smaller ligand. Ideally peak areas should be equal and proportional to the bound ligand [67, 43].

Analytical ultracentrifugation is utilised to investigate larger sample volumes (100-200 µL) measuring ultraviolet- (UV) absorbance in correlation with sedimentation. The higher molecular mass complex hereby sediments faster as free protein/ligand resulting in a sharp UV-peak while migrating down the cell [68, 43].

Useful data from nucleic acid-protein interactions has been derived from **filter assays**, where enzymes are immobilised on nitrocellulose filters and free ligands, however, are not retained. In special cases this economical procedure provides useful data for assaying binding [69, 43].

Spectroscopic methods such as measuring the Trp-fluorescence of a protein and/or a ligand are popular methods to observe protein-interactions. However, the concentration of free ligand is not directly accessible and often titration experiments with the ligand are performed. Fitting the fluorescence data yields the dissociation constant at relatively low sample concentrations and volumes [43].

Isothermal titration calorimetry (ITC) is a method to directly measure the specific heat change upon ligand binding under isothermal conditions. Depending on the dissociation constant (K_d) of the system, different sample concentrations yield information about binding stoichiometry, enthalpy and K_d [22, 43].

A recently developed methodology uses refractive indices to determine concentrations of proteins and/or ligands immobilised on a glass slide to calculate K_d's from concentration changes. Hence, light passes between two media with low and high refractive indices on a conducting surface, inducing an electric field causing photon/plasmon energy conversion, when constructive interference occurs. This results in a resonance effect, termed **surface plasmon resonance** (SPR). Nevertheless, high accuracy data represents an immobilised state of a protein and care must be taken comparing these results with other methods [22].

In the field of **mass spectrometry** a variety of techniques have emerged to observe protein and protein-ligand interactions in the gaseous and aqueous phase and to study structural properties of these biological systems. Since the first observations of non-covalent complexes in the gas phase by Ganem, Li and Henion [70] a lot of work has been done on quantifying these properties, as reviewed in [71, 72, 73, 74, 75]. The dialectic character of how well gas-phase properties reflect those in solution have been demonstrated *i.a.* by Aplin *et al.* [76] and Robinson and co-workers on the *E. coli* chaperonin groEL and tandem mass spectrometry [77], exhibiting low and high grade of reproducibility for gas- and solution phase determined information. These findings triggered the evolvement of indirect methods to observe protein-ligand interactions such as hydrogen-deuterium exchange methods (Section 1.3), PLIMSTEX (Section 1.5) and SUPREX (Section 1.6).

Tandem mass spectrometry describes the process of multiple rounds of isolation of a particular ionic species and dissociation followed by mass analysis and has been widely employed for proteomic analysis. Dissociation is achieved *via* vibrational and

electronic mediated processes. The former utilises *i.a.* neutral buffer gas molecules as reactants for fragmentation and is referred to as collision induced dissociation (CID) or collisionally activated dissociation (CAD) [78]. CID is perhaps the most widely used fragmentation technique in the field of MS and has been well studied over the years, as reviewed in [79].
Another vibrational dissociation technique is surface-induced dissociation (SID) whereby collisions between gaseous ions and a surface increase the internal energy of the ionic species, culminating in fragmentation as demonstrated by Wysocki, Futrell and co-workers [80, 81].
Electronic mediated fragmentation processes such as electron capture dissociation (ECD) were first described by Zubarev, Kelleher and McLafferty in 1998 [82], thereby electron capture leads to charge reduction and electron mediated dissociation. Since then, ECD is a well applied method for protein structure elucidation, probing protein properties and nucleic acid sequencing as demonstrated by Breuker *et al.* [83, 84].

In the last 25 years ion mobility mass spectrometry (IM-MS) has become an important analytical tool to study the shape of compounds and has recently been applied to investigate biological systems. It is based on determining the mobility of an analyte ion in an electric field and a buffer gas environment, resulting in an averaged collisional cross section for the compound in question, as reviewed in [85]. Over the years protein systems of all sizes have been investigated ranging from small peptides by Bowers *et al.* [86] to moderate size proteins, such as cytochrome C, haemoglobin and calmodulin probed by Barran and co-workers [87] and large biological systems such as groEL, investigated by Robinson and Heck *et al.* [88, 89].

1.3 Hydrogen Deuterium Exchange

Since the detection of deuterium in 1932 by Urey and Brickedde [90], its exchange with hydrogen has been the subject of intensive study. In 1933 Bonhöffer and Klar showed that little hydrogen-deuterium exchange occurs in small organic molecules in heavy water [91]. The pioneering work of Linderstrøm-Lang and Hvidt in the mid 50's established HDX as a central technique for studying proteins [92, 93]. While the majority of protein HDX experiments still employ high resolution NMR to observe exchange kinetics [94] the ground breaking work of Katta and Chait firstly demonstrated the great potential [95] of marrying HDX with MS and laid the foundation for several MS based HDX methods [96, 97, 98, 99].

1.3.1 HDX in Macromolecules

Proteins posses three different types of hydrogen atoms distinguished by their binding partner and their intrinsic rates of HD-exchange (Fig. 1.6) [100].

The hetero atom bound hydrogens of the side chains are coined **type 1** hydrogen atoms undergoing a fast reversible exchange under all buffer conditions [100] (Fig. 1.6a).

Amide bound hydrogen atoms of the protein backbone are referred to as **type 2** hydrogens exhibiting solvent depending behaviour. Low pH and temperature conditions slow down the exchange rate and these features are widely used in HDX experiments [94].

The aliphatic and aromatic bound hydrogens are named **type 3** hydrogen atoms and show no exchange within the time of an usual HDX-MS experiment [91].

In choosing the right pH conditions the intrinsic rate of exchange (k_{int}) of an amide hydrogen can be lowered four orders of magnitude, whereas temperature control adds another order of magnitude (Fig. 1.6).

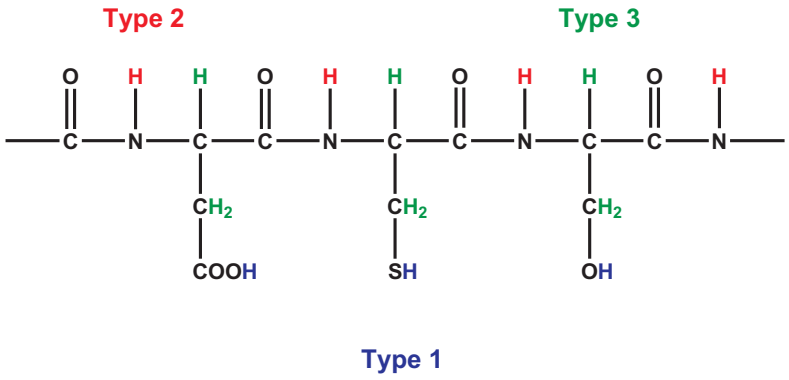

Figure 1.5: Types of hydrogens in an enzyme with: type 1 hydrogen atoms in blue, type 2 (red) and type 3 (green; visualised with ChemDraw - CambridgeSoft - Cambridge, USA).

1.3.2 HDX Models

In enzymes global HDX depends on the nature of the hydrogen atom to be exchanged and its rate constant for exchange. Type 2 hydrogens are nearly all involved in H-bonding, either intramolecularly or with water. Also, amide protons are often less

solvent accessible due to the folded state of a protein and therefore show reduced exchange rates [98]. At physiological pH, HDX is base catalysed (Section 1.3.3), however, at low pH acid catalysis (Section 1.3.3) plays an important role [101]. The rate constant for hydrogen deuterium exchange k_{ex} for proteins with equilibrium unfolding behaviour following a two state process (folded - unfolded) [102] HDX can be described by [103, 104, 105]:

$$P_{cl}^{H} \underset{k_{cl}}{\overset{k_{op}}{\rightleftharpoons}} P_{op}^{H} \overset{k_{int}}{\rightarrow} P_{op}^{D} \underset{k_{op'}}{\overset{k_{cl'}}{\rightleftharpoons}} P_{cl}^{D} \tag{11}$$

with P_{cl}^{H} the protonated folded, P_{op}^{H} the protonated unfolded, P_{op}^{D} the unfolded deuterated and P_{cl}^{D} the deuterated folded species. k_{op} and k_{cl} being the rate constants for the unfolding/refolding process and k_{int} the intrinsic exchange rate for amide HDX to occur. The overall HDX rate constant k_{ex} can be written as:

$$k_{ex} = \frac{k_{op}k_{int}}{k_{op} + k_{cl} + k_{int}} \tag{12}$$

When $k_{int} \gg k_{cl}$ and $k_{int} \gg k_{op}$ (termed EX1 kinetics) the exchange rate k_{ex} is given by the unfolding rate constant k_{op}:

$$k_{ex} = k_{op} \tag{13}$$

Per contra, under physiological conditions it is more common for $k_{cl} \gg k_{op}$ and $k_{cl} \gg k_{int}$. In this case (EX2 kinetics) the exchange rate k_{ex} is given by:

$$k_{ex} = \frac{k_{op}k_{int}}{k_{cl}} \tag{14}$$

k_{op} and k_{cl} can be rewritten as the equilibrium constant for the unfolding reaction:

$$k_{ex} = K_{op}k_{int} \tag{15}$$

While only a few proteins show EX1 kinetics naturally, all proteins undergo EX2 kinetics under physiological conditions and exchange can be influenced towards the EX1 under denaturing conditions, *e.g* denaturant or pH increase [106].

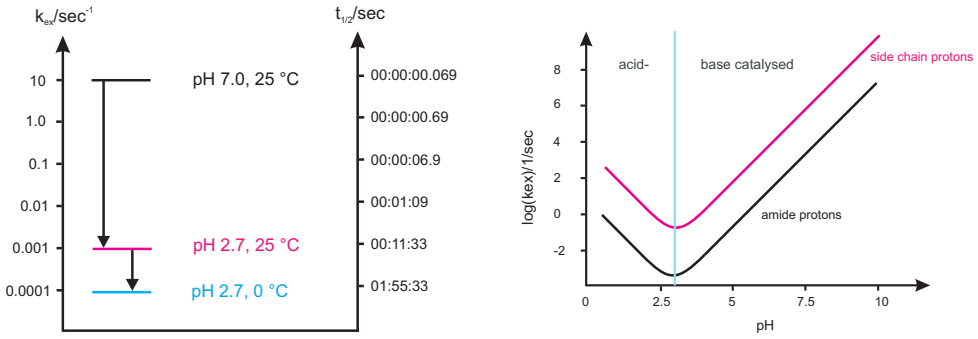

Figure 1.6: Amide bond exchange rates. (a) Rate constants and half lifes for amide HDX at different pH and temperature settings (reproduced from: homepage Engen JR, http://www.hxms.neu.edu). (b) Average exchange rates of amide- (black) and side chain bound hydrogen atoms [22, 94].

1.3.3 Mechanisms of Exchange

Hydrogen exchange at unprotected sites in a protein is pH dependent, both acid- and base-catalysed mechanisms are important. The overall intrinsic exchange rate (k_{int}) is usually presented:

$$k_{int} = k_{acid}[H^+] + k_{base}[OH^-] + k_{H_2O} \tag{16}$$

with k_{acid} the acid-catalysed rate constant, k_{base} the base-catalysed rate constant and k_{H_2O} the spontaneous rate constant in water. The absolute and relative values for k_{int} are aa-residue dependent and have been tabulated by Englander and co-workers [107].

Base-catalysis occurs *via* the imidate anion caused by amide proton abstraction of the base (Fig. 1.7). Acid-catalysis takes place by one of the two suggested pathways. The first occurs *via* an ionic amide intermediate analogue to the basic-catalysed pathway. The second, involves deuteron abstraction by the α-carbonyl group *via* the imidic acid mechanism (Fig. 1.7c) [94].

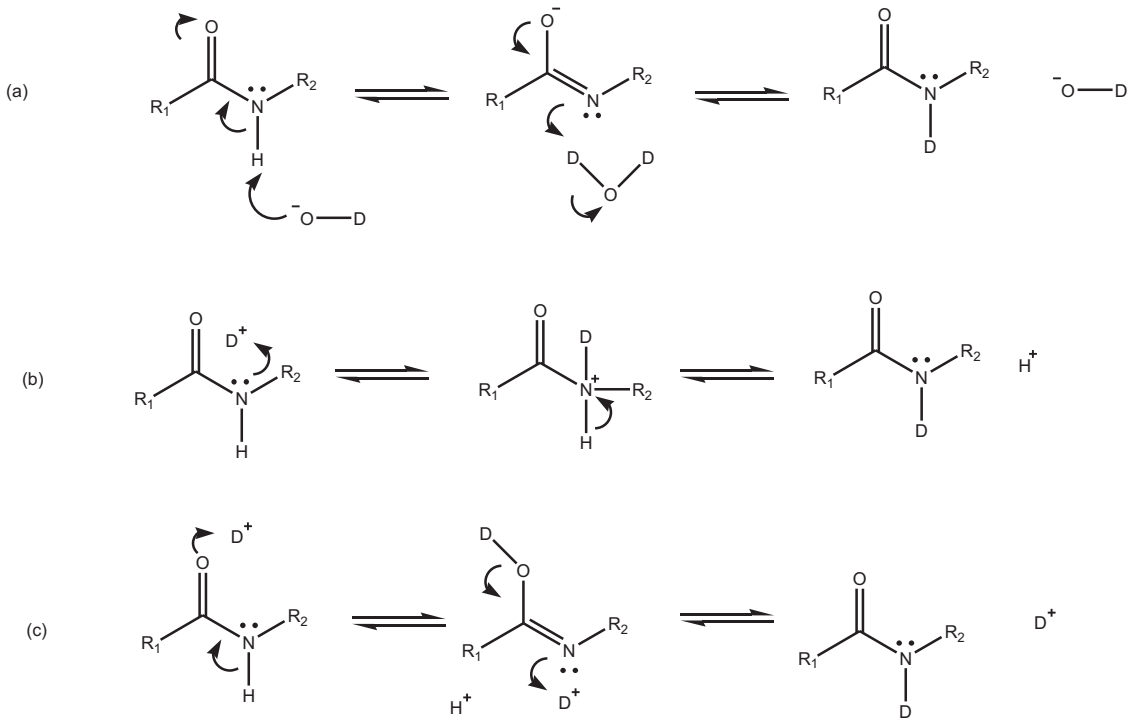

Figure 1.7: Proposed HDX mechanisms for acid- and base-catalysis. (a) Base-catalysed HDX mechanism *via* imidate anion. (b) First acid-catalysed mechanism *via* positive charged amide nitrogen. (c) Second acid-catalysed mechanism *via* imidic acid mechanism (adapted from [94]).

1.4 Biological Systems

1.4.1 The Peptidyl-Prolyl *cis-trans* Isomerase Family

Since the discovery of cyclophilin A in 1984 by Handschumacher *et al.* and Harding *et al.* [108] as a binding partner to cyclosporin A (K_d 30 nM) resulting in an immune suppression reaction, there has been keen interest in the immunophilin protein family. In 1989 another protein was identified binding the immunosuppressive drug FK506 and named FK506-binding protein (FKBP) [109, 110]. In the same period it was demonstrated that cyclophilins and peptidyl-prolyl-*cis-trans* isomerases (PPIase) are species variants of the same protein [111, 112]. In 1994 a third member of the PPIase family was discovered, the parvulins, which are in contrast to CypA and FKBP, irreversibly inhibited by juglone, 5-hydroxy-1,4-naphthoquinone [113, 114, 115].

Protein folding was initially thought to be a spontaneous process, transforming the amino acid sequence in a well defined three-dimensional structure, suggesting all information for proper folding is located in the primary sequence [49]. Refolding

experiments of denatured globular single-domain proteins showed refolding events occurring in a second to millisecond time scale. However, the *cis-trans* isomerisation of the peptidyl-prolyl bond is the rate limiting step in protein folding and takes significantly more time [116]. During biosynthesis of proteins in the ribosomes the *trans* isomer is most abundant, as it is in most native peptides. Nonetheless, both isomers are accessible in the peptide backbone. The PPIases lower the energy barrier of this rate limiting step and thereby accelerate protein folding [112]. However, knockout experiments in *E. coli* [117] and *A. calcoacet.* [118] did not show any significant phenotype in growth. *Per contra*, mutation experiments in *Drosophila* and *C. elegans* showed severe effects on sight and fertility, respectively [119, 120]. Based on these findings it was concluded that the immunophilins do not play a general essential role in protein folding but rather may perform specific functions through interactions with unique sets of restricted partner proteins that remain to be fully identified.

The immunosuppressive actions exerted of CsA and FK506 have been numerously reviewed [121, 122] and are visualised in Figure 1.8. During T cell activation calmodulin (CaM) binds to the phosphatase calcineurin (CN) as a result of elevated levels of intracellular Ca^{2+}. The complex dephosphorylates the nuclear factor of activated T cells (NF-AT), now able to cross the nuclear membrane. In the nucleus dephosphorylated NF-AT acts as transcriptional activator for the early T-cell-activation gene product interleukin-2 (IL-2). Binding of CsA to CypA alters the structure of CsA, enabling binding to CN and therefore blocking the phosphatase activity of the CN/CaM complex. Inhibition of the CN/CaM phosphatase activity with FK506 and FKBP works in an analogous way (Fig. 1.8).

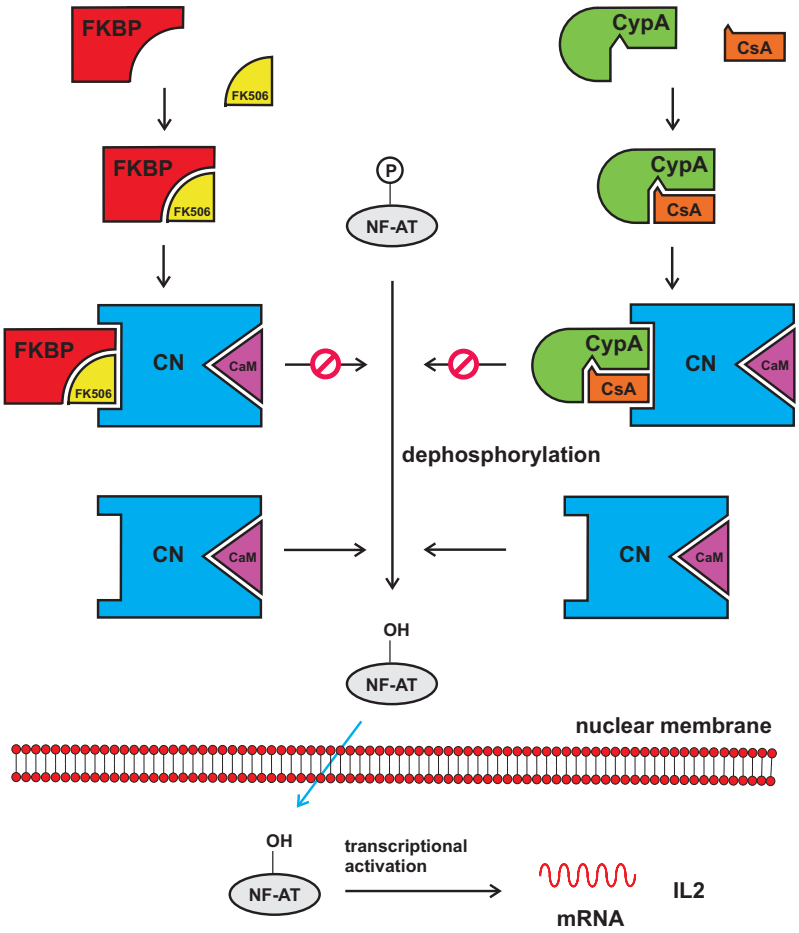

Figure 1.8: Possible pathways associated with CypA-CsA and FKBP-FK506 complexation during T cell activation. During T cell activation CaM binds to CN due to high Ca^{2+} levels resulting in dephosphorylation of NF-AT. In the nucleus NF-AT acts as activator for IL-2 transcription (adapted from [123]).

Cyclophilin A

The cyclophilins are ubiquitous proteins found in almost all cell types, *i.a.* bacteria, yeasts, fungi, plants and vertebrates. The CypA family is highly conserved in structure and consists of CypA, B, C and D. Human CypA is a cytosolic 165 aa, 18 kDa protein comprising two α-helices and eight β-strands forming the hydrophobic core of the protein. Despite structural differences, FKBP and CypA share a common domain involving residues Tyr48 and Phe53 in the hydrophobic core, Tyr79 on the surface and Phe60 in the CsA binding pocket [124]. Intensive x-ray crystallography and NMR structural studies by Wüthrich, Walkinshaw *et al.* [125, 126, 127, 124, 128, 129, 130, 131, 132] identified residues Arg55, Ile57, Phe60, Met61, Gln63, Gly72, Thr73, Ala101, Asn102, Ala103, Gln111, Phe113, Trp121, Leu122, His126 being involved in CsA binding and therefore form a 15·20·10 Å

binding pocket (Fig. 1.9). It has been shown that up to 5 water molecules are essential for CsA binding [133, 134]. More recent calculations of Lazaridis *et al.* [135] suggest the involvement of only 4 water molecules.

Lately, studies have shown the involvement of CypA in replication and infectivity of the human immunodeficiency virus type 1 (HIV-1), which encodes *i.a.* the viral protein R (Vpr) involved in the induction of G2 host cell cycle and the translocation of the *pre*-integration complex of the incoming virus to the nucleus [136, 137]. The N-terminus of this 96 aa enzyme comprises a highly conserved proline rich region, from which two show a preference for the *cis* conformation of the imidic bond, suggesting a regulation of the isomerisation of Vpr by the host PPIase. As a result CypA is incorporated into HIV-1 virons by binding to Pro222 in the proline rich region of the HIV-1 capsid protein. This specific interaction disables detection by inhibitory host factors such as Ref-1, which facilitates the infection [138, 139, 140].

Cyclosporin A

The undecapeptide CsA (Fig. 1.10) binding to CypA is a cyclic peptide with a mass of 1202.65 Da and a pronounced hydrophobic character, first isolated from the fungus *Tolypocladium inflatum*. Since its discovery in the early 1980's (Section 1.4.1) it has been used as an immunosuppressive drug to prevent graft rejection after organ transplantation [108]. Side effects such as nephrotoxicity led to the search for new metabolites [141] and the synthesis of new compounds.
Due to its hydrophobic character, CsA studies in different solvents showed a conformational polymorphism of CsA [142]. In the complexed form with CypA all peptide bonds are in the *trans* conformation and none of the intramolecular hydrogen bonds, found in the free structure are present. Nonetheless, one hydrogen bond is formed between the hydroxyl group of the Bmt-1 side chain and carbonyl oxygen of MeLeu-4 (Fig. 1.10). In the complex only residues 1, 2, 3, 9, 10 and 11 of CsA are in contact; the remaining residues 4-8 protrude out of the CypA surface. This hydrophobic protrusion is referred to as the "effector loop", which is implicated in the specific interaction with CN. Conclusively, this explains the phenomenon that binding of a CsA analogue was a requirement, but not sufficient, for immunosuppressive activity [143, 144, 134].

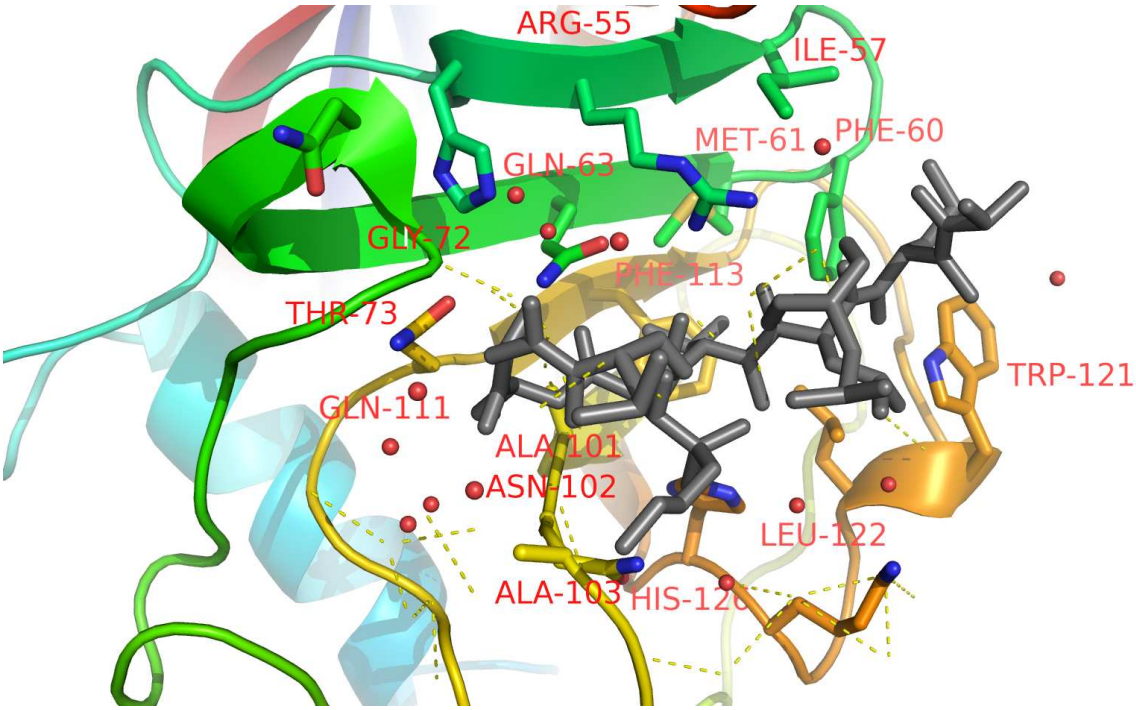

Figure 1.9: The CypA-CsA binding pocket with Arg55, Ile57, Phe60, Met61, Gln63, Gly72, Thr73, Ala101, Asn102, Ala103, Gln111, Phe113, Trp121, Leu122, His126 residues involved in CsA binding. Cyclosporin represented in grey (pdb file 1cwb visualised with pymol (DeLano Scientific LLC - Palo Alto, USA)).

FKBP12

Members of the FKBP protein family range from 12 to 52 kDa. FKBP12 is a 107 aa small ubiquitous protein (~12 kDa) with all seven proline residues in the *trans* conformation [145]. It is a PPIase and induces immune suppression (Section 1.4.1, Fig. 1.8) by binding to FK506 or rapamycin. Dissociation constants for the FKBP-FK506 and FKBP-rapamycin complex have been determined to 0.4 nM and 0.2 nM, respectively [146, 147, 148].

Its structure has been solved to atomic resolution, identifying residues Tyr82, Ile92, Phe36, Phe99, Tyr26, Phe46, Phe48, Val55, Ile56 and Trp59 forming a hydrophobic pocket, responsible for ligand binding [149, 150, 151, 152]. It was found that the volume of this binding pocket only accommodates a five-membered or a six-membered ring [147] and in 1998 Denesyuk *et al.* identified the 6-membered pipecolinyl ring of FK506 or rapamycin being responsible for binding in FKBP-FK506 and FKBP-Rapamycin complex [153].

FK506/Rapamycin

The immunosuppressive drug FK506 is a 788 Da polyketide and mainly produced by the bacterium *Streptomyces tsukubaesis* first discovered in a soil sample in Tsukuba, Japan [154]. It is structurally related to rapamycin, 901.5 Da (Fig. 1.10), isolated from *Streptomyces hygroscopicus* found on Easter Island in 1975. Both act as an immunosuppressive drug and find wide medical application [155, 156]. To find less toxic analogues a variety of compounds have been synthesised and investigated [157] as reviewed by Etzkorn in 2006 [155].

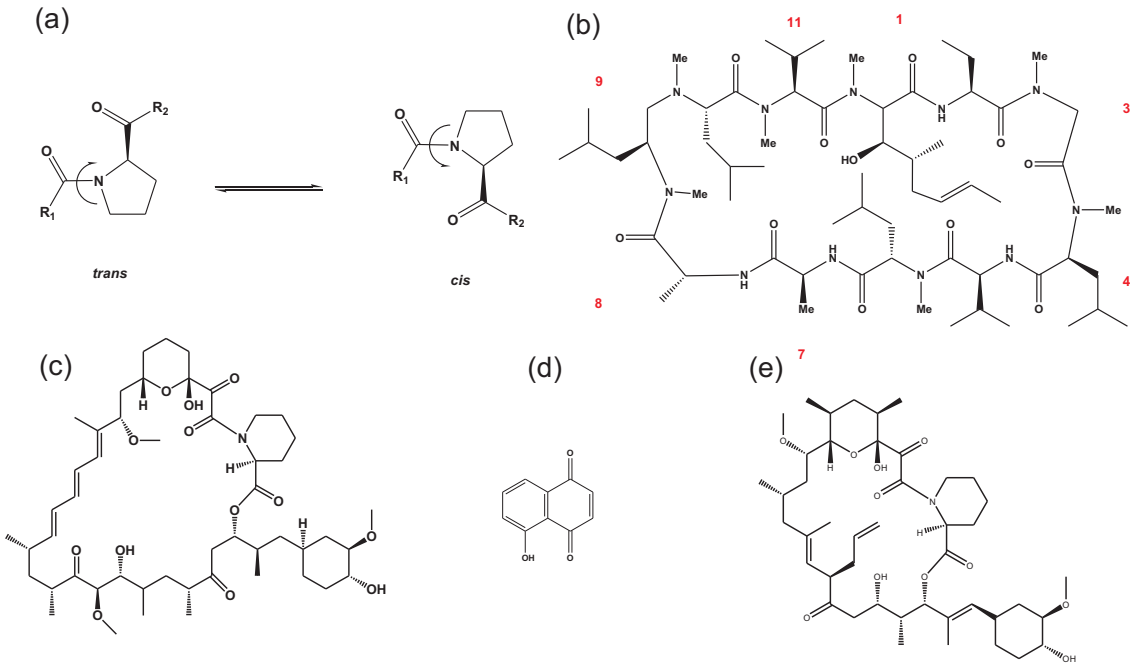

Figure 1.10: Structures of immunophilin binding ligands. (a) The *cis-trans* isomerisation of the proline imidic bond. (b) Cylosporin A, 1. 4R-4[(E)-2-butenyl]-4, *N*-dimethyl-L-threonine (MeBmt); 2. L-α-aminobutyric acid (Abu); 3. sacrosine (Sar); 4. leucine (Leu); 5. valine (Val); 6. *N*-methylleucine (meLeu); 7. alanine (Ala); 8. D-Ala; 9. MeLeu; 10. MeLeu; 11. *N*-methylvaline (MeVal). (c) Rapamycin. (d) 5-Hydroxy-1,4-naphthoquinone (juglone). (e) FK506. Structures visualised with ChemDraw - CambridgeSoft - Cambridge, USA.

1.4.2 The GroEL/GroES *E.coli* Chaperon System

Molecular chaperones, or chaperonins were initially identified in bacteria, archaea and eukaryotic cells as reviewed in [158, 159, 39]. Chaperonins seem to provide kinetic assistance in protein folding of newly translated or translocated polypeptides. Although Anfinsen identified in 1973 that all steric information specifying the final three-dimensional structure of a protein is contained in its primary sequence [49],

there is an apparent disposition under certain conditions for many proteins to misfold and aggregate irreversibly *in vivo* [160]. By preventing this from happening, molecular chaperons facilitate the production of native state proteins under conditions in which the native form would otherwise not be achieved [161]. Conclusively, their actions increase the yield of properly folded proteins but rarely increase the inherent rate of the folding reaction [162, 160].

The *E.coli* chaperon system groEL/groES is one of the most studied molecular chaperon systems and is expressed from the groE operon of the bacterium, whereby L stands for large and S for small. GroEL comprises 14 identical subunits with a relative mass of ~58 kDa each, which are arranged in two stacked heptameric toroids, constituting a cylinder of 145 Å height, 135 Å diameter and a central inner channel of 45 Å (Fig. 1.11). Each groEL protein is composed of three clearly defined domains: apical (a), intermediate (i) and equatorial (e). The apical domain is formed by aa residue 191-376 and provides the binding site for non-native proteins and the co-chaperon groES. It has been found that the non-native protein target is bound at the edge of the inner channel co-assisted by the end-surfaces of the groEL cylinder containing hydrophobic clusters for extra fixation [163, 164, 165, 166, 167]. The largest (equatorial) domain (aa residue 6-133 and 409-523) delivers the majority of inter-subunit and inter-ring contacts and hosts the ATP/ADP binding site on the upper part of the inner channel surface [168]. The intermediate domain contains 89 aa (134-190 and 377-408) and connects a- and e-domain providing large scale conformational changes of the protein during ligand interactions [168, 164, 160]).

The co-chaperon groES contains seven identical ~10 kDa subunits assembled in one heptameric dome shaped ring 30 Å in height, 70-80 Å in diameter incorporating a hole of 10 Å in diameter. In the presence of Mg-ATP/ADP, groES interacts with the a- and i-domain of the groEL protein inducing large scale movements enabling the formation of the large inner chamber (Anfinson's cage) [164, 166, 160, 169, 170, 89].

The model for groEL/ES assisted productive folding includes several steps (Fig. 1.12). First, binding of non-native proteins to the a-domain of the preexisting groEL/ES triggers a conformational change releasing groES. In the presence of ATP groES binds once again to groEL forming the Anfinsen's cage. Cooperative hydrolysis of ATP by the *cis* ring of groEL enhances its affinity to groES resulting in a conformational change in the a-domain releasing the non-native protein into the

Anfinson's cage for spontaneous folding in a state, isolated from external medium. ATP binding to the opposite *trans* ring triggers cooperative hydrolysis and allosteric conformational changes in the *cis* ring, dissociating groES and releasing the native protein from the Anfinson's cage [171, 172, 173, 174, 175]. In case one cycle is not enough for the final folding of the protein, it reoccurs once again.

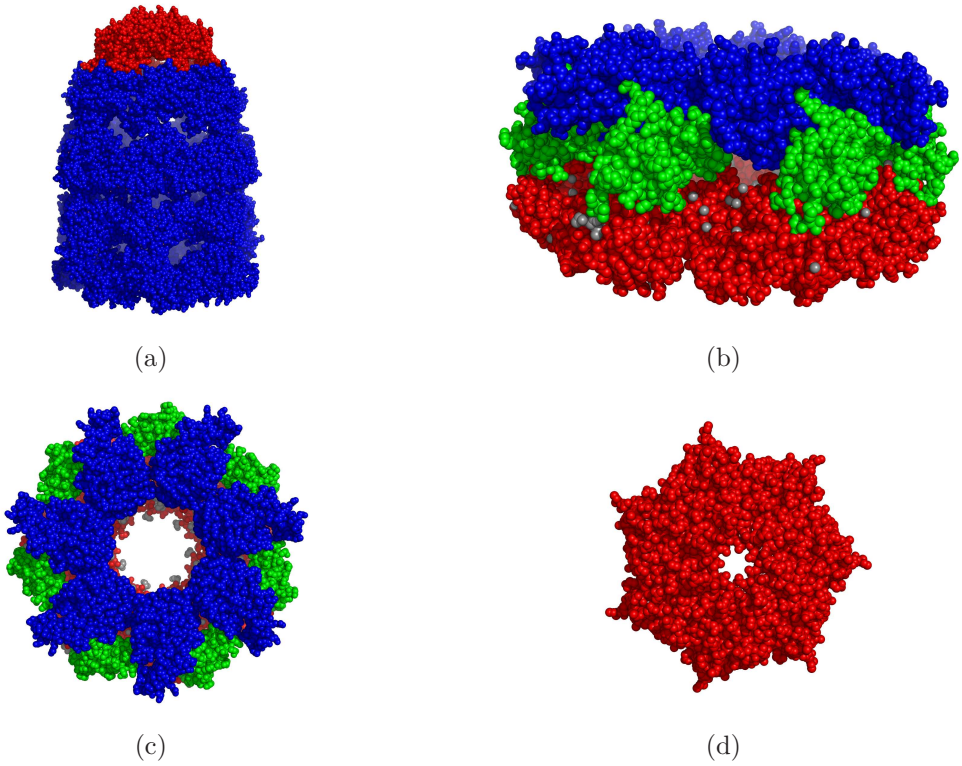

Figure 1.11: Protein structures of groEL/ES. (a) The groEL/groES complex. (b) A single groEL toroid with apical- (blue), equatorial- (red) and intermediate- (green) domain. (c) Top view into the groEL cavity. (d) Top view of the 10 subunit-groES protein (pdb file 1oel visualised with pymol (DeLano Scientific LLC - Palo Alto, USA).

Over time, it has been shown that groEL/ES also chaperones protein folding in proteins too big for the inner cavity and the groES-lid, as shown for the mitochondrial aconitase [176], a 82 kDa protein and maltodextrin glucosidase [177] with 62 kDa. Studies on rhodanese and cyclophilin without the groEL ligands K^+, Mg^{2+}, ADP, ATP and the co-chaperonin groES revealed protein folding attributes solely contributed to groEL [178, 179, 162]. The findings of the groEL-CypA interaction will be further discussed in Chapter 5. GroEL has been well investigated in the field of MS *inter alia* by van Duijn and Heck *et al.* [170, 89].

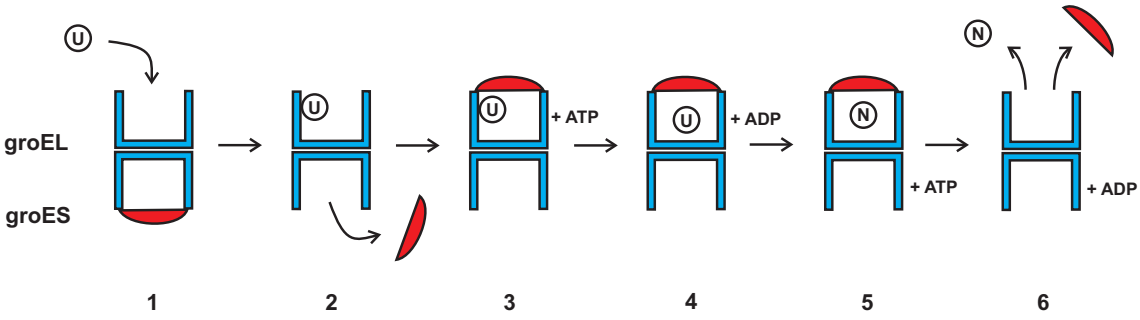

Figure 1.12: GroEL/ES folding mechanism. With U standing for the unfolded protein and N representing the native folded protein (adapted from [162]).

Conclusively , after almost 40 years of investigation a basic mechanism of the groEL/ES chaperonin activity has been established. However, there is still discussion about alternative mechanisms as reviewed by Marchenkov [162].

1.4.3 AGr2

Anterior gradient 2, also known as gob-4 [180] or hAG-2 [181] is a 175 aa, ~20 kDa protein found to play a key role in cancer development and survival [182].
It is the human orthologue of the *Xenopus laevis* AGr2 protein, XAG-2. In the frog embryo it has a putative role in ectodermal patterning and is regulated by a number of fundamental embryonic molecules like noggin and chordin [183]. XAG-2 is secreted and induces cement gland differentiation and expression of neural markers. The role of AGr2 in humans is uncertain. Liu *et al.* suggested that AGr2 in humans is secreted as well [184]. Others proposed, based on basic local alignment search tool (BLAST) analysis [185], that AGr2 represents a novel member of the protein disulfide isomerase family, involved in protein maturation in the endoplasmatic reticulum (ER) [186, 187].
Hupp and co-workers found, that the over expression of AGr2 attenuates the activation of p53 in UV-damaged cancer cells, suggesting AGr2 acting as a survival factor through p53 inhibition [188]. Experiments conducted in rat mammary tumor cells over expressing AGr2 demonstrated enhanced adhesion to substrate and increased metastatic potential [184]. The profiling of expressed genes of circulating tumor cells in peripheral blood from metastatic cancers such as colorectal and pancreatic cancers illustrated the presence of AGr2 [182, 189]. Furthermore, it has been shown to be expressed in breast [190, 181, 191], prostate [192], fibrolamellar carcinoma [193] and lung cancers [194], although its role in these diseases remains unclear.

Hupp *et al.* demonstrated a universal up-regulation of the AGr2 expression in Barrett's epithelium or Barrett's oesophagus [195, 196], morphological intermediates also referred to as metaplasia and dysplasia in the development of an oesophageal adenocarcinoma [188]. Whang and co-workers found AGr2 acting as an oncogene by promoting tumor growth, cell migration and cellular transformation in the same type of human cancer [197].
So far there is little known about the structure of AGr2 as no crystal or NMR-structures have been determined, yet.

1.4.4 The Complement System and Factor H

The complement system is part of the innate immune system responsible for recognition and elimination of damaged and modified self structures, as well as foreign invading microbes [198] and was first described by Ehrlich and Bordet in the 1890's [199].

The Complement System

Individual complement components act in a cascade type manner (Fig. 1.13a) and are linked together to form an important immune surveillance system. The classical pathway activation is triggered by immune antigen-antibody complexes, whereas the lectin pathway is activated by carbohydrate complexes on microbial surfaces [200]. *Per contra*, the alternative pathway is constantly activated at a low level caused by spontaneous conformational changes of the complement component 3 (C3). This 'tick over' activation initiates a powerful amplification cycle, generating multiple C3b, cleavage products of C3, by the C3 convertase C3bBb which further triggers immune response, by releasing anaphylatoxins (*e.g.* C3a and C5a) and formation of the membrane attack complex. The latter is responsible for cell lysis, whereas anaphylatoxins lead to inflammation reactions (Fig. 1.13a), ultimately leading to elimination and safe removal of a foreign or modified particle. The activation cascade is controlled by proteins belonging to the regulators of complement activation (RCA) family, *i.a.* factor H (fH), complement regulator 1 (CR1) and the membrane control protein (MCP) [201, 202, 203].

Factor H

Factor H is a single peptide chain plasma glycoprotein of ~155 kDa in mass. It was first discovered by Nilsson and Müller-Eberhard in 1965 as β1H globulin and is abundant in the blood plasma at concentrations of several hundred µg/mL [204].

Inhibition of complement activation by fH occurs on the level of the C3 convertase by preventing and inhibiting formation of the C3 convertase, enhancement of dissociation of a performed convertase (decay-accelerating activity) and acting as a co-factor for the C3b cleaving serine protease factor 1 [198, 205, 205].

It has been shown that sequence modifications and gene truncations can be associated with several, quite different diseases [202]. FH mutations and sequence variations are directly linked to renal diseases such as haemolytic uraemic syndrome (HUS) [206, 207], dense deposit disease (DDD) [208] or membranoproliferative glomerulonephratitis (MPGN) [209] or retinal diseases such as age related macular degeneration (AMD) [210, 211].

FH is composed of of 20 complement control proteins modules (CCP) that resemble beads on a flexible string in the transmission electron microscope [212, 213]. The N-terminal four CCPs (module 1-4) encompass the region capable of co-factor and decay accelerating activity as well as binding to C3b [214, 215, 216, 217]. A second principal binding site lies within the C-terminal pair of CCP's 19-20 [218, 219]. It has been shown that at least two sites on fH (*i.e.* CCP 7 and 20) interact with heparin and other poly anions [220, 221, 222, 223, 224, 225, 226, 227]. Furthermore, the C-terminal side additionally binds sialic acids [220, 224, 227].

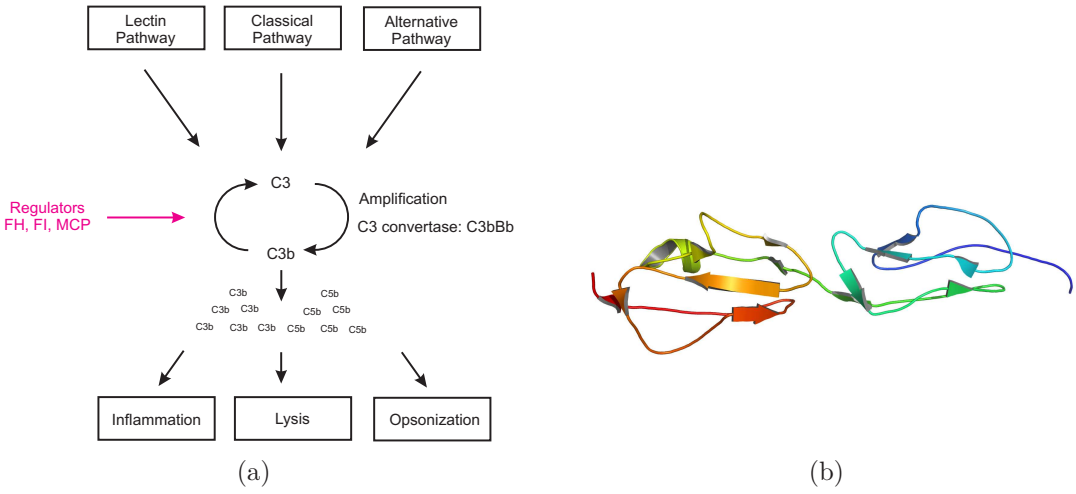

Figure 1.13: Complement mechanism and protein structure of factor H CCP modules 19-20. (a) Complement mechanism (adapted from [198]). (b) NMR protein structure of fH CCP module 19-20 (pdb file 2bzm visualised with pymol (DeLano Scientific LLC - Palo Alto, USA)).

1.5 PLIMSTEX

A methodology employing solution phase HDX to quantify protein ligand interactions with the sensitivity and specificity of MS was developed by Gross and coworkers in 2003 and named PLIMSTEX (**p**rotein-**l**igand **i**nteractions in solution by **MS**, **t**itration and HD **ex**change) [1]. For affinity quantification the method requires a change to occur in HDX during titration. The PLIMSTEX method is based on reactivity similar to footprinting experiments [228], but it is also analogous to titration monitoring by spectroscopic methods. It relies on spectral position shifts (Δm_i) rather than spectral absorbances.

Figure 1.14 visualises the individual steps involved in a PLIMSTEX experiment. The protein of question is first equilibrated with different concentrations of the ligand in a non-deuterating environment, before HDX is initiated with a deuterated buffer. After reaching near steady state conditions HDX is quenched by lowering the temperature to 0 °C and the pH to 2.5. The solution is loaded on a guard column for desalting and back exchange of the T1 deuterons of the side chains of the immobilised protein. Elution with an organic gradient into the MS for analysis reveals the deuterium uptake due to HDX of T2 hydrogens, reflecting the protein's state prior quenching.

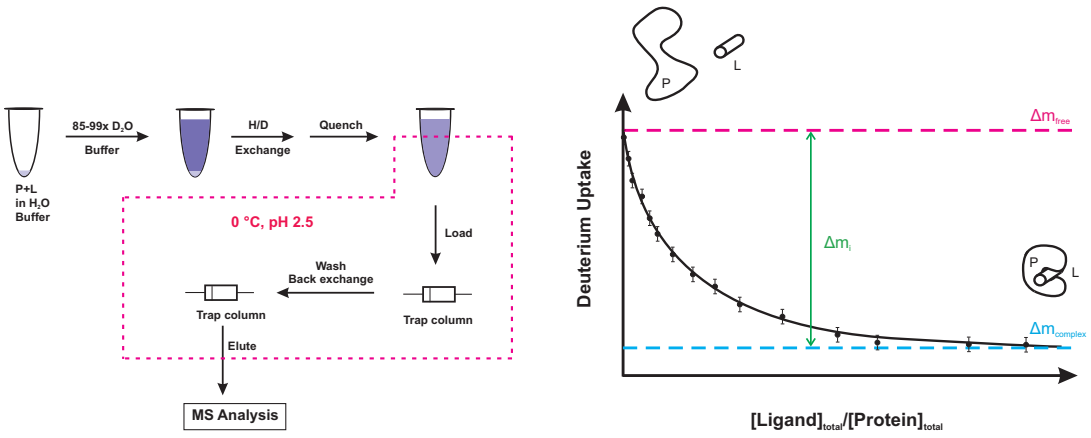

(a) (b)

Figure 1.14: The PLIMSTEX protocol. (a) Methodology of a PLIMSTEX experiment. (b) The resulting PLIMSTEX curve (images modified from [229]).

The quenching and desalting process causes the ligands to dissociate and be washed of the column, liberating the protein for which the number of solvent accessible amide deuteriums can be determined by MS. A plot of the mass difference of the deuterated and the non-deuterated enzyme *vs.* the total ligand concentration

results in the PLIMSTEX curve (Fig. 1.14b). Δm_{free} describes the deuterium level of the apo protein, $\Delta m_{complex}$ of the holo protein and Δm_s is the difference between Δm_{free} and $\Delta m_{complex}$ describing the change in Δm_i upon ligand binding from a 1:1 to a 1:n protein-ligand ratio. This change describes the degree of protection due to ligand binding and thereby induced changes in protein conformation. PLIMSTEX curves are sensitive to the total protein concentration and do not yield reliable K values when the protein is titrated at concentrations higher than ~100 times the K_d. Nevertheless, when the concentration is too high, 'sharp-break' curves (Fig. 1.15a are obtained and can be used for stoichometric evaluation of the protein-ligand complex [229]. For a 1:1 protein-ligand system Equation 54 (page 188) is applicable (derivation in Appendix 9.8). However, for 1:n protein-ligand systems a more sophisticated approach was developed including statistical re-sampling [230, 231].

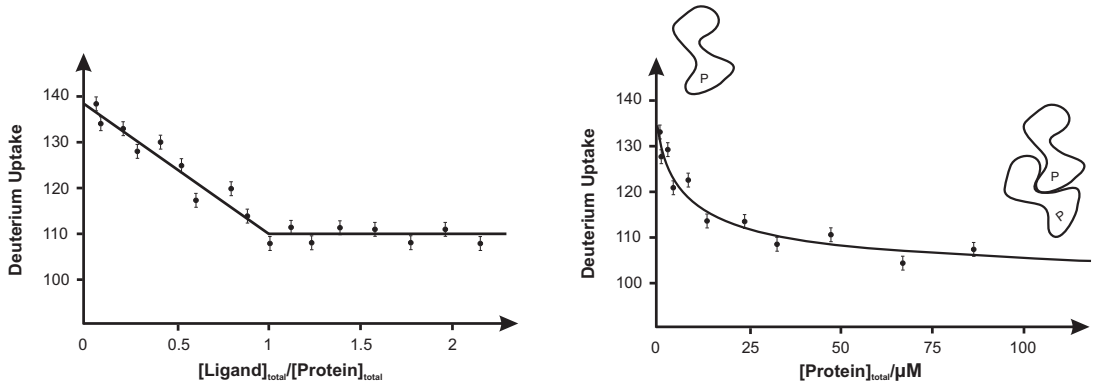

(a) (b)

Figure 1.15: Sharp-break PLIMSTEX and SIMSTEX curves. (a) Sharp-break PLIMSTEX curve for a model protein-ligand system (image modified from [229]). (b) SIMSTEX curves for an aggregating model protein (adapted from [232]).

1.5.1 SIMSTEX

In 2006 Gross *et al.* adapted PLIMSTEX to determine solution phase self-association equilibrium constants of insulin analogues [232]. SIMSTEX stands for **s**elf-association **i**nteractions using **MS**, self-**t**itration and HD **ex**change. It first requires the determination of the deuterium uptake of the monomeric protein species at steady state equilibrium as a function of the total protein concentration (Fig. 1.15b). The process for calculating the affinity constants from the SIMSTEX curves starts with the PLIMSTEX modeling procedure [230]. However, the equations for the oligomer solution concentrations were modified to accommodate self-association as described in [233] yielding affinity constants for different stages of oligomerisation. A detailed

derivation of the SIMSTEX equations along with the results for insulin analogues can be found in [232].

1.6 SUPREX

Another method utilising HDX-MS to probe protein-ligand behavior is SUPREX. The '**s**tability of **u**npurified **p**roteins from **r**ates of H/D **ex**hange' technique was first reported by Fitzgerald and coworkers [2] in 2000 and since then has become well applied. The approach is based on measuring the stability (*i.e.* the standard free energy of protein folding (ΔG_f) of a protein or a protein-ligand system by denaturation with a chemical denaturant utilising the reactions of globally protected amide protons during HDX. Generally ΔG_f reflects the stability of a protein in its 'native' conformation and therefore differs in miss-folded proteins or protein-ligand complexes. In the first instance, a miss-folded protein is generally less stable than it's 'native' conformation [234] whereas ligand-binding has a stabilising effect [235]. Once ΔG_f values have been determined, K_d and m-values can be calculated for the protein-ligand complex [236, 237]. SUPREX is an alternative way to circumvent time consuming spectroscopic based methods like fluorescence or circular dichroism (CD) [238] with the advantage of using 1-2 orders of magnitude less sample [239]. The fact that no highly purified protein samples were needed and that the process was automated with MALDI or LC-ESI-MS analysis make it a versatile method to investigate biological systems and properties (*e.g. in vivo* protein studies [240], multimeric proteins [241], protein-DNA complexes [242] and multi-domain proteins [243]) in a high-throughput fashion [244, 245].

1.6.1 The SUPREX Protocol

The SUPREX technique relies on measuring the mass increase (Δm), due to the HDX reaction of globally protected amide protons of an enzyme or an enzyme-substrate system due to denaturation and deuteration of the protein in various concentrations of a chemical denaturant (*e.g.* urea or guanidinium hydrochloride). Therefore the protein in question is incubated for different time periods at different concentrations of the chemical denaturant in the deuterated buffer. The denaturant destabilises the protein's structure, which has the effect of increasing the rate of global HDX and increasing the rate of deuterium incorporation into the protein. After quenching with 2 M HCl, the solution is loaded on a guard column, washed with non-deuterated buffer to back exchange T1 deuterons followed by elution with

an organic gradient into the MS (process described for developed LC-ESI-MS, Fig. 1.16c). Ultimately, Δm is detected *via* MS analysis and plotting the different Δm values at different concentrations of the denaturant yields the SUPREX curve (Fig. 1.16a). Fitting the data with Equation 17 extracts the midpoint ($C^{1/2}_{SUPREX}$) of the SUPREX curve.

$$\Delta\mathrm{m} = \Delta M_0 + \frac{a}{1 + e^{-\frac{[Denaturant] - C^{1/2}_{SUPREX}}{b}}} \tag{17}$$

Where ΔM_0 represents Δm before global exchange, a is the amplitude of the curve in Da, [Denaturant] is the molar concentration of the chemical denaturant and b is a parameter that describes the steepness of the transition [237]. At this point it should be noted that the $C^{1/2}_{SUPREX}$ values are not midpoints of denaturing curves in the classical way where $C^{1/2}_{den}$ depends on the protein stability and the m-value of the protein [2, 241]. In SUPREX the midpoint is not only a function of this parameters but also depends on the time of exchange t and the average intrinsic exchange rate of an amide proton $\langle k_{int}\rangle$ in Equation 18. The values for $\langle k_{int}\rangle$ can either be estimated by averaging the values for all the backbone amide hydrogens as shown by Englander, Bai and coworkers [107, 246], or the simple relationship $\langle k_{int}\rangle = 10^{pH-5}$ min^{-1} could be used as shown by Fitzgerald *et al.* [2].

$$C^{1/2}_{SUPREX} = C^{1/2}_{den} - \frac{RT}{m}\ln\left(\frac{\langle k_{int}\rangle t}{0.693} - 1\right) \tag{18}$$

Once $C^{1/2}_{SUPREX}$ values have been determined according to Equation 61 (Appendix 9.14) plotting $-RTln(\langle k_{int}\rangle t/0.693 - 1)$ *vs.* $C^{1/2}_{SUPREX}$ followed by linear square fit analysis yields ΔG_f at a 0 M concentration of the denaturant as the intercept with the ordinate and the m value as the slope of (Fig. 1.16b). In 1975 Schellman reported a way to calculate dissociation constants of protein-ligand complexes from free energies [235], hence Equation 63 (Appendix 9.14) can be used to determine K_d's.

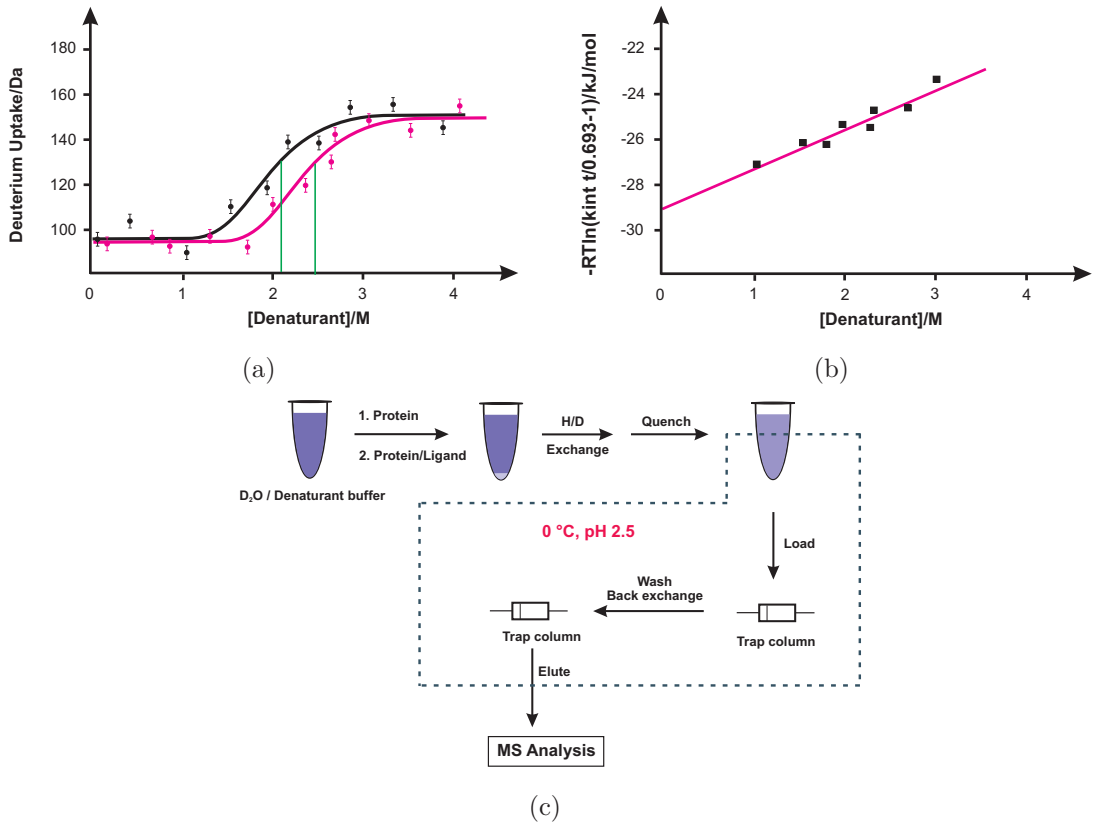

Figure 1.16: SUPREX methodology and curves for a model protein. (a) Theoretical SUPREX curve for an apo model protein (black), holo protein (magenta) at a single incubation time and resulting in a stabilisation of the complex. (b) Evaluation of SUPREX, free energy of protein folding *vs.* $C_{SUPREX}^{1/2}$ (images a and b modified from [2]). (c) SUPREX methodology modified for LC-ESI-MS usage.

1.6.2 Precision and Accuracy

The precision of SUPREX under well defined two-state unfolding and EX2 exchange conditions is mainly dependent on the precision of the $C_{SUPREX}^{1/2}$-value. SUPREX experiments with various proteins (*i.a.* β-trypsin) showed an average standard deviation of ~10 %. The accuracy under the same conditions with the same set of proteins was within 46 % of ΔG_f values previously reported by NMR, CD, fluorescence and calorimetry [247].

SUPREX was developed to gain information about the standard free energy of protein folding. Therefore EX2 exchange conditions (Section 1.3) and two-state unfolding are necessary to guarantee the accuracy of the SUPREX approach. To investigate SUPREX accuracy under non-EX2/unknown conditions, unfolding studies with ubiquitin [248, 249] have been performed. Thereby good agreement for ΔG_f values were obtained as long as experiments were performed at lower pH conditions

(to favor EX2 conditions) and H/D exchange times to yield $C^{1/2}_{SUPREX}$ at lower denaturant concentrations (*i.e.*, less than 2 M). Non-linearity of acquired SUPREX data and large deviations in the correlation coefficient in the non-linear least-squares analysis might indicate non-two-state, non-EX2 or EXX exchange behavior (Section 1.3).

1.6.3 Single Point SUPREX and SPROX

To increase throughput of SUPREX enabling more efficient screening, a single point SUPREX approach has been devised [244]. For quantitative analysis of protein-ligand behaviour a SUPREX curve has to be recorded (Fig. 1.16). However, this process would be more time and sample consuming than a single point SUPREX experiment. Therefore a SUPREX experiment at a wisely chosen single denaturant concentration and time would be sufficient. It would of course be necessary to perform a full SUPREX experiment to investigate the protein in question's thermodynamic properties. Fitzgerald and coworkers presented in 2004 and 2008 the feasibility of the MALDI single point SUPREX approach on protein-S and CypA [244, 245].

Based on SUPREX a methodology of chemical modification combined with MALDI-/LC-MS was presented by Fitzgerald and coworkers in 2008, termed **s**tability of **p**roteins from **r**ates of **ox**idation (SPROX). It is, like SUPREX, based on measuring the thermodynamic properties of an enzyme-substrate system, however, utilising oxidation rates of globally protected sites in a protein instead of HDX. One advantage of SPROX is the irreversibility of the oxidation compared to HDX. However, it is limited to the number of globally protected methionine residues providing only a relatively low resolution probe for studying conformational changes in proteins. Despite this, various protein-ligand systems have been investigated, *i.a.* CypA, ubiquitin, ribonuclease A and bovine carbonic anhydrase II [250] (Table 3.1, Section 3).

2 Experimental and Method Development

2.1 Bacterial Work

To increase the amount of DNA for protein expression mini- and maxi-preparations were performed. Therefore the *E. coli* strains Origami™ B (DE3) pLysS (Novagen - Darmstadt, Germany), XL1-Blue Quick Change (Stratagene - La Jolla, USA) and Top 10 (Invitrogen - Paisley, UK) were used. For protein expression chemical competent *E. coli* hosts BL 21™ and BL 21 Star™ (Novagen - Darmstadt, Germany) were used.

2.1.1 Preparation of Electrocompetent Cells

E. coli is unlike other bacteria, such as *Bacillus subtilis*, not able to incorporate foreign DNA. Therefore it is important to make *E. coli* competent to transform a reasonable amount of foreign DNA. Hence, a 15 mL centrifuge tube containing 6 mL of LB-medium (Section 2.1.6) was inoculated with a single colony of *E. coli* from a 1.5 % agar plate and incubated at 225 rpm at 37 °C (Stuart Orbital Incubator SI50 - Bibby Scientific - Staffordshire, UK) overnight. Then a 2 L Erlenmeyer flask with 500 mL *pre*-warmed LB-medium was inoculated with 25 mL of the overnight culture and further incubated until an OD_{600} value of 0.4. The cell growth was stopped by transferring the flask in an ice-bath for 15-30 min. The cultures were then transferred to *pre*-cooled centrifuge bottles and centrifuged for 15 min at 4 °C at 2500 rpm (1000 xg - Sorvall RC26 plus - Waltham, USA). The supernatant was discarded and the cell-pellet was washed once with 250 mL ice-cold H_2O_{dd} water and once with 10 % glycerol to remove the buffer salts. After centrifugation the cell pellet was dissolved in ice-cold 2x YT-medium (Section 2.1.6) and diluted to an OD_{600} of 1.0 (*ca.* 2.5 x 108 cells). To make sure that during the electroporation no arcing occurs, 40 µL of the cell solution was transferred to an ice-cold electroporation cuvette and an electrical pulse was applied (5 ms, 12.5 kV/cm). After ensuring that the conductivity is sufficiently low, the cell solution was dispensed in 40 µL aliquots in a micro centrifuge tube, shock frozen in liquid nitrogen and stored at -80 °C.

2.1.2 Chemical Transformation of Recombinant DNA

To transform plasmid DNA into chemically competent *E. coli* a slightly modified protocol of Hanahan [251] was used. A single micro centrifuge tube with chemically competent cells was thawed on ice followed by the addition of 5-10 ng of DNA. After

30 min incubation on ice a heat shock was applied by putting the cells for 45 s in a 42 °C water bath (SUB14 - Grant - Shepreth, UK) followed by another 5 min incubation on ice. Then 1 mL of *pre*-warmed SOC medium (Sigma-Aldrich - Derset, UK) was added and the suspension was incubated for 1 h at 37 °C and gentle rotations (Stuart Orbital Incubator SI50 - Bibby Scientific - Staffordshire, UK). Then 50, 100 and 150 µL were streaked out on an *pre*-warmed LB-agar ampicilin plate (100 µg/mL; Section 2.1.6) and incubated overnight at 37 °C.

2.1.3 Transformation of Recombinant DNA *via* Electroporation

To transform recombinant DNA into electro competent bacteria cells the following procedure was applied. A micro centrifuge tube containing 40 µL of electro competent cells was thawed on ice. After transferring the cells into an ice-cold electroporation cuvette 25 ng of DNA in a volume of 1-5 µL were added and incubated for 60 s. Then an electrical pulse of 25 µF capacitance, 2.5 kV and 200 Ω resistance was applied (Gene Pulser II, Pulse Controller plus and Capacitance Extender plus - Bio Rad - Hercules, USA) to the cuvette followed by the addition of 1 mL of *pre*-warmed SOC-medium (Sigma-Aldrich - Derset, UK). The cells were then transferred into a 1.5 mL micro centrifuge tube and incubated with gentle rotation for 1 h at 225 rpm and 37 °C (Stuart Orbital Incubator SI50 - Bibby Scientific - Staffordshire, UK), streaked out on a pre-warmed LB-agar ampicilin plate (100 µg/mL) and incubated overnight at 37 °C.

2.1.4 Isolation of Plasmid DNA (Minipreparation)

For the isolation of small amounts of DNA up to 20 µg the QIAgen spin plasmid DNA-kit was used (QIAgen - Crawley, UK). Therefore the DNA of question was transformed into *E. coli* as described above (Section 2.1.3, 2.1.2). A 15 mL centrifuge tube containing 5 mL of 2x YT/LB media was inoculated with a single colony from the overnight culture and incubated overnight at 37 °C and 225 rpm (Stuart Orbital Incubator SI50 - Bibby Scientific - Staffordshire, UK). The cells of the overnight culture were spun for 15 min at room temperature (RT) at ~4300 rpm (~4000 xg - Sorvall RC26 plus - Waltham, USA) and the supernatant was discarded. The cell pellet was re-suspended in 250 µL buffer P1 and then transferred in a 1.5 mL micro centrifuge tube. Then 250 µL of cell lysis buffer P2 were added and incubated for 5 min at room temperature (RT). After the incubation 350 µL of ice cold N3 buffer were added to neutralise the basic cell lysis and inverted 5 times before incubating for

5 min on ice. Another centrifugation step for 10 min at RT at 14000 rpm (~10000 xg - Eppendorf 5515C - Hamburg, Germany) the supernatant was applied to a QIAprep-spin column (QIAgen - Crawley, UK) sitting in a 2 mL micro centrifuge tube and spun for 1 min at RT at 14000 rpm (~10000 xg - Eppendorf 5515C - Hamburg, Germany). The flow through was discarded and the column was washed once with 750 µL of PE buffer. After spinning for another minute the flow through was discarded again and an additional spinning step was applied to get rid of excess buffer. The plasmid-DNA was eluted by adding 50 µL Tris/HCl buffer (2.5 mM, pH 7.5) on to the column and incubation for 2 minutes, followed by placing the column in a micro centrifuge tube and centrifugation for 1 min at RT at 14000 rpm (~10000 xg - Eppendorf 5515C - Hamburg, Germany). DNA was stored at -20 °C.

2.1.5 Isolation of Plasmid DNA (Maxipreparation)

For isolation of larger amounts of DNA up to 1500 µg the Jet Star DNA purification kit was used (Genomed - Löhne, Germany). Therefore the DNA of interest was transformed into appropriate *E. coli* (Section 2.1.3, 2.1.2) and colonies of interest were picked from a LB-carbenicillin/ampicilin (Sigma-Aldrich - Derset, UK) plate (100 µg/mL) and transferred into a 5 mL carbenicillin/ampicilin (100 µg/mL) containing 2x YT *pre*-culture. After 4-5 h of incubation at 37 °C and 225 rpm (Stuart Orbital Incubator SI50 - Bibby Scientific - Staffordshire, UK) a 200 mL LB-carbenicillin/ampicilin (100 µg/mL) containing 1 L Erlenmeyer flask was inoculated with 50-200 µL of the *pre*-culture depending on the cell growth and incubated overnight at 37 °C and 225 rpm (Stuart Orbital Incubator SI50 - Bibby Scientific - Staffordshire, UK). At first a maxi-column was equilibrated with 30 mL of E4 Buffer. The overnight culture was transferred in a 250 mL centrifuge bottle and spun for 15 min at 37 °C and 6000 rpm (~4000 xg - Sorvall RC26 plus - Waltham, USA) and the supernatant discarded. The *E. coli* cell pellet was re-dissolved in 10 mL E1 buffer and transferred to a 50 mL centrifuge tube. Then cell lysis was induced by adding 10 mL of E2 buffer and gently inverted. After 5 min of incubation lysis was stopped by adding E3 neutralisation buffer and gently inverting before incubating for another 5 min. The cell debris was spun down for 30 min at 37 °C and 10000 rpm (~10000 xg - Sorvall RC26 plus - Waltham, USA) and the supernatant was filtered through a paper filter (Whatman - GE Healthcare - Chalfont St Giles, UK) and applied to the equilibrated maxi-column. The column was emptied by gravity flow and washed once with 60 mL of E5 buffer. The plasmid DNA was eluted from the column into a 30 mL centrifuge tube by applying 15 mL E6 elution buffer and precipitated by

the addition of 10.5 mL of 2-propanol (Fisher Scientific - Loughborough, UK) and incubation for 2 h at -20 °C. After centrifugation for 30 min at 4 °C and 10000 rpm (~10000 xg - Sorvall RC26 plus - Waltham, USA) the DNA pellet was washed with 1 mL 70 % ethanol (Fisher Scientific - Loughborough, UK). After centrifugation for 10 min at 4 °C and 10000 rpm (~10000 xg - Sorvall RC26 plus - Waltham, USA) the supernatant was discarded and the DNA pellet was air-dried for 15 min before dissolving in 1 mL 2.5 mM Tris/HCl pH 7.0 and storage at -20 °C.

2.1.6 Buffers and Media

LB-Medium

For LB-medium 10 g trypton (Oxoid - Basingstoke, UK), 10 g sodium chloride (Fisher Scientific - Loughborough, UK) and 5 g yeast extract (Bacto - Liverpool, Australia) were dissolved in 1 L H_2O_{dd}. The pH was adjusted to 7.3 by using 1 M and 10 M sodium hydroxide (Sigma-Aldrich - Derset, UK). The medium was autoclaved (Boxer 200/150L - Hertfordshire, UK) and stored at 4 °C.

2x YT-Medium

16 g trypton (Oxoid - Basingstoke, UK), 10 g sodium chloride (Fisher Scientific - Loughborough, UK) and 5 g yeast extract (Bacto - Liverpool, Australia) were dissolved in 1 L H_2O_{dd}. The pH was adjusted to 7.0 by using 1 M and 10 M sodium hydroxide (Sigma-Aldrich - Derset, UK). The medium was autoclaved (Boxer 200/150L - Hertfordshire, UK) and stored at 4 °C.

Ampicilin/Carbenicillin Containing LB-Agar-Plates

In the first instance 1 L of LB-medium was prepared (Section 2.1.6) and 1.5 % (w/v) of agar was added followed by autoclaving (Boxer 200/150L - Hertfordshire, UK) the medium. The still hot medium was allowed to cool down to ~40 °C at RT, then 1 mL of an ampicilin/carbenicilin (Sigma-Aldrich - Derset, UK) stock solution (100 µL/µL) was added to 1 L medium to achieve a final concentration of 100 µg/mL. After mixing the solution was poured in sterile petri dishes. The cold plates were stored at 4 °C in the dark.

2.2 Protein Expression and Purification

Various proteins were expressed and appropriate purification procedures applied.

2.2.1 Cyclophilin A Expression and Purification

For the expression of CypA in *E. coli* the psw3-003 vector containing the CypA gene [252] (kindly donated by Prof. M Walkinshaw) was chemically transformed (Section 2.1.2) in BL 21 Star^{TM} (Novagen - Darmstadt, Germany) cells. Then a starter culture was incubated overnight in 15 mL 2x YT containing 100 µg/mL ampicilin (Sigma-Aldrich - Derset, UK) at 37 °C and 225 rpm (Stuart Orbital Incubator SI50 - Bibby Scientific - Staffordshire, UK). Four 2 L Erlenmeyer flasks containing 1 L 2x TY (100 µg/mL ampicilin) each were inoculated with 2 mL of the starter culture and incubated at 225 rpm (Stuart Orbital Incubator SI50 - Bibby Scientific - Staffordshire, UK) and 37 °C (Model G 25 - New Brunswick Scientific - Edison, USA). The OD_{600} was checked every hour until ~0.6 was reached. Then 1 mL of a 1 M isopropyl *β-D*-1-thiogalactopyranoside (IPTG) (VWR - West Chester, USA) stock solution was added and incubated for another 3 h. After stopping the cell growth on ice, the suspension was transferred to four 1 L centrifuge bottles and centrifuged for 15 min at 4 °C at ~3000 xg (Sorvall RC26 plus - Waltham, USA). After decanting the supernatant the cells were washed once with 100 µL ice cold lysis buffer and centrifuged at 4 °C at ~3000 xg (Sorvall RC26 plus - Waltham, USA). The cell pellet was then re-suspended in 10 % (w/v) ice cold lysis buffer containing an excess of protease inhibitor cocktail (Sigma-Aldrich - Derset, UK) and sonicated on ice for 6 x 30 s bursts (Soniprep 150 - MSE - London, UK), with 30 s cooling in between. The cell lysate was subjected to centrifugation for 2 h at 4 °C at ~20000 xg (Sorvall RC26 plus - Waltham, USA) and the supernatant was exhaustively dialysed overnight against 50 mM 4-(2-hydroxyethyl)-1-piperazineethanesulfonic acid (HEPES, Sigma-Aldrich - Derset, UK), 1 mM dithiothreitol (DTT, Acros Organics - Geel, Belgium), 2.5 mM ethylenediaminetetraacetic acid (EDTA, Sigma-Aldrich - Derset, UK), 1 mM NaN_3 (Sigma-Aldrich - Derset, UK), 100 µM phenylmethylsulphonyl fluoride (PMSF,MP Biomedicals - Cambridge, UK), 100 µM Benzamidine (Sigma-Aldrich - Derset, UK); pH 6.8. Then the solution was filtered through a 0.2 µm filter (Satorius - Göttingen, Germany) and applied to an SP-sepharose column (XK 26 - GE Healthcare - Chalfont St Giles, UK) pre-equilibrated in 50 mM HEPES (Sigma-Aldrich - Derset, UK), 1 mM DTT (Acros Organics - Geel, Belgium), 2.5 mM EDTA (Sigma-Aldrich - Derset, UK), 1 mM NaN_3 (Sigma-Aldrich - Derset, UK);

pH 6.8. Proteins were eluted with a 0-400 mM NaCl gradient (Fig. 2.1a, b) using the same buffer over 200 mL and then analysed *via* SDS-PAGE (Section 2.2.3, Fig. 2.1c). Fractions containing CypA, eluting between 160 mM and 250 mM NaCl, were pooled and concentrated to ~1 mL. After filtering through a 0.2 µm filter (Satorius - Göttingen, Germany) the solution was loaded onto a XK 16/Sephacryl-200 HR gel filtration column (GE Healthcare - Chalfont St Giles, UK), pre-equilibrated in 25 mM Tris (Sigma-Aldrich - Derset, UK) and 1 mM NaN_3. CypA was eluted ~90 % pure as judged by SDS-PAGE (Fig. 2.2). The protein was concentrated to a concentration of ~500 µM and stored on ice at 4 °C for 6 to 8 weeks at most.

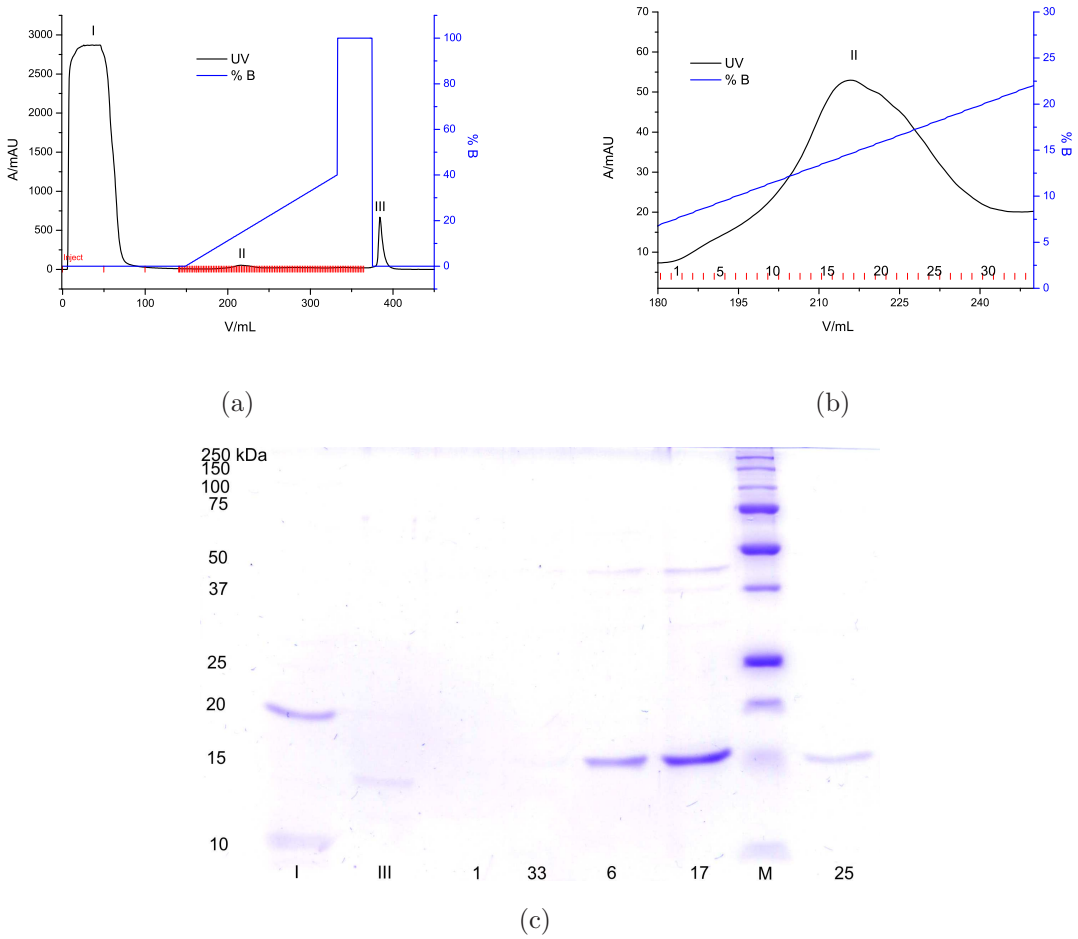

Figure 2.1: Cation exchange chromatography for cyclophilin A. (a) Overview of cation exchange chromatogram with UV trace (black) and percentage of elution buffer (blue). (b) Enlargement of peak II with fractions collected. (c) 12.5 % SDS-PAGE gel of collected fractions. Chromatograms visualised with Origin - Microcal, USA; gel images enhanced with Fireworks - Adobe, USA.

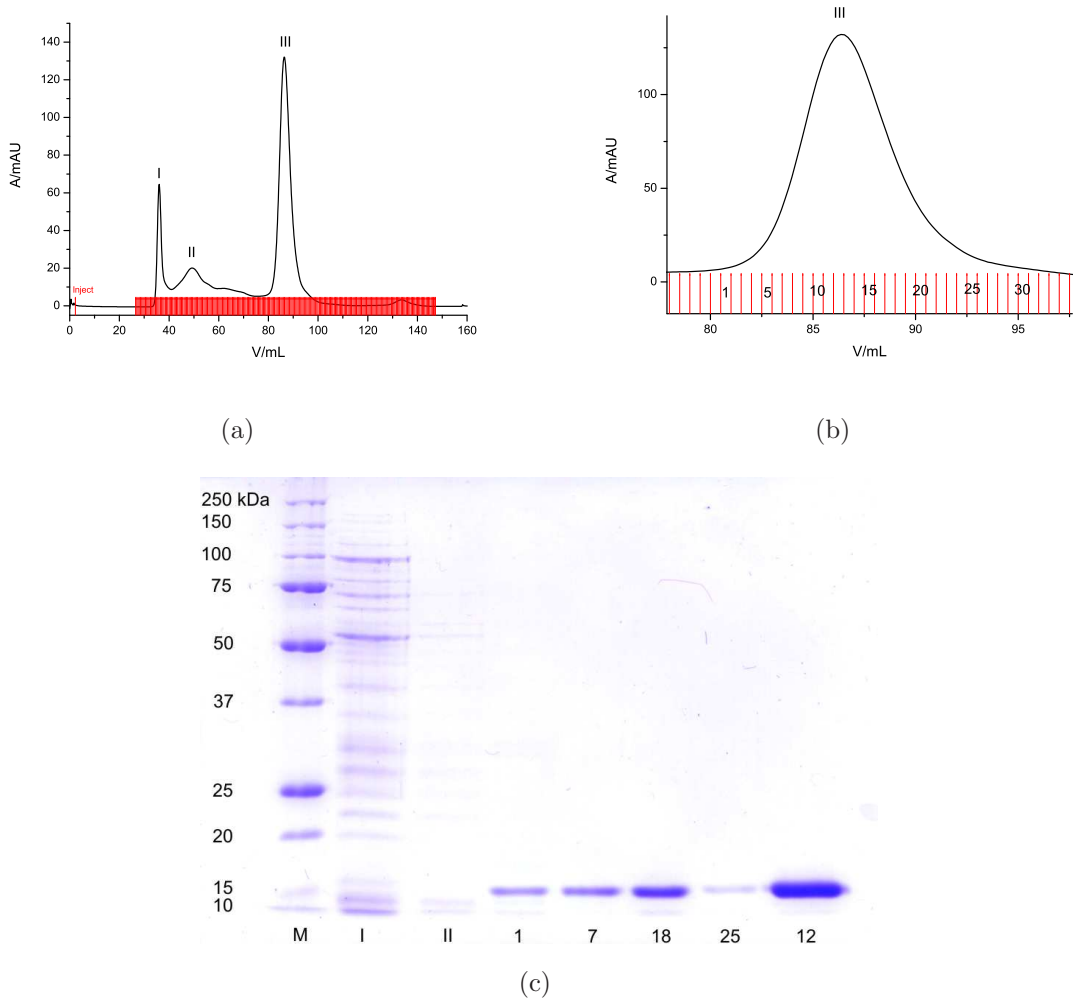

Figure 2.2: Gel filtration chromatography for cyclophilin A. (a) Overview of gel filtration elution profile. (b) Enlargement of peak III with fractions collected. (c) 10 % SDS-PAGE gel of collected fractions. Chromatograms visualised with Origin - Microcal, USA; gel images enhanced with Fireworks - Adobe, USA.

Further CypA expressions were carried out by Dr. John White in the fermentation suite in the Edinburgh Protein Interaction Centre (EPIC). Therefore freshly transformed psw3-003 [252] in BL 21 Star^{TM} (Novagen - Darmstadt, Germany) was grown up in a 10 L fermenter (BioFlo4500s - New Brunswick - Edison USA) to the appropriate OD_{600}, protein over expression was induced and cells were harvested as described above. The cell pellet was stored at -20 °C until further purification.

2.2.2 GroEL Expression and Purification

GroEL was expressed from a pET11a (Novagen - Darmstadt, Germany) expression vector containing the groEL coding frame according to a modified protocol from [160]. Initially the expression vector (kindly donated by Dr. D Campopiano, originated from [160]) was multiplied by maxi preparation (Section 2.1.5). A starter culture was incubated overnight in 15 mL LB-medium containing 100 µg/mL ampicilin (Sigma-Aldrich - Derset, UK) at 37 °C and 225 rpm (Stuart Orbital Incubator SI50 - Bibby Scientific - Staffordshire, UK). Then four 2 L Erlenmeyer flasks containing 1 L LB-medium (100 µg/mL ampicilin) each, were inoculated with 2 mL of the starter culture and incubated at 225 rpm (Stuart Orbital Incubator SI50 - Bibby Scientific - Staffordshire, UK) and 37 °C (Model G 25 - New Brunswick Scientific - Edison, USA). The OD_{600} was checked until ~1.0 was reached, followed by induction with 1 M IPTG for 3 h and harvesting of the cells (Section 2.2.1). The cell pellet was then re-suspended in 10 % (w/v) ice cold buffer A (50 mM Tris-HCl, 10 mM $MgCl_2$, 1 mM DTT, 0.5 mM KCl, 1 mM EDTA, 0.05 % NaN_3 and 50 µg/mL PMSF, [pH 7.5]). Cell lysis was performed at 21 kPa and 4 °C utilising a cell disruptor (TS Series - Constant Systems - Daventry, UK). After centrifugation for 70 min at 4 °C and ~50000 xg (Sorvall RC26 plus - Waltham, USA) the supernatant was filtered (0.2 µm; Satorius - Göttingen, Germany) and loaded onto a HiPrep^{TM} DEAE FF column (GE Healthcare - Chalfont St Giles, UK), pre-equilibrated in buffer A. Proteins were eluted with a 0-500 mM NaCl gradient using buffer A over 200 mL and then analysed *via* SDS-PAGE (Fig. 2.3). Fractions containing groEL were pooled and concentrated to ~1 mL and applied onto a HiPrep^{TM} 16/60 S300 HR gel filtration column (GE Healthcare - Chalfont St Giles, UK) using 50 mM Tris-HCl, 0.05 % NaN_3, [pH 7.5]. Fractions containing groEL eluted close to the void volume of the column (Fig. 2.4), were collected and applied on a MonoQ 5/50 GL anion exchange column (GE Healthcare - Chalfont St Giles, UK). After elution over 200 mL with a 0-500 mM NaCl gradient using buffer A, fractions containing groEL were analysed *via* SDS-PAGE (Fig. 2.5) and concentrated to ~200 µL. Protein samples for imminent use were kept at 4 °C. For long term storage groEL was frozen in $N_{2,(l)}$ in buffer A and kept at -80 °C.

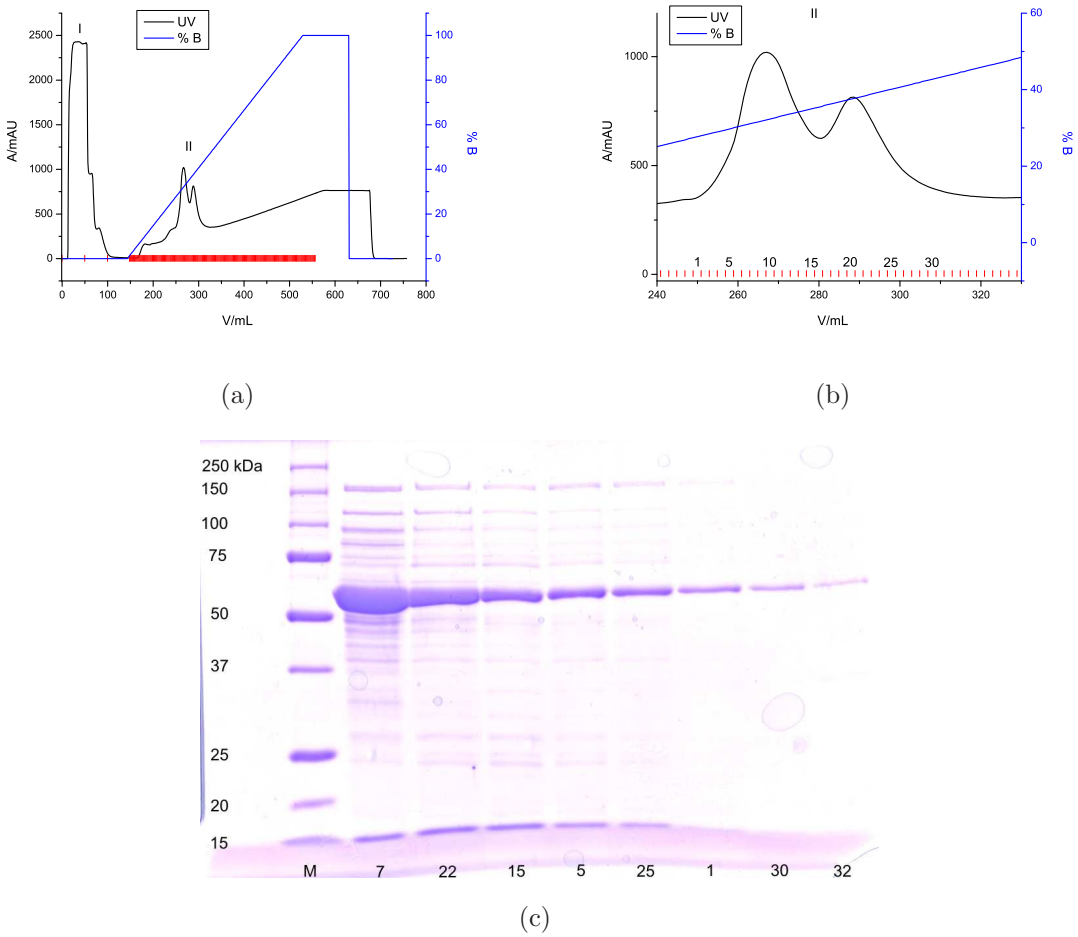

Figure 2.3: Weak anion exchange chromatography for groEL. (a) Overview of weak anion exchange chromatogram with UV trace (black) and percentage of elution buffer (blue). (b) Enlargement of peak II with fractions collected. (c) 7.5 % SDS-PAGE gel of collected fractions. Chromatograms visualised with Origin - Microcal, USA; gel images enhanced with Fireworks - Adobe, USA.

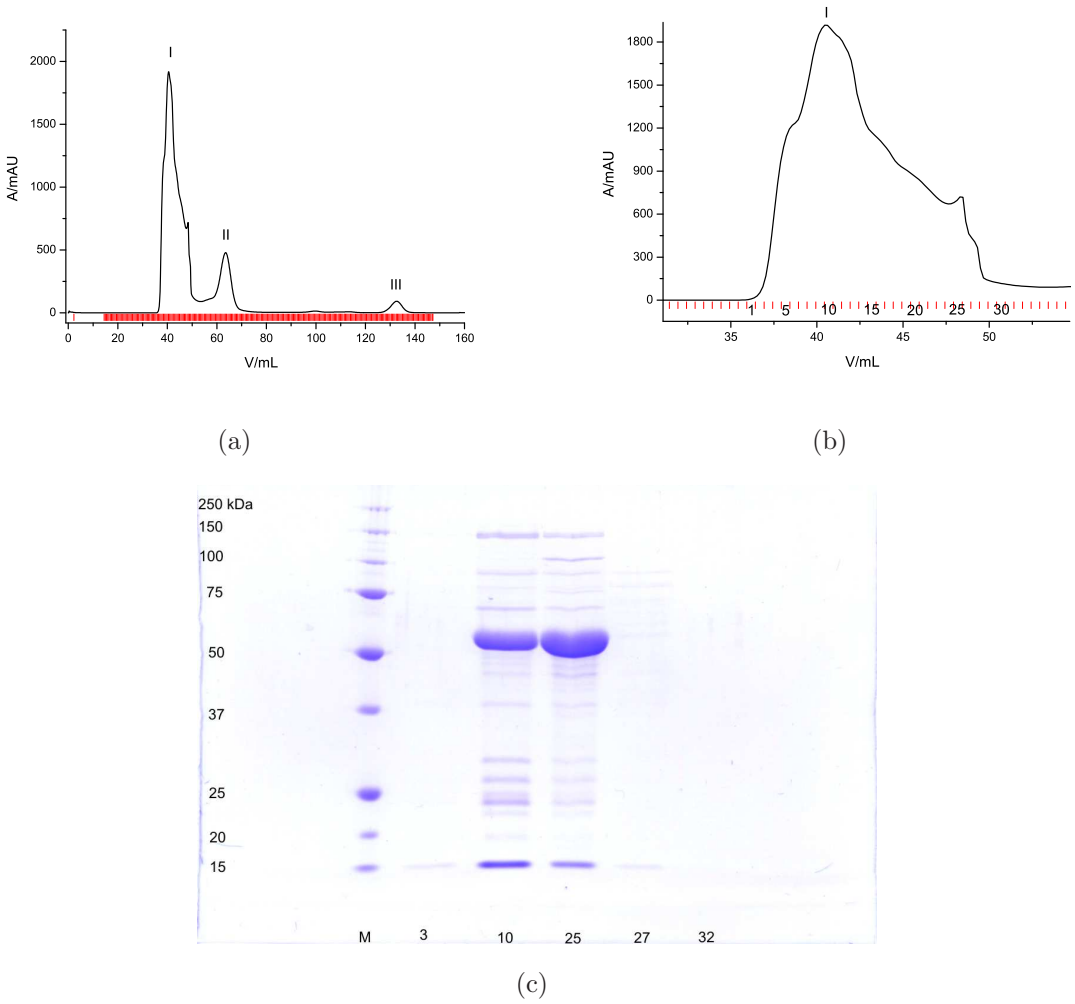

Figure 2.4: Gel filtration chromatography for groEL. (a) Overview of gel filtration elution profile. (b) Enlargement of peak I with fractions collected. (c) 7.5 % SDS-PAGE gel of collected fractions. Chromatograms visualised with Origin - Microcal, USA; gel images enhanced with Fireworks - Adobe, USA.

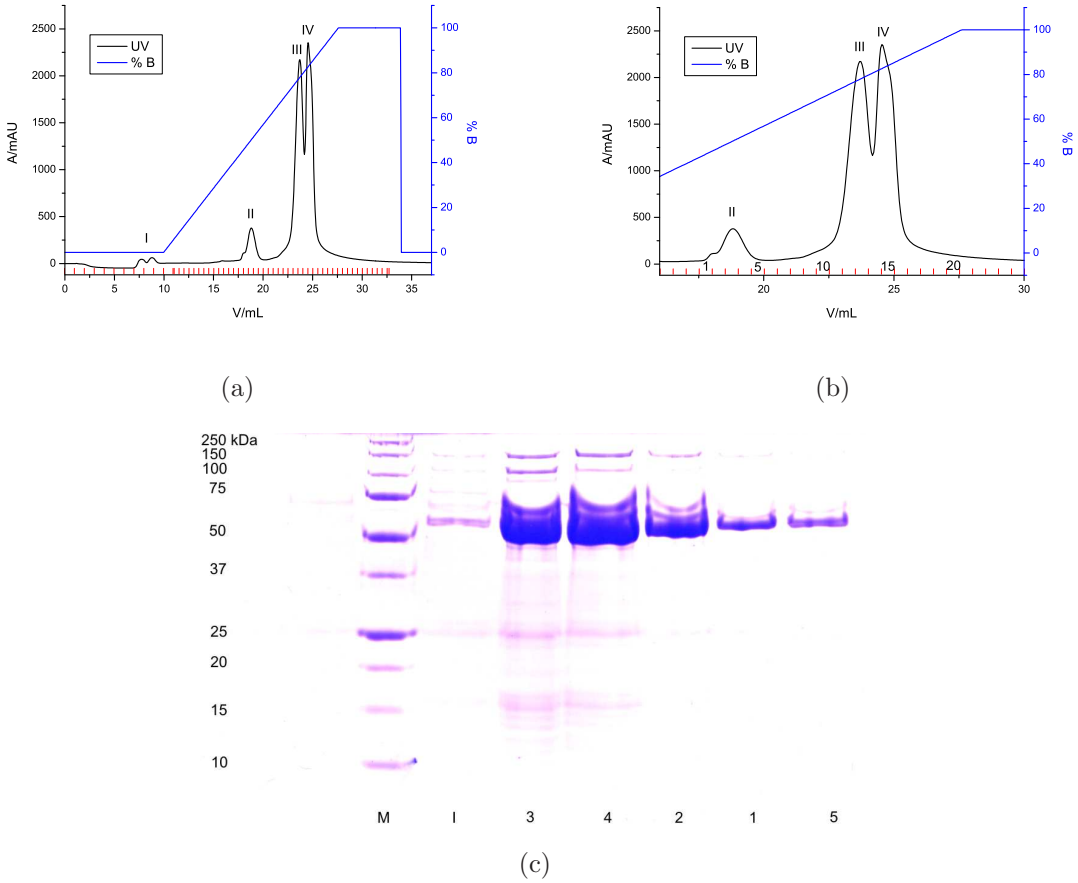

Figure 2.5: Strong anion exchange chromatography for groEL. (a) Overview of strong anion exchange chromatogram with UV trace (black) and percentage of elution buffer (blue). (b) Enlargement of peaks II, III and IV with fractions collected. (c) 7.5 % SDS-PAGE gel of collected fractions. Chromatograms visualised with Origin - Microcal, USA; gel images enhanced with Fireworks - Adobe, USA.

2.2.3 SDS-PAGE

To estimate molecular weights and purity of proteins sodium dodecyl sulfate polyacrylamide gel electrophoresis (SDS-PAGE) was performed. Therefore self cast (Table 2.1) or precast SDS-PAGE gels (Bio Rad - Hercules, USA) were used.

Table 2.1: Self cast SDS-PAGE gels with different percentages of acrylamide for different protein sizes.

Chemical	7.5 %	10 %	12.5 % (V/mL)	15.0 %	18.0 %
1.5 M Tris-HCl buffer, pH 8.8[a]	5.00	5.00	5.00	5.00	5.00
30 % Acrylamide[a]	5.00	6.70	8.30	10.00	12.00
H_2O_{dd}[b]	10.00	8.30	6.70	5.00	3.00
APS (25 % w/v)[c]	0.06	0.06	0.06	0.06	0.06
TEMED[a]	0.03	0.03	0.03	0.03	0.03

[a] Bio Rad - Hercules, USA.

[b] Satorius - Göttingen, Germany.

[c] Sigma-Aldrich - Derset, UK.

For all SDS-PAGE running gels at different acrylamide concentrations 5 % stacking gels were used (2.5 mL 1.5 M Tris-HCl buffer, pH 8.8; 1.25 mL 30 % acrylamide; 5.83 mL H_2O; 60 µL ammonium persulfate (APS, 25 % w/v); 60 µL tetramethylethylenediamine (TEMED). SDS-PAGE gels were mounted in the electrophoresis cell (Mini-protean tetra cell - Bio Rad - Hercules, USA), filled with Tris-glycine electrophoresis buffer (prepared from 10 x Tris/Glycine/SDS buffer (Bio Rad - Hercules, USA)). Then 12 µL protein sample were mixed with 12 µL 2x SDS sample buffer (Bio Rad - Hercules, USA) and heated for 3 min at 95 °C (Dry Block Heater HBS-130 - Anachem - Bedfordshire, UK)). After cooling down the samples were loaded on the appropriate SDS-PAGE gel together with a molecular weight ladder (Precision Plus Protein Standart^{TM} - Bio Rad - Hercules, USA). The power supply (Power Pac basic - Bio Rad - Hercules, USA) was connected and a voltage of 10 V/cm was applied. The gel was run until the blue marker front reached the bottom of the gel (~50 min). After staining the gel for 1 h in coomassie brilliant blue (Sigma-Aldrich - Derset, UK) with gentle rotation (The belly dancer - Sorvall - Waltham, USA) the gel was destained by soaking in 10 % acetic acid, 10 % methanol and 80 % water for 1 h with gentle rotation (The belly dancer - Sorvall - Waltham, USA).

2.2.4 Bradford Assay

To determine protein concentrations after purification a Bradford assay was conducted [253]. Therefore 2 mL of Bradford dye reagent concentrate (Bio Rad - Hercules, USA) were diluted in 8 mL H_2O_{dd} in a 15 mL centrifuge tube and incubated

for 10 minutes. The solution was aliquoted in 1.5 mL micro centrifuge tubes at 1 mL each. Then the standard samples for the calibration curve were prepared at different concentrations by adding different amounts of bovine serum albumin (BSA; Sigma-Aldrich - Derset, UK) to the aliquoted Bradford reagent and further incubation for 10 min. For the micro Bradford assay the amount of BSA was between 0 and 10 µg. 1 µL of the unknown protein sample was diluted in 9 µL H_2O_{dd} and 1 to 10 µL were added to the aliquoted Bradford reagent each. The absorbance was read at 595 nm using a UV/VIS Biophotometer (Biophotometer 600 - Eppendorf - Hamburg, Germany). Plotting the readouts on the calibration curve (Appendix 9.1 for CypA) and considering the dilution factor, the protein concentration was calculated.

2.3 Reagents and General Sample Preparation

All buffer solutions were prepared using high purity water from a Satorius - Arrium 611 UV water purification unit (Satorius - Göttingen, Germany) delivering double distilled grade, 0.2 µm sterile filtered (H_2O_{dd}). The buffer salts were weighed out using either a Mettler - Toledo PB 1501, Mettler - Toledo AB 204 or a Mettler AC 100 (Mettler-Toledo - Leicester, UK) to an accuracy of ± 0.1 g and ± 0.0001 g respectively. The pH adjustments were performed using a Jenway 3305 (Bibby Scientific - Staffordshire, UK) with a range of concentrations between 0.1-10 M of NaOH and HCl. Solvents for HPLC analysis met analytical HPLC grade and were 0.2 µm sterile filtered prior usage.

2.3.1 Protein Sample Preparation

Protein standards such as myoglobin and insulin were purchased from Sigma-Aldrich (Derset, UK). However, AGr2 and fH19-20 protein samples were kindly donated by Dr. H. Florance, Ms. J. Nicholson and Dr. A. Herbert, respectively. Unless stated otherwise proteins of interest were dissolved/diluted in 10 mM NH_4OAc (Fisher Scientific - Loughborough, UK) at different concentrations prior analysis.

2.3.2 Ligand Preparation

Ligands for direct infusion, HDX-labeling, PLIMSTEX and SUPREX experiments were sourced and diluted/dissolved according to Table 2.2.

Table 2.2: Preparation and origin of ligands.

Ligand	System	Solvent	Source
CsA [a]	CypA	36.88 % MeOH in H_2O	Prof. M. Walkinshaw
KM184 [b]	CypA	36.88 % MeOH in H_2O	Prof. M. Walkinshaw
ES1234 [b]	CypA	36.88 % MeOH in H_2O	Prof. M. Walkinshaw
FK506[b]	FKBP12	MeOH	Ms. E. Blackburn
Rapamycin[b]	FKBP12	MeOH	Ms. E. Blackburn
PTTIYY-Pen [b]	AGr2	H_2O	Ms. J. Nicholson
PATIAA-Pen[b]	AGr2	H_2O	Ms. J. Nicholson
Fondaparinux[b]	fH19-20	H_2O	Dr. A. Herbert

[a] fresh prepared with every batch of fresh CypA (6-8 weeks).

[b] imminent use after preparation (1-2 weeks).

2.3.3 MS-Sample Introduction

Generating protein ions in the gas phase for direct infusion, HDX labeling, PLIMSTEX and SUPREX experiments was achieved using electrospray (Section 2.3.3) and nano-electrospray ionisation (Section 2.3.3).

Electrospray

ESI (Section 1.1.1) was performed using a set of gas tight syringes (Gasthigt 1725-1750 - Hamilton - Bonaduz, Switzerland) containing 250 µL-500 µL of sample, mounted on a syringe pump (Harvard apparatus - Kent, UK) connected to the ESI-probe. Flow rates varied between 10 µL/min-40 µL/min.

Nano-Electrospray

Nano-ESI (Section 1.1.1) was carried out with in house pulled glass tips of different taper shapes and diameters using borosilicate capillaries (0.12 x 10.16 cm; World Precision Instruments Inc. - Savasota, USA; P97 - Sutter Instrument co. - Novato, USA). 20 µL of sample were loaded into the capillary, platinum wire (99.99 % purity; Sigma-Aldrich - Derset, UK) inserted and mounted onto the nESI probe.

2.3.4 Direct Infusion

For direct infusion (DI) ESI(Section 2.3.3) or nano-ESI (Section 2.3.3) experiments under native like conditions the purified protein sample of interest was diluted into

10 mM NH_4OAc (Fisher Scientific - Loughborough, UK), pH 6.88. Under denaturing conditions 5 % of formic acid (FA, Fisher Scientific - Loughborough, UK) was added to the sample. For direct infusion analysis of AGr2 and fH19-20 buffer exchange/dialysis (Section 2.4.1) was performed prior to the experiment. For high-throughput DI the automated SUPREX HPLC setup (Section 2.7.3) was used with a sample pick up of 65 µL, loading onto a 50 µL sample loop and transferred to the MS.

2.3.5 HDX Labeling Experiments

HDX experiments were conducted with deuterated 10 mM *d*-NH_4OAc. Therefore NH_4OAc (Fisher Scientific - Loughborough, UK) was dissolved in D_2O (Sigma-Aldrich - Derset, UK). The pH corrections for *d*-buffers of 0.4 according to [254] were applied, where appropriate.
For HDX labeling experiments the apo protein of interest was diluted into *d*-NH_4OAc and incubated for a particular time period. In the presence of ligand the same procedure was applied after incubation with the ligand for 20 min. Mass increase *vs.* time was analysed *via* various HPLC-MS setups (Section 2.6.2, 2.6.3, 2.7.3). For the latter, an automated sample pick up of 65 µL, loading onto guard column/sample loop (DI) and washing for 8 min at 0 °C was carried out (Section 2.6.4). The detailed LC method program is described in Appendix 9.5.

2.4 General Experimental Procedures

2.4.1 Buffer Exchange/Dialysis

Proteins for DI-MS-analysis or as part of a protein purification step were dialysed/buffer exchanged using appropriate dialysis tubing according to sample volume or desalting columns. For volumes <1 mL dialysis tubing with a diameter of ~2 cm was used. Samples <100 µL were dialysed using disposable 'Dispo-Biodialyzer'. All used dialysis equipment had a molecular weight cut off of 10 kDa and was purchased from Sigma-Aldrich - Derset, UK. Protein samples were exhaustively dialysed overnight against 4 L of 10 mM NH_4OAc, 1 mM NaN_3 (Fisher Scientific - Loughborough, UK), pH 6.8 for 24 h at 4 °C, exchanging buffer every 3 h at gentle rotations. For desalting a PD10 column (Amersham Biosciences - Little Chalfont, UK) was equilibrated with 2.5 mL 10 mM NH_4OAc (Fisher Scientific - Loughborough, UK), the protein sample applied in 2.5 mL volume and the flow through discarded. Elution with 3.5 mL 10 mM NH_4OAc (Fisher Scientific - Loughborough, UK) into a

micro centrifuge tube was often followed by sample concentration *via* viva-spin concentrators (Satorius - Göttingen, Germany) differing between 0.1-2 mL of sample volume.

2.4.2 Instrument Calibration

Platform II

For accurate mass measurements the Micromass Platform II was calibrated every 3 months. Therefore a calibration mixture containing NaCsI (2mg/mL NaI, 0.05 mg/mL CsI in 1:1 2-propanol, H_2O_{dd}) was sprayed *via* DI-ESI at 5 µL/min and the automatic calibration routine started. The calibration was verified by comparison of the NaCsI reference peak list with the mass spectrum just acquired. Once deviations were within a particular threshold the calibration was accepted and applied.

QTOF Ultima/ QTOF 2

To guarantee mass accuracy the Micromass "QTOF Ultima" and "QTOF 2" were calibrated on a weekly basis. Therefore NaCsI (2mg/mL NaI, 0.05 mg/mL CsI in 1:1 2-propanol, H_2O_{dd}) was injected *via* nano-ESI and a spectrum recorded over ~50 scans using the 'uncal'-calibration file. The 'calibrate from file'-option was used to calibrate the quadrupole- and TOF-analysers after manually checking the correct peak assignment. To test the accuracy of the calibration a protein standard was investigated and the calibration procedure repeated, if necessary.

2.4.3 Instrumental Parameters

Depending on mass spectrometric instrumentation, different tuning parameters were used.

The Platform II (Micromass - Manchester, UK) was operated throughout in positive ionisation mode at a capillary voltage of 3.5 kV, a cone voltage of 50 V, a source temperature of 85 °C and a multiplier setting of 650 arbitrary units.

The QTOF-2 and -Ultima were used at capillary voltages of 3.5 kV for ESI and 0.8-1.8 kV for nESI, a cone voltage between 30-60V and a source temperature of ~90 °C. The MCP settings were 2000 V and 2400 V on the QTOF-2 and -Ultima, respectively.

2.5 General Data Processing

After mass spectrometric data has been collected in DI-, HDX-labeling, PLIMSTEX- and SUPREX experiments it was deconvoluted using particular software depending on the instrument used. Most of the data was produced using Micromass (UK) instrumentation. Nevertheless, some manual SUPREX work (Section 3.6) was carried out with a LCQ classic (Thermo Corporation, UK) requiring different data processing.

MassLynx

Utilising Micromass mass spectrometers (Platform II, QTOF-2 and QTOF-Ultima) MassLynx versions 3.5-4.1 have been used. Post acquisition the individual spectrum was smoothed with 2-6 Da peak width and 10-20 smoothing steps using a Savitzky Golay algorithm after combining over the acquired DI- (Appendix 9.2) or HPLC chromatogram (Appendix 9.3). The baseline subtraction was performed with a 5^{th} order polynomial for signals less than 40 % of the maximum intensity. The peaks were centered with 4 channels at the minimum peak width at half height at 80 % centroid top of the peak (Fig. 3.1, Chapter 3.2). To determine the mass from a spectrum two adjacent peaks were manually selected and the transform option within the MassLynx software was employed for deconvolution. Some of the CypA PLIMSTEX data (Section 3.4) was deconvoluted manually due to high s/n-ratio and low signal intensities. Therefore the spectrum was processed as described above, but the centered spectrum list was exported to Microsoft Excel XP to identify adjacent peaks, before calculating the mass (Eq 19) for each charge state and averaging.

$$\text{mass} = (m/z \cdot \text{cs}) - \text{cs} \tag{19}$$

With m/z the mass to charge ratio and cs the individual charge state.

Xcalibur

Data acquired with with a LCQ classic (Thermo Corporation, UK) was processed using the instrument software Xcalibur 2.0. Spectra were smoothed using the 15 points gaussian smoothing routine and centered. The m/z values were manually transferred to Microsoft Excel XP and the average mass calculated as described above.

2.6 PLIMSTEX Method Development

2.6.1 PLIMSTEX Buffers and Sample Preparation

According to the PLIMSTEX protocol (Section 1.5) the deuteration buffer was prepared as for the HDX labeling experiment (Section 2.3.5) and ligands prepared as described previously (Section 2.3.2).

HPLC buffer for priming and loading the C4 guard column was denoted as washing buffer (WB; 97 % H_2O, 3 % acetonitrile, [pH 2.5]). For elution of the protein from the guard column elution buffer (EB, 96 % acetonitrile, 4 % H_2O, [pH 2.5]) was used.

For the first PLIMSTEX experiments (Section 2.6.2) and for the manual PLIMSTEX approach (Section 2.6.3), 2 µL of the protein in question was incubated with 2 µL of ligand at different concentrations, ranging from a 0-20 fold excess of ligand. After 20 min incubation 96 µL of 10 mM *d*-NH_4OAc (Fisher Scientific - Loughborough, UK) were added to initiate HDX. The total sample volume was 100 µL with a total protein concentration of 2 µM-4 µM.

The automated PLIMSTEX approach (Section 2.6.4) utilised the same protein-ligand concentrations and ratios. However, the total sample volume was shrunk to 70 µL. Thereby 2 µL protein (122 µM stock) and 1 µL of ligand at different concentrations (Section 2.3.2) were placed in a 250 µL, 12x32 mm autosampler vial each and sealed with a snap cap (magenta, Fig. 2.6a). Final ligand concentrations reached from 0-20 equivalents of the total protein concentration. 3 mL of 10 mM *d*-NH_4OAc (Fisher Scientific - Loughborough, UK) were filled in a 22.5x45 mm headspace vial and crimped with a 20 mm headspace cap and placed in a 48 well plate (orange, Fig. 2.6a).

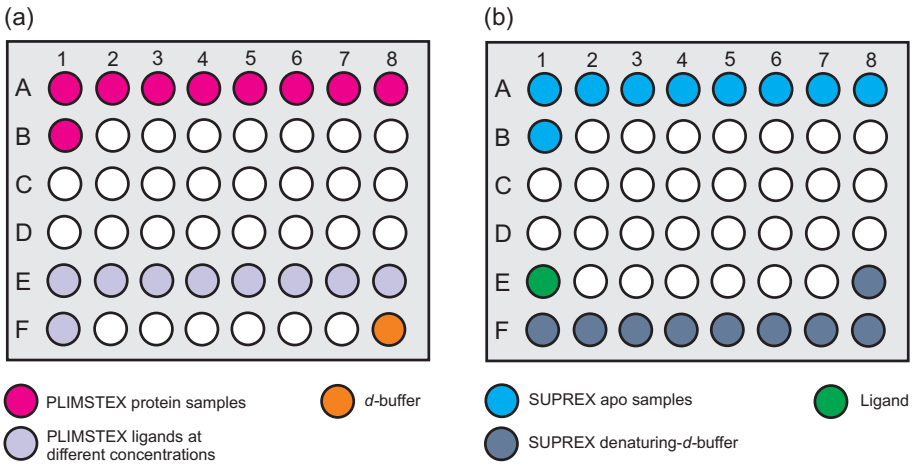

Figure 2.6: PLIMSTEX and SUPREX 48 well plate sample array. (a) Nine protein PLIMSTEX samples (magenta) and nine ligand samples (violet). Orange, 10 mM *d*-NH_4OAc. (b) Nine apo protein SUPREX samples, cyan. Blue, nine different denaturing concentrations in 10 mM *d*-NH_4OAc. Green, 10-20 fold excess of ligand.

2.6.2 The Beginning; First Steps

The development of the HPLC front end for the PLIMSTEX (Section 1.5) approach was first undertaken. Therefore the sample was placed in a 250 µL gas tight syringe (Gasthigt 1725-1750 - Hamilton - Bonaduz, Switzerland) mounted on a syringe pump (Harvard apparatus - Kent, UK; Fig. 2.7). The needle was connected to 1/16 peek^{TM} tubing with 0.005 in inner diameter (ID) *via* a 0.010 in 10-32 ZDV peek^{TM} union. Between sample and MS a C4 guard column (Optimize Technologies - Oregon City, USA) was placed into the sample line, packed in ice in a polystyrene box. If not otherwise stated all HPLC accessories were purchased from Anachem - Luton, UK.

To perform a PLIMSTEX experiment the syringe was filled with 200 µL washing buffer and attached to the sample line, priming the column at a flow rate of 10 µL-30 µL. Flow through was collected in a separate container. Then 100 µL of sample (Section 2.6.1) was quenched after a 90 min of incubation by adding 2 µ L of 2 M HCl and lowering the temperature by placing the sample on ice. After loading the sample onto the syringe and connecting to the C4 guard column, injection was started and the time closely monitored with a stop watch. This was important to guarantee the best possible reproducibility. The flow through was discarded and the protein loaded/washed on the column. After 4 min of washing the buffer in the syringe was changed to elution buffer and the protein was eluted after connecting the HPLC tubing to the Platform II. The data acquired was mass deconvoluted (Section 2.5)

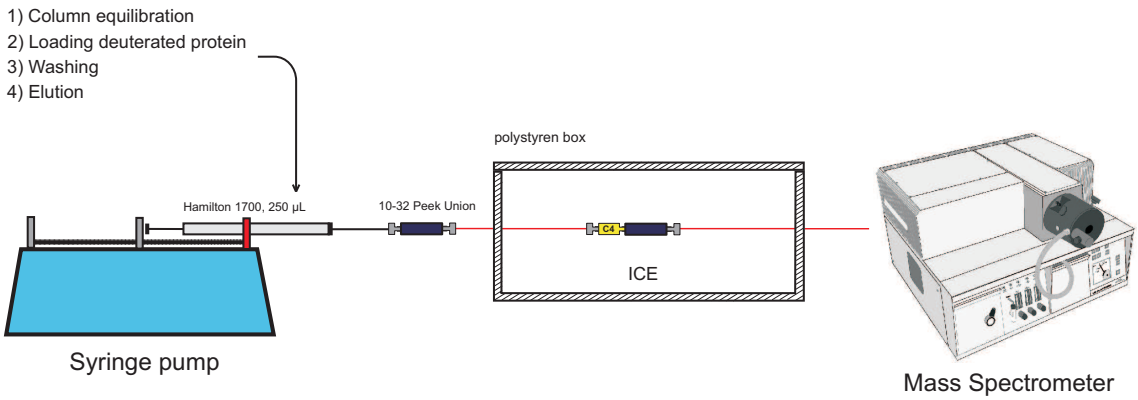

Figure 2.7: First developed PLIMSTEX setup. Showing a syringe pump with gas-thight syringe connected to a C4 guard column, sitting on ice in a polystyrene box, connected to the mass spectrometer. (1) C4 column was primed with washing buffer. (2) Sample applied to the syringe and loaded onto guard column. (3) Washing step. (4) Elution into Platform II for mass analysis.

and further analysed according to the PLIMSTEX routine (Section 2.6.5).

First HDX Labeling Experiment

Before PLIMSTEX experiments were performed with the CypA-CsA system the setup developed was tested by carrying out HDX labeling experiments with apo CypA. Therefore a 4 µM CypA sample in 100 µL was prepared (Section 2.3.5) and subjected to the PLIMSTEX routine (Section 2.6.2) at a flow rate of 30 µL. The washing time, which was crucial for the back exchange, was held constant at 4 min. Each incubation time was repeated at least twice. However, not every experiment resulted in a mass. Figure 2.8 shows the deuterium uptake of CypA *vs.* time, indicating findings were not reproducible for short incubation times. This was mainly attributed to errors made in timing the experiment, handling the individual steps and due to flow rate issues caused by leakages of the syringe. This was due to machine fatigue as a result of the chosen flow rate in conjunction with the back pressure generated by the HPLC tubing and the guard column. The inaccuracy of the apo CypA results emphasised the necessity of a better flow rate management, which led to the development of a more sophisticated HPLC front-end (Section 2.6.3).

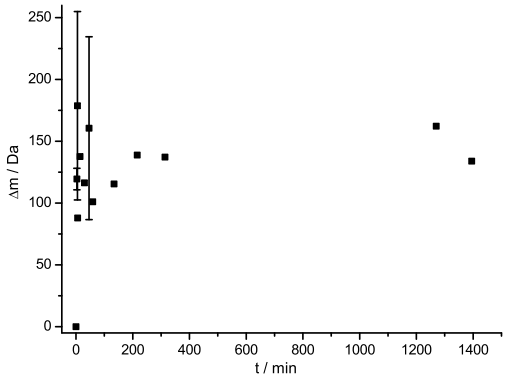

Figure 2.8: First HPLC HDX labeling experiment with developed setup and apo CypA. Error bars represent standard deviation of at least two independent experiments.

2.6.3 The Manual Approach

To circumvent the flow rate issue a set of HPLC pumps (PU980 - Jasco - Essex, UK) was used to deliver a constant flow, adjusted to 30 µL/min for washing and elution buffer. Figure 2.9 provides an overview of the total setup. For diversion of the flow paths 3 Rheodyne valves (7725, 7000 - IDEX Health & Science - Wertheim-Mondfeld, Germany) were mounted on a metal plate and connected with low ID 1/16 peek^{TM} tubing (ID 0.005 in)[2]. The metal plate holding the valves was positioned on a polystyrene box filled with ice, immersing the valves in ice to guarantee a sample temperature close to 0 °C. To further assist low temperature conditions stainless steel (ss) loops were bend and installed between HPLC pumps and Rheodyne valves, buried in ice. For sample injection a 100 µL ss sample loop was employed in conjunction with a C4 guard column (Optimize Technologies - Oregon City, USA) for protein 'trapping' (Fig. 2.9a). PLIMSTEX (Section 2.6.1) or HDX labeling samples (Section 2.3.5) were quenched precisely as in Section 2.6.2 and loaded onto the sample loop with a 250 µL gasthight syringe *via* the needle port of valve I in the load position (blue ports connected), while valve II remained in the inject position (magenta ports connected) to allow flow over the guard column and valve III in the load position (blue ports connected) going to waste. After loading, the sample valve I was switched to the inject position allowing washing buffer to empty the sample loop and loading the quenched protein sample onto the guard column. The moment the switch was turned for loading/washing the sample onto the column, time acquisition was started and the protein was washed with non-deuterated buffer for

[2]thanks to Dr. H. Husi for advise on general HPLC questions.

as close to 4 min as possible. Then mass acquisition was started and valves II and III were switched to the load and inject position, respectively. Elution buffer now ran over the C4 column eluting the protein into the MS, followed by data analysis (Section 2.5, 2.6.5).

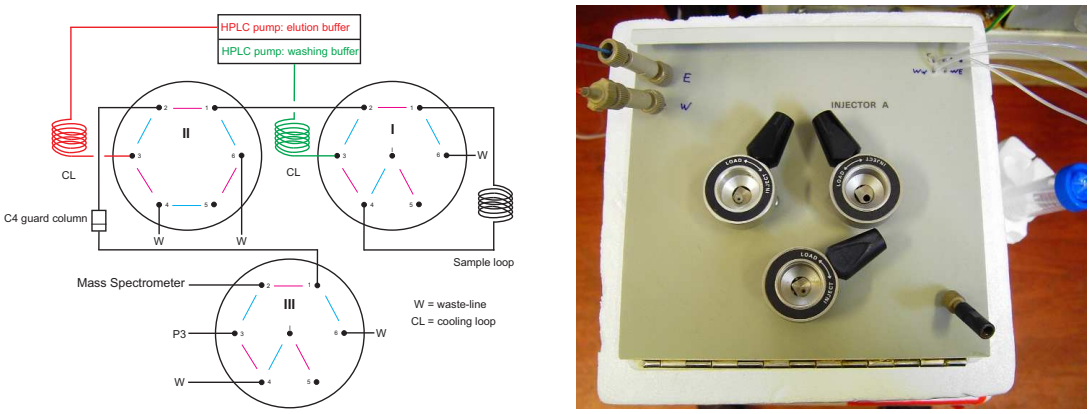

(a) (b)

Figure 2.9: Manual PLIMSTEX and SUPREX setup. (a) Flow path schematic of wash/elution buffer. (b) Image of the HPLC switches on top of the polystyrene ice box.

Flow Rates

To get an idea about the error associated with the uncertainty of the flow rates, both wash and elution buffer flow rates were determined and recorded for every experimental day. Therefor an empty 250 µL gasthight syringe was connected to port 2 of valve III (Fig. 2.9). Using a stop watch the elapsed time was measured until the syringe was filled with buffer and the average flow rate calculated. Figure 2.10a shows the flow rate deviation from the set value of 30 µL/min for wash and elution buffer. Deviations for the washing buffer are relatively small and within a range of ±2 µL/min. However, for the elution buffer discrepancies are larger, compared to the wash buffer, within a range of ±10 µL/min. This might be due to the solvent properties of the elution buffer in context with a lower backpressure of the system relative to the washing buffer.

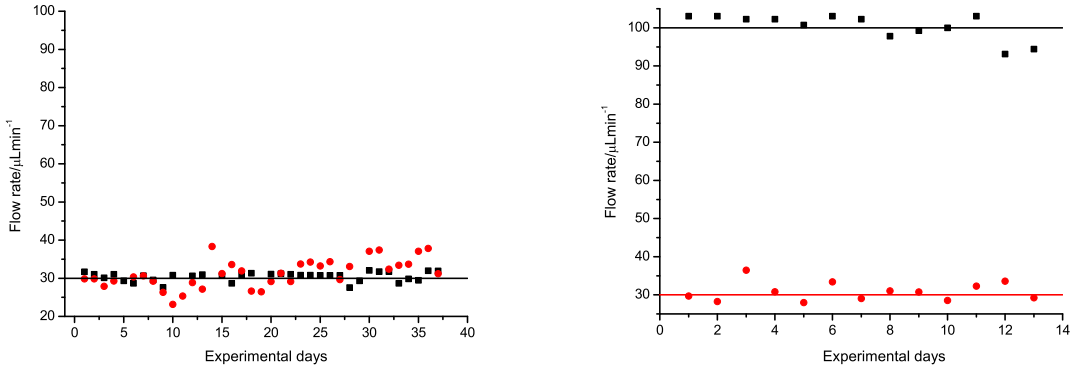

(a) (b)

Figure 2.10: Flow rates for manual PLIMSTEX and SUPREX. (a) Deviations from 30 µL/min shown for washing (black) and elution buffer (red) for manual PLIMSTEX. (b) Deviations from 100 µL/min and 30 µL/min for washing (black) and elution buffer (red) for manual SUPREX experiment.

HDX Labeling Experiment with the Manual Setup

The manual setup was tested repeating the same HDX labling experiment as with the first PLIMSTEX setup (Section 2.6.2). As Figure 2.11a visualises the reproducibility is much better than in the previous experiment and more data points could be collected.

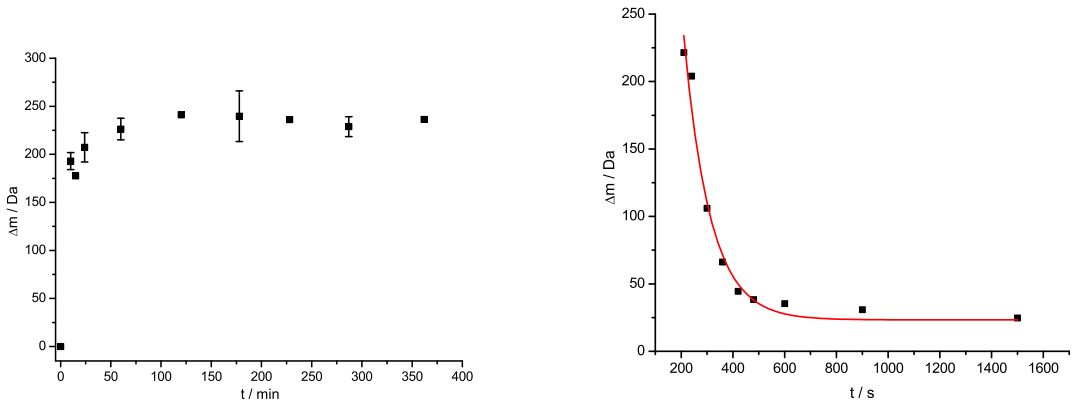

(a) (b)

Figure 2.11: CypA HPLC-HDX labling experiment and back exchange optimisation. (a) HDX labeling experiment with the manual PLIMSTEX setup. (b) Back exchange optimisation for CypA.

Back Exchange Optimisation

To minimise the experimental error on PLIMSTEX data it was necessary to get an idea of the back exchange profile of the utilised system. Therefore CypA was incubated in 10 mM *d*-NH_4OAc (Fisher Scientific - Loughborough, UK) at a concentration of 4 µM for 120 min before quenching (Section 2.6.2) and loading 100 µL of the sample onto the 'manual setup' (Fig. 2.9). Loading/washing the sample for different time periods yielded the different changes in mass of CypA due to back exchange of type 1 and type 2 deuterium atoms (Section 1.3). Figure 2.11b shows the change in the mass difference between undeuterated and deuterated CypA depending on the washing time on the guard column. The rapid decrease at short washing times is due to the back exchange of the fast exchanging type 1 deuterons, whereas the plateau for times longer than 400 s represents the slower back exchange of the amide bound T2 deuterons. A compromise between a too low deuterium level and big fluctuations in the T1 back exchange region was a washing time of ~6-9 min. Further manual PLIMSTEX experiments were carried out at this very washing time.

CypA-CsA PLIMSTEX

After optimising the washing step a PLIMSTEX experiment (Section 2.6.3) with the CypA-CsA system was conducted. An example mass spectrum for CypA-CsA PLIMSTEX experiments is visualised in Appendix 9.4. Figure 2.12 shows the PLIMSTEX curve for the system (quantitative discussion of manual CypA-CsA PLIMSTEX data in Chapter 3.4). Two sets of experiments were run and the standard deviation was plotted as error bars. The errors are within a reasonable threshold, finally emphasising the usefulness of the developed PLIMSTEX HPLC-front end. However, as all steps within the developed protocol (Section 2.6.3) were manually timed and executed there was still room for improvement of reproducibility and increasing the throughput.

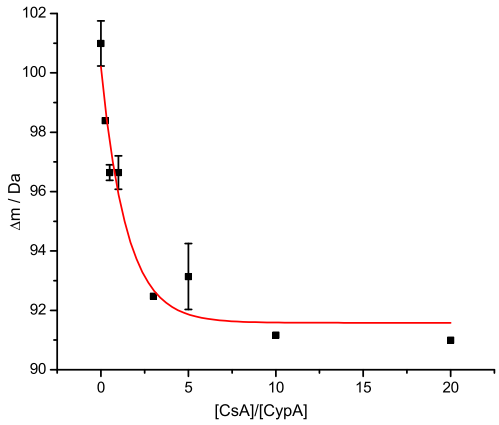

Figure 2.12: Manual CypA-CsA PLIMSTEX curve. Error bars represent standard deviation of two independent runs.

2.6.4 The Automated Method

As the manual acquisition of PLIMSTEX experiments limited throughput and accuracy, a fully automated approach was developed.

Hardware

A software controlled HPLC system was employed comprising a Dionex Ultimate 3000 quaternary analytical pump (Dionex - Sunnyvale, USA) with a flow accuracy of ± 0.1 % accuracy for better flow rate management. Sample handling was taken care of by a Famos Micro Autosampler (Dionex - Sunnyvale, USA), which was further equipped with a 100 µL syringe (Dionex - Sunnyvale, USA) to accelerate handling of larger sample volumes. The standard 2.4 µL sample needle was replaced with a self built 15 µL one (Fig. 2.13a). Fused glass capillary tubing (SGE Europe Ltd - Kiln Farm Milton Keynes, UK) was glued into grey 1/16 peek^{TM} tubing (Anachem - Bedfordshire, UK) using a two component epoxy adhesive (Araldite - Huntsman Advanced Materials - Cambridge, UK) and dried/hardened for ~ 7 days. A stopper was placed at a particular position to guarantee exact sample needle height. All measures are visualised in Figure 2.13a. Individual HPLC components were connected with fused glass capillary tubing of different diameters (PLIMSTEX: 50 µm, SUPREX: 75 µm) and lengths to keep the tubing dead volume as low as possible. The methodology was identical for the preparation of the autosampler needles (Fig. 2.13b). It was necessary to adapt tubing inner diameters (ID) to the flow rate of the individual HDX experiment (PLIMSTEX or SUPREX) to guarantee

a back pressure of at least 50 bar for optimal performance of the HPLC pump.

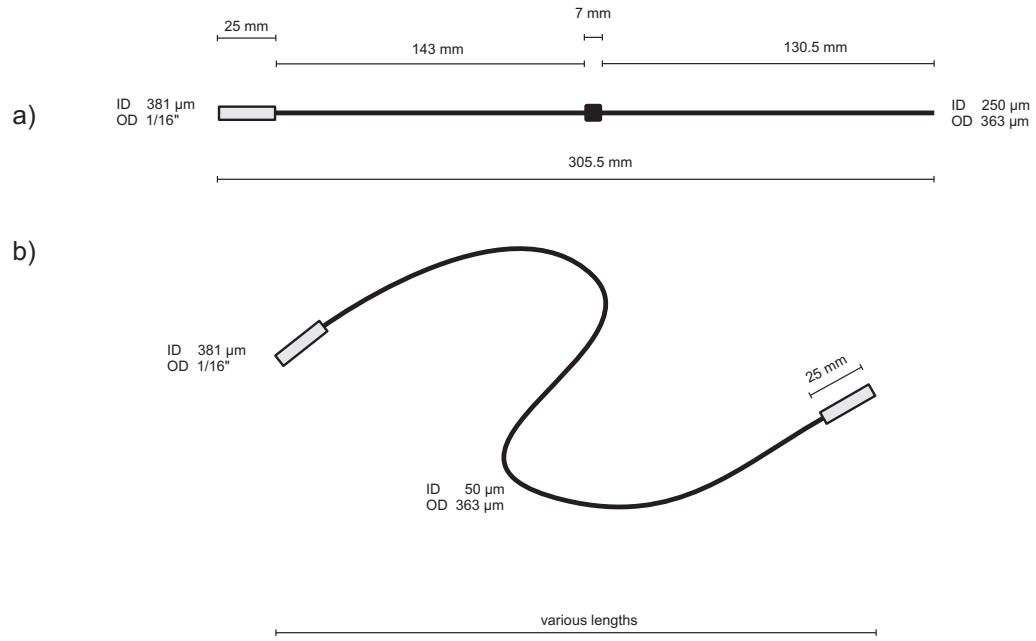

Figure 2.13: Autosampler tubing. (a) In house made 15 µL needle for Famos Micro Autosampler. (b) Fused glass capillary tubing in different lengths and ID's.

For sample injection different sized sample loops were prepared. Utilising 0.02 in 1/16 peek^{TM} tubing in the lengths of 14.8, 24.7, 29.6 and 49.34 cm sample loops of 30, 50, 60 and 100 µL were built.

The main issue of any automation attempt was the low temperature needed for the quenching of the HDX reaction. To circumvent this issue a device was required, which was able to hold a reasonable amount of ice for at least 24 h. A ss box was built[3] matching the dimensions to fit a polystyrene box. HPLC connections were established *via* two 0.020 in 10-32 ZDV ss unions (Anachem - Luton, UK), silver soldered into the ss box according to Figure 2.14. A C4 guard column was attached from the inside of the box and connected with 50 µm ID fused glass capillary tubing at the inside and the outside. Now water tight, the ss box was put into the polystyrene box and filled with a water/ice mixture for better heat transmission.

Figure 2.15 provides an overview of the automated PLIMSTEX setup.

Methodology

For automated PLIMSTEX experiments, samples were prepared according to Sec-

[3]Mr. D. Paden, University of Edinburgh

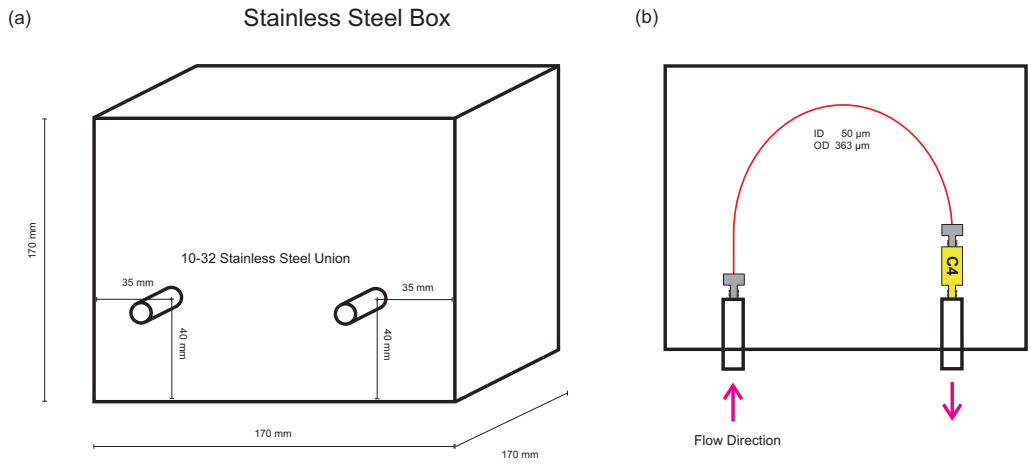

Figure 2.14: HPLC ice box. (a) Front view with dimensions of the ice box. (b) Top view, with column assembly.

tion 2.6.1, put in a 48 well plate according Figure 2.6a and positioned in the autosampler. The LC method program (Appendix 9.7) used for PLIMSTEX involved:

- ligand addition (1 µL) to protein sample (1 µL; Fig. 2.6a)
- waiting block of 20 min
- pick up of 66 µL 10 mM *d*-NH_4OAc from headspace vial and dispense into individual sample vial
- waiting block for 90 min to allow HDX
- sample pick up of 65 µL, loading onto guard column and washing for 8 min (Section 2.6.4)
- sample elution into MS.

At this point it is important to emphasise the lack of an explicit pH quenching step due to the time it would take to perform this. However, due to the pH of the washing buffer the sample was instead quenched 'online' while been loaded/washed. Duration of an individual experiment was ~105 min, allowing ~14 samples being investigated within 24 h. Data analysis was performed as described in Section 2.5 and 2.6.5.

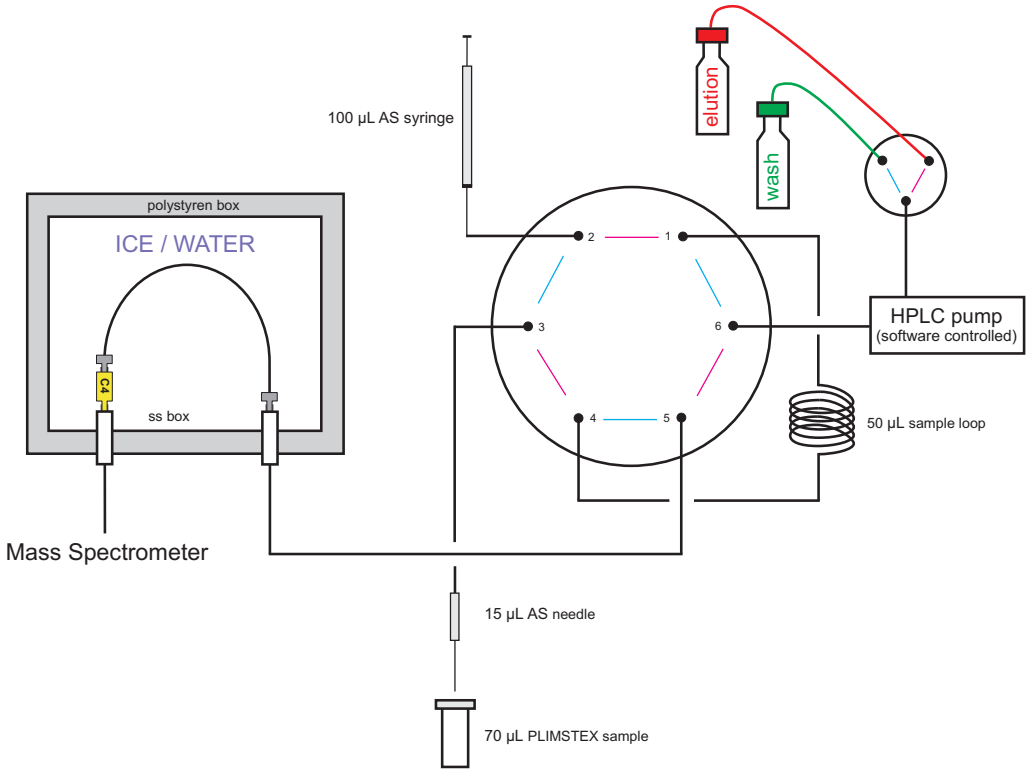

Figure 2.15: Automated PLIMSTEX overview with software controlled HPLC pump, autosampler, ice box and mass spectrometer.

Automated Back Exchange Optimisation

Before PLIMSTEX experiments were conducted, the time for loading/washing the quenched protein sample was optimised. Horse heart myoglobin (HHM; Section 2.7.6) was used as a standard due to easy and cheap accessibility. A 1 mL HHM sample was prepared (Section 2.3.1) in 10 mM *d*-NH_4OAc at a concentration of 4 µM and incubated for 120 min. Then 65 µL *d*-HHM sample were loaded *via* the autosampler on the sample loop and loaded onto the column, where different washing times were applied. Figure 2.16a illustrates the different retention times of the sample due to different washing times. The associated changes in mass are visualised in Fig. 2.16b. In comparison with the back exchange experiment of the manual setup (Fig. 2.11), data shows a more linear decrease of the protein deuterium level in time, indicating T2 deuterons already back exchanging. Due to the fact that one HPLC pump serves two buffers (wash/elution) the shortest retention time was shown to be 7 min. Meaning, directly after sample injection the flow path was changed to the elution buffer, taking 7 min for elution to occur. To compromise between run duration and deuterium level of the protein a washing time of 1 min,

resulting in a retention time of 8 min was chosen for further automated PLIMSTEX experiments.

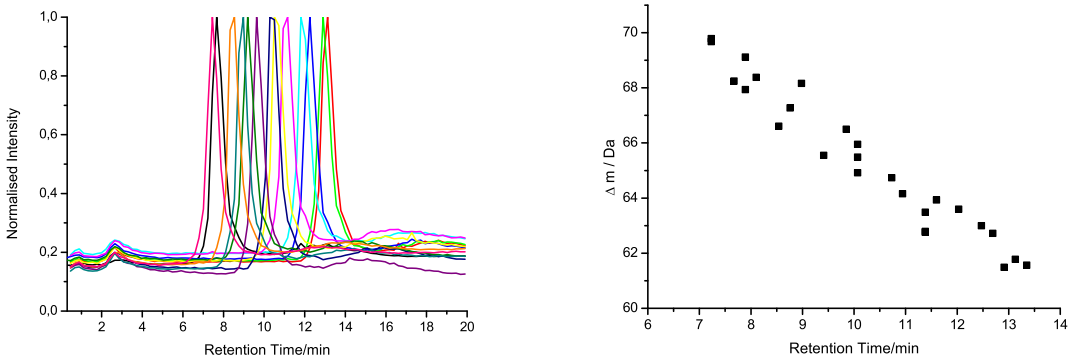

(a) (b)

Figure 2.16: Back exchange optimisation for the automated PLIMSTEX setup using HHM. (a) MS chromatogram for HHM elution with retention times between 7-14 min. (b) Associated mass shifts of HHM due to different retention times.

2.6.5 PLIMSTEX Data Processing

The experimental PLIMSTEX data was processed (Section 2.5) and plotted in a PLIMSTEX curve (Fig. 1.14a) before modeling the data according [1], [230] and [229]. Therefore a methodology has been developed by Dr. Phillip Camp (University of Edinburgh) to model 1:1 binding behaviour by using equation 54 (Appendix 9.8) in conjunction with Microcal - Origin 7.5 to fit and plot experimental PLIMSTEX data, yielding values for Δm_{free}, $\Delta m_{complex}$, and K the mass difference due to deuterium uptake of the free protein, the fully complexed protein and the affinity constant, respectively. A further detailed derivation can be found in Appendix 9.8.

2.6.6 PLIMSTEX Optimisation

Due to the self-assembly capabilities of insulin, the new developed automated PLIMSTEX setup was tested with recombinant (r) human insulin.

Insulin

Insulin is 51 aa protein (Section 9.9) with a mass of 5808 Da. It is a hetero dimer [255] consisting of an α- and β-subunit with 21 and 30 amino acids covalently connected *via* two disulfide bonds (Fig. 2.17a). It is produced in the pancreas as a monomer to regulate blood glucose levels and self-associates in solution. However, storage takes place in the pancreas as a hexamer [256]. Dissociation into the monomeric active form is needed for absorption into the blood stream [232, 257]. Recombinant human insulin is widely used for type 1 diabetes. Therefore it's structural form plays an important role in terms of bioavailability and duration of action. Hereby one hypothesis is that the higher the tendency of an insulin to self-associate, the longer it takes to act [258].

(a) (b)

Figure 2.17: Human insulin structure. (a) Heterodimer (pdb file 1a7f). (b) Phenol stabilised hexamer (pdb file 1ai0 visualised with pymol (DeLano Scientific LLC - Palo Alto, USA)).

Gross *et al.* investigated the self-assembly properties of r-human, porcine, bovine and lispro insulin and other insulin mutants utilising an adaptation of PLIMSTEX, termed SIMSTEX (Section 1.5.1). Equilibrium constants for the oligomerisation of the various insulin analogs have been reported [232]. These findings demonstrate the presence of the dimeric, tetrameric and hexameric insulin form in solution and the existence of a trimeric and pentameric form in the gas phase.

Insulin PLIMSTEX

The insulin SIMSTEX experiment (Section 2.6.6) was carried out with DI mass spectrometry. As a proof of principle and to optimise the automated PLIMSTEX setup self-association LC-experiments were carried out. At first a HDX labeling experiment (Section 2.3.5) with the automated setup (Section 2.7.3) was performed to

gain information about exchange kinetics and deuterium levels of r-human insulin. Figure 2.18a shows the HDX labeling curve at a fixed concentration of 40 µM. In conjunction with a 30 µL/min for wash/elution buffer the maximum deuterium incorporation could be determined to be ~28 amide deuterons, compared to the total number of 50 exchangeable hydrogens, meaning 22 amide protons were shielded due to protein structure and therefore showed no exchange. However, some degree of back exchange also contributed to this finding as the back exchange experiments with HHM (Section 2.6.4) indicated. Nevertheless, as PLIMSTEX experiments were performed under identical experimental conditions using the automated HPLC front-end (Section 2.6.4), back exchange was not further investigated but considered as constant.
For low sample concentrations of insulin the high s/n ratio and the low signal intensities were problematic. Figure 2.18b illustrates the increasing signal intensity of the chromatogram with increasing insulin concentration, taken from the elution peak maximum.

Insulin PLIMSTEX experiments (Section 2.6.4) clearly emphasise the applicability of the developed setup, as the resulting PLIMSTEX curve (Fig. 2.18c) showed the expected trend.

2.7 SUPREX Method Development

In 2000 SUPREX was initially designed for MALDI-MS analysis [2]. So it was necessary to adapt the method for ESI-LC-MS application. As it turned out the previously developed PLIMSTEX setup was applicable for SUPREX as well.

2.7.1 SUPREX Buffers and Sample Preparation

SUPREX experiments were performed according to the SUPREX protocol (Section 1.6.1). Therefore a series of SUPREX-buffers with different denaturing concentrations were prepared from urea and guanidinium hydrochloride stock solutions (Table 2.3) and 10 mM *d*-NH_4OAc (Fisher Scientific - Loughborough, UK). Stock solutions were prepared according to [259] by dissolving 1.103 g of urea in 1 mL of 10 mM *d*-NH_4OAc (Fisher Scientific - Loughborough, UK) to yield a 10 M stock. For guanidinium hydrochloride 1.816 g/mL resulted in a 8 M stock solution. Concentrations were verified using an Abbe-refractometer (Carl Zeiss - Jena, Germany) at RT and 10 mM *d*-NH_4OAc (Fisher Scientific - Loughborough, UK) as blank. Refractive indices were transformed into concentrations using equation 20 for urea and 21 for

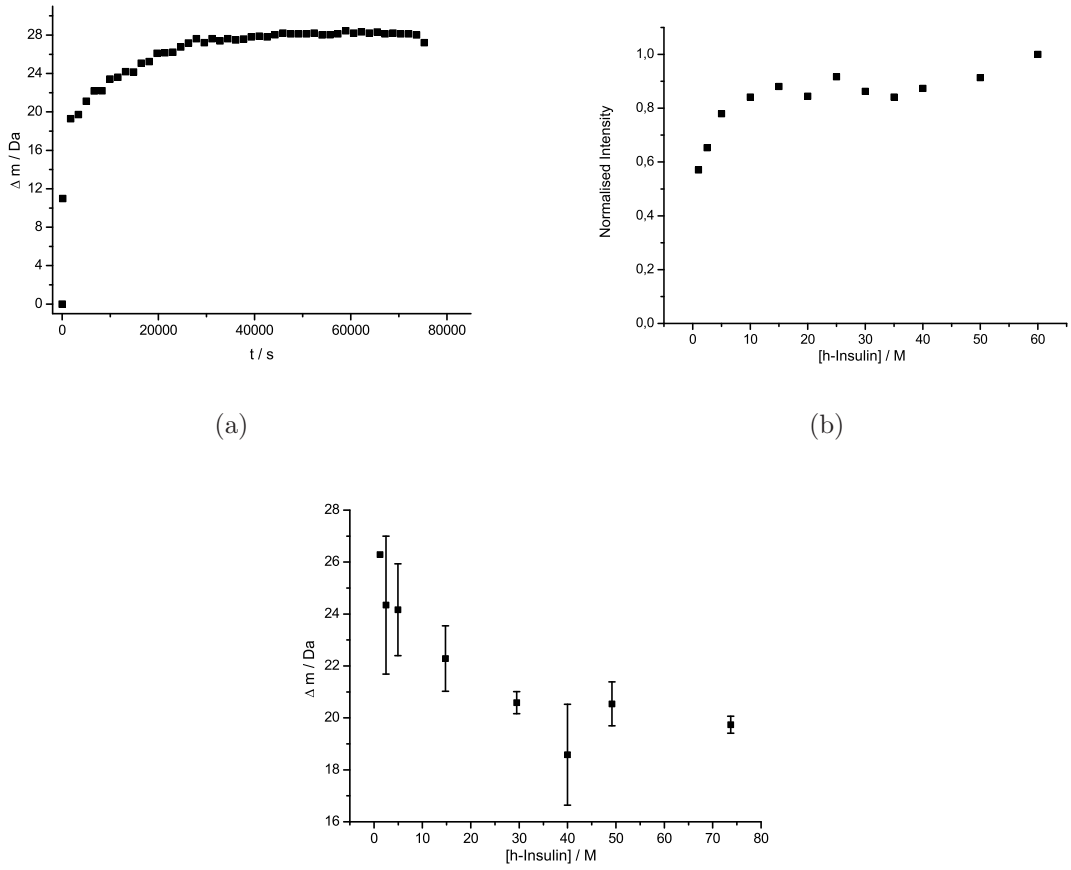

(a) (b)

(c)

Figure 2.18: Insulin HDX overview. (a) Deuterium uptake *vs.* time. (b) Elution chromatogram intensity with respect to insulin concentration. (c) Insulin PLIMSTEX curve. Error bars represent standard deviation of two independent runs.

guanidinium hydrochloride [259].

$$[\mathrm{c}] = 117.66(\Delta N) + 29.753(\Delta N)^2 + 185.56(\Delta N)^3 \tag{20}$$

$$[\mathrm{c}] = 57.147(\Delta N) + 38.68(\Delta N)^2 - 91.60(\Delta N)^3 \tag{21}$$

With [c] concentration in molL^{-1} and ΔN the difference in the refractive index between the denaturant solution and *d*-buffer at the sodium D-line.

For the manual SUPREX approach (Section 2.7.2) 1 µL of the apo protein in question was added to a micro centrifuge tube followed by the addition of 96 µL of the SUPREX-buffer at a particular GDH concentration, resulting in a 4 µM total protein concentration. After incubation between 10-420 min the HDX reaction was

quenched by adding 2 µL of 2 M HCl (Fisher Scientific - Loughborough, UK). The same procedure was applied for the holo protein apart an additional 20 min waiting period prior SUPREX-buffer addition due to complex formation.

For the automated SUPREX approach (Section 2.7.3) the final protein concentration was between 4 µM-5 µM, depending on the protein ligand system, and the final volume was 70 µL. Therefore 4 µL protein (60 µM stock) was placed in a 250 µL, 12x32 mm autosampler vial and sealed with a snap cap. The SUPREX-buffers were pipetted and sealed in identical vials according to their concentration. Where a holo experiment was performed n+1 volume equivalents of ligand were filled in an additional vial at concentrations between 10-20 fold excess to the apo protein (Fig. 2.6b).

Table 2.3: Guanidinium hydrochloride and urea stock solutions for SUPREX. Volumes to prepare 1 mL of SUPREX buffer.

$c_{denaturat}$ $molL^{-1}$	$V_{GDHstock}$[a] mL	V_{NH_4OAc} mL	$V_{ureastock}$[b] mL	V_{NH_4OAc} mL
0.00	0.00	1000.00	0.00	1000.00
0.25	38.75	961.25	25.23	974.77
0.30	46.50	953.50	30.28	960.32
0.50	77.50	922.50	50.46	949.54
0.60	93.00	907.00	60.50	939.50
0.75	116.25	883.75	75.70	924.30
1.00	155.00	845.00	100.93	899.07
1.25	193.75	806.25	126.16	873.84
1.50	232.50	767.50	151.39	848.61
1.75	271.25	728.75	176.62	823.38
2.00	310.01	689.99	201.86	798.14
2.25	348.76	651.24	227.09	772.91
2.50	387.51	612.49	252.32	747.68
2.75	426.26	573.74	277.55	722.45
3.00	465.01	534.99	302.79	697.21
3.25	503.76	496.24	328.02	671.98
3.50	542.51	457.49	353.25	646.75
3.75	581.26	418.74	378.48	621.52
4.00	620.01	379.99	403.71	596.29
4.25	658.76	341.24	428.95	571.05
4.50	697.51	302.49	454.18	545.82
4.75	736.26	263.74	479.41	520.59
5.00	775.01	224.99	504.64	495.36
5.25	813.76	186.24	529.87	470.13
5.50	852.51	147.49	555.11	444.89
5.75	891.27	108.73	580.34	419.66
6.00	930.02	69.98	605.57	394.43
6.25	968.77	31.23	630.80	369.20
6.50			656.04	343.96
6.75			681.27	318.73
7.00			706.50	293.50
7.25			731.73	268.27
7.50			756.96	243.04
7.75			782.20	217.80
8.00			807.43	192.57
8.25			832.66	167.34
8.50			857.89	142.11
8.75			883.12	116.88
9.00			908.36	91.64

[a] prepared from 6.45 M guanidinium hydrochloride stock.

[b] prepared from 9.91 M urea stock M.

2.7.2 Manual SUPREX

For manual SUPREX experiments the previously developed manual PLIMSTEX setup (Section 2.6.3) was used. For desalting purposes it was necessary to increase the WB flow rate and time dramatically. Therefore a flow rate of 100 µL/min for the WB was used, whereas the EB flow rate remained the same at 30 µL/min. For error estimation flow rates were determined every experimental day and recorded (Section 2.6.3, Fig. 2.10b). The quenched samples (Section 2.7.1) were loaded onto the manual HPLC-setup (Fig. 2.9), washed/loaded with the appropriate buffer for 8 min, followed by elution into the mass spectrometer (precisely as in Section 2.6.3) and mass analysis (Section 2.5, 2.7.5).

2.7.3 Automated SUPREX

Hardware

The developed automated PLIMSTEX setup in Section 2.6.4 was, again, a good starting point for automated SUPREX experiments in a more high throughput fashion. As Fig. 2.15 illustrates, there is just one flow path to the MS, meaning all desalting solvent of a SUPREX sample goes into the instrument, limiting the number of possible SUPREX experiments to ~6 on the Platform II (Micromass - Manchester, UK) due to contamination. Finally, having the opportunity to use a 'Famos Switchos Unit' (Dionex - Sunnyvale, USA) with two software controlled 10-port valves and HPLC pump, circumvented this issue. It also reduced the time between switching from washing to elution buffer from ~8 min to <1 min, increasing LC efficiency and throughput. Individual HPLC components were connected with in house prepared 75 µm ID fused glass capillary (Section 2.6.4) due to the higher washing flow rate of 160 µL/min, increasing the back pressure significantly. Figure 2.19 visualises the overall setup.

Software

The one remaining bottle neck was the chromelion software, only allowing one sample to be investigated at a time. Meaning, during long HDX incubation times the system would sit idle, wasting resources. The only option to get round this problem was to program each LC step individually, designing a unique sample list with continuous sample mixing and analysis for each incubation time. A basic LC method for a SUPREX experiment consists of 4 blocks: ligand addition, ligand incubation, buffer addition and LC analysis. According to sample preparation (Section 2.7.1)

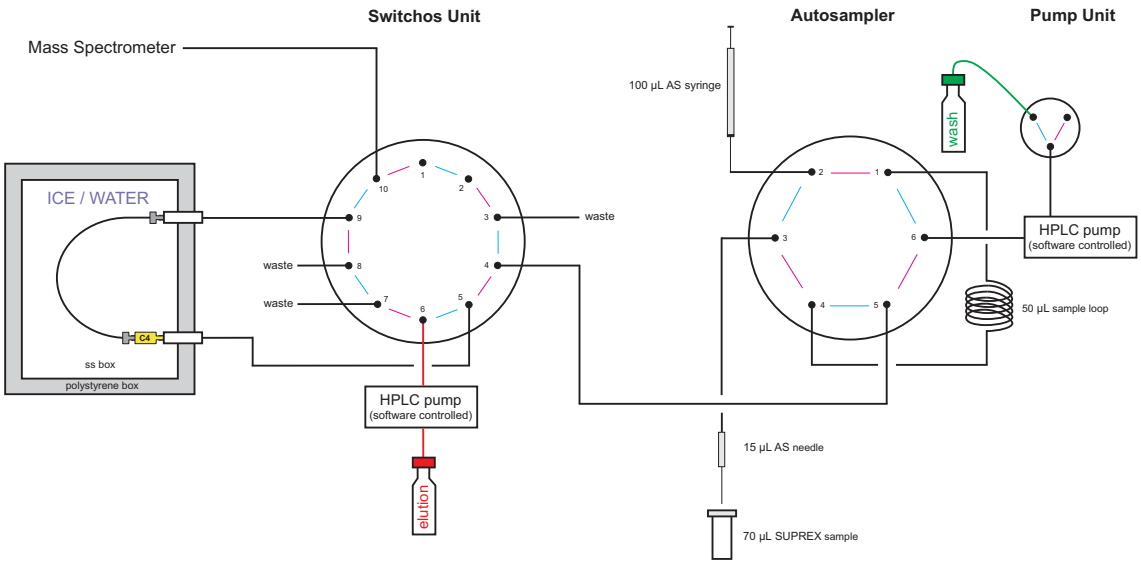

Figure 2.19: Automated SUPREX overview with software controlled HPLC pump unit, autosampler, switchos system, ice box and mass spectrometer.

the individual block durations were illustrated in Table 2.4. Every LC step was timed three times and average values taken.

Table 2.4: Duration of LC method programmes for SUPREX.

Event	Duration	Average Duration/Reaction time
Ligand addition [a]	02 min 47 s	
	02 min 56 s	02 min 56 s
	02 min 57 s	
Waiting block [b]	01 min 00 s	01 min 23 s
	02 min 00 s	02 min 23 s
	03 min 00 s	03 min 23 s
Buffer addition [c]	02 min 54 s	
	02 min 52 s	02 min 52 s
	02 min 52 s	
LC run [d]	13 min 01 s	
	13 min 02 s	13 min 01 s
	13 min 01 s	

[a] time it took to add ligand to apo protein sample.

[b] duration of waiting block.

[c] time it took to add *d*-buffer to holo protein sample.

[d] duration of LC analysis.

Having determined the duration of each individual LC step, sample lists for apo and holo SUPREX experiments were prepared. For HDX incubation times <60 min it was more efficient to utilise the individual genuine LC method program precisely as described in Section 2.6.4. However, for incubation times >60 min the prepared apo and holo sample lists at least doubled throughput efficiency due to less idle time of the system. Detailed sample lists for 10 and 18 samples for even and odd incubation times can be found in Appendix 9.10, 9.11 and 9.12.

Methodology

SUPREX samples were prepared according to Section 2.7 for apo and holo protein experiments and placed into a 48-well plate (Fig. 2.6b). According to Section 2.7.3 samples for HDX incubation times <60 min were carried out with a single LC method program involving:

- (ligand addition of 4 µL to apo protein sample)
- (waiting block for 20 min to allow protein ligand incubation)
- pick up of 66 µL (62 µL) 10 mM *d*-NH_4OAc containing different concentrations of the chemical denaturant and dispense into individual sample vial
- waiting block for various SUPREX times to allow HDX
- sample pick up of 65 µL, loading onto guard column and washing for 8 min (Section 2.6.4)
- sample elution into mass spectrometer.

Steps in brackets designate a holo SUPREX experiment. For incubation times >60 min the same procedure in terms of sample volumes and incubation times was applied. However, the sample lists were manually designed (Section 2.7.3) for each individual incubation time to reduce idle time of the system as much as possible Appendix 9.10, 9.11 and 9.12. This two approaches allowed a throughput of 33 apo SUPREX samples and 21 holo SUPREX samples within a 24 h period.

2.7.4 Temperature Dependent Automated SUPREX

All PLIMSTEX and SUPREX experiments were carried out at constant 22 °C in an air conditioned lab and are referred to as RT. However, investigation of temperature dependent SUPREX experiments needed precise temperature control. Therefore a

48-well plate containing heating and cooling channels was designed. On the basis of a standard 48-well plate for the Famos Micro Autosampler (Dionex - Sunnyvale, USA) a replicate was made[4] from aluminium comprising channels for a secondary heating/cooling device (Fig. 2.20). Mains water was used to heat/cool the sample tray in conjunction with a copper spiral immersed in a water bath (JB12 - Grant - Shepreth, UK) connected *via* plastic tubing (5 mm ID, Nalgene - Thermo Corporation, UK). For low temperature measurements the copper coil was put in an ice box. Two temperatures, different from 22 °C, were investigated. Adjusting the the water bath temperature to 85 °C at a flow rate of ~ 500 mL/min resulted in a 50 °C sample temperature, measured with a glycerol sample and a thermometer. For the low temperature experiment at the same flow rate a sample temperature of 15 °C could be observed. Temperature dependent SUPREX experiments were carried out as those previously described in Sections 2.7.1, 2.7.3 and 2.7.3.

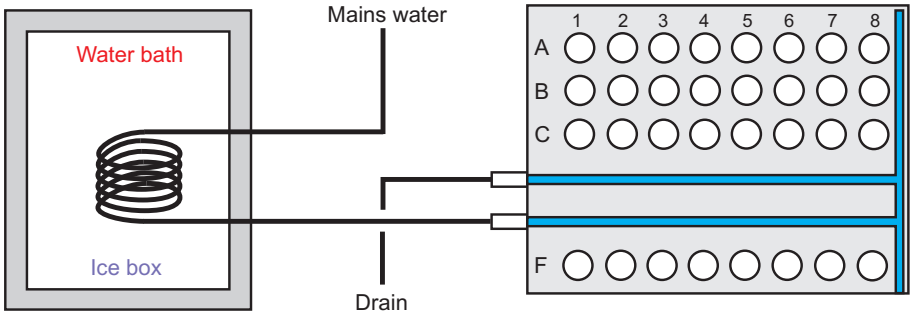

Figure 2.20: Heated 48-well sample tray for SUPREX experiments.

2.7.5 SUPREX Data Processing

Post acquisition, SUPREX mass spectra (illustrated on apo CypA in Appendix 9.13) were processed as described in Section 2.5 and the change in mass shift due to deuteration and denaturation was plotted *versus* the concentration of the chemical denaturant, utilising Microcal - Origin 7.5. Data fitting with equation 17 was carried out as described in Section 1.6.1. ΔG_f's were determined using equation 61 (Appendix 9.14) and plotting $-RTln(\langle k_{int}\rangle t/0.693 - 1)$ *vs.* $C^{1/2}_{SUPREX}$. $\langle k_{int}\rangle$ values were calculated according to Bai *et al.* [107] employing SPHERE, a server program for HDX rate estimation[5]. Dissociation constants were extracted from changes in ΔG_f for the apo and holo systems according to equation 63 (Appendix 9.14).

[4]Mr. D. Paden, University of Edinburgh
[5]http://www.fccc.edu/research/labs/roder/sphere/sphere.html

2.7.6 SUPREX Optimisation

Before wasting valuable protein resources on the automated SUPREX methodology developed, myoglobin was investigated as a protein standard.

Myoglobin

Myoglobin is a 153 aa protein (Appendix 9.15) responsible for oxygen storage in muscle tissue in a non-cooperative way, compared to haemoglobin and the oxygen transport chain. A proximal histidine-bound iron protoporphyrin IX allows oxygen uptake, whereas a distal histidine prevents carbon monoxide from binding [48]. Figure 2.21 illustrates the eight α-helices in the secondary structure of HHM with the heme group in the hydrophobic core. The mass of apo and holo HHM is 16951 Da and 17567 Da, respectively. Due to its easy accessibility it has been widely used as a protein standard not only in the field of mass spectrometry and its properties have been well characterised over the years as shown *inter alia* by Feng *et al.* in 1993 [260] and Konermann *et al.* in 2000 [261].

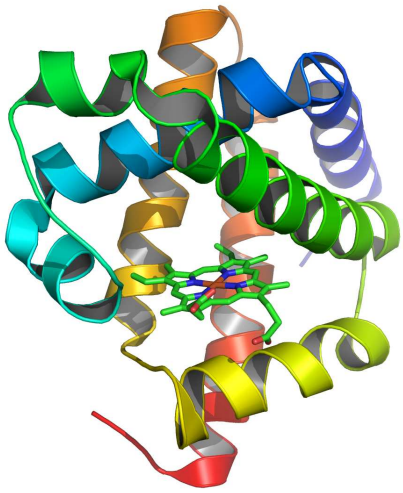

Figure 2.21: X-ray cristal structure of azide stabilised horse heart myoglobin (pdb file 1azi visualised with pymol (DeLano Scientific LLC - Palo Alto, USA)).

Myoglobin SUPREX Results

Automated SUPREX experiments were conducted and evaluated according to Section 2.7.1, 2.7.3 and 2.7.5. Table 2.5 summarises the $C^{1/2}_{SUPREX}$ values for horse heart myoglobin at different incubation times. Figure 2.22a illustrates the change of the SUPREX midpoints with different incubation times. Due to clarity only 10, 60, 120 and 180 min incubation are shown. SUPREX curves at each individual incubation

time can be found in Appendix 9.16. The average intrinsic exchange rate $\langle k_{int} \rangle t$ was calculated with SPHERE to 4.53 s^{-1} at 22 °C. All SUPREX inflexion points gathered at different guanidinium hydrochloride concentrations were plotted *versus* ΔG_f. Figure 2.22b gives an overview of the free energy of protein folding *vs.* denaturant concentration. ΔG_f for myoglobin at a 0 M denaturant concentration was determined to be -26.90 ±1.05 $kJmol^{-1}$. The *m*-value was calculated to 5.40 ±1.63 $kJmol^{-1}M^{-1}$.
Fitzgerald and coworkers [262] reported thermodynamic properties for horse skeletal muscle myoglobin by conventional denaturing experiments and MALDI-SUPREX. ΔG_f was determined to -24.27 ±0.84 $kJmol^{-1}$ with an associated *m*-value of 22.60 ±0.84 $kJmol^{-1}M^{-1}$. However, no thermodynamic parameters different than the $C^{1/2}_{SUPREX}$ values could be extracted from graphs *via* MALDI-SUPREX due to the non-linearity of the ΔG_f *vs.* denaturant concentration plots as reported by Pace and Vanderburg in 1975 [263]. This might indicate a non-two state folding behaviour due to the population of partially unfolded intermediates.
However, Ahmad *et al.* observed linear unfolding behaviour and determined ΔG_f and *m*-values for horse heart myoglobin to -22.43 ±0.42 $kJmol^{-1}$ and 18.58 ±0.42 $kJmol^{-1}M^{-1}$ at a pH of 5.88 utilising conventional spectroscopic denaturing experiments [264].

In conclusion, SUPREX data acquired with the automated ESI-LC SUPREX setup showed good reproducibility as Figure 2.22a emphasises and is within a 10-15 % range to conventional unfolding data for HHM. The effect of different solvents in the denaturing buffer affecting ΔG_f and *m*-values also contributes to the difference in reported values [262, 263, 264]. However, the non-two state behaviour reported with MALDI-SUPREX [262] and spectroscopic methods [263] could not be confirmed suggesting that sample preparation and analysis also have an effect on the nature of protein unfolding.

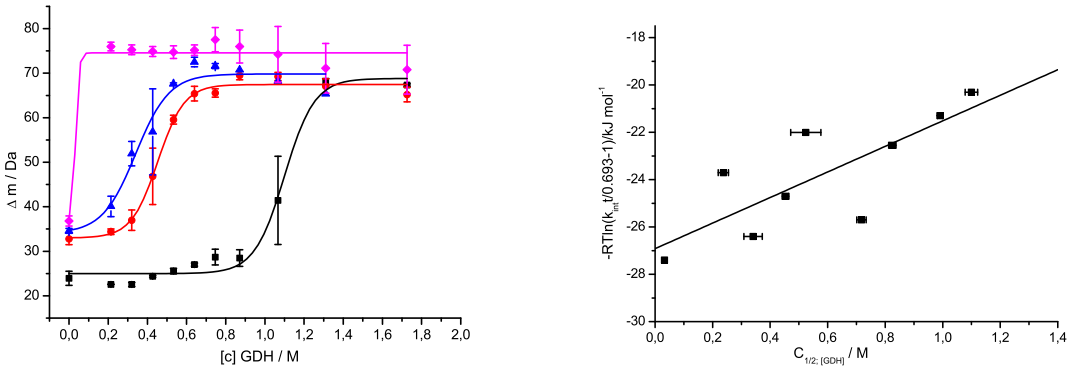

(a) (b)

Figure 2.22: SUPREX curves for HHM and free energy *vs.* denaturant concentration plots. (a) Incubation times of 10 (black), 60 (red), 120 (blue) and 180 min (magenta). Error bars represent standard deviation of 2 runs. (b) Free energy *vs.* denaturant concentration plot for HHM. Error bars represent $C_{SUPREX}^{1/2}$ error due to least-square analysis.

Table 2.5: Horse heart myoglobin SUPREX results with the automated setup.

Incubation time/min	$C_{SUPREX}^{1/2}$ [a] /M
10	1.10
15	1.00
20	0.52
25	0.82
40	0.24
60	0.45
90	0.72
120	0.34
180	0.03

[a] visualised in Fig. 2.22 and Appendix 9.16.

3 SUPREX and PLIMSTEX of the Immunophilins

In this Chapter the HPLC front ends developed for high throughput ESI-PLIMSTEX and SUPREX are tested with enzymes of the PPIase protein family. CypA and FKBP12 were investigated with potentially binding ligands (Section 2.3.2) and compared to data derived from other techniques.

3.1 Introduction

Mass spectrometry screening applications play an important role in drug discovery and multiple methodologies have been elaborated to reflect gas phase behaviour of protein-ligand systems *via* DI-ESI [265, 266, 267, 19]. In contrast, PLIMSTEX and SUPREX have the potential to deliver solution phase information based on HDX reverse phase LC-MS with ESI-MS or MALDI-MS. In the last six years several enzyme-substrate systems have been investigated, including CypA/CsA as illustrated in Table 3.1.

Since Gross *et al.* established PLIMSTEX in 2003 [1] five enzyme/substrate systems have been investigated as visualised in Table 3.1. Those PLIMSTEX determined K_a's and K_d's are within a factor of two for reported proteins-ligand systems.

Fitzgerald and co-workers utilised MALDI-SUPREX in 2004 [268] to determine free energies of protein folding and dissociation constants of CsA with purified CypA and CypA extracted from lung tumor tissue. $\Delta\Delta G_f$ values of -19.66 ± 3.35 kJ/mol and K_d's of 77 ± 17 nM and -17.57 ± 4.2 kJ/mol and 32 ± 20 nM have been determined for the purified and extracted CypA, respectively. Reported dissociation constants are in the range of K_d's determined with other techniques (Table 3.2). In 2008 SPROX (Section 1.6.3) was utilised to investigate CypA/CsA resulting in a K_d of 86 nM [269]. Single point MALDI-SUPREX screening of a 880 member library of potential CypA binding ligands did not detect any new ligands, however, CsA could be identified as a positive hit at a throughput of 3 min *per* ligand [245].

Exchange rates for aa-residues in CypA have been measured by NMR and calculated by Shi and co-workers [270], resulting in three different classes of exchange speed, exhibiting fast, moderate and slow exchange. The CypA/CsA system was investigated to further characterise newly synthesised PPIase ligands (Section 2.3.2) with the new devised LC-ESI-SUPREX setup in a high-throughput fashion to gain

solution phase binding data. After *in silico* screening approaches Walkinshaw *et al.* discovered dimedone analogues to bind to CypA [141]. Synthesised compounds showed K_d's between 11.2-170 µM with KM184 being the most potent candidate (Table 3.2). Table 3.2 provides an overview of PPIase ligand dissociation constants, for ligands investigated in this thesis, derived with different techniques (Section 1.2.6). DI-ESI-MS data was acquired with automated MS equipment utilising ESI and nano-ESI (NanoMate^{TM}) MS techniques by Florance [19] (Table 3.2). It is noteworthy, that dimedone analogue ES1234 is referred to as compound 5 in [141] and KM5 in [19].

Table 3.1: Proteins investigated with different mass spectrometry solution phase HDX methods.

Protein	Method	Year	Reference
		PLIMSTEX	
intestinal fatty acid binding protein (IFABP), Ras-GDP[a] , calomdulin (CaM)	ESI	2003	[1]
CaM	ESI	2003	[231]
IFABP, CaM	ESI	2003	[230]
recombinant human insulin (rh-insulin)	ESI	2004	[229]
human telomeric binding factor 2 (hTRF2)	ESI	2008	[271]
		SIMSTEX	
rh-insulin, insulin analogues	ESI	2006	[232]
		SUPREX	
maltose binding protein, monomeric λ repressor	MALDI	2000	[2]
ribonuclease A (RNaseA) - bovine pancreas	MALDI	2001	[239]
monomeric λ repressor (*in vivo*)	MALDI	2001	[240]
GCN4p1 dimer, coil-V_aL_d trimer, 4-OT hexamer, TrpR dimer, ArcR dimer, (DOA20)ArcR dimer[b]	MALDI	2002	[241]
protein G, S-protein, TrpR,	MALDI	2002	[236]
abelson tyrosine kinase SH3 domain-S-Protein	MALDI	2003	[237]
CopG, equine cytochrome C, β-lactoglobulin A, protein L, β-trypsin, ubiquitin, lysozyme[c]	MALDI	2003	[247]
CopG, ArcR	MALDI	2003	[242]
S-protein	MALDI	2003	[244]
unpurified/purified cyclophilin A	MALDI	2004	[268]
membrane bound lytic transglycosylase B (MltB)	MALDI	2004	[272]
ferric binding protein (FbpA)	MALDI	2004	[273]
ubiquitin	MALDI	2005	[274]
molybdopterin (MPT)	MALDI	2005	[275]
MltB	MALDI	2006	[276]
α-lactalbumin, cytochrome C, IFABP, horse skeletal muscle myoglobin	MALDI	2006	[262]
ubiquitin	MALDI	2006	[248]
protein kinase C Θ (PKCΘ)	ESI	2006	[277]
sortase A (SrtA)	MALDI	2007	[278]
CaM, BCAII, RmlB, Bcl-x_L[d]	MALDI	2007	[279]
CaM, Fyn-construct[e] , human serum transferin	MALDI	2007	[243]
CaM	MALDI	2007	[238]
ferric binding protein (FbpA)	MALDI	2008	[280, 281]
cyclophilin A (CypA)	MALDI	2008	[245]
		SPROX	
ubiquitin, RNaseA, CypA, BCAII	MALDI/ESI	2008	[269]

[a] Ras-GDP: GDP-bound human $p21^{H-ras}$ protein.

[b] with 4-OT: 4-oxolatocrotonate tautomerase, TrpR: Trp repressor, ArcR: Arc repressor and Arc mutant DOA20.

[c] β-lactoglobulin A, β-trypsin and ubiquitin from bovine, hen egg lysozyme.

[d] BCAII: bovine carbonic anhydrase II, RmlB: d-TDP-*D*-glucose 4,6-dehydratase, Bcl-x_L: pro-apoptotic factor Bcl-x_L.

[e] Fyn-construct: a linked SH3- and SH2-domain.

3.1.1 The Dissociation Constant

The affinity constant K_a of an enzyme/substrate system measures the affinity, protein and ligand have to each other. It is usually determined by measuring the free ligand concentration (*e.g.* equilibrium dialysis (Section 1.2.6)). According to the law of mass action, assuming an equilibrated state, K_a will remain constant under a given set of conditions:

$$P + L \underset{K_d}{\overset{K_a}{\rightleftharpoons}} PL \qquad \text{and;} \qquad K_a = \frac{[PL]}{[P] \cdot [L]} \tag{22}$$

The dissociation constant is the reciprocal of the association constant, therefore:

$$K_d = \frac{1}{K_a} \qquad \text{and} \qquad K_d = \frac{[P] \cdot [L]}{[PL]} \qquad \text{therefore;} \qquad \frac{[PL]}{[P]} = \frac{1}{K_d}[L] \tag{23}$$

If the free ligand concentration $[L]$ is less than the K_d there is little association, as binding conditions favor excess of ligand [235]. In contrast, if K_d and $[L]$ are equal half of the protein is complexed (eq. 23) [19].

3.2 Direct Infusion

Each freshly expressed CypA batch (Section 2.2.1) was tested for binding with a freshly prepared CsA stock solution (Section 2.3.2) *via* DI-ESI (Section 2.3.4) under native like conditions with a two fold excess of ligand at a total protein concentration of ~40 µM, acquired on a QTOF-Ultima. Figure 3.1a visualises the apo protein spectrum for CypA showing a charge state distribution from 7+ to 24+, resulting in a deconvoluted mass of 18144 Da, however, according to the CypA sequence (Appendix 10.1) a theoretical mass of 18012 Da should be expected. The mass difference of 132 Da suggests an additional N-terminal methionine residue of CypA attributable to the *E. coli* expression system. The mass spectrum of the CypA-CsA complex (Fig. 3.1) demonstrates the same charge state distribution as the apo CypA spectrum plus additional CypA-CsA complex peaks of charge states 7+, 8+ and 9+. Deconvolution results in a mass of 19346 Da for the complex, which agrees well as the sum of individual CypA and CsA. Unbound CsA is present in a 2+ charge state at a *m/z* value of 601. DI-ESI-MS findings for CypA-CsA emphasise the strong interaction of enzyme and substrate and confirm a successful cyclophilin A protein expression.

Table 3.2: Comparison of dissociation constants of the investigated immunophilins with different biophysical and biological methods.

Protein	Ligand	Structure	Mass/Da	K_d^{DI-ESI}	K_d^{SPR}	K_d^{FL}	K_d^{ITC}	K_d^{PPIase}	$IC_{50}^{in\ vivo}$
CypA									
	CsA	Fig. 1.10	1202.61		38.5 ± 10.4 nM[a]	26 ± 9 nM [b]	11.4 ± 3.9 nM[c] 47.6 nM[d]	6.3 ± 3.8 nM[b] 1.6 ± 0.4 nM[b] 20 nM[b]	
	KM184	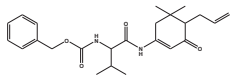	412.5	189 ± 43 µM[e]	36 µM[b] 42 ± 7 µM[f]	12.2 ± 9.2 µM[b] 11.2 ± 9.2 µM[f]		22 ± 7.8 µM[f]	190 ± 60 µM[f]
	ES1234	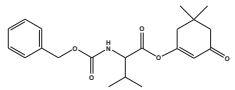	373.44	271.97 µM[e]	~50 µM[f]	19.5 ± 5 µM[f]		27.3 ± 9.2 µM[f]	
FKBP12	Rapamycin	Fig. 1.10	914.17				2.0 nM[g]	20 nM[b]	

[a] from [282].
[b] from [252].
[c] from [283].
[d] from [284].
[e] from [19].
[f] from [141].
[g] from [145].

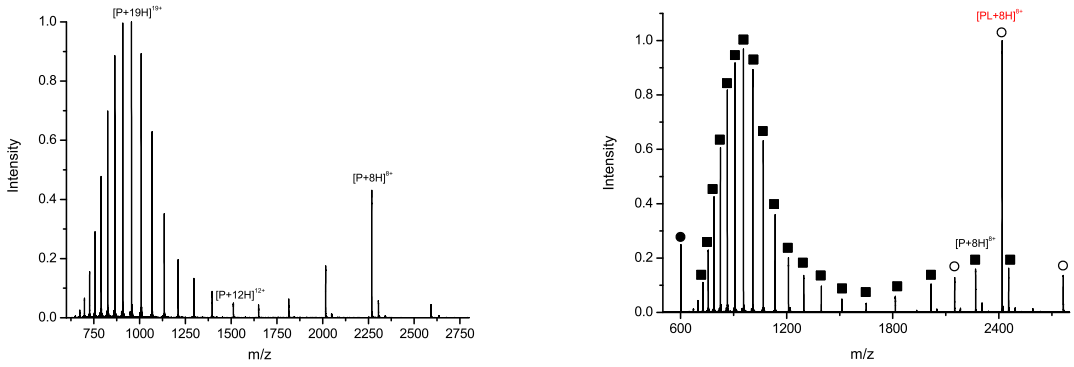

(a) (b)

Figure 3.1: Direct infusion spectrum CypA-CsA. (a) CypA sprayed under native like conditions from 10 mM NH_4OAc exhibiting charge states from 7+ to 24+. (b) CypA-CsA complex spectrum under native like conditions from 10 mM NH_4OAc with uncomplexed CypA (black squares), CypA-CsA complex peaks at charge states 7+, 8+ and 9+ (black filled circle) and excess ligand at charge state 2+ (black circles).

Before PLIMSTEX and SUPREX experiments with potential immunophilin ligands KM184 and ES1234 were conducted, DI-ESI-MS studies were employed for compound characterisation. The KM184 ligand was sprayed from pure methanol containing 5 % FA, resulting in singly charged analyte ions with a deconvoluted mass of 413 Da, showing good agreement with the theoretical mass of 412.5 Da (Fig. 3.2a). CypA-KM184 complex was investigated under native like conditions displaying free protein signals at charge state 8+ and 2269.9 m/z, complexed KM184 at 2321.7 m/z and charge state 8+ and CypA complexed with a KM184 fragment at m/z of 2306.5 and charge state 8+ (Fig. 3.2b). Masses are calculated to 18151.7, 18444.0 and 18565.7 Da for apo and complexed CypA, verifying the correct mass of CypA-KM184 at m/z 2321.7 and yielding a fragment mass of 292.3 Da. Fragmentation/degradation can either occur by cleavage by CypA or degradation caused by storage at 4 °C, the latter being the most likely explanation. The fact the degradation product does not appear in the DI-ESI-MS spectrum of the ligand (Fig. 3.2a), suggests poor ionisation properties of the fragment.

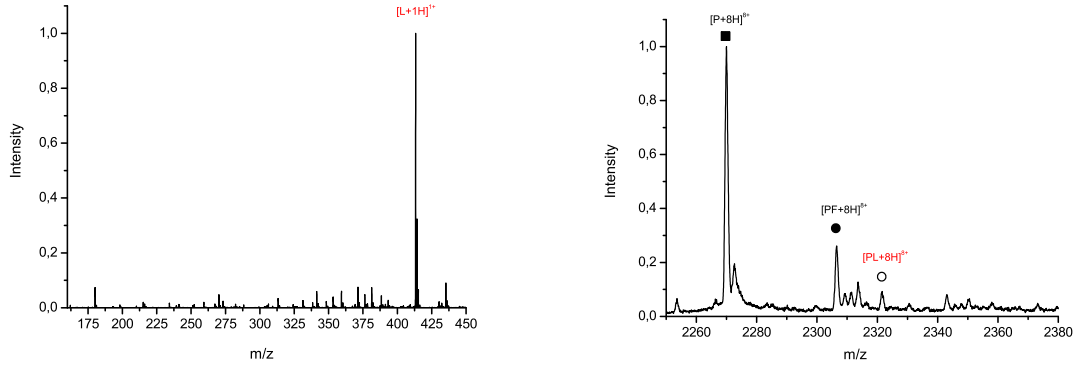

(a) (b)

Figure 3.2: DI-ESI spectrum of CypA-KM184. (a) KM184 sprayed from pure methanol containing 5 % FA with a mass of 412.5 Da. (b) CypA-KM184 complex (red) and CypA-KM184-fragment complex (black) sprayed under native like conditions from 10 mM NH_4OAc.

DI-ESI-MS for ES1234 sprayed from pure methanol containing 5 % FA reveals singly charged ligand containing one sodium ion at m/z 395.7 (Fig. 3.3a). Two singly charged fragmentation/degradation products of ES1234 are identified at m/z 287.7 and 230.8 showing binding to CypA at m/z 2306.51 and 2299.00 in Figure 3.3b. Florance and Yang *et al.* [19, 141] confirmed a CypA-ES1234 interaction with K_d's between 19 and 272 µM utilising DI-ESI-MS, SPR and fluorescence methodologies (Table 3.2).

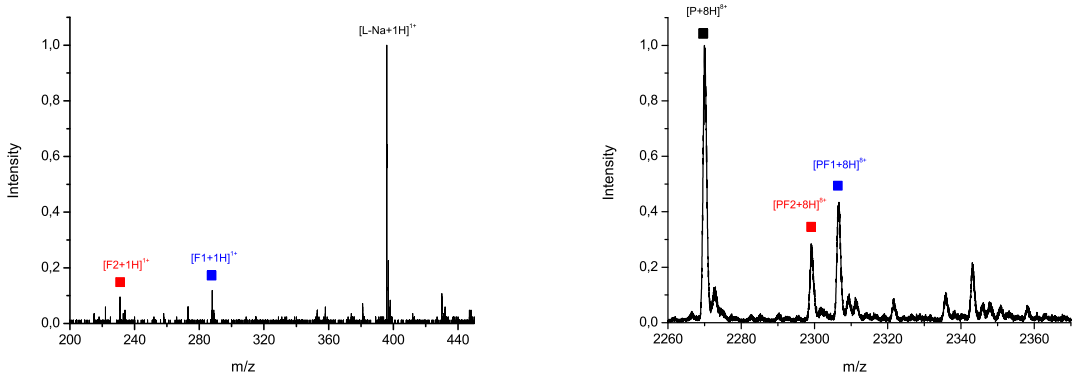

(a) (b)

Figure 3.3: DI-ESI spectrum of CypA-ES1234. (a) ES1234 sprayed from pure methanol containing 5 % FA with a mass of 373.44 Da. Peak at 396.44 *m/z* corresponds to charge state 1+ of ES1234 with one sodium ion. Ligand fragments/degradation products F2/F1 at 233.73 and 292.45 *m/z* shown in red and blue, respectively. (b) CypA complexed with ES1234 fragments F2 (233.73 Da) and F1 (292.45 Da) sprayed under native like conditions from 10 mM NH_4OAc.

Rapamycin was sprayed from pure methanol containing 5 % FA exhibiting a series of species at the 2+ charge state comprising free ligand (460.5 *m/z*), ligand plus one sodium (469.7 *m/z*) and ligand with two sodium ions (476.4 *m/z*; Fig. 3.4). Singly charged rapamycin containing one sodium atom at an *m/z* value of 913.19 shows good agreement with the expected theoretical average mass of 914.17 (Table 3.2). A native like spectrum of the FKBP-rapamycin complex comprises charge state distributions for free and complexed protein ranging from 7+ to 21+ and 7+ to 10+, respectively. Deconvolution yields masses for apo FKBP12 of 13275.05 Da and FKBP12-rapamycin 14190.38 Da resulting in a mass of 915.33 Da for rapamycin, exhibiting good agreement with the free ligand studies (Fig. 3.4).

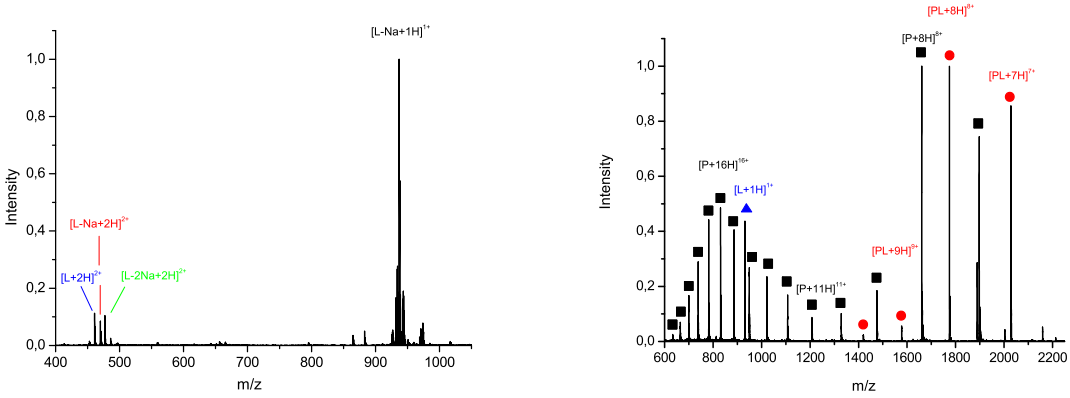

(a) (b)

Figure 3.4: DI-ESI spectrum of FKBP12-rapamycin. (a) Rapamycin sprayed from pure methanol containing 5 % FA with a mass of 914.17 Da. Peak at 936 *m/z* corresponds to charge state 1+ of rapamycin with one sodium ion. Charge state 2+ for rapamycin comprising 0, 1 and 2 sodium ions shown in blue, red and green respectively. (b) Two overlaid spectra of apo FKBP12 (black squares) and FKBP12-rapamycin complex (red circles) with uncomplexed rapamycin (blue triangle) sprayed under native like conditions from 10 mM NH_4OAc.

3.3 Labeling Experiments

Protein-ligand systems investigated were subjected to HDX labeling experiments to ascertain amide HDX properties. Samples were prepared as described in Section 2.3.5 at a final enzyme concentration of 5 µM in conjunction with the automated SUPREX setup (Section 2.7.3).

According to the sequence of CypA (Appendix 10.1) the total number of hydrogens within the protein are 1245 considering one additional methionine, comprising 125 T1, 160 T2 and 952 T3 hydrogen atoms. In Figure 3.5 apo CypA exhibits the lowest exchange rate and deuterium level, with about 275 min to reach a HDX equilibrium at ~43 T2 hydrogens. These 43 T2 protons represent 27 % of all available backbone amide protons remaining after back exchange and protection, enabling qualitative comparisons to ligand exposed CypA.

As all immunophilin ligands were dissolved in 36.88 % MeOH/water, which was the lowest methanol concentration still guaranteeing complete solvation of the compound, the final MeOH ratio for protein-ligand incubation was 18 % and for the protein-ligand complex in the deuterated buffer 2.3 %. The curve representing CypA in a total methanol ratio of 2.3 % MeOH exhibits the highest exchange rate and deuterium level, reaching HDX equilibrium after 451 min. This indicates partial alcohol

denaturation of CypA in the presence of methanol. All investigated CypA-ligand complexes display lower exchange rates and deuterium levels, due to interaction with CypA. Surprisingly ES1234 demonstrates the lowest exchange rate and deuterium level of the three ligands, however close to CsA, displaying a HDX equilibrium after 395 min. This indicates a strong interaction with CypA similar to CsA with a K_d of 30-300 nM. Deuterium levels of CypA-CsA reach HDX equilibrium after 457 min. KM184 exhibits an exchange rate and deuterium level close to apo CypA in 2.3 % MeOH, suggesting a weaker interaction compared to CsA and ES1234 with CypA. HDX equilibrium is reached after approximately 457 min.

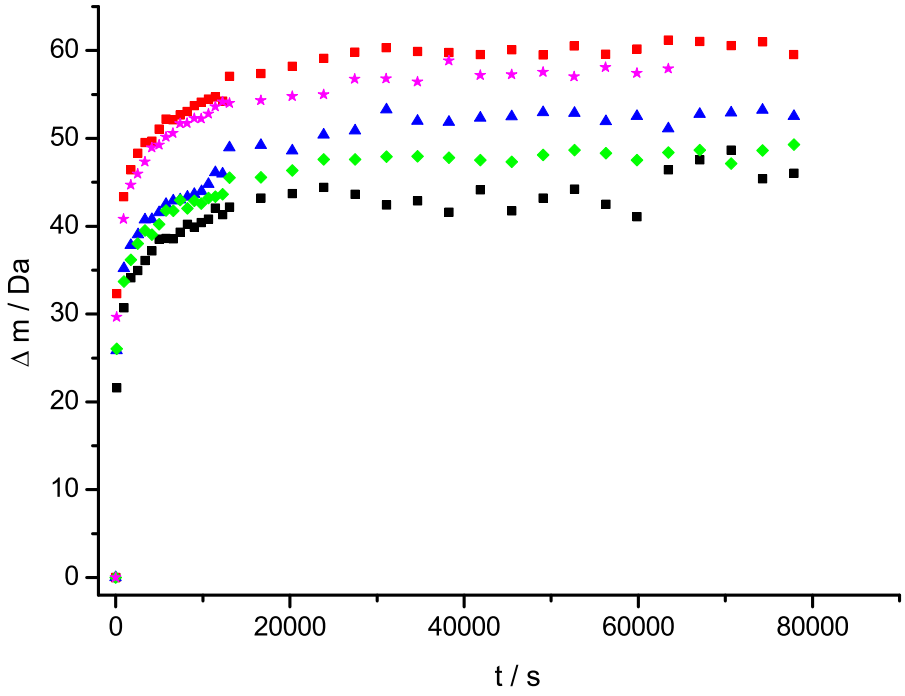

Figure 3.5: Automated CypA HDX labeling. Deuterium uptake *versus* time for apo CypA (black squares), apo CypA in 2.3 % MeOH (red squares), CypA-CsA in 2.3 % MeOH (blue triangle), CypA-ES1234 in 2.3 % MeOH (green diamond) and CypA-KM184 in 2.3 % MeOH (magenta star).

To get an idea about exchange rates and deuterium levels in the presence of the chemical denaturant guanidinium hydrochloride, mass increase over time of CypA complexed with ES1234 at one molar GDH was measured. Figure 3.6 illustrates the HDX profile of CypA-ES1234 at 1 M GDH. The exchange rate and deuterium level is almost twice as much as for the apo enzyme. In comparison with CypA-ES1234

without GDH present, the deuterium level is already higher after 28 min, indicating denaturation.

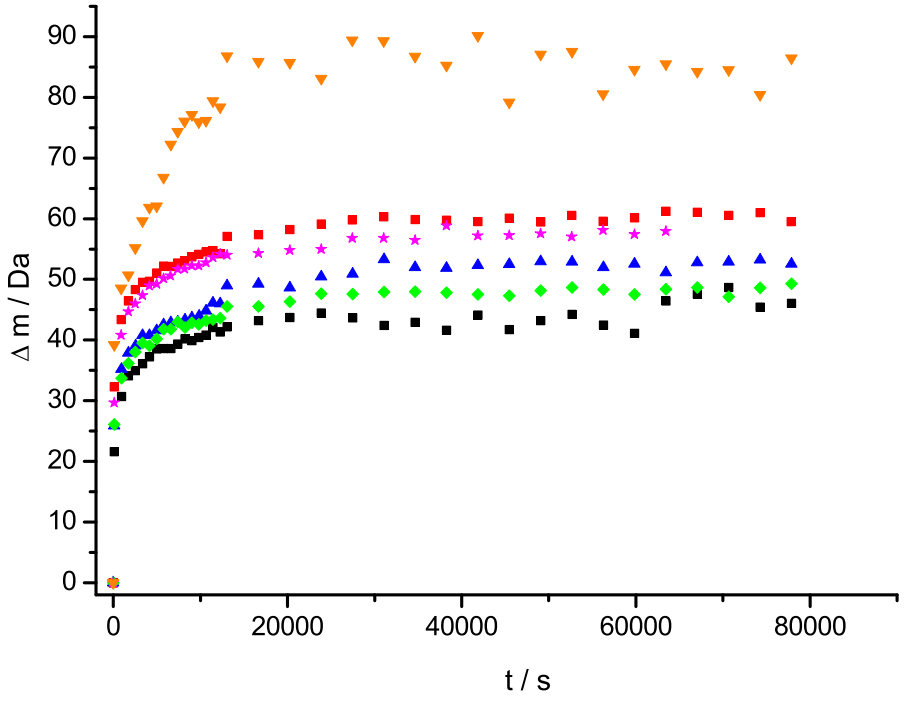

Figure 3.6: Automated CypA HDX labeling. Deuterium uptake *versus* time for apo CypA (black squares), apo CypA in 2.3 % MeOH (red squares), CypA-CsA in 2.3 % MeOH (blue triangle), CypA-ES1234 in 2.3 % MeOH (green diamond), CypA-KM184 in 2.3 % MeOH (magenta star) and CypA-ES1234 in 2.3 % MeOH in 1 M GDH (orange triangle).

3.4 PLIMSTEX - Manual

Manually executed PLIMSTEX experiments employed the devised manual HPLC front end (Section 2.6.3) in conjunction with the Platform II MS. Sample preparation and procedure was undertaken as described in Section 2.6.1 and 2.6.3.
Back exchange and washing time optimisation (Section 2.6.3) resulted in a loading/washing time of 6-9 minutes, with the latter taken for all manual immunophilin-ligand PLIMSTEX experiments to guarantee the best possible accuracy.
Apo CypA subjected to the PLIMSTEX procedure shows a Δm_{free} value of 37.32 $\pm$ 0.33 Da resulting in a mass of 18181 Da for deuterated CypA without any ligand present. Titrating the ligand to the enzyme up to a 20-fold excess of ligand induces a conformational change or a change in stability of the protein and therefore shows

a decrease in deuterium uptake or an increase in protection due to the presence of the ligand. Employing the PLIMSTEX fitting procedure (Section 2.6.5, Appendix 9.8) values for $\Delta m_{complex}$ and Δm_s are determined to 29.69 ± 0.25 Da and 7.60 Da, resulting in a K_a of $3.12 \cdot 10^6 \pm 1.24 \cdot 10^6$ M^{-1} and a K_d of 321 ± 128 nM (Fig. 3.7).

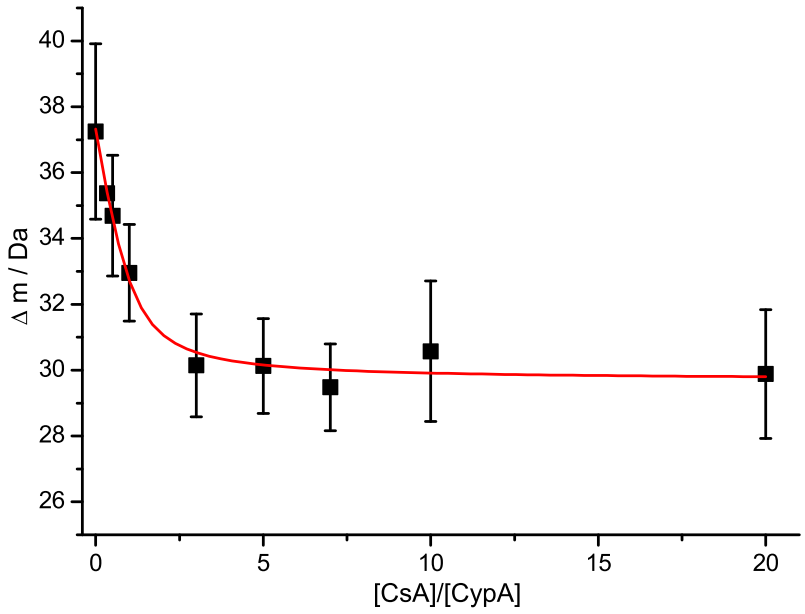

Figure 3.7: Manual CypA-CsA PLIMSTEX data, with Δm_{free} 37.32 ± 0.33 Da, $\Delta m_{complex}$ 29.69 ± 0.25 Da, Δm_s 7.60 Da, K_a $3.12 \cdot 10^6 \pm 1.24 \cdot 10^6$ M^{-1} and a K_d of 321 ± 128 nM. Error bars represent standard deviation from five independent experiments.

Under identical conditions the KM184 ligand was titrated to CypA resulting in Δm_{free} value of 33.35 ± 0.08 Da, $\Delta m_{complex}$ 31.54 ± 0.06 and Δm_s 1.81 Da, resulting in a K_a value of $8.20 \cdot 10^6 \pm 4.84 \cdot 10^6$ M^{-1} and a K_d of 121 ± 71 nM (Fig. 3.8).

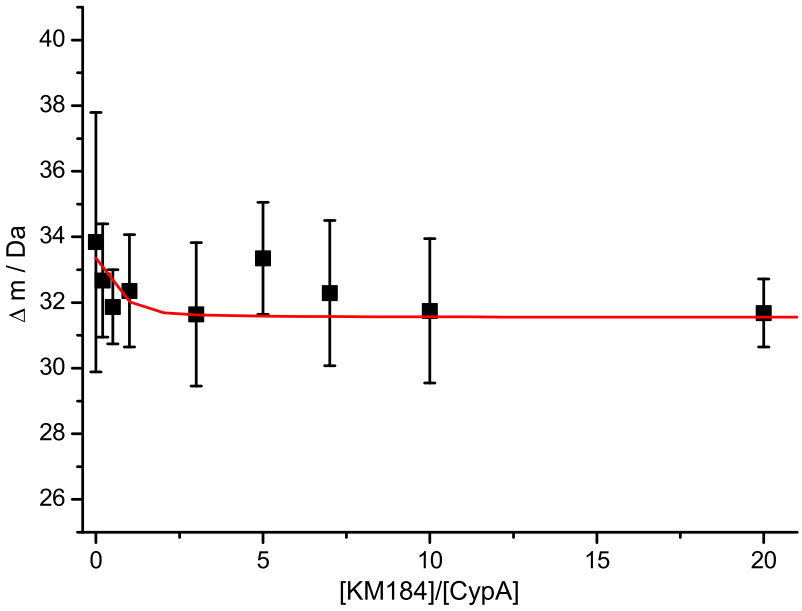

Figure 3.8: Manual CypA-KM184 PLIMSTEX data, with Δm_{free} 33.35 ± 0.08 Da, $\Delta m_{complex}$ 31.54 ± 0.06 Da, Δm_s 1.81 Da, K_a 8.20 · 10^6 ± 4.84 · 10^6 M^{-1} and a K_d of 121 ± 71 nM. Error bars represent standard deviation from four independent experiments.

FKBP12-rapamycin PLIMSTEX experiments yield a deuterated mass of 13311.74 Da resulting in a Δm_{free} value of 35.05 ± 0.08 Da. $\Delta m_{complex}$ and Δm_s values are determined to 28.00 ± 0.05 Da and 7.05 Da culminating in K_a/K_d value of 4.89 · 10^{10} ± 4.83 · 10^6 M^{-1} and 0.02 nM, respectively (Fig. 3.9).

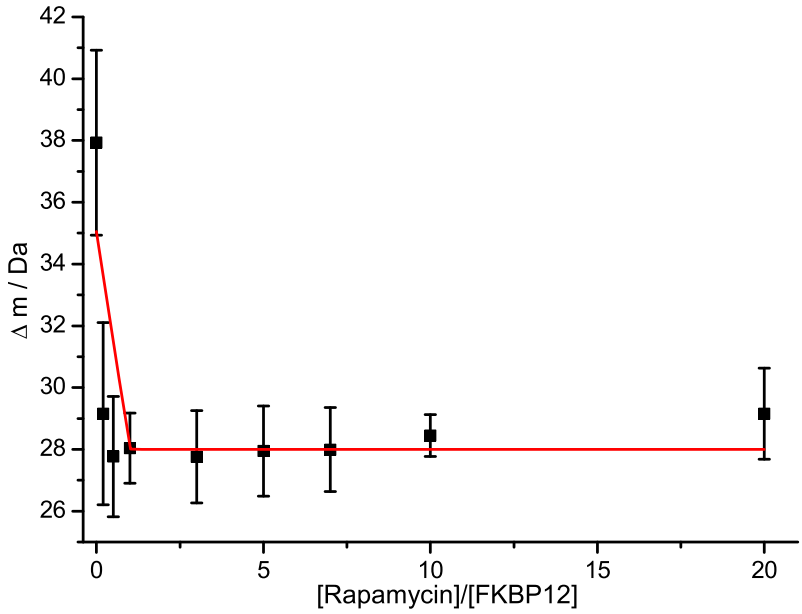

Figure 3.9: Manual FKBP12-Rapamycin PLIMSTEX data, with Δm_{free} 35.05 ± 0.08 Da, $\Delta m_{complex}$ 28.00 ± 0.05 Da, Δm_s 7.05 Da, K_a 4.89 · 10^{10} ± 4.83 · 10^6 M^{-1} and a K_d of 0.02 nM. Error bars represent standard deviation from five independent experiments.

The PLIMSTEX K_d value of 321 nM for CypA-CsA is within one order of magnitude to values reported in the literature (Table 3.2). For KM184 the PLIMSTEX curve (Fig. 3.8) shows a steeper decrease of the deuterium level of CypA suggesting a 'stronger' interaction compared to CsA, which is reflected by the K_d of 121 nM being within two orders of magnitude from values previously reported (Table 3.2). However, a Δm_s of 1.8 Da indicates no increased protection upon ligand presence and with values being within the margin of experimental error no quantitative information can be gained. Data for FKBP12-rapamycin indicates an even 'stronger' interaction as CypA-CsA as the PLIMSTEX curve shows a very rapid decrease of the deuterium level, which is not well represented by the PLIMSTEX fitting procedure (Fig. 3.9). Nevertheless, a calculated K_d of 0.02, which is within two orders magnitude from K_d's reported previously (Table 3.2), emphasises the strong interaction.

Manually timed and executed PLIMSTEX experiments yield a throughput efficiency of ~20 min *per* experiment after a particular incubation time, which was determined to 80 min with regards to showing different deuterium levels for apo

and holo protein, after 20 min incubation of protein and ligand, resulting in a total number of ~14 experiments per day.
As PLIMSTEX relies on conformational changes or a stability change of the protein in presence of the ligand, this change has to be reflected by amide protection, otherwise PLIMSTEX would not be applicable. On that account knowledge of the enzyme-substrate system in question is vital for PLIMSTEX data extraction, as *a priori* screening of unknown protein-ligand systems does not yield any useful data. The success of the method, furthermore, depends on the degree of amide protection due to the presence of the ligand, *id est* the larger the protection the more reliable data can be extracted. Systems investigated by Gross *et al.* (Table 3.1) showed Δm_s values between 12 and 30 Da. *Per contra*, the investigated immunophilin-ligand systems showed Δm_s values between 1.8 and 7.6 Da complicating data analysis, especially for the CypA-KM184 system with Δm_s being 1.81, which is clearly within the error margin of the experiment (Fig. 3.8).
Nevertheless, if some knowledge of the system of interest is present, PLIMSTEX might deliver qualitative information comparing different ligands, provided sufficient protection due to the presence of the ligand occurs.

3.5 PLIMSTEX - Automated

3.5.1 Bulk Incubation

Increased throughput potential was achieved with the developed HPLC-front end (Section 2.6.4). To get a first impression about applicability of the automated approach, PLIMSTEX was performed after bulk incubation of the protein with ligand in the PLIMSTEX buffer. Deviating from the standard PLIMSTEX sample preparation protocol (Section 2.6.1), n+1 sets of PLIMSTEX samples for n sets of experiments were prepared in one sample vial and incubated for two hours to reach near steady state HDX equilibrium (Section 3.3) and subjected analysis. One set of samples describes 11 different ligand-protein ratios (0-20). Thereby one set of samples was investigated from low to high ligand-protein rations and *vice versa*, before analysing the next set of identical samples. This approach resulted in different incubation times over a 24 h period, however, improved the throughput by a factor of three from 14 experiments *per* day to 44.
CypA-CsA PLIMSTEX data acquired with this approach does not exhibit the expected trend as with increasing ligand concentration the protection of amide hydrogen atoms decreases. In theory a PLIMSTEX curve occurs for each set of samples

with only slight differences in Δm due to not reaching steady state conditions. Acquired data, however, shows decreased protection with an increasing CsA ratio, indicating denaturation of CypA by CsA over time, as samples were prepared at a time t_0 and from then on further incubated until analysis (Fig. 3.10a). The effect of not reaching exact steady state HDX conditions is acceptable within $\pm$ 5 Da (Fig. 3.10a), which agrees well with the HDX labeling experiments conducted on CypA-CsA (Section 3.3). This effect was partially counteracted by reversing the order of sample analysis from high to low substrate-enzyme ratios (Fig. 3.10b). A different batch of CypA and freshly prepared CsA stock solutions still resulted in the same findings (Fig. 3.10c, d).

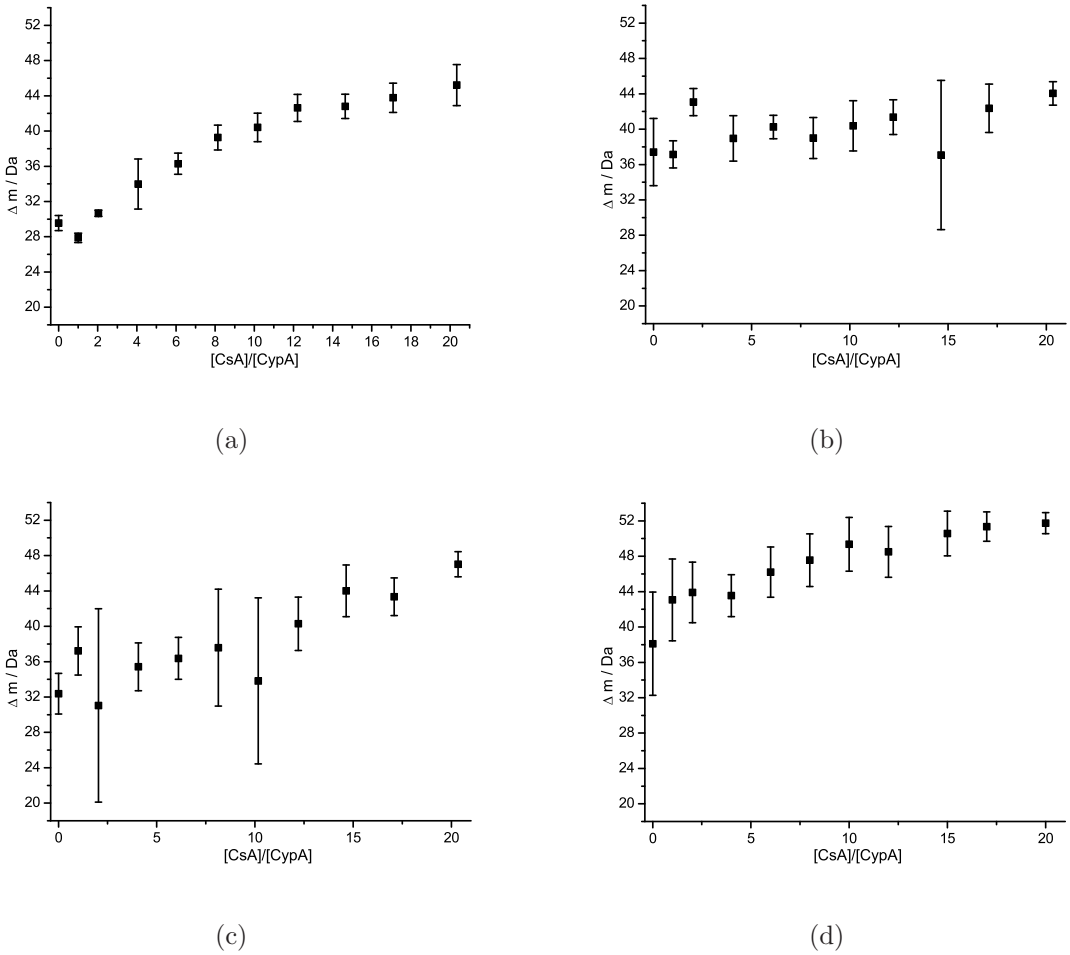

Figure 3.10: Automated PLIMSTEX CypA-CsA bulk incubation. (a) Data acquired from low to high ligand/protein ratios. (b) Data acquired from high to low ligand/protein ratios. (c) Data acquired from low to high ligand/protein ratios using fresh protein and ligand stocks. (d) Data acquired from high to low ligand/protein ratios using fresh protein and ligand stocks. Error bars represent standard deviation of three independent (a, c) and four independent experiments (b, d).

For FKBP12 and rapamycin the same automated experiment was conducted, culminating in controversial PLIMSTEX data.
As Figure 3.11 illustrates, the protection of amide protons increases with increasing ligand-protein ratios, not considering 0 and 0.5 ratios. Fitting PLIMSTEX data, neglecting FKBP12-rapamycin ratios 0, 0.5 and 7, a K_d value of 74.77 ± 7.85 nM is calculated, with Δm_{free} 79.73 ± 2.07, $\Delta m_{complex}$ 35.59 ± 0.05 and K_a $1.34 \cdot 10^7$ ± $0.14 \cdot 10^7$ M^{-1}. The K_d is within one order of magnitude to values previously reported (Table 3.2) and within three orders of magnitude to manually determined PLIMSTEX K_d. Presented data represents averaged data of two individual sets of experiments each executed from low to high ligand-protein ratio and *vice versa* with standard deviation as error bars.
On the contrary FKBP12-rapamycin data exhibits the same trend as CypA-CsA data and only the larger Δm_s value of ~8 Da facilitates the PLIMSTEX fit.

The automated PLIMSTEX approach with bulk incubation of CypA, CsA and PLIMSTEX buffer demonstrates the denaturing capabilities of CsA impeding K_d calculations. For the FKBP12-rapamycin system a dissociation constant of 74.77 ± 7.85 nM is calculated, in contrast to the manually determined PLIMSTEX K_d of 0.02 nM.

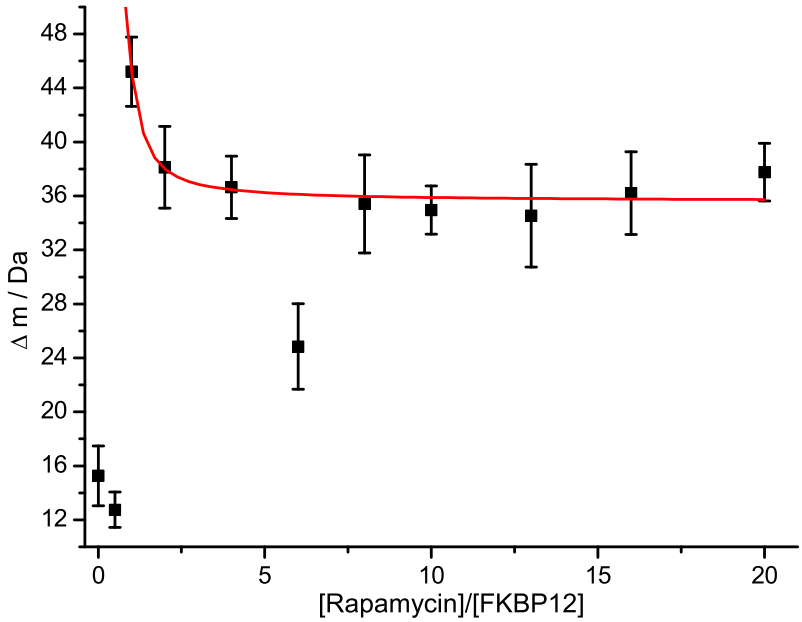

Figure 3.11: Automated FKBP12-rapamycin PLIMSTEX data. Error bars represent standard deviation from four independent experiments. Ligand/protein rations 0, 0.5 and 6 are not included in data fitting.

3.5.2 Individual Incubation

For the CypA-CsA system individually executed automated PLIMSTEX experiments were performed according to the PLIMSTEX protocol in Section 2.6.1 guaranteeing constant protein-ligand incubation times (20 min) and HDX PLIMSTEX buffer incubation (80 min) to circumvent denaturing issues with CsA and guaranteeing equal non-steady state conditions. Four independent sets of runs were performed and analysed. Figure 3.12 visualises individual PLIMSTEX data. Curve fitting results in values for Δm_{free} of 52.11 ± 0.32 Da, $\Delta m_{complex}$ of 47.43 ± 0.08 Da, Δm_s of 4.63 Da, K_a $1.27 \cdot 10^6 \pm 0.26 \cdot 10^6$ M^{-1} and a K_d of 789.4 ± 164.2 nM, whereby ligand-protein ratios 10 and 20 are neglected, 6, 12 and 17 are accounted for 80 % and 0 is weighted for 5 %. The dissociation constant of 789.4 nM is within the same order of magnitude as the manually determined PLIMSTEX K_d and within one order of magnitude to values reported previously (Table 3.2), however, it is questionable as the Δm_s of 4.63 Da is within the margin of the experimental error (Fig. 3.12).

By executing each PLIMSTEX experiment individually, throughput decreases to 12 samples in a 24 h period due to software restrictions in the utilised HPLC control

software, disabling usage of system idle time during HDX incubation periods. Nevertheless, automated sample handling and timing should eliminate manually executed and timed errors.

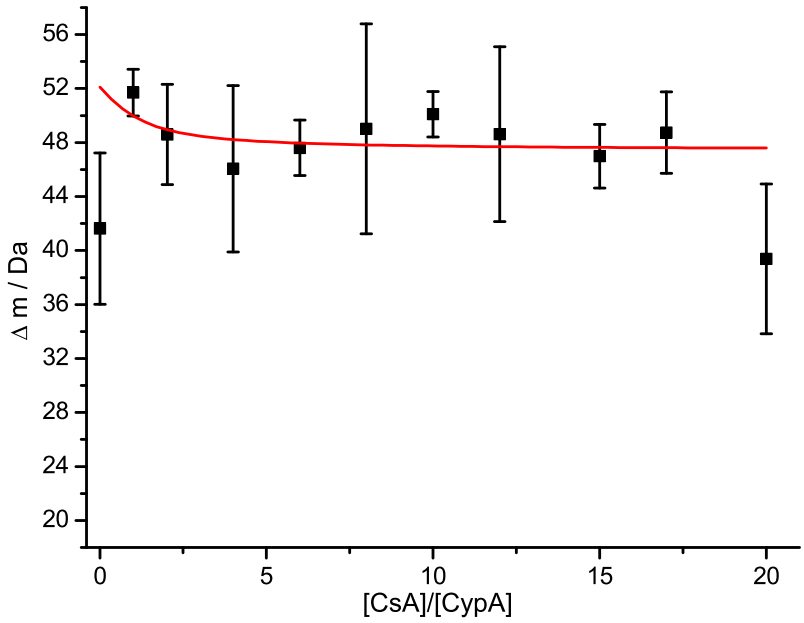

Figure 3.12: Single automated CypA-CsA PLIMSTEX data. Error bars represent standard deviation from four independent experiments. Ligand/protein rations 10 and 20 are not included in data fitting. Ratios 6, 12 and 17 are subjected a weighted fitting procedure and are accounted for 80 %. The starting ratio 0 is weighted to gain Δm_{free} of 52 Da, resulting in a 5 % weighting.

3.6 Cyclophilin A Manual SUPREX

Data in this Section (3.6) was acquired by L. Baillie in fulfilment with her masters degree at the University of Edinburgh and is reproduced with her kind permission.

The developed manual HPLC front end (Section 2.6.3) was utilised in conjunction with the manual SUPREX procedure (Section 2.7.1). The intrinsic exchange rate $\langle k_{int} \rangle$ was calculated to be 5.59 s^{-1} at 22 °C (Section 2.7.5). Sample concentrations throughout were 2 µM for CypA and 4 µM for CsA and ES1234 and GDH was used a denaturant.

SUPREX $C^{1/2}$ values are determined to be 2.20, 1.94, 1.51 and 1.50 M (Table

3.3 and Section 2.7.5) for apo CypA resulting in a ΔG_f value of -28.91 kJmol^{-1} and an m-value of 2.43 kJmol^{-1}M^{-1} (Fig. 3.13a, d). For the CypA-CsA complex midpoints of the SUPREX curve are at 2.76, 2.42, 1.75 and 1.92 M (Table 3.3) with an associated ΔG_f value of -30.84 kJmol^{-1} and a stabilisation of -1.92 kJmol^{-1} with a m value of 2.72 kJmol^{-1}M^{-1}, ultimately resulting in a K_d of 3.3 µM (Fig. 3.13b, d). The inflexion points of the CypA-ES1234 SUPREX curves are determined to be 2.42, 2.50, 1.50 and 1.99 M (Table 3.3), impeding calculation of thermodynamic properties (Fig. 3.13d). Manual SUPREX CypA data is visualised in Table 3.3 and all SUPREX curves at different incubation times are displayed in Appendix 10.3.

SUPREX buffer conditions were chosen to favor EX2 exchange behaviour and two state unfolding behaviour was assumed, as no intermediate species was detected with the instrumentation used. As Figure 3.13 illustrates cyclophilin A is stabilised by the presence of cyclosporin A. For 10, 40 and 60 min incubation $C^{1/2}_{SUPREX}$ values are shifted by 0.56, 0.48 and 0.42 M to higher denaturant concentrations. The pre-transition baseline for the 10 and 40 min incubation of CypA complexed with CsA is lower compared to the free protein indicating increased protection of backbone protons in the complex. In contrast, for the 60 min incubation the pretransition baseline is higher as in the free protein, suggesting denaturation of CypA by CsA over time as concluded in the HDX labeling- (Section 3.3) and bulk incubated PLIMSTEX experiment (Section 3.5.1). Also the decreasing stabilisation over time corroborates this finding.
The calculated K_d of 3.3 µM is within two orders of magnitudes of values presented earlier (Table 3.2) and within one order of magnitude to manual and automated PLIMSTEX results implying that PLIMSTEX better represents protein-ligand properties. SUPREX offers more potential for accuracy, as the change in mass measured upon denaturation is much bigger than Δm_s upon protection/shielding in a PLIMSTEX experiment. The four SUPREX data points for all CypA-ligand complexes are not well represented by the linear curve fit (Fig. 3.13), therefore more data points should be acquired to get more precise thermodynamic data of CypA and its ligands, as the automated SUPREX approach will provide (Section 3.7).
CypA in complex with ES1234 exhibits a slightly weaker stabilisation by 0.22, 0.56 and 0 M for the incubation times 10, 40 and 60 min (Table 3.3). The pre-transition baseline is lower for the 10 min incubation time and the same for 40 and 60 min, suggesting a less denaturating effect on CypA compared to CsA. The four acquired $C^{1/2}_{SUPREX}$ values were not subjected to a linear fitting routine as results would have

been questionable.

Manually timed and executed SUPREX experiments demonstrate similar throughput rates as manual PLIMSTEX experiments with ~14 runs per day.

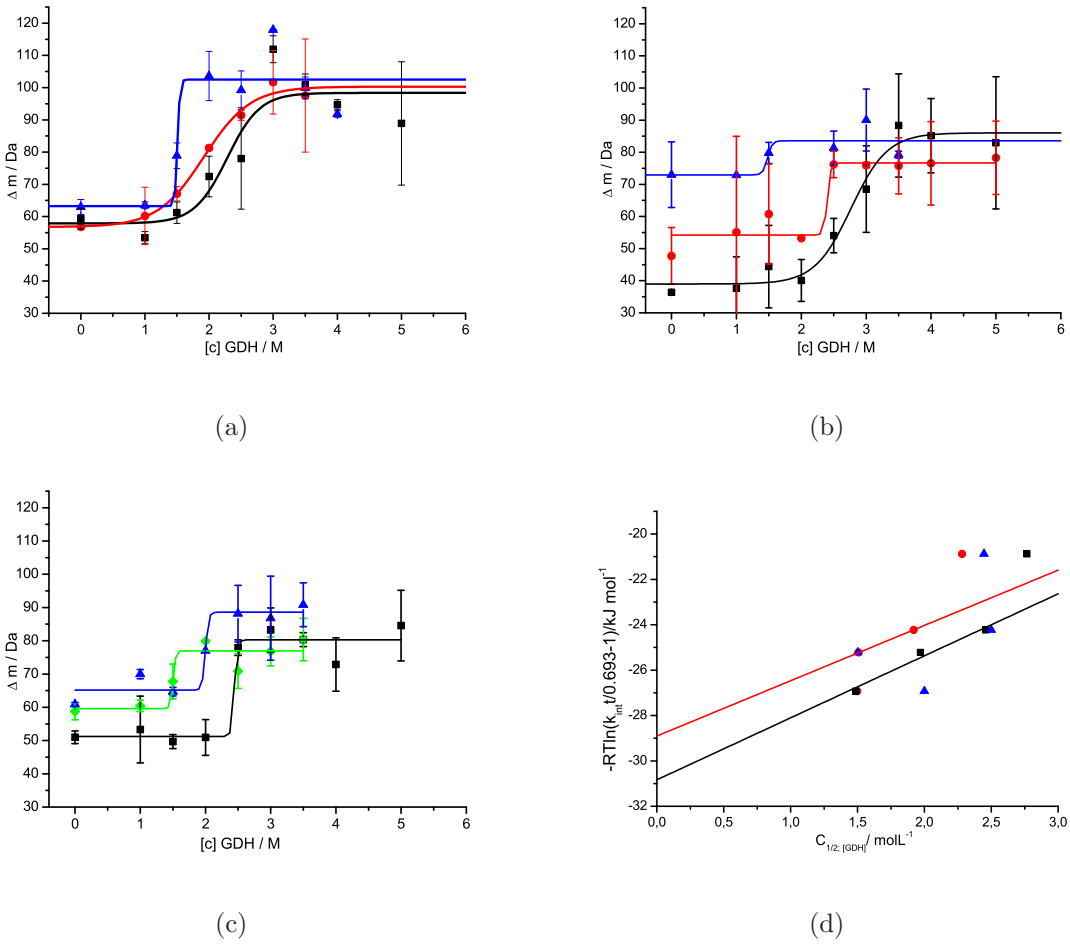

Figure 3.13: Manual CypA-CsA SUPREX data.(a) Apo CypA incubation at 10 (black), 40 (red) and 60 min (blue) with $C^{1/2}_{SUPREX}$ values of 2.20, 1.94 and 1.51 M. (b) CypA-CsA SUPREX incubation at 10 (black), 40 (red) and 60 min (blue) with $C^{1/2}_{SUPREX}$ values of 2.76, 2.42 and 1.75 M. (c) CypA-ES1234 with 10 (black), 60 (blue) and 120 min (green) incubation with $C^{1/2}_{SUPREX}$ values of 2.42, 2.50 and 1.75 M. (d) Free energy *vs.* denaturant concentration plot for CypA (red) CypA-CsA (black) and CypA-ES1234 (blue), resulting in ΔG_f values of -28.91 and -30.84 kJmol^{-1} and m values of 2.43 and 2.72 kJmol^{-1}M^{-1} for apo CypA and CypA-CsA, respectively. $\Delta\Delta G_f$ for the CypA-CsA complex is -1.92 kJmol^{-1}, resulting in a K_d of 3.3 µM. All error bars represent standard deviation of 2 runs.

Table 3.3: Manual CypA SUPREX results.

Incubation time/min	Apo CypA	CypA-CsA $C_{SUPREX}^{1/2}$ [a] /M	CypA-ES1234
10	2.20	2.76	2.42
40	1.94	2.42	2.50
60	1.51	1.75	1.50
120	1.50	1.92	1.99
ΔG_f/kJmol^{-1}	-28.91	-30.84	N/A
$\Delta\Delta G_f$/kJmol^{-1}		-1.92	N/A
m/kJmol^{-1}M^{-1}	2.43	2.72	N/A
K_d/µM		3.3	N/A

[a] visualised in Fig. 3.13 and Appendix 10.3, 10.4 and 10.5.

3.7 SUPREX - Automated

After the automated method for ESI-SUPREX was devised (Section 2.7.3) and exchange- and back exchange behaviour was optimised with HHM (Section 2.7.6), CypA was further investigated with potential binding ligands. An automated SUPREX approach with self created/timed sample lists doubled the throughput to 33 apo and 21 holo samples in a 24 h period.

3.7.1 Apo Cyclophilin A

Apo CypA was subjected the automated SUPREX methodology (Section 2.7.3) and $C_{SUPREX}^{1/2}$ values for incubation times 10, 15, 30, 45, 60, 90, 120, 150, 180 and 420 min are determined (Table 3.4). Figure 3.14a illustrates 10 and 60 min incubation and the induced shift to lower denaturation concentrations at increased exposure. The complete set of SUPREX curves is displayed in Appendix 10.6. The deuterium level pre-transition is ~25 Da and post-transition ~55 Da, resulting in a 30 Da increase in mass upon denaturation. Due to different flow rate settings and washing times, deuterium levels are lower in the automated approach, compared to the manual approach (Section 3.6), however, the deuterium uptake upon deuteration is similar, indicating identical pre- and post-transition CypA species. Plotting $C_{SUPREX}^{1/2}$ *vs.* ΔG_f with $\langle k_{int} \rangle$ being 5.59 s^{-1} at 22 °C, for all further CypA SUPREX experiments, results in a free energy of protein folding of -32.43 ± 1.88 kJmol^{-1} (Fig. 3.14b). The abscissa related errors in Figure 3.14b represent the standard error associated with the non-linear curve fitting procedure of $C_{SUPREX}^{1/2}$ values, whereas the ΔG_f associ-

ated error reflects the standard error of the linear fit. The m value is calculated to 12.38 ± 3.01 kJmol^{-1}M^{-1}.

In comparison ESI-SUPREX ΔG_f values are within those obtained by MALDI-SUPREX and SPROX by Fitzgerald *et al.* for purified apo CypA -47.28 ± 2.93 kJmol^{-1} and unpurified apo CypA -39.33 ± 0.84 kJmol^{-1} [268] and -19.25 ± 1.67 kJmol^{-1} [269] for apo CypA. Differences in ΔG_f values might be the result of comparing different protein species in different environments, as purified and unpurified CypA samples show ΔG_f differences of 7.95 kJmol^{-1}, mainly attributed to the protein mix of the unpurified sample. Different buffer conditions also affect relative protein stability and in this thesis solely 10 mM NH_4OAc was utilised, however, Fitzgerald and co-workers solely employed 20 mM sodium phosphate. SUPREX derived ΔG_f and m values are not meaningful in themselves, however, relative changes in ΔG_f are used to calculate comparative dissociation constants.

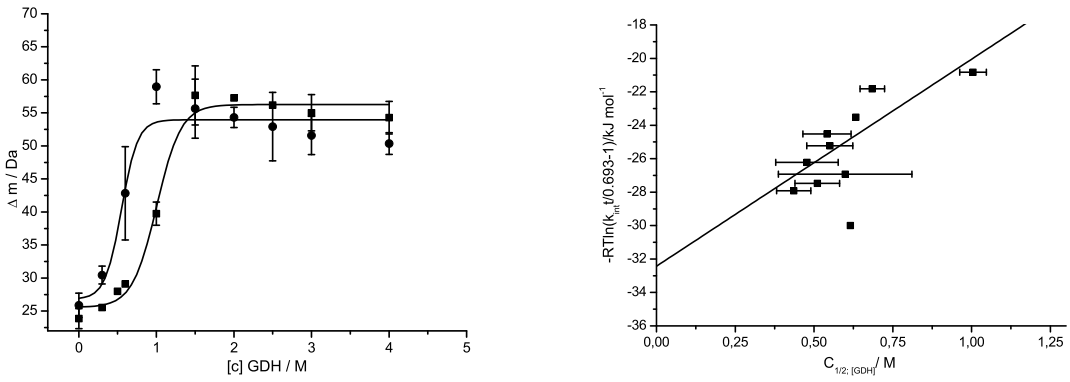

(a) (b)

Figure 3.14: Automated apo CypA SUPREX data. (a) SUPREX curves at 10 and 60 min incubation with $C^{1/2}_{SUPREX}$ values 1.00 and 0.55 M respectively. Error bars represent standard deviation from two independent experiments. (b) Free energy of protein folding *vs.* $C^{1/2}_{SUPREX}$. ΔG_f is determined to -32.43 ± 1.88 kJmol^{-1} and m to 12.38 ± 3.01 kJmol^{-1}M^{-1}. Error bars represent standard error from fitting SUPREX curves.

3.7.2 Cyclophilin A-2.3 % MeOH

All immunophilin ligands were dissolved in 36.88 % methanol, resulting in a final methanol ratio of 18 % for the enzyme-substrate incubation and 2.3 % for the protein-ligand system in the HDX/SUPREX/PLIMSTEX-buffer. Therefore thermodynamic properties of apo CypA were determined under these very conditions. Methodology and sample preparation did not deviate from previous de-

scriptions (Section 2.7.3), with 2.3 % MeOH/10 mM NH_4OAc without any ligand. All SUPREX curves for apo CypA in 2.3 % MeOH are illustrated in Appendix 10.7. ΔG_f values determined for apo CypA in the presence of 2.3 % MeOH indicate a stabilisation as $C^{1/2}_{SUPREX}$ values are shifted to higher denaturant concentrations by 0.27, 0.39, 0.34 and 0.34 M for incubation times 10, 30, 60 and 120 min, respectively (Fig. 3.15a and Table 3.4). The pre-transition baseline illustrates an increased deuterium level by about 10 Da for 30 min incubation, or a decreased protection of amide protons suggesting alcohol denaturation of CypA in the presence of methanol. HDX labeling experiments (Section 3.3) support this findings (Fig. 3.5). The post-transition baseline also shows elevated deuterium levels for all incubation times but 10 min.

The free energy of protein folding is calculated to be -38.74 ± 5.06 kJmol^{-1} resulting in a stabilisation of -6.32 ± 5.40 kJmol^{-1} and a m value of 14.14 ± 4.60 kJmol^{-1}M^{-1}. The increased m value in the 2.3 % MeOH containing CypA apo sample compared to the pure buffer indicates an increased surface exposure of the protein, further confirming a more unfolded state of CypA with a different $C^{1/2}_{SUPREX}$ value.

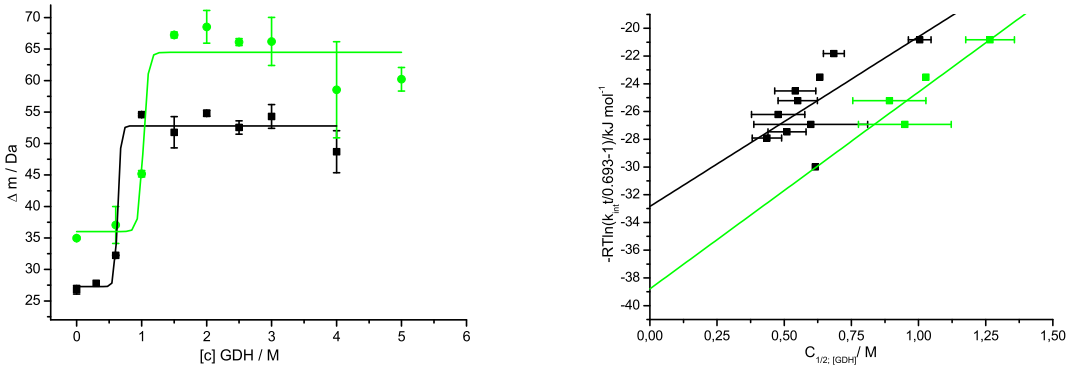

(a) (b)

Figure 3.15: Automated CypA-2.3 % MeOH SUPREX data. (a) SUPREX curves at 30 min incubation for apo CypA (black) and CypA-2.3 % MeOH (green) with $C^{1/2}_{SUPREX}$ values 0.63 and 1.03 M respectively. Error bars represent standard deviation from two independent experiments. (b) Free energy of protein folding *vs.* $C^{1/2}_{SUPREX}$. ΔG_f is determined to -32.43 ± 1.88 kJmol^{-1} and m to 12.38 ± 3.01 kJmol^{-1}M^{-1} for apo CypA (black) and -38.74 ± 5.06 kJmol^{-1} and m to 14.14 ± 4.60 kJmol^{-1}M^{-1} for CypA-2.3 % MeOH (green). Error bars represent standard error from fitting SUPREX curves.

3.7.3 Cyclophilin A-Cyclosporin A

Thermodynamic parameters for CypA-CsA are determined according to Table 3.4 for incubation times from 10 to 420 min. SUPREX curves for 10 min incubation can be found in Figure 3.16, whereas the complete set of curves is visualised in Appendix 10.8.

The free energy of protein folding is determined to be -44.48 ± 4.35 kJmol^{-1} resulting in a stabilisation of -12.05 ± 4.73 kJmol^{-1}, compared to apo CypA. Figure 3.16a emphasises the strength of the CypA-CsA interaction as for the 10 min incubation the stabilisation is 1.57 M (Table 3.4). Average shifts of $C_{SUPREX}^{1/2}$ values are between 1.57 and 2.39 M. The m value is calculated to 7.11 ± 1.63 kJmol^{-1}M^{-1}, exhibiting less surface exposure of CypA in complex with CsA during the unfolding process compared to the free protein (Section 3.7.1). The dissociation constant is determined to 596.7 ± 234.7 nM.

The deuterium level of the pre-transition baseline is similar for all CypA and CypA-CsA curves, however, the post-transition baseline is slightly lower for the CypA-CsA complex compared to the free protein, indicating a more compact structure of CypA in the complex. The lower m value of 7.11 ± 1.63 kJmol^{-1}M^{-1}, compared to the free CypA, further indicates less solvent exposure due to a more compact state.

The longest incubation time investigated is 180 min in the presence of CsA, beyond that incubation time no CypA could be detected due to degradation.

The K$_d$ of 596.7 ± 234.7 nM determined is within the same order of magnitude as manual and automated PLIMSTEX experiments and shows better accuracy than manual SUPREX (Section 3.6) as a comparison of Figure 3.13d and 3.16b illustrates. Reported values for ΔG_f and $\Delta\Delta G_f$ by Fitzgerald and co-workers are -64.85 ± 2.93 and -58.99 ± 3.34 kJmol^{-1} and -17.57 ± 4.2 and -19.66 ± 3.35 kJmol^{-1}, for purified and unpurified CypA, respectively [268] and thereby 1.5 times larger than ESI-SUPREX values. As different buffer conditions explain the discrepancy of absolute ΔG_f values, however, resulting $\Delta\Delta G_f$ values are within the error associated with the SUPREX approach as emphasised by reported values and uncertainties culminating in the differences in reported dissociation constants.

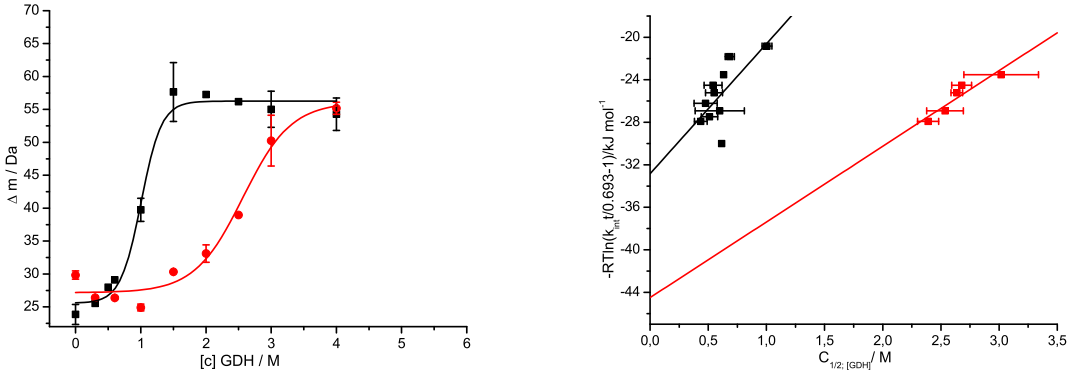

(a) (b)

Figure 3.16: Automated CypA-CsA SUPREX data. (a) SUPREX curves at 10 min incubation for apo CypA (black) and CypA-CsA (red) with $C^{1/2}_{SUPREX}$ values 1.00 and 2.57 M respectively. Error bars represent standard deviation from two independent experiments. (b) Free energy of protein folding *vs.* $C^{1/2}_{SUPREX}$. ΔG_f is determined to -32.43 ± 1.88 kJmol^{-1} and m to 12.38 ± 3.01 kJmol^{-1}M^{-1} for apo CypA and -44.48 ± 4.35 kJmol^{-1} and m to 7.11 ± 1.63 kJmol^{-1}M^{-1} for CypA-CsA (red). Error bars represent standard error from fitting SUPREX curves.

3.7.4 Cyclophilin A-KM184

Automated SUPREX curves for CypA-KM184 at 30 min incubation time are illustrated in Figure 3.17a, whereas the complete set of curves is illustrated in Appendix 10.9.

ΔG_f is determined to -35.52 ± 1.46 kJmol^{-1} with a stabilisation of -3.10 ± 2.38 kJmol^{-1} compared to uncomplexed CypA (Fig. 3.17b). The m value is determined to 10.25 ± 1.34 kJmol^{-1}M^{-1}, culminating in a K_d of 32.4 ± 24.9 µM. The $C^{1/2}_{SUPREX}$ values exhibit smaller shifts to higher denaturant concentrations, compared to free CypA indicating a weaker interaction between CypA and KM184, relatively, in comparison with the CypA-CsA system (Table 3.4). This is assisted by the m value, as this is smaller as for the uncomplexed protein, but higher as in the CypA-CsA complex. The K_d of 32.4 ± 24.9 µM is within the margin of error of the SPR and fluorescence determined K_d's and within one order of magnitude to *in vivo* and DI-ESI-MS values.

Deuterium levels of the pre-transition baseline demonstrate higher deuterium uptake of the KM184 complexed CypA, suggesting a more unfolded conformation before denaturation. In contrast, the post-transition baseline reveals a more compact conformation, as deuterium levels are lower than in the apo protein.

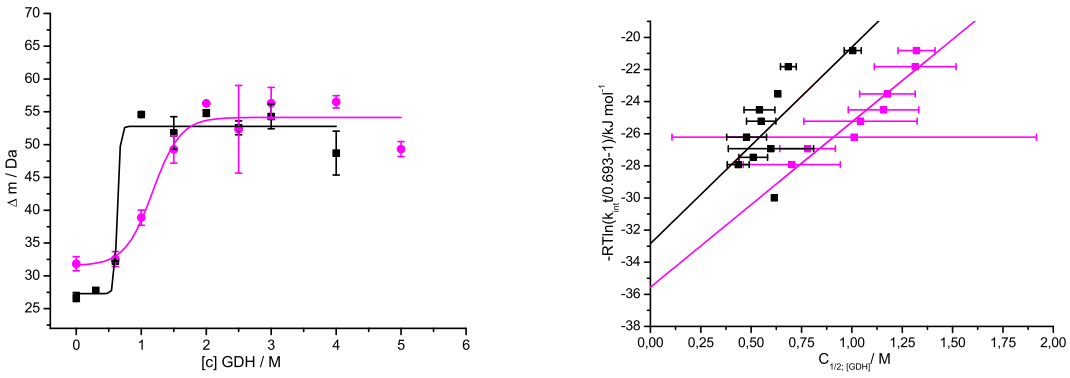

(a) (b)

Figure 3.17: Automated CypA-KM184 SUPREX data. (a) SUPREX curves at 30 min incubation for apo CypA (black) and CypA-KM184 (magenta) with $C_{SUPREX}^{1/2}$ values 0.63 and 1.18 M respectively. Error bars represent standard deviation from two independent experiments. (b) Free energy of protein folding *vs.* $C_{SUPREX}^{1/2}$. ΔG_f is determined to -32.43 ± 1.88 kJmol^{-1} and m to 12.38 ± 3.01 kJmol^{-1}M^{-1} for apo CypA (black) and -35.52 ± 1.46 kJmol^{-1} and m to 10.25 ± 1.34 kJmol^{-1}M^{-1} for CypA-KM184 (magenta). Error bars represent standard error from fitting SUPREX curves.

3.7.5 Cyclophilin A-ES1234

SUPREX data for CypA in complex with ES1234 is shown for 30 min incubation in Figure 3.18b, all other incubation times are displayed in Appendix 10.10.
Individually $C_{SUPREX}^{1/2}$ values show stabilisation from 0.21 to 0.55 M to higher guanidinium hydrochloride concentrations over an incubation time from 10 to 90 min. However, absolute changes of $C_{SUPREX}^{1/2}$ are not as big as observed with other immunophilin ligands, resulting in little change of the $C_{SUPREX}^{1/2}$ values over time. This dramatically affects ΔG_f, calculated to be -47.86 ± 10.84 kJmol^{-1} and a resulting stabilisation of -15.44 ± 11.00 kJmol^{-1}. The calculated K_d of 149.9 ± 106.8 nM is the lowest, determined for the immunophilin ligands and is even lower than the CypA-CsA K_d, in contrast with biological assays and DI-ESI-MS (Table 3.4). Where K_d's between 19.5 and 270 µM have been reported, differing between two to three orders of magnitude. Figure 3.18b shows the steepest slope for the ΔG_f-fit of the investigated immunophilin ligands, resulting in a high m value of 22.51 ± 10.04 kJmol^{-1}M^{-1}, suggesting either higher exposure of CypA upon unfolding compared to other CypA-ligands or non-two state unfolding of CypA in the presence of ES1234 or observed ligand fragments (Fig. 3.3).

Deuterium levels of the pre-transition baseline are comparable with those of the uncomplexed cyclophilin, whereas the posttransition baseline shows similar levels up to 30 min incubation and then decreasing levels, similar to those of the CypA-CsA complex. This phenomenon and the fact of lower $\Delta C^{1/2}_{SUPREX}$ compared to CsA, suggests a non-two state unfolding behaviour of CypA in the presence of the ES1234 ligand. Labeling experiments of CypA with the immunophilin ligands (Section 3.3) further supports the findings as deuterium levels of CypA-ES1234 are lower, compared to CypA-CsA which suggests less surface exposure prior to denaturation.

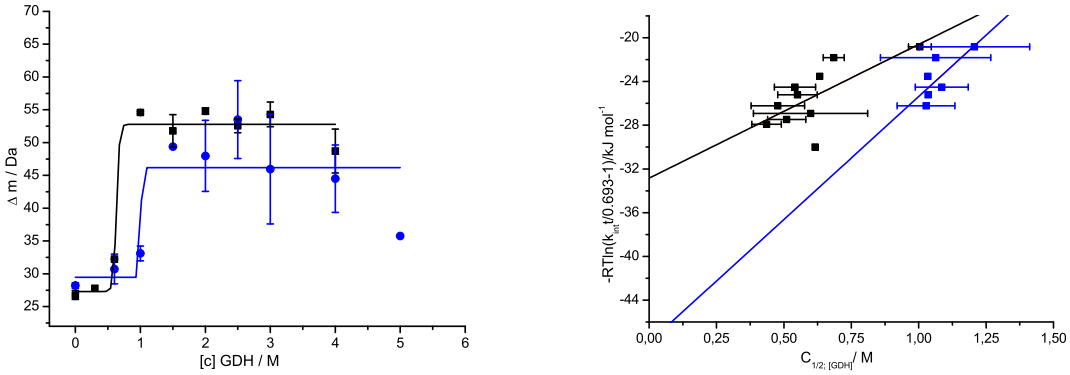

(a) (b)

Figure 3.18: Automated CypA-ES1234 SUPREX data. (a) SUPREX curves at 30 min incubation for apo CypA (black) and CypA-ES1234 (blue) with $C^{1/2}_{SUPREX}$ values 0.63 and 1.03 M respectively. Error bars represent standard deviation from two independent experiments. (b) Free energy of protein folding *vs.* $C^{1/2}_{SUPREX}$. ΔG_f is determined to -32.43 $\pm$ 1.88 kJmol^{-1} and m to 12.38 $\pm$ 3.01 kJmol^{-1}M^{-1} for apo CypA (black) and -47.86 $\pm$ 10.84 kJmol^{-1} and m to 22.51 $\pm$ 10.04 kJmol^{-1}M^{-1} for CypA-ES1234 (magenta). Error bars represent standard error from fitting SUPREX curves.

3.8 Denaturant Effect on HD-Exchange Behavior

The SUPREX experiments conducted with CypA and ligands show a decrease in the deuterium level at high concentrations with the chemical denaturant guanidinium hydrochloride. Tanford *et al.* [64] proposed that interactions of the denaturant with the protein are more favorable than interactions of the protein with water. Therefore a decrease in HDX with increasing GDH concentration would agree with these findings. Myers and co-workers demonstrated that GDH is twice as effective as urea in denaturation experiments [66], therefore a denaturing experiment of CypA with urea would clarify the decrease of the deuterium level.

Table 3.4: Automated CypA SUPREX results (values in brackets denote shift in $C^{1/2}_{SUPREX}$ due to stabilisation compared to apo CypA).

Incubation time/min	Apo CypA[a]	CypA-MeOH[b]	CypA-CsA[c] $C^{1/2}_{SUPREX}$/M	CypA-KM184[d]	CypA-ES1234[e]	Apo CypA in Urea[f]
10	1.00	1.27 (0.27)	2.57 (1.57)	1.32 (0.32)	1.21 (0.21)	
15	0.68		2.39 (1.71)	1.31 (0.63)	1.06 (0.38)	
30	0.63	1.02 (0.39)	3.02 (2.39)	1.17 (0.54)	1.03 (0.40)	
45	0.54		2.68 (2.14)	1.16 (0.62)	1.09 (0.55)	
60	0.55	0.89 (0.34)	2.64 (2.09)	1.04 (0.49)	1.03 (0.48)	2.64
90	0.48			1.01 (0.53)	1.03 (0.55)	
120	0.60	0.94 (0.34)	2.53 (1.93)	0.78 (0.18)		
150	0.51					
180	0.44		2.39 (1.95)	0.70 (0.26)		
420	0.62					
ΔG_f/kJmol^{-1}	-32.43 ± 1.88	-38.74 ± 5.06	-44.48 ± 4.35	-35.52 ± 1.46	-47.86 ± 10.84	
$\Delta\Delta G_f$/kJmol^{-1}		-6.32 ± 5.40	-12.05 ± 4.73	-3.10 ± 2.38	-15.44 ± 11.00	
m/kJmol^{-1}M^{-1}	12.38 ± 3.01	14.14 ± 4.60	7.11 ± 1.63	10.25 ± 1.34	22.51 ± 10.04	
K_d			596.7 ± 234.7 nM	32.4 ± 24.9 µM	149.9 ± 106.8 nM	

[a] visualised in Section 3.7.1 Fig. 3.14 and Appendix 10.6.
[b] visualised in Section 3.7.2 Fig. 3.15 and Appendix 10.7.
[c] visualised in Section 3.7.3 Fig. 3.16 and Appendix 10.8.
[d] visualised in Section 3.7.4 Fig. 3.17 and Appendix 10.9.
[e] visualised in Section 3.7.5 Fig. 3.18 and Appendix 10.10.

The conducted SUPREX experiment with the automated setup (Section 2.7.3) of apo CypA denatured with urea is visualised in Figure 3.19. Deuterium uptake *vs.* denaturant concentration was measured for urea concentrations between 0 and 8 M at a single incubation time of 60 min. Evaluation reveals a $C_{SUPREX}^{1/2}$ value of 2.64 (Table 3.4), shifted by 2.09 M to higher denaturant concentrations compared to apo CypA denaturation with GDH.

Interestingly, the deuterium level of the pre-transition baseline is slightly higher in the urea denaturation with 33 Da, compared to 25 Da in the GDH SUPREX experiment, resulting in a difference of ~8 deuterons (Fig. 3.19), under identical experimental conditions. The same trend is observed for the post-transition baseline, being 55 Da for GDH- and 70 Da for urea-denaturation, culminating in a difference of 15 Da. The change in protection upon unfolding is similar, with 30 Da and 35 Da for GDH and urea, respectively, suggesting pre- and post-denatured CypA species are identical in both denaturation experiments.
This comparison emphasises the higher denaturation efficiency of GDH over urea at the expense of lower deuterium levels due to a stronger interaction of denaturant molecules with the protein, reducing HDX rates and efficiency.

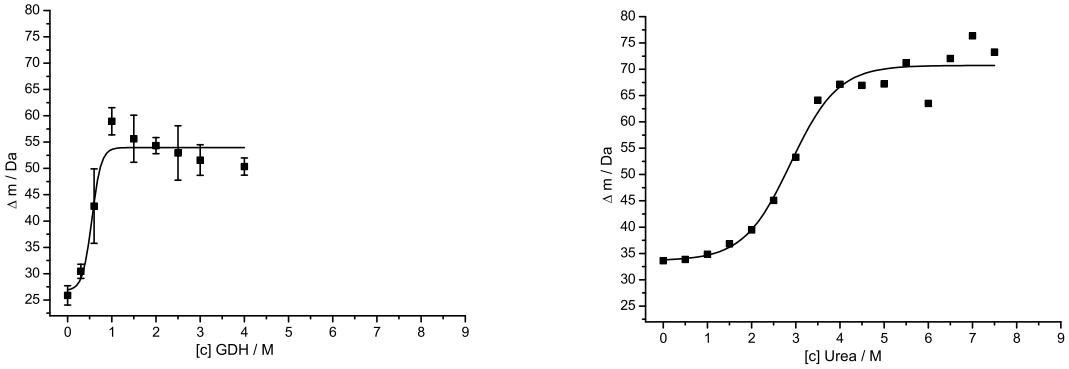

(a) (b)

Figure 3.19: Automated CypA SUPREX with urea. (a) SUPREX curve for 60 min incubation of apo CypA with GDH denaturation. $C_{SUPREX}^{1/2}$ is 0.55 M, error bars represent standard deviation from two independent runs. (b) SUPREX curve for apo CypA urea denaturation at 60 min incubation with $C_{SUPREX}^{1/2}$ 2.89 M. Data represents a single experiment.

3.9 Conclusion

In conclusion, apo masses for all the undeuterated immunophilin proteins used have been determined as well as free ligand masses, showing good agreement with theoretical calculated average masses. DI-ESI-MS experiments confirm ligand binding for cyclosporin A, KM184 and rapamycin as well as the activity of the self purified cyclophilin A. Under the same conditions DI-data of cyclophilin with the ES1234 ligand does not exhibit any intact protein-ligand complex, rather CypA complexed with fragments/degraded ligand with masses of 287.7 and 230.81 Da, respectively. Intact ES1234 is observed sprayed from solely methanol containing 5 % FA identifying the intact ligand as the major component in the sample. The reason for this discrepancy is not clear.

Hydrogen deuterium labeling experiments emphasise the partially denaturating effect of methanol present at final concentrations of 18 % for protein-ligand incubation and 2.3 % for incubation with the deuterated buffer. Despite this, all immunophillin ligands investigated display more protection of amide protons compared to the apo CypA sample in 2.3 % MeOH. Thereby CsA and ES1234 show similar exchange rates and ES1234 slightly lower deuterium levels, suggesting a similar, if not stronger, binding potential to CypA. The investigation of KM184 exhibits a similar exchange pattern as the apo CypA in 2.3 % MeOH, indicating a weaker interaction compared to CsA and ES1234 upon fewer protection. Adding the chemical denaturant to the CypA-ES1234 complex reveals hydrogen deuterium exchange patterns for the denaturation process, demonstrating an additional deuterium incorporation or deprotection of 30-40 deuterium atoms.

Manually timed and executed PLIMSTEX experiments exhibit a qualitative nature of acquired data, with K_d's within one to two orders of magnitude of the values previously reported. Important for reliable PLIMSTEX data is that investigated protein-ligand systems show a sufficient degree of protection of amide protons in the presence of the ligand. Unfortunately the immunophilins investigated show little protection upon ligand binding complicating PLIMSTEX data analysis. Nevertheless, with extensive knowledge of the enzyme-substrate system in question and tedious setup optimisation a qualitative trend of relative ligand affinity is demonstrated.

The automated PLIMSTEX application with bulk incubation of CypA, CsA and PLIMSTEX buffer does not provide reliable PLIMSTEX data on grounds of different incubation times for each individual sample. Incubation at near steady state HDX conditions exhibits accountable deviations in deuterium levels of the protein. *Per contra*, the denaturing properties of CsA prohibit bulk incubation as steady state HDX occurs within a couple of hours and the data acquired would represent a questionable native state of the protein. The low Δm_s value of CypA also contributes to this finding, whereas a higher Δm_s value found for FKBP12-rapamycin culminates in a determinable K_d. Bulk incubation shows three times higher throughput rates compared to the manual approach and therefore would be favorable.
Individually incubated automated PLIMSTEX experiments circumvent non equilibrium HDX states and denaturing issues at the expense of decreased throughput rates. Denaturation of CypA by CsA still occurrs, however, it is put into perspective by identical incubation times. Throughput rates decreased to 12 samples in a 24 h period, however, guaranteeing constant sample handling and incubation times. Once more, automated PLIMSTEX emphasises how little protection of the amide protons is attributed to CypA upon ligand binding, resulting in a K_d in the same order of magnitude as the manually determined, and within one order of magnitude to values previously reported (Table 3.2).

Manual SUPREX results clearly indicate a stabilisation of CypA by binding to CsA for all incubation times. However, relative stabilisation decreases from low to high incubation times emphasising the denaturing character of CsA over time, as bulk incubated PLIMSTEX experiments suggest. This is further supported by comparing the pretransition baseline of apo and CsA complexed CypA as protection of backbone protons decreases over time, when CsA present. The calculated dissociation constant is within two order of magnitudes of data previously presented and within one order of magnitude of PLIMSTEX K_d's. SUPREX offers better potential for data accuracy as measured changes in mass are bigger upon unfolding as protection upon complexation. Automation will increase throughput and accuracy of determined dissociation constants as more data points become available.

Automated SUPREX for the CypA-CsA complex exhibits good data reproducibility and accuracy within reported margins for SUPREX. However, different CypA species show different thermodynamical properties, therefore recombinant human cyclophilin A comprising an additional N-terminal methionine, complexed

with CsA demonstrates good agreement with data previously reported. The pre-and post-transition baselines and the $C^{1/2}_{SUPREX}$ values of CypA incubated in 18/2.3 % methanol reveal a denaturing and stabilising effect. The solely denaturating properties of CsA, determined in the manual SUPREX approach is not supported by automated SUPREX data, as relative stabilisation and m values expose. In complex with KM184, CypA displays binding properties very close to results determined with biological and other biophysical assays. Contextualising ES1234-CypA results would suggest a stronger interaction of CypA with ES1234 than CsA judged on the differences of the free energy of protein folding, which is contrasted by the lower absolute stabilisation of the individual SUPREX curves. This could also reveal a non-two state unfolding behaviour for CypA in the presence of ES1234.
The automated ESI-SUPREX methodology developed demonstrates the capability of K_d determination within a reasonable margin to previously reported values. Deviations might indicate that basic SUPREX assumptions of two state unfolding and EX2 HDX conditions are not fulfilled. Meeting this criteria is crucial to gain useable data from SUPREX derived methods, making it a very system-dependent method unable to deliver accurate binding data on *a priori* screening approaches of unknown protein ligand systems. Nevertheless, with well investigated and well behaved enzyme-substrate systems good quality data can be achieved.
In terms of throughput, the developed ESI-MS-SUPREX approach utilises 5.5 days for a complete screen of the apo protein in question comprising ten duplicate runs, each run comprising nine experiments and 8.5 days for the holo system. Increased throughput can be achieved at the expense of accuracy by decreasing the number of different incubation times down to a single point SUPREX experiment for screening a ligand library as performed by Fitzgerald and co-workers.

A comparison of apo CypA denatured in a SUPREX experiment with guanidinium hydrochloride and urea reveals that decreasing post-transition deuterium levels are specific to denaturation with GDH. Furthermore a higher denaturation efficiency of GDH over urea at the expense of lower deuterium levels in general, has been demonstrated. However, changes in protection upon unfolding are similar, suggesting identical CypA species pre- and post-transition with both denaturants.

4 SUPREX of AGr2 and FH19-20

4.1 Introduction

This chapter describes the use of automated SUPREX (Section 2.7.3) for screening the 'unknown' protein-ligand systems AGr2 and FH19-20 and potential binding ligands. Anterior gradient 2 from biological samples (as described in Section 1.4.3) was positively identified by Myung *et al.* [285] in 2008 by MS analysis. Thereby two dimensional gel electrophoresis, in gel digestion and MALDI analysis revealed a 100 % sequence coverage.

In 2007 Hupp *et al.* [286] demonstrated the binding capabilities of a short hexa-peptide PTTIYY to AGr2 utilising a microarray assay based on the usage of peptide aptamers. Based on these findings, peptide variants were developed to probe binding properties with AGr2. Peptides such as RRMKWKKSGSG-PTTIYY and RRMKWKKSGSG-PTTIYY comprise a SGSG linker unit and a cell penetrating part RRMKWKK for *in vivo* analysis (personal communication). The linker unit and the cell penetrating component will be abbreviated as 'Pen' coining the hendeca-tagged hexa-peptides to PTTIYY-Pen and PATIAA-Pen. Figure 4.1 displays minimum energy structures of PTTIYY-Pen and PATIAA-Pen employing Gaussian 03 with a semi-empirical PM3 method and a 3-21g basis set[6]. Images emphasise the steric demand of the cell penetrating part of the hendeca-tagged hexa-peptide.

Competition fluorescence anisotropy experiments with the tagged peptides undertaken by Hupp and co-workers have revealed a dissociation constant of 25-40 µM (unpublished data). The dissociation constant for the interaction of AGr2 with PATIAA-Pen has not been determined and remains, as yet unknown.

In this chapter two different batches of AGr2 are discussed, only differing in the way of purification by H. Florance and J. Nicholson and are referred to as Nicholson- and Florance-batch. For purification purposes the AGr2 protein comprises a 27 aa long His-tag containing six histidines, as visualised in Appendix 11.1.

[6]kindly conducted by Ms. I. Pechtl

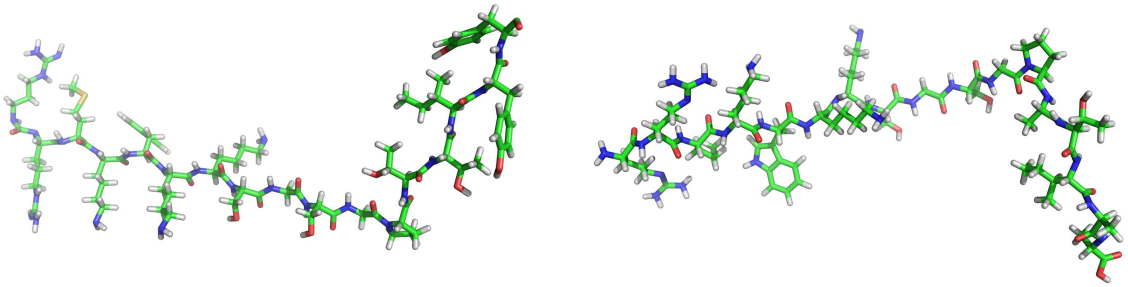

(a) RRMKWKWKKSGSG-PTTIYY (b) RRMKWKWKKSGSG-PATIAA

Figure 4.1: AGr2 binding hendeca-tagged hexa-peptides. (a) PTTIYY-Pen structure optimised with Gaussian 03 employing a PM3 method and a 3-21g basis set. Displayed structure did not reach self consistency. (b) PATIAA-Pen structure identically optimised (kindly conducted by Ms. I Pechtl; pdb files visualised with pymol (DeLano Scientific LLC - Palo Alto, USA)).

As described in Section 1.4.4 the C-terminal pair of CCP's (CCP 19-20) has been shown to interact with polyanions such as heparin, heparan sulfate, dextran sulfate and sialic acid [222]. Herbert *et al.* determined a dissociation constant of 9.0 ± 2.5 µM for heparin and fH19-20 employing two dimensional NMR titration techniques [287]. Furthermore no aggregation of fH19-20 was observed in the presence of the tetrasaccharide which suggests a specific and localised interaction, which causes little, if any changes to the structure of the protein.
Ferreira *et al.* investigated the binding properties of wild type fH19-20 and sequence variants with respect to C3b and polyanion binding *via* heparin affinity chromatography and gel-mobility shift assays to conclude an increased binding potential of mutated fH19-20 variants exhibiting a gain of positive charges [227].

Based on the finding that fH19-20 exhibited a K_d of 9.0 ± 2.5 µM with heparin, the target was to investigate the binding properties of fH19-20 with the pentasaccharide fondaparinux (FPX, Fig. 4.2), as no binding properties of this system have been reported yet. Within this Chapter possible binding interactions of the fH19-20-FPX system will be investigated with the manual- and automated ESI-SUPREX methodology.

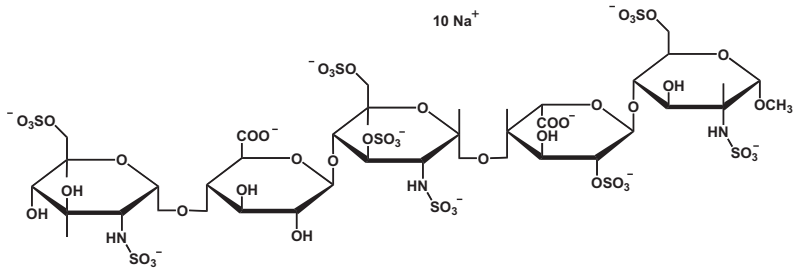

Figure 4.2: Structure of the pentasaccharide, fondaparinux, as the deca-sodium salt (visualised with ChemDraw - CambridgeSoft - Cambridge, USA).

4.2 Direct Infusion

Nano-ESI direct infusion experiments were conducted in positive ion mode to verify protein and ligand masses before automated ESI-SUPREX was employed.
Each batch of AGr2 was sprayed under denaturing conditions comprising 5 % FA (Section 2.3.4) culminating in identical charge state distributions, ranging from 9+ to 16+ and an identical deconvoluted mass of 21041 Da (Fig. 4.9a). The theoretical mass according to its sequence (Appendix 11.1) is 21173.24 Da, resulting in a difference of 132.24 Da. This suggests the absence of the N-terminal methionine residue of the 27 aa His-tag. The presence of AGr2 dimer peaks in charge states ranging from 20+ to 32+ under denaturing conditions, can be attributed to the formation of a covalently bound dimer. Formation must occur upon storage at 4 °C over time as automated SUPREX experiments conducted at an earlier stage do not exhibit the dimeric species. The tendency of AGr2 forming aggregates, competent of peptide binding, is further demonstrated in native DI-ESI-MS experiments by Faull (unpublished PhD Thesis). However, under denaturing conditions only the AGr2 monomer is observable suggesting a non-covalent aggregation. *Per contra*, Clark *et al.* brought evidence for a covalent dimer in the gas phase conducting FT-ICR experiments in the gas phase (unpublished data).
The hendeca-tagged hexa-peptides were sprayed under native like conditions (Section 2.3.4), demonstrating deconvoluted experimental masses of 2059.87 and 1845.83 Da for PTTIYY-Pen and PATIAA-Pen, respectively (Fig. 4.9b and c). Theoretical masses of 2059.42 Da and 1845.20 Da for PTTIYY-Pen and PATIAA-Pen are in very good agreement with experimental derived data.

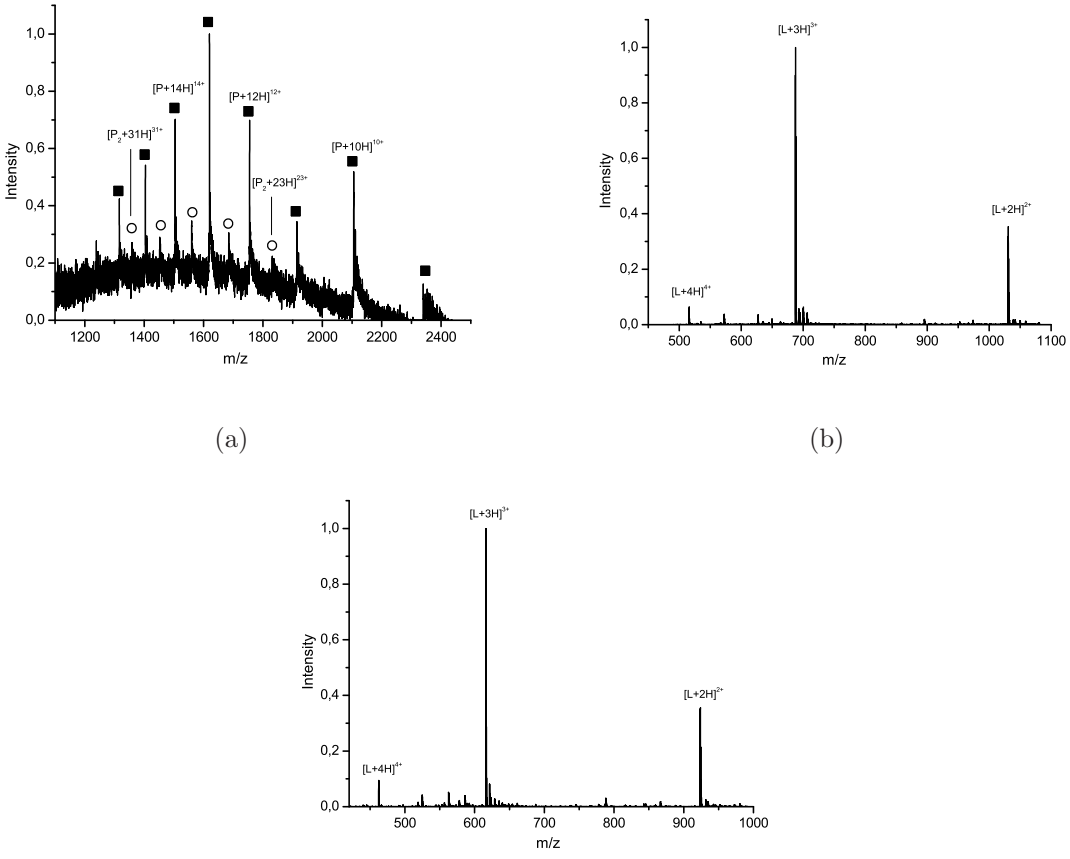

(a) (b)

(c)

Figure 4.3: Direct infusion spectrum of AGr2 and ligands. (a) Nicholson-Agr2 sprayed under denaturing conditions from 10 mM NH_4OAc with 5 % FA exhibiting monomer charge states (squares) from 9+ to 16+, dimer charge states (circles) from 20+ to 32+ resulting in a deconvoluted mass of 21041 and 42085 Da. (b) PTTIYY-Pen sprayed from native like conditions displaying charge states 2+ to 4+ with an associated mass of 2059.87 Da. (c) PATIAA-Pen sprayed from native like conditions displaying charge states 2+ to 4+ and a deconvoluted mass of 1845.83 Da.

FH19-20 was sprayed under denaturing conditions with 10 % FA resulting in two different species ranging from a 7+ to 9+ charge state with a deconvoluted mass of 14738.5 and 14938.8 Da. Apo fH19-20's theoretical mass according to its sequence (Appendix 11.2) is 14745.76 and 14945.9 Da in the oxidised form with four disulfide bridges present. The difference of 200.3 Da is due to additional Glu-Ala (EA) aa residues on 129 aa apo fH19-20, which is a well known phenomenon in using the *Pichia pastoris* expression system [288]. The theoretical mass of the 131 aa fH19-20 is 14936.04 Da and therefore demonstrates good agreement with deconvoluted data (Fig. 4.9a).

The pentasaccharose FPX was sprayed from native-like conditions with 5 % MeOH exhibiting different degrees of sodiation ranging from 6-10 sodium atoms in the 1+ charge state (Fig. 4.9b). The deconvoluted mass of FPX is 1726.77 Da and therefore exhibits good agreement with the theoretical mass of 1728 Da of the deca-sodium salt. The presence of salt complicates DI-ESI-MS analysis, however, is tolerated in automated LC-ESI SUPREX experiments. A FPX fragment comprising different amounts of sodium atoms was detected, however, could not be identified (red circles Fig. 4.9).

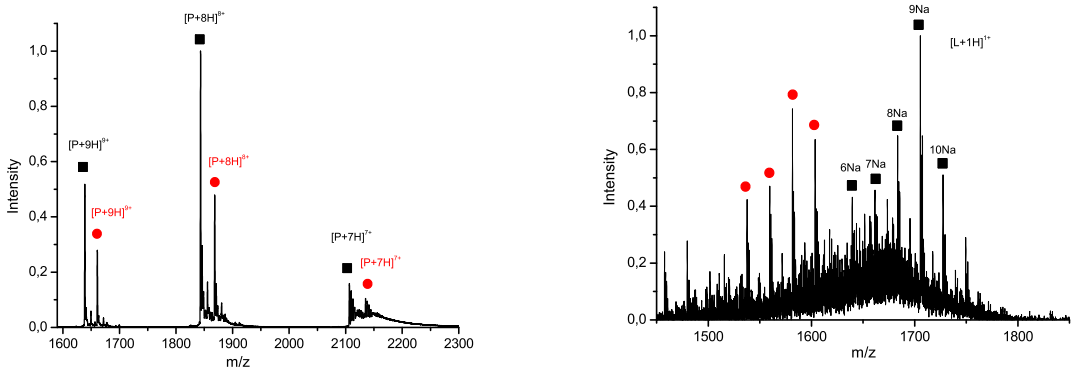

(a) (b)

Figure 4.4: Direct infusion spectrum of fH19-20 and fondaparinux. (a) FH19-20 sprayed under denaturing conditions sprayed from 10 mM NH_4OAc with 10 % FA exhibiting charge states from 7+ to 9+ (black squares) and fH19-20 with an additional EA expression artefact (red circles). (b) Fondaparinux under native-like conditions sprayed from 10 mM NH_4OAc with 5 % MeOH exhibiting the 1+ charge state comprising 6 to 10 sodium atoms (black squares) and a series of FPX fragments comprising various sodium adducts (red circles).

4.3 Labeling Experiments

AGr2 and fH19-20 systems were investigated *via* HDX labeling (Section 2.3.5) utilising the automated SUPREX setup (Section 2.7.3).

AGr2 comprises, according to its sequence including the His-tag (Appendix 11.1), 165 T1, 174 T2 and 1158 T3 hydrogen atoms. Figure 4.5 illustrates the deuterium incorporation with regard to time for Nicholson apo AGr2 and in complex with PTTIYY-Pen and PATIAA-Pen. All three systems exhibit similar exchange rates, however, slightly different equilibrium deuterium levels. Apo AGr2 displays the highest level with ~77 deuterons incorporated, followed by AGr2-PATIAA-Pen with ~75 deuterons and AGr2-PTTIYY-Pen with approximately 73 hydrogen atoms ex-

changed. As all peptides were dissolved in water, all observed changes in deuterium levels can solely be attributed to interaction with AGr2. This suggests an interaction of both hendeca-tagged peptides with the His-tagged AGr2, resulting in an increased protection of AGr2 in complex with PTTIYY-Pen and PATIAA-Pen due to conformational changes upon binding and/or shielding of the ligand. Thereby a qualitatively stronger interaction can be attributed to the PTTIYY-Pen ligand in comparison to PATIAA-Pen.

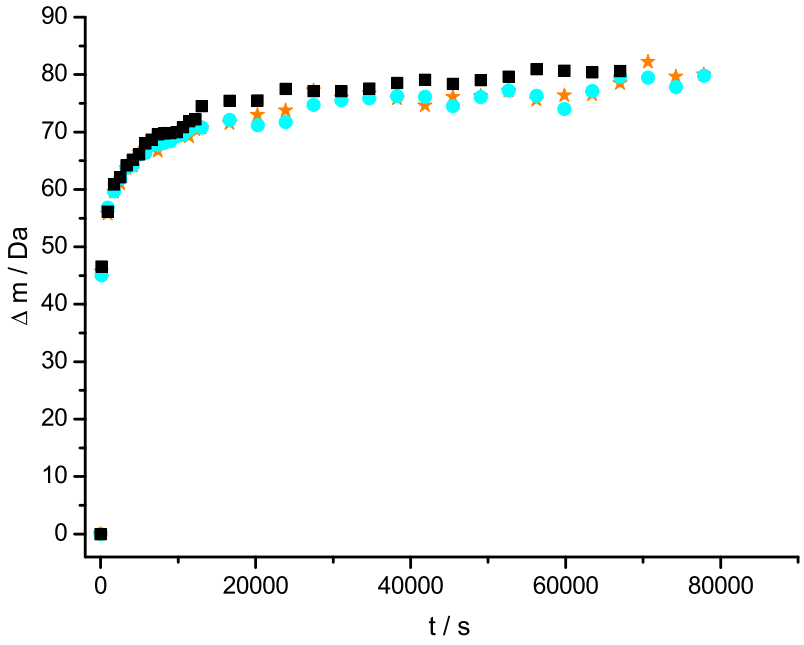

Figure 4.5: Automated AGr2-ligand HDX labeling. Deuterium uptake *versus* time for apo Agr2 (black squares), AGr2-PTTIYY-Pen (cyan circles) and AGr2-PATIAA-PEN (orange stars).

Temperature dependent HDX labeling experiments for AGr2 with the temperature controllable ESI-SUPREX setup (Section 2.7.4) are illustrated in Figure 4.6. Time course experiments were conducted at 14, 22 and 50 °C, where 22 °C is defined as RT. Room temperature runs for apo-, PTTIYY-Pen- and PATIAA-Pen are also included. At 14 °C apo AGr2 demonstrates the lowest exchange rate and deuterium level, with an equilibrium deuterium level of about 71 deuterons. In contrast, an increased sample temperature of 50 °C results in a high exchange rate and a high initial equilibrium deuterium level for short incubation times. Over time the formation of a covalent homodimeric AGr2 species is observed appearing after ~160

min, suggesting some degree of aggregation and precipitation occurring, as visually confirmed after ~18.5 h.

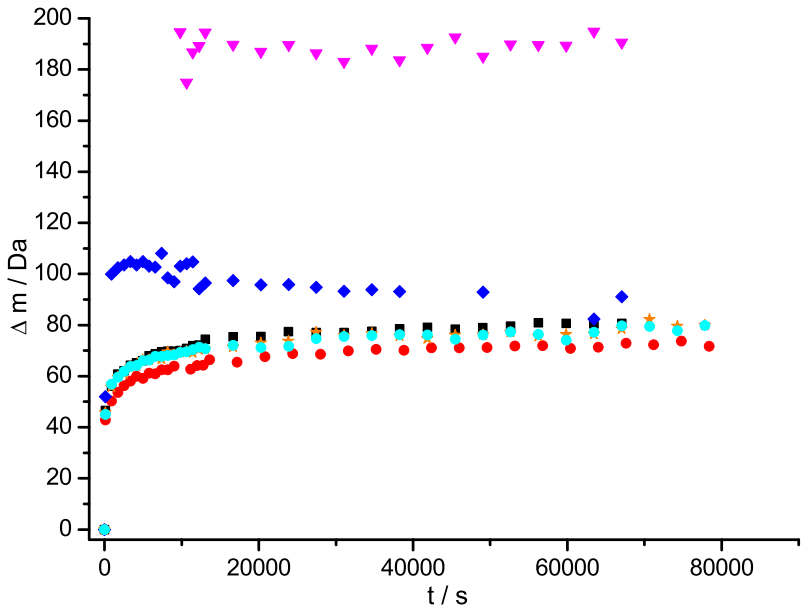

Figure 4.6: Automated AGr2 temperature HDX labeling. Deuterium uptake *versus* time for apo AGr2 at RT (black squares), apo AGr2 at 14 °C (red circles), monomeric apo AGr2 at 50 °C (blue diamonds), dimeric apo AGr2 at 50 °C (magenta triangles), AGr2-PTTIYY-Pen at RT (cyan circles) and AGr2-PATIAA-Pen at RT (orange stars).

FH19-20 has 129 T1, 119 T2 and 762 T3 hydrogen atoms for the 129 aa species and 131 T1, 121 T2 and 771 T3 hydrogen atoms for the 131 aa species, which contains an additional Glu and Ala residue. HDX labeling data for the 129 aa species is visualised in Figure 4.7 demonstrating exchange properties for apo and FPX complexed fh19-20. The apo protein displays a lower exchange rate and deuterium level than the FPX complexed one, resulting in an equilibrium deuterium level of ~82 and ~95 deuterons. Figure 4.8 illustrates the time course experiment for the 131 aa fH19-20 species exhibiting the same trend for exchange rates and deuterium levels as the 129 aa variant. Equilibrium HDX levels are ~84-97 deuterium atoms for the 131 aa species.

Interestingly, a high degree of HDX is observed for fH19-20 compared to previous studies with CypA (Section 3.3) under identical experimental conditions. The degree of amide backbone HDX is between 69-71 % for 129 and 131 aa fH19-20 and

27.5 % for apo CypA, suggesting a more solvent accessible structure of the fH protein. A closer look at the fH19-20 structure (Fig. 1.13b) reveals a less structured secondary structure in comparison to CypA. CCP module 19 exhibits six short β-sheets connected by loops and a complete absence of α-helices, whereas CCP 20 comprises six β-sheets and one α-helix with approximately 1.5 turns involving ~5 amino acid residues. These findings account for the high degree of deuteration of fH19-20 and therefore we can attribute the lower deuterium levels in HDX labeling experiments for CypA to be structure related, rather than back exchange under identical experimental conditions (Section 3.3).

The comparison between apo- and FPX-complexed, fH19-20 of both the 129 and 131 aa species, demonstrates a higher degree of exchange in the complex than in the free protein. This suggests conformational changes occur upon FPX binding to CCP module 19-20, unshielding apo buried amide protons, which contrasts with the heparin experiments of Herbert *et al.* [287]. The difference of ~10 deuterons between the apo and the complexed form of both species indicate a structural opening upon complexation.

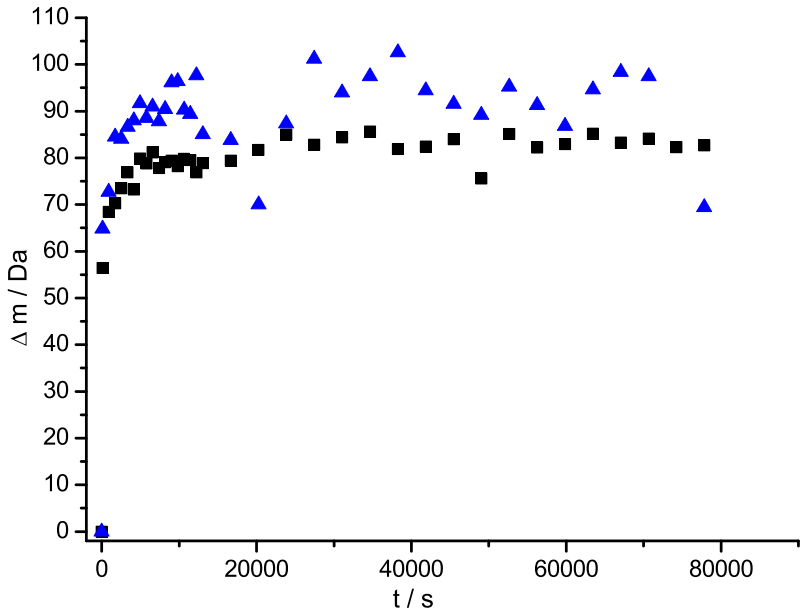

Figure 4.7: Automated fH19-20-FPX HDX labeling. Deuterium uptake *versus* time for apo fH19-20 (129 aa) at RT (black squares) and in complex with FPX (blue triangles).

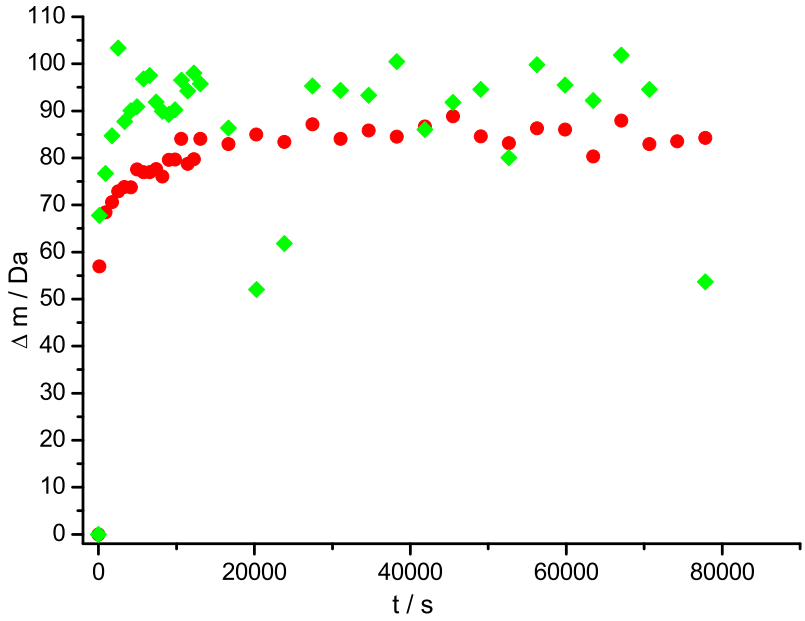

Figure 4.8: Automated fH19-20-FPX HDX labeling. Deuterium uptake *versus* time for apo fH19-20 (131 aa) at RT (red circles) and in complex with FPX (green diamonds).

4.4 SUPREX - Manual

For manual ESI-SUPREX (Section 2.7.2) average intrinsic exchange rates were determined, according the method mentioned in Section 2.7.5, to be 3.98 s^{-1} for AGr2 based on its sequence (Appendix 11.1) and 6.89 s^{-1} for both fH19-20 species (Appendix 11.2). For all experiments a total AGr2 and fH19-20 concentration of 2.5 µM was utilised along with tenfold excess of hendeca-tagged hexapeptides and FPX.

4.4.1 AGr2 SUPREX

In conjunction with the devised manual ESI-SUPREX setup apo AGr2 from the Florance batch was investigated, yielding SUPREX curves and midpoints for the incubation times at 10, 40, 60 and 180 min. The complete set of SUPREX curves is displayed in Appendix 11.3, whereas Figure 4.9a provides an overview of 10, 60 and 180 min incubation. Midpoint concentrations are calculated to be 2.18, 1.55 and 1.29 M for 10, 60 and 180 min incubation, respectively.

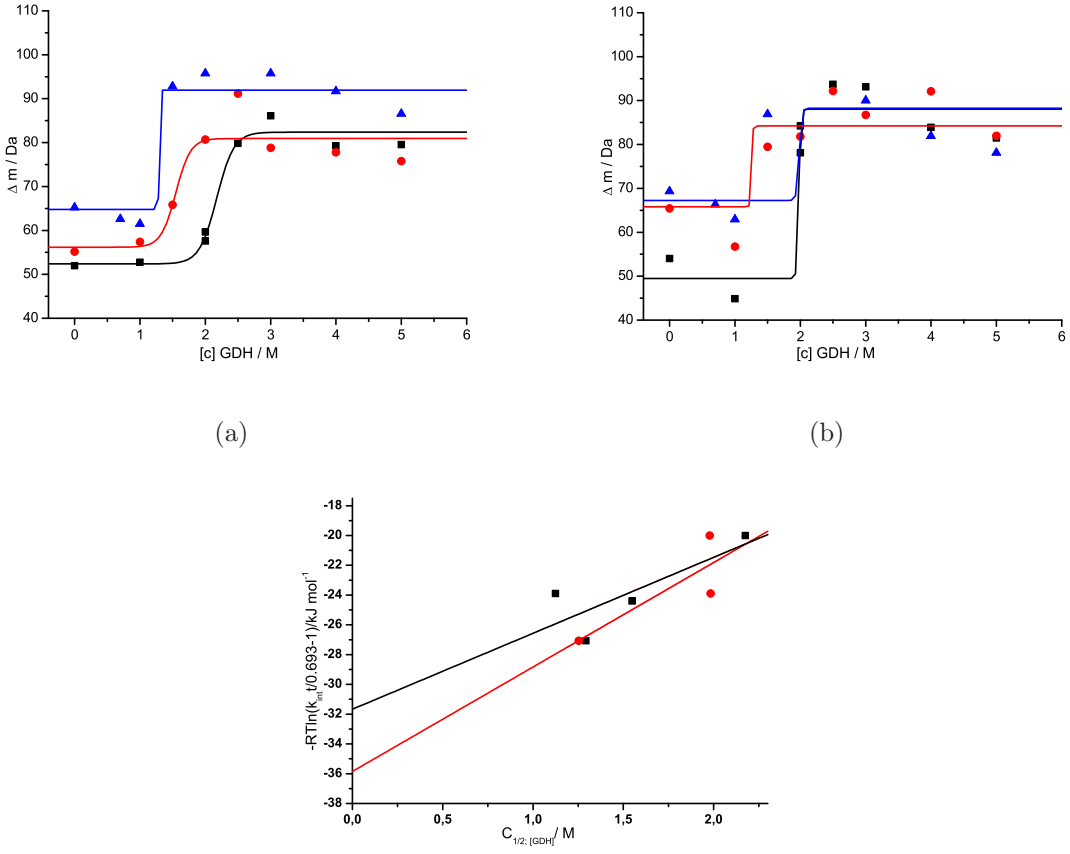

Figure 4.9: Manual AGr2 SUPREX data. (a) Overview of apo AGr2 manual SUPREX curves for incubation times 10, 60 and 180 min with $C^{1/2}_{SUPREX}$ values of 2.18, 1.55 and 1.29 M. (b) Overview of AGr2-PTTIYY-Pen manual SUPREX curves for incubation times 10, 60 and 180 min with $C^{1/2}_{SUPREX}$ values of 1.98, 1.98 and 1.25 M. (c) Free energy *vs.* $C^{1/2}_{SUPREX}$ plot resulting in -31.05 ± 36.28 kJmol^{-1} for apo AGr2, -36.28 ± 7.23 kJmol^{-1} for the AGr2-PTTIYY-Pen complex and a m value of 4.77 ± 2.93 kJmol^{-1}M^{-1} and 7.36 ± 4.06 kJmol^{-1}M^{-1}, resulting in a $\Delta\Delta G_f$ value of -5.23 ± 8.62 kJmol^{-1} and a K_d of 3.37 ± 5.55 µM.

AGr2 in complex with PTTIYY-Pen at the same incubation times is shown in Figure 4.9b. The full set of SUPREX curves for the holo system is displayed in Appendix 11.4. $C^{1/2}_{SUPREX}$ values for holo fH19-20 are determined to be 1.98, 1.98 and 1.25 M for the 10, 60 and 180 min incubation period, resulting in a slight destabilisation of the 10 and 180 min experiment and stronger stabilisation of 0.86 M for the 40 min incubation experiment (Table 4.1). Plotting SUPREX midpoints *vs.* the free energy of protein folding results in values of -31.05 ± 4.69 and -36.28 ± 7.23 kJmol^{-1} for apo- and PTTIYY-complexed AGr2 culminating in a K_d of 3.37 ± 5.55

µM. The m value is calculated to be 4.77 ± 2.93 kJmol^{-1}M^{-1} for the apo protein and 7.36 ± 4.06 kJmol^{-1}M^{-1} for the complexed form, suggesting apo AGr2 exhibiting a lower degree of unfolding upon denaturation and thereby demonstrating fewer surface exposure. The limitation of experimental data points is, again, preventing a more detailed and more accurate ESI-SUPREX data evaluation. The automated ESI-SUPREX methodology offers a higher degree of automation therefore it ought to give a more detailed insight into AGr2-ligand interactions.

4.4.2 FH19-20 SUPREX

Identical experimental procedures were used for manual ESI-SUPREX of apo fH19-20 as for AGr2 in the previous Section. SUPREX curves for both, the 129 and 131 aa species were recorded and midpoints extracted for 10, 60 and 180 min incubation (Fig. 4.10). For 10 min incubation with the chemical denaturant GDH, $C^{1/2}_{SUPREX}$ values are determined for the 129 and 131 aa species of 4.11 and 4.07 M, respectively (Fig. 4.10a). Different deuterium levels of the pre-transition baseline can be attributed to different solution structures of the two protein species and to their relative lengths. Errors in timing and execution of the manual experiment results in a big standard deviation in the transition region, where the methodology is very sensitive to non-consistency in the experimental protocol. Incubation of fH19-20 for 60 min in GDH culminates only in one midpoint for the 131 aa fH19-20 species of 3.07 M, as for the 129 aa variant there is no transition observable (Fig. 4.10b). This finding is supportive of the observations from HDX labeling experiments (Section 4.3) suggesting a non-compact tertiary structure with a large number of solvent accessible amide protons. This is further supported by the 180 min experiment demonstrating no transition at all, but a level of deuteration equal to the post-transition on of the 10 min incubation experiment (Fig. 4.10c). This suggests, that SUPREX is suitable to only a limited extent for the determination of thermodynamical data of the complement control proteins 19-20. The decrease in the deuterium level at high denaturant concentrations can be attributed to strong interaction of GDH with the protein as demonstrated for CypA in Chapter 3.8.

Table 4.1: Manual SUPREX results for AGr2 and FH19-20.

Incubation time/min	Apo AGr2[a]	AGr2-PTTIYY-Pen[a] $C_{SUPREX}^{1/2}$ [a] /M	Apo fH19-20[b]	Apo fH19-20[c]
10	2.18	1.98 (-0.20)	4.11	4.07
40	1.12	1.98 (+0.86)		
60	1.55	N/A	N/A	3.07
180	1.29	1.25 (-0.04)	N/A	N/A
ΔG_f/kJmol^{-1}	-31.05 ± 4.69	-36.28 ± 7.23		-38.66
$\Delta\Delta G_f$/kJmol^{-1}		-5.23 ± 8.62		
m/kJmol^{-1}M^{-1}	4.77 ± 2.93	7.36 ± 4.06		4.23
K_d		3.37 ± 5.55 µM		

[a] Florance expressed batch.

[b] 129 aa apo fH19-20.

[c] 131 aa apo fH19-20, comprising an additional EA expression artefact.

Nevertheless, plotting the two extracted SUPREX midpoints in a ΔG_f *vs.* $C_{SUPREX}^{1/2}$ plot results in a free energy of -38.66 kJmol^{-1} for the 131 aa fH19-20 species and a m value of 4.23 kJmol^{-1}M^{-1} (Fig. 4.10d) as tabulated in Table 4.1. In comparison to CypA, fH19-20 seems to have a higher stability against denaturation as for the 10 min incubation given that the midpoint concentration was almost twice as much as for CypA.

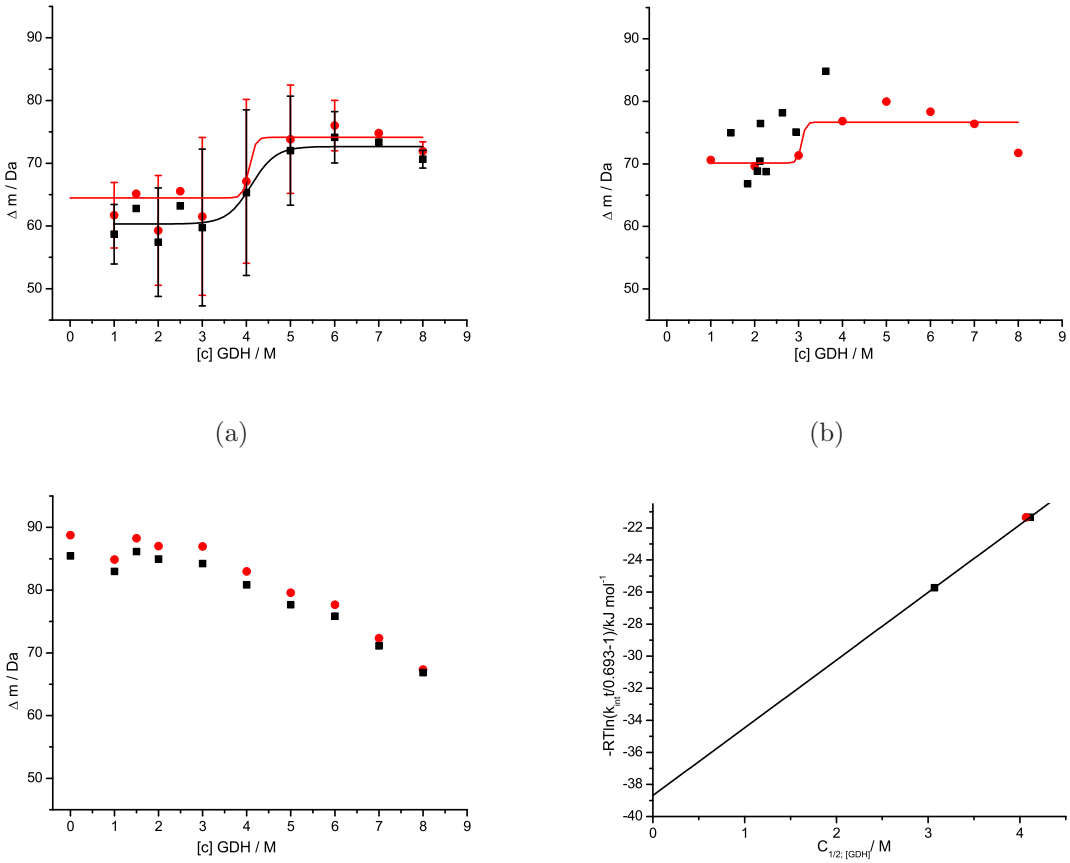

Figure 4.10: Manual fH19-20 SUPREX data. (a) Apo fH19-20 manual SUPREX curves for 10 min incubation with fH19-20 (black squares) and with an additional EA expression artefact (red circles) resulting in $C^{1/2}_{SUPREX}$ values of 4.11 and 4.07 M (error bars represent standard deviation of two sets of experiments). (b) Apo fH19-20 manual SUPREX curves for 60 min incubation with fH19-20 (black squares) and with an additional EA expression artefact (red circles), the latter resulting in a $C^{1/2}_{SUPREX}$ value of 3.07 M. (c) Apo fH19-20 manual SUPREX curves for 180 min incubation with fH19-20 (black squares) and with an additional EA expression artefact (red circles). (d) Free energy *vs.* $C^{1/2}_{SUPREX}$ plot resulting in -38.66 kJmol^{-1} free energy of protein folding and a m value of 4.23 kJmol^{-1}M^{-1}.

4.5 SUPREX - Automated

4.5.1 AGr2 SUPREX

Automated ESI-SUPREX experiments were performed as described in Section 2.7.3 with both AGr2 batches at incubation times from 10 to 180 min. AGr2 from the Florance batch exhibits (for all investigated incubation times) somewhat higher denaturing midpoint concentrations compared with the same protein expressed and

purified by Nicholson. Since the proteins have identical masses (Section 4.2) this must be attributed to buffer effects (detergent *vs.* non-detergent) and/or different levels of oligomerisation caused by these buffer conditions, which reflects once more the dependence of the relative stability of a protein on its environment. In the automated SUPREX experiments conducted at room temperature, no covalently bound homodimeric AGr2 was observed. Therefore it was not considered in the data evaluation process, however, accounted for in discussing SUPREX results.
Figure 4.11a displays the two different AGr2 batches for a 10 min incubation period, resulting in $C^{1/2}_{SUPREX}$ values 1.55 and 1.06 M for Florance and Nicholson AGr2 under identical experimental conditions. At this point it is noteworthy that manual SUPREX buffers for fH19-20 were not refractively verified, hence higher relative midpoint concentrations are observed. However, this does not affect K_d calculations as these are determined from relative $\Delta\Delta G_f$ values. SUPREX midpoints for both proteins are summarised in Table 4.2, whereas an overview of the complete set of SUPREX curves is illustrated in Appendix 11.5 and 11.6 for Florance and Nicholson expressed and purified AGr2. Figure 4.11b displays the 90 min incubation with GDH, culminating in SUPREX midpoint concentrations of 2.02 and 0.90 M for Florance and Nicholson Agr2, respectively.
Both protein batches exhibit a similar trend in destabilisation with respect to the incubation time in GDH, however, absolute stabilities vary due to different buffer conditions. Florance AGr2 was treated with detergents, such as polysorbate products to prevent unspecific binding and increase solubility. Over time the purification protocol was refined and the application of detergents was no longer necessary, as in the Nicholson AGr2 batch. As previously described (Section 1.6), these absolute differences in $C^{1/2}_{SUPREX}$ values do not affect the calculated dissociation constant, as the differences of SUPREX derived free energies, which are not comparable to other techniques, are utilised for K_d calculations.

Evaluation of the SUPREX curves by assuming two-state unfolding and linear fitting results in a ΔG_f value of -27.82 ± 1.30 kJmol^{-1} and an associated m value of 3.64 ± 0.92 kJmol^{-1}M^{-1} for Florance AGr2 (Fig. 4.11c). In contrast, plotting ΔG_f *vs.* $C^{1/2}_{SUPREX}$ of the Nicholson batch offers three potential fitting possibilities, as visualised in Figure 4.11d. Linear fitting all collected data points as performed with the Florance batch (black line Fig. 4.11d) results in a free energy of protein folding of -31.88 ± 4.48 kJmol^{-1} and a m value of 9.62 ± 5.23 kJmol^{-1}M^{-1}, indicating that the AGr2 in the Nicholson batch is more stable. The m value suggests in

comparison a higher degree of unfolding and higher surface exposure upon unfolding in the Nicholson batch, which is consistent with the deuterium level of the 10 min incubation (Fig. 4.11a), however, not by the deuterium level upon unfolding in the 90 min incubation experiment (Fig. 4.11b).
Neglecting the 10 and 120 min incubation period in the SUPREX evaluation routine, linear fitting culminates in a ΔG_f value of -109.75 ± 8.70 kJmol^{-1} and associated m value of 98.49 ± 9.99 kJmol^{-1}M^{-1} (blue fit Fig. 4.11d), indicating a high stability and a high degree of unfolding upon denaturation in Nicholson AGr2. Error bars are visualised where an error was possible to be calculated.
In the case where a sigmoidal curve interpretation was applied no ΔG_f value was calculated (red line 4.11d). Nevertheless, these findings would suggest a non-two state unfolding behaviour for apo Agr2 (Nicholson batch) probably caused by non-covalent oligomerisation in solution as covalent aggregates are not evident in any of the acquired SUPREX mass spectra, except high in temperature SUPREX experiments (Section 4.6) and DI-ESI MS experiments of long-term-stored AGr2 (Section 4.2).

Contextualising Nicholson AGr2 findings with those obtained from the Florance batch utilising polysorbates to prevent unspecific binding, a non-two state unfolding behaviour caused by at least partial oligomerisation of AGr2 in the Nicholson batch seems the most likely conclusion. Even though only monomeric AGr2 was detected, aggregation plays, a yet unknown, role explaining previous findings.

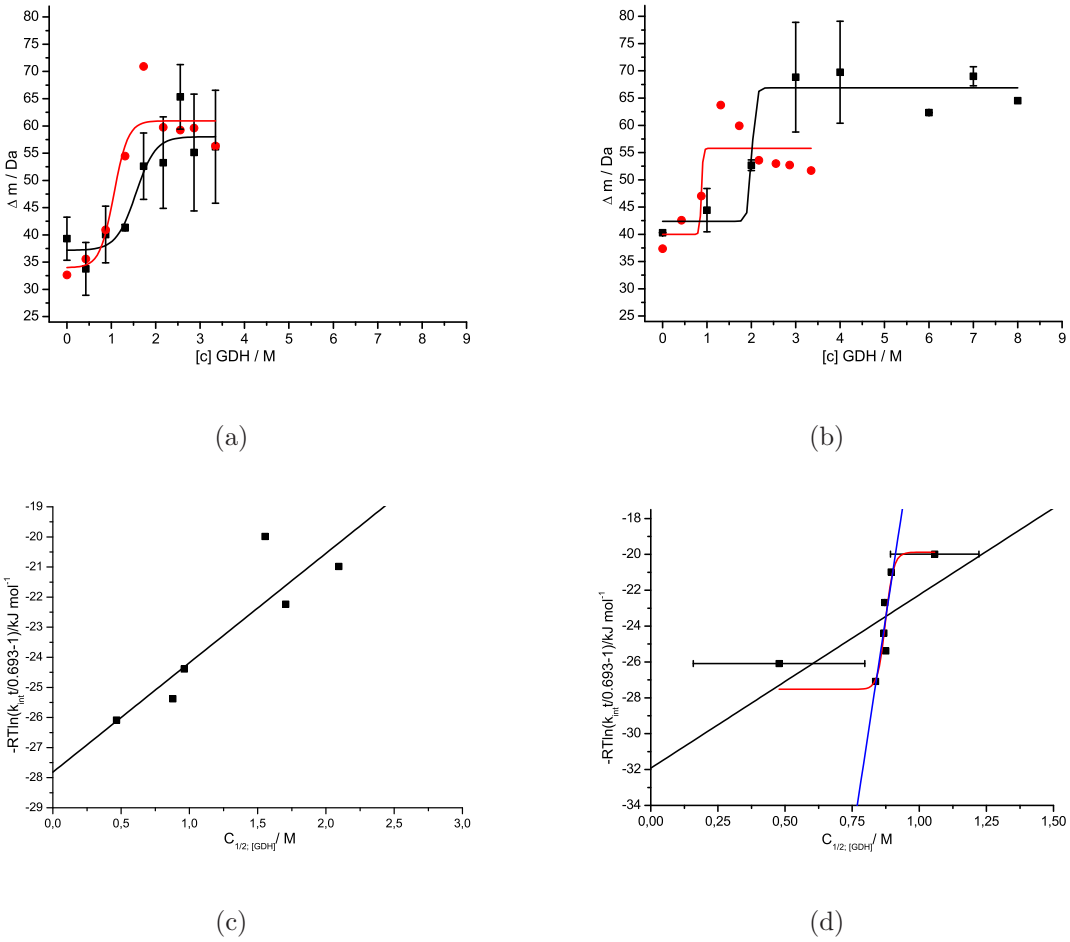

Figure 4.11: Automated apo AGr2 SUPREX data of the two batches. (a) Florance (black squares) and Nicholson (red circles) apo AGr2 incubated for 10 min, resulting in $C_{SUPREX}^{1/2}$ values of 1.55 M and 1.06 M. (b) The Florance (black squares) and Nicholson (red circles) AGr2 incubated for 90 min, result in 2.02 and 0.86 M SUPREX midpoints (error bars represent standard deviation of two sets of experiments). (c) Florance AGr2, free energy *vs.* $C_{SUPREX}^{1/2}$ plot resulting in a ΔG_f value of -27.82 $\pm$ 1.30 kJmol^{-1} and a m value of 3.64 $\pm$ 0.92 kJmol^{-1}M^{-1}. (d) ΔG_f *vs.* $C_{SUPREX}^{1/2}$ plot resulting in a free energy of protein folding of -31.88 $\pm$ 4.48 kJmol^{-1} and a m value of 9.62 $\pm$ 5.23 kJmol^{-1}M^{-1}, if all experimental data is incorporated in the fit (black line). Neglect of 10 and 120 min incubation results in a ΔG_f of -109.75 $\pm$ 8.70 kJmol^{-1} and a m value of 98.49 $\pm$ 3.99 kJmol^{-1}M^{-1} (blue line). Neglect of 120 min incubation and sigmoidal fitting would indicate non-two state unfolding behaviour (red line).

ESI-SUPREX experiments with PTTIYY-Pen were conducted throughout with Nicholson expressed and purified AGr2. All SUPREX curves of the complex are available in Appendix 11.7. Figure 4.12a provides an overview of apo and PTTIYY-Pen-complexed AGr2 for a 120 min incubation period, resulting in $C_{SUPREX}^{1/2}$ values of 0.48 and 0.88 M for apo and complexed AGr2. The 0.40 M stabilisation of AGr2

at 120 min incubation is the only measured positive stabilisation (Table 4.2). All other incubation times yield destabilisation of AGr2 in a range of 0.17 and 0.29 M or exhibit similar SUPREX midpoint concentrations as the apo enzyme. Evaluation of all acquired $C^{1/2}_{SUPREX}$ values results in a ΔG_f of -33.97 ± 7.24 kJmol^{-1} and a m value of 12.09 ± 8.62 kJmol^{-1}M^{-1} with an associated $\Delta\Delta G_f$ value of -2.09 ± 4.64 kJmol^{-1}, culminating in K_d of 24.52 ± 54.43 µM (red line Fig. 4.12b), which is within the same order of magnitude as the manual determined K_d of 3.39 µM. However, the fitting approach utilised does not represent experimental data very well and the lack of error bars due to large deviations in the $C^{1/2}_{SUPREX}$ value extraction, further complicates quantitative analysis.

In contrast, plotting the free energy of protein folding *vs.* $C^{1/2}_{SUPREX}$ values with the neglect of the 180 min incubation time, a steep linear fit is extracted resulting in a ΔG_f of -251.67 ± 71.50 kJmol^{-1} and a m value of 258.91 ± 81.09 kJmol^{-1}M^{-1} (black line Fig. 4.12b). A $\Delta\Delta G_f$ value of -223.80 ± 71.50 kJmol^{-1} is not supported by measured SUPREX midpoint concentrations of apo- and holo protein, where just a single stabilisation of 0.40 M for the 120 min incubation time is observed. In comparison, CypA in complex with CsA exhibits an average stabilisation of 1.5 - 2 M resulting in a $\Delta\Delta G_f$ value of -12.05 kJmol^{-1}. These thermodynamic parameters do not encourage K_d calculations, as results would not reflect biological properties.

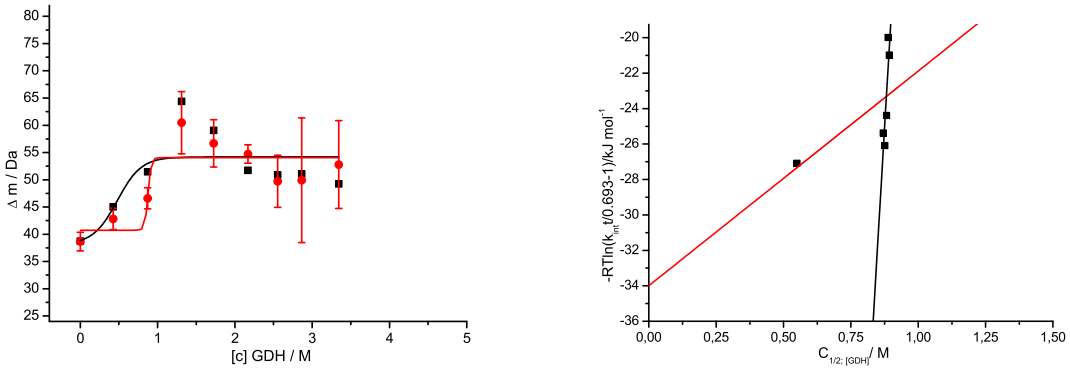

(a) (b)

Figure 4.12: Automated AGr2-PTTIYY-Pen SUPREX data. (a) Comparison of free (black squares) and PTTIYY-Pen complexed (red circles) AGr2 at 120 min incubation, resulting in $C^{1/2}_{SUPREX}$ values of 0.48 and 0.88 M, respectively (error bars represent standard deviation of two sets of experiments). (b) Evaluation, neglecting 180 min incubation (black line), results in a ΔG_f of -251.67 ± 71.50 kJmol^{-1} and a m value of 258.91 ± 81.09 kJmol^{-1}M^{-1}, whereas incorporating all experimental data points culminates in a ΔG_f of -33.97 ± 7.24 kJmol^{-1} and a m value of 12.09 ± 8.62 kJmol^{-1}M^{-1} (red line).

For the AGr2-PATIAA-Pen system ESI-SUPREX experiments were carried out with Nicholson expressed and purified AGr2 and the complete set of SUPREX curves is visualised in Appendix 11.8.
Extracted SUPREX inflexion points demonstrate almost identical $C^{1/2}_{SUPREX}$ values as for the AGr2-PTTIYY-Pen system apart from the 60 min incubation, exhibiting a destabilisation of 0.19 M (Table 4.2). The most drastic change in protein stabilisation is identical to the PTTIYY-Pen experiment at 120 min incubation with a stabilisation of 0.41 M, as illustrated in Figure 4.13a. Thermodynamic analysis of all experimental data acquired reveals a free energy of protein folding of -32.25 ± 6.07 kJmol^{-1} and an associated m value of 10.50 ± 7.57 kJmol^{-1}M^{-1} resulting in a K$_d$ of 198.98 ± 3278.00 µM (black line Fig. 4.13a). If 60 and 180 min incubation times are neglected a ΔG_f of -128.07 ± 17.61 kJmol^{-1} and a m value of 118.99 ± 19.96 kJmol^{-1}M^{-1} is observable, culminating in a large -96.19 ± 17.66 kJmol^{-1} stabilisation (blue line Fig. 4.13b), which is not supported by extracted $C^{1/2}_{SUPREX}$ values. Again, quantitative K$_d$ evaluation is not advised as biological relevance would be questionable.

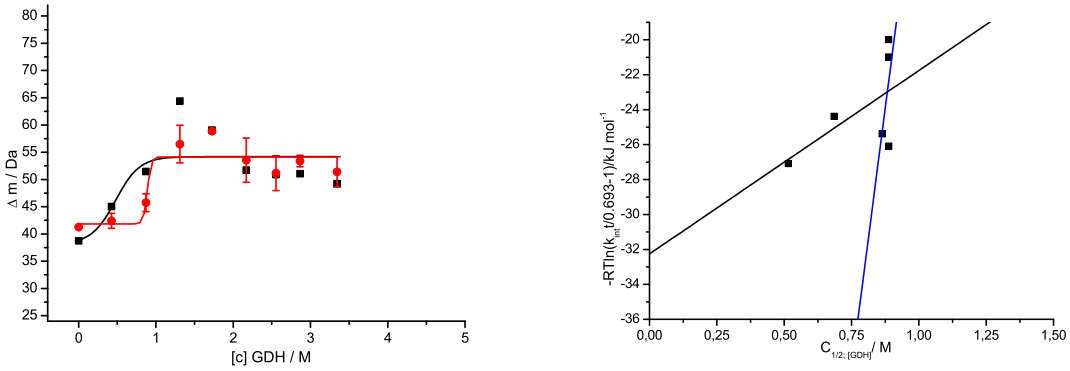

(a) (b)

Figure 4.13: Automated AGr2-PATIAA-Pen SUPREX data. (a) Comparison of free (black squares) and PATIAA-Pen complexed (red circles) AGr2 at 120 min incubation, resulting in $C^{1/2}_{SUPREX}$ values of 0.48 and 0.89 M, respectively (error bars represent standard deviation of two sets of experiments). (b) ΔG_f *vs.* $C^{1/2}_{SUPREX}$ plot comprising all experimental data (black line), results in a free energy of protein folding of -32.25 ± 6.07 kJmol^{-1} and a m value of 10.50 ± 7.57 kJmol^{-1}M^{-1}. Neglect of 60 and 180 min incubation, results in a ΔG_f value of -128.07 ± 17.61 kJmol^{-1} and a m value of 118.99 ± 19.96 kJmol^{-1}M^{-1} (blue line).

Qualitative comparison of m values of all five investigated sets of thermodynamic data suggests an increased surface area upon denaturation for all holo-AGr2 systems and all associated evaluation approaches, conclude a more open structure of AGr2 in the presence of the hendeca-tagged hexapeptides.
Besides large errors associated with the free energy calculation, the determined dissociation constant of 24.52 ± 54.43 µM for PTTIYY-Pen complexed AGr2 shows good agreement with K_d's determined with competition fluorescence anisotropy of 25-40 µM (Section 4.1). The K_d for AGr2-PATIAA-Pen of 198.98 ± 3278.00 µM can not yet be properly evaluated, as there is no comparable data available. However, *in vivo* experiments might indicate a weaker binding of PATIAA-Pen in comparison to PTTIYY-Pen (personal communication). These findings would exculpate the higher dissociation constant of PATIAA-Pen. In addition DI-ESI-MS data by Faull does not show any interaction of this peptide with AGr2 (unpublished PhD thesis).

Table 4.2: Automated AGr2 SUPREX results (values in brackets denote shift in $C^{1/2}_{SUPREX}$ due to stabilisation compared to apo AGr2[a]).

Incubation/min	Apo AGr2[a]	Apo Agr2[b]	AGr2-PTTIYY[b] $C^{1/2}_{SUPREX}$/M	AGr2-PATIAA[b]
10	1.55	1.06	0.89 (-0.17)	0.89 (-0.17)
15	2.09	0.90	0.89 (-0.01)	0.89 (-0.01)
25	1.71			
30		0.87		
60	0.96	0.87	0.88 (+0.01)	0.69 (-0.19)
90	2.02	0.88	0.87 (-0.01)	0.86 (-0.02)
120	0.47	0.48	0.88 (+0.40)	0.89 (+0.41)
180		0.84	0.55 (-0.29)	0.52 (-0.03)
ΔG_f/kJmol^{-1}/[c]	-27.82 ± 1.30	-31.88 ± 4.48	-33.97 ± 7.24	-32.25 ± 6.07
$\Delta\Delta G_f$/kJmol^{-1}/[c]			-2.09 ± 4.64	-0.38 ± 6.19
m/kJmol^{-1}M^{-1}/[c]	3.64 ± 0.92	9.62 ± 5.23	12.09 ± 8.62	10.50 ± 7.57
K_d[c]			24.52 ± 54.43 µM	198.98 ± 3278.00 µM
ΔG_f/kJmol^{-1}/[d]		-109.75 ± 8.70	-251.67 ± 71.50	-128.07 ± 17.61
$\Delta\Delta G_f$/kJmol^{-1}/[d]			-223.80 ± 71.50	-96.19 ± 17.66
m/kJmol^{-1}M^{-1}/[d]		98.49 ± 9.99	258.91 ± 81.09	118.99 ± 19.96
K_d[d]			N/A	N/A

[a] expressed and purified by H. Florance.

[b] expressed and purified by J. Nicholson.

[c] all experimental data incorporated.

[d] selected data points as individually visualised in Figure 4.11d, 4.12b and 4.13b.

4.5.2 FH19-20 SUPREX

Automated ESI-SUPREX experiments for fH19-20 were conducted according to Section 2.7.3 with incubation times ranging from 10 to 180 min. All SUPREX curves for the two apo and holo fH species are displayed in Appendix 11.9 and 11.10. Apo fH19-20 SUPREX midpoint concentrations for both species are summarised in Table 4.3.

The 129 aa species displays an almost constant denaturing behaviour for the incubation period between 10-60 min, followed by a decrease in the denaturing concentration for incubation times longer 180 min. In contrast, the 131 aa species does exhibit a continuous destabilisation with increased incubation time. Thermo-

dynamic analysis for both species reveal ΔG_f values of -30.38 ± 3.22 and -29.58 ± 3.10 kJmol^{-1} for the 129 and 131 aa variant. Associated m values are calculated to 3.30 ± 1.84 and 3.10 ± 0.71 kJmol^{-1}M^{-1} for the 129 and 131 aa species, respectively (Fig. 4.14c). Interestingly, lower m values are determined as for the CypA- and AGr2-system, suggesting a lower surface exposure upon unfolding for the fH19-20 protein. This finding is in agreement with fH19-20 possessing two disulfide bonds *per* CCP module, culminating in 4 disulfide bonds for the complete fH19-20 enzyme, making it more stable against denaturation. The absolute denaturant concentration also reflects this stability, as values are twice as big as in protein systems previously investigated. This stability is contrasted by the degree of HDX occurring in labeling experiments (Section 4.3). FH19-20 retains on average 70 % of its amide backbone deuterons in the conducted ESI-SUPREX experiments, indicating a very solvent exposed tertiary structure, experiencing further deprotection upon binding of FPX, as illustrated in Figure 4.14a. Thereby the 129 aa species at a 30 min incubation time is displayed with and without FPX. In the presence of FPX, deuterium levels of both, the pre- and post-transition baseline exhibit elevation, resulting in a decrease of deuterium uptake upon denaturation. Remarkably, the presence of FPX destabilises fH19-20 and shifts the SUPREX midpoints to lower concentrations. The same trend is observable for the 131 aa variant at 10 min incubation as visualised in Figure 4.14b with a destabilisation of 0.30 M compared to the apo protein. Thermodynamic analysis reveals a ΔG_f value of -27.82 ± 1.30 kJmol^{-1} and a m value of 2.97 ± 0.84 kJmol^{-1}M^{-1}, resulting in a destabilisation of 2.55 ± 3.47 kJmol^{-1} for the 129 aa species (Fig. 4.14d). Analysis of the 131 aa variant culminates in a single SUPREX point due to high s/n ratios, which is destabilised by 0.30 M. The decreased m value indicates a further increase in surface exposure upon denaturation, which well agrees with the deuterium levels of pre- and post-transition baseline of apo and holo fH19-20 both species variants.

The combination of possessing four disulfide bridges, gaining stability with the accompanying structural restrictions and a secondary structure mainly comprising loop regions, complicate general SUPREX quantification. Incubation times longer 60 min do not yield any useful data and the low change of mass incorporation upon unshielding of amide backbone protons due to denaturation make fH19-20-FPX an unsuitable protein-ligand system for investigation *via* SUPREX.

Table 4.3: Automated fH19-20 SUPREX results.

Incubation time/min	Apo fH19-20[a]	Apo fH19-20[b]	fH19-20-FPX[c] $C_{SUPREX}^{1/2}$/M	fH19-20-FPX[d]
10	2.00	2.25	2.02 (+0.02)	1.95 (-0.30)
30	2.02	2.02	1.51 (-0.51)	N/A
60	2.01	1.54	0.62 (-1.39)	N/A
120	N/A	0.35		
180	0.60	0.59		
ΔG_f/kJmol^{-1}	-30.38 ± 3.22	-29.58 ± 3.10	-27.82 ± 1.30	
$\Delta\Delta G_f$/kJmol^{-1}			+2.55 ± 3.47	
m/kJmol^{-1}M^{-1}	3.30 ± 1.84	3.10 ± 0.71	2.97 ± 0.84	

[a] 129 aa apo fh19-20.

[b] 131 aa apo fH19-20, comprising an additional EA expression artefact.

[c] FPX complexed with 129 aa apo fh19-20.

[d] FPX complexed with 131 aa apo fH19-20, comprising an additional EA expression artefact.

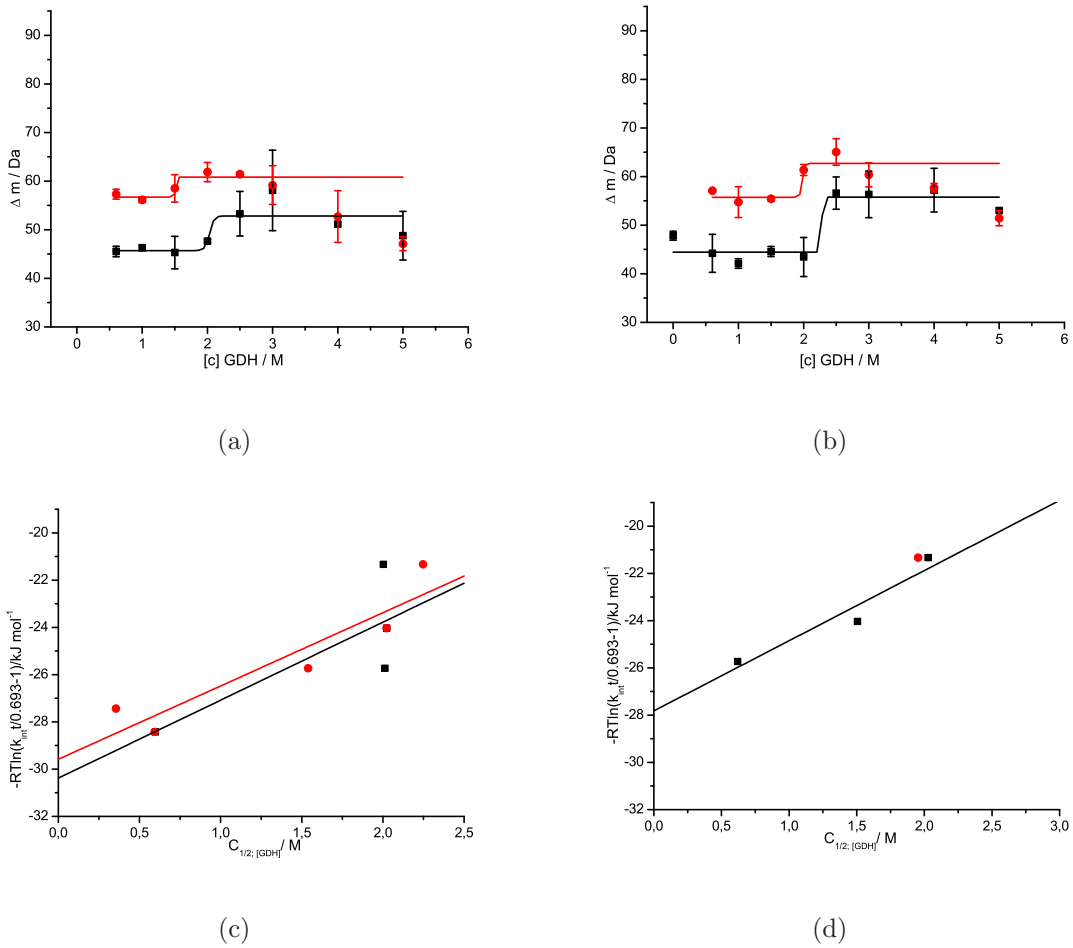

Figure 4.14: Automated fH19-20-FPX SUPREX data. (a) SUPREX curves for apo fH (129 aa, black squares) and in complex with FPX (red circles) at 30 min incubation, resulting in $C^{1/2}_{SUPREX}$ values of 2.02 M and 1.51 M for the apo and the complexed protein. (b) SUPREX curves for apo fH (131 aa, black squares) and in complex with FPX (red circles) at 10 min incubation, resulting in $C^{1/2}_{SUPREX}$ values of 2.25 M and 1.95 M for the apo and the complexed protein. (c) Free energy *vs.* $C^{1/2}_{SUPREX}$ values result in ΔG_f values of -30.38 ± 3.22 kJmol^{-1} and -29.58 ± 3.10 kJmol^{-1} for apo fH19-20 with 129 aa (black line) and 131 aa (red line), respectively. The m values are 3.30 ± 1.84 kJmol^{-1}M^{-1} and 3.10 ± 0.71 kJmol^{-1}M^{-1} for the 129 and 131 aa species. (d) Free energy *vs.* $C^{1/2}_{SUPREX}$ plot of FPX complexed fH19-20 results in a ΔG_f value of -27.82 ± 1.30 kJmol^{-1} and a m value of 2.97 ± 0.84 kJmol^{-1}M^{-1} for the 129 aa fH19-20 species (black line). For the 131 aa species, a single SUPREX midpoint at 1.95 M is displayed in red. Error bars, if present, represent standard deviation of two sets of experiments.

4.6 Automated Temperature Dependent SUPREX of AGr2

AGr2 from the Nicholson batch was subjected a SUPREX experiment identical to that in Section 4.5.1 at an incubation temperature of 50 °C with the developed

temperature adjustable sample rack (Section 2.7.4).

Figure 4.15 provides an overview of an automated ESI-SUPREX experiment at the shortest incubation of 10 min at 22 and 50 °C. Figure 4.15a shows the results of the 22 °C experiment, resulting in a $C^{1/2}_{SUPREX}$ value of 1.06 M. The 50 °C experiment is demonstrated in Figure 4.15b exhibiting SUPREX data points with large discrepancies, especially in the pre-transition region, between two repeats of identical experiment. Derived SUPREX data does not allow midpoint extraction of the 50 °C run. The deuterium levels over the complete range of chemical denaturant are equal to the post-transition baseline of apo AGr2 experiments at ambient temperature (Appendix 11.6). This indicates that complete HDX has occurred at the lowest incubation time and a zero concentration of GDH. Interestingly, the zero molar denaturant concentration exhibits the highest deuterium uptake, decreasing with increasing GDH concentration, which further emphasises the increasing interaction of GDH with the protein in question with increasing denaturant concentration, as demonstrated with CypA in Chapter 3.8.

A lower temperature might result in extractable SUPREX data, however, the way the temperature adjustable sample rack was developed (Section 2.7.4) a fine adjustment of the temperature used is not possible. A thermostat with a pump attached to the sample rack would circumvent this issue, however, this was not available.

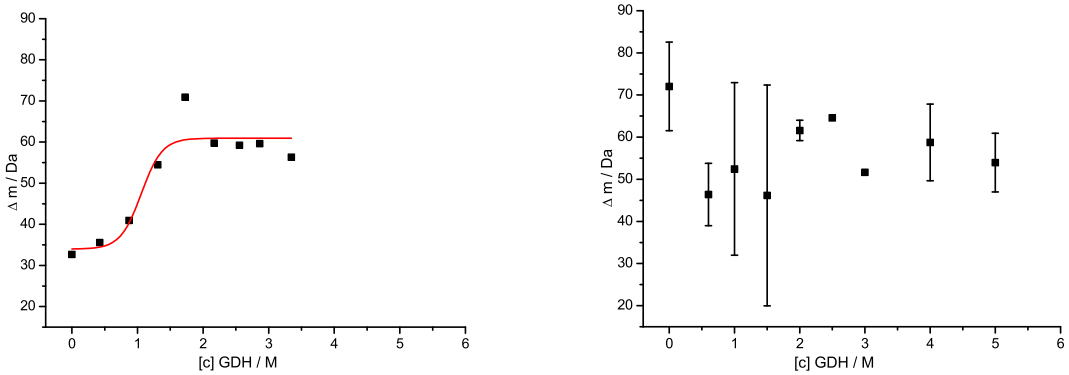

(a) (b)

Figure 4.15: Automated temperature dependent AGr2 SUPREX data. (a) Automated SUPREX experiment of apo AGr2 at 22 °C and 10 min incubation time, resulting in a $C^{1/2}_{SUPREX}$ value of 1.06 M. (b) Automated SUPREX experiment of apo AGr2 at 50 °C and 10 min incubation time (error bars, if present, represent standard deviation of two sets of experiments).

4.7 Conclusion

DI-ESI experiments confirm the masses of both AGr2 batches and the hendeca-tagged hexa-peptides. The fH19-20 protein is positively identified along with a related fH19-20 species comprising an additional Glu and Ala amino acid residue due to the expression in *Pichia pastoris*. The interaction of fH19-20 with fondaparinux has been studied.

HDX labeling experiments for AGr2 display an overall similar exchange behaviour for apo-, PTTIYY-Pen and PATIAA-Pen complexed AGr2. Nevertheless a slightly lower deuterium level was found for PTTIYY-Pen and PATIAA-Pen as for the apo protein, suggesting structural tightening/shielding upon interaction with the ligand. Temperature controlled HDX time course experiments reveal irreversible aggregation and precipitation of AGr2 after a 2.5 h period of incubation at 50 °C, indicating a thermal instability of AGr2.
FH19-20 HDX labeling data exhibits a high degree of deuteration, which can be attributed to the tertiary structure affected by the low degree of secondary structure, emphasising the solvent shielding effects of the CypA tertiary structure with respect to the back exchange behaviour upon liquid chromatography handling. The high deuterium level is further increased by the presence of the pentasaccharide FPX suggesting a conformational opening in the fH19-20 protein contrasting previous findings. SUPREX experiments were performed to investigate, if the structural opening is associated with a stabilising or destabilising effect on fH19-20-FPX protein stability.

Manual ESI-SUPREX experiments conclude a dissociation constant of 3.37 ± 5.55 µM for the AGr2-PTTIYY interaction from the Florance batch.
Manual factor H 19-20 SUPREX experiments demonstrate a higher relative stability of both, the 129 and 131 aa species in comparison with CypA. Furthermore, HDX equilibrium is reached between 60 and 180 min in the absence of the chemical denaturant as no transition occurs upon unfolding, indicating either a very dynamic structure or a non-compact structure with a large number of solvent accessible backbone hydrogen atoms. The latter finding is supported by the conformational restriction of the protein *via* the four disulfide bonds.

Automated ESI-SUPREX experiments for apo AGr2 of the two different protein batches offer multiple possible conclusions. Findings suggest either a non-two state

unfolding behaviour of AGr2 or a two state unfolding event associated with large experimental errors. The most likely event, if results from the two protein batches are reviewed, seems to be a non-two state unfolding behaviour upon oligomerisation of the AGr2 protein forming aggregates in solution. SUPREX experiments with PTTIYY-Pen and AGr2 demonstrate large experimental errors and multiple evaluation approaches. Nevertheless, if all acquired data is incorporated and two-state unfolding behaviour assumed, a dissociation constant close to a previously reported one can be extracted from the developed automated ESI-SUPREX approach. Experiments with the second hendeca-tagged hexa-peptide PATIAA-Pen indicate one order of magnitude weaker binding and postulate the first reported dissociation constant for this interactions. Absolute values might be considered with care as two-state unfolding is questionable, however, magnitudes of reported values agree well with data reported in the literature so far.

SUPREX experiments with the automated ESI-setup reveal a higher relative stability of both fH19-20 species in comparison with the resulting free energy of protein folding, suggesting a low degree of unfolding during denaturation, caused by the four disulfide bonds in fH CCP module 19 and 20. In the presence of FPX a destabilisation of both, the relative stability and the free energy of protein folding is observed complicating the determination of a dissociation constant. Gaining stability *via* the disulfide bridges, which also restricts the degree of unfolding, and the good solvent accessibility culminating in a high degree of HDX prior denaturation make fH19-20 an unsuitable candidate for general SUPREX applications.

Temperature dependent SUPREX experiments at 50 °C and 10 min incubation already display post-transition deuterium levels, suggesting thermal denaturation occurs before chemical assisted denaturation, or both contribute.

5 SUPREX of CypA and GroEL

5.1 Introduction

The molecular chaperonin groEL/groES and its effect on other proteins has been well studied with various biochemical and biophysical methods over the last four decades. Mutagenisis [165] and cryo-electron studies [164] gave insight into the mechanism of action. Denaturing studies with urea and solution x-ray scattering revealed the reassembly properties of the *E. coli* chaperonin, indicating concentration dependent distinct partial dissociation and cooperative unfolding [289]. The effects on other proteins have been investigated *i.a.* with CD [161], fluorescence-denaturation [177] and fluorescence anisotropy experiments [175], just to name a few.

In the field of MS the *E. coli* chaperonin system groEL/groES has been of keen interest. Robinson, Gross and Ashcroft *et al.* investigated the chaperonin and chaperon-bound protein properties utilising ESI-MS [290, 291, 292, 293, 294, 295]. More recently van Duijn and Heck *et al.* probed groEL-substrate behaviour employing tandem [296], ESI [170] and ESI ion mobility mass spectrometry techniques [89]. Direct MALDI-MS was employed by Ohtsu *et al.* to identify large enzymes, *i.a.* groEL and groES on immunoblotting membranes [297].

Three different classes of exchange speed were observed for CypA exhibiting fast, moderate and slow exchange behaviour [270]. In 1994 Zahn *et al.* [298] investigated the HDX behaviour of amide protons by NMR, concluding three association/dissociation cycles are needed to completely exchange the T2 hydrogen atoms in CypA, indicating a destabilisation of the entire protein in the complex with groEL. These findings have been confirmed by Zahn in 1996 by conducting experiments on only the apical domain of the groEL protein [178] and by Wüthrich *et al.* [179] in 1997. The speed of complex formation of groEL-CypA is pH dependent and has been found to occur between 5.0 and 7.0, whereas lower pH conditions trigger aggregation of CypA. Furthermore the dissociation of the complex is assisted by low temperature conditions (6 °C), whereas ambient temperatures favour association [179].

In conclusion, it has been shown that CypA undergoes reversible global unfolding once bound to groEL. The unfolded state of CypA is stabilised by binding of the hydrophobic side chains in the central cavity of the groEL cylinder. Multi-

ple denaturation/renaturation cycles would allow misfolded, kinetically trapped or folding-incompetent species to find a folding-pathway, resulting in the proper folded state [179].

The ambition here is to unfold CypA with groEL[7] in the absence of the co-factors and utilising the developed ESI-SUPREX approach to detect the unfolded CypA species stabilised in the groEL-CypA complex.

5.2 Direct Infusion

After groEL was expressed, purified and positively identified by SDS-PAGE (Chapter 2.2.2) a DI-MS experiment was conducted for further characterisation. Therefore groEL was prepared under denaturing conditions containing 10 % FA to a final concentration of 10 µM as described in Chapter 2.3.1 and subjected to DI-nano-ESI-MS on a QTOF2 mass spectrometer (Section 2.3.4). There was no evidence for the groEL tetradecamer but this was not expected under non-native ESI conditions. Nevertheless Heck *et al.* reported the oligomeric species under almost identical buffer conditions [89]. Furthermore gel filtration purification (Section 2.2.2 Fig. 2.4) suggests the presence of the groEL tetradecamer.
Figure 5.1 illustrates a wide charge state distribution ranging from 25+ to 70+ of a single groEL subunit. Deconvolution results in a mass of 57211 ± 13 Da indicating a methionine loss, compared to the full 548 aa sequence (Appendix 12.1) with a mass of 57329 Da. The theoretical mass lacking one methionine residue is 57197 Da being within the margin of error of the DI-ESI-MS data acquired, culminating in a mass for the intact groEL of 800954 ± 182 Da, which is further utilised for automated ESI-SUPREX experiments. The assumption of expressed groEL lacking a methionine is strengthened by the fact that van Duijn *et al.* report an identical apo groEL mass of 57197 Da for the individual subunit and 800.758 kDa for the intact groEL [89].

[7] utilisation of the term groEL refers to the tetradecameric form of groEL

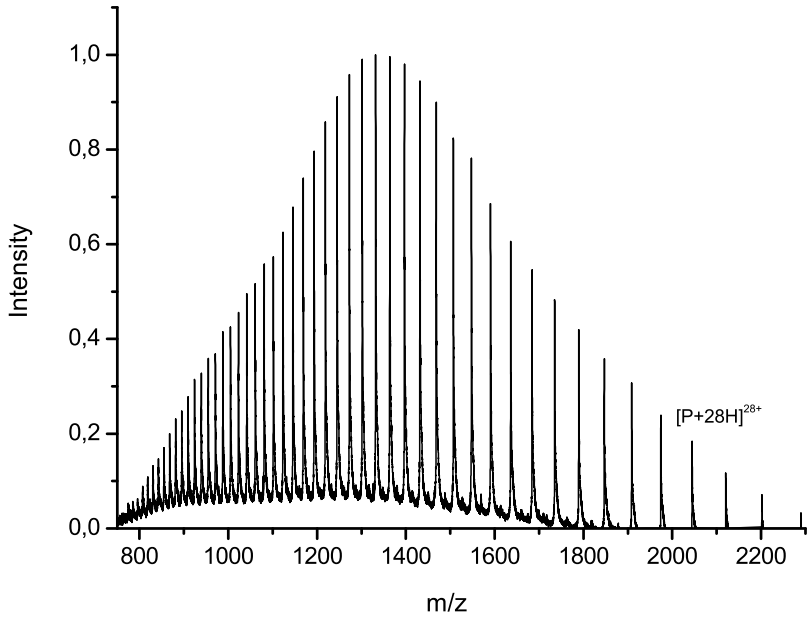

Figure 5.1: Direct infusion spectrum of apo groEL. Sprayed under denaturing conditions from 10 mM NH_4OAc containing 10 % FA at a total concentration of 10 µM with charge states 25+ to 70+.

5.3 Labeling Experiments

The groEL-CypA system was subjected to HDX labeling experiments (Section 2.3.5) with the devised automated SUPREX setup (Section 2.7.3) at a final CypA concentration of 5 µM probing exchange behaviour of both proteins. As the ESI-SUPREX method developed is based on HPLC analysis of quenched/denatured proteins, the sheer size of groEL complicates a stoichiometric use of groEL, as upon denaturation for each equivalent of intact groEL 14 equivalents of subunits are observed. A compromise between massively overloading the guard column and still detecting CypA resulted in the utilisation of the oligomeric groEL at a third of the CypA starting concentration, however, a stoichiometric application would have been desirable. The LC-programs/conditions employed were identical to the HDX labeling studies previously presented (3.3, 4.3), enabling direct data comparison.

Figure 5.2a visualises the deuterium uptake with regard to time for apo CypA in the presence of groEL and 18/2.3 % MeOH for comparison. Apo CypA displays the slowest exchange rate and the lowest deuterium level with ~43 Da. Exchange rates for CypA in complex with groEL and in the presence of methanol are higher, compared to the free protein, however almost similar, as are the deuterium levels of

~57 Da and ~59 Da. These findings suggest similar degrees of denaturation upon alcohol denaturation and unfolding of CypA *via* groEL resulting in stabilisation of an unfolded state in the groEL-CypA complex. The non-stoichometric application of groEL with CypA might have disfavoured stabilisation of the entire unfolded CypA population. Nevertheless, the comparison with CypA HDX labeling experiments (Section 3.3), in particular the time course experiment with ES1234 and 1 M GDH, suggests a lower degree of unfolding and HDX of CypA in the groEL complex than when denatured with GDH (Fig. 5.2a). As proposed by Wüthrich *et al.* one would assume a similar degree of exchange as groEL complexed CypA undergoes unfolding with the stabilisation of a globally unfolded state [179]. CypA HDX labeling experiments conducted in the presence of tetradecameric groEL do not support this idea of stabilisation of globally unfolded CypA.

According to its sequence (Appendix 12.1) lacking one methionine residue, groEL comprises a total of 4126 hydrogen atoms, split in 380 T1, 533 T2 and 3213 T3 hydrogen atoms for each of the 14 subunits. Deuterium uptake *versus* time is displayed in Figure 5.2b indicating an equilibrium deuterium level of 269 incorporation after approximately 204 min. Upon these findings 50 % of the amide backbone protons are subjected to back exchange and/or experienced solvent protection by virtue of the tertiary structure of the enzyme. Interestingly the HDX-rate and deuterium level increases by 29 Da to 298 after complexation with CypA, suggesting that in the complex more T2 protons are solvent accessible on grounds of deprotection and conformational changes upon CypA binding. This contrasts somewhat with the idea of a more compact conformation and an increased amide protection due to binding of CypA in the inner cavity of groEL.

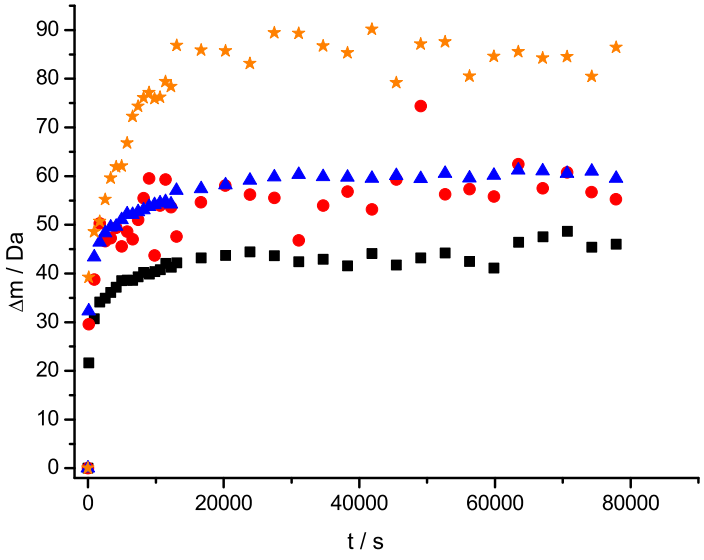

(a)

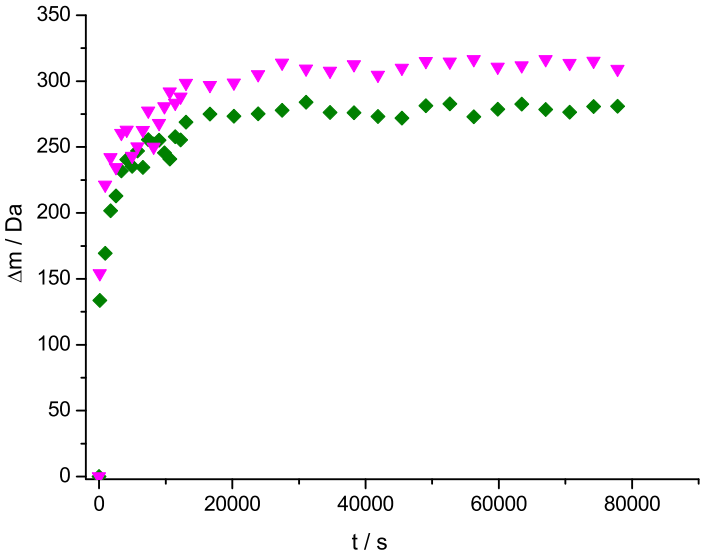

(b)

Figure 5.2: HDX labeling experiments for the CypA-groEL system. (a) Deuterium uptake *vs.* time of apo CypA (black squares), CypA in the presence of groEL (red circles), CypA in 18/2.4 % MeOH (blue triangles) and CypA with ES1234 in 1M GDH (orange stars). (b) Deuterium uptake *vs.* time of apo groEL (green diamonds) and groEL in the presence of CypA (magenta triangles).

5.4 SUPREX - Automated

Automated ESI-SUPREX was conducted as described in Section 2.7.3. To simultaneously observe CypA and groEL in a SUPREX experiment with GDH it was necessary to further decrease the chaperonin concentration to a tenth of the CypA concentration, which was for all groEL-CypA SUPREX experiments 5 µM (CypA). *In vivo* the basal level of groEL is ~4 µM, whereas the concentration of nascent protein-chains is ~35 µM [159], resulting in a chaperonin/unfolded protein ratio of ~11 %. Hence, experimental conditions are comparable to those *in vivo* with respect to the chaperonin/unfolded protein ratio.
ESI-SUPREX data for apo CypA and in the complex with CsA is displayed in Chapter 3.7 and summarised in Table 3.4.

5.4.1 Apo GroEL

Freshly expressed and purified groEL was subjected to ESI-SUPREX analysis and $C^{1/2}_{SUPREX}$ values are determined for 10, 30, 45, 60, 90, 120 and 180 min incubation and are summarised in Table 5.1. Figure 5.3a demonstrates the destabilisation of the chaperonin with the associated shift to lower $C^{1/2}_{SUPREX}$ values with increasing incubation time with GDH for 30 and 120 min. The complete set of ESI-SUPREX curves acquired is arranged in Appendix 12.2. Incubation times longer than 180 min do not yield useful SUPREX data due to very high s/n ratios associated with protein degradation of both proteins. Analysis of SUPREX inflexion points results in values of -32.55 ± 4.23 kJmol^{-1} for ΔG_f and a resulting m value of 5.90 ± 2.94 kJmol^{-1}M^{-1} utilising a linear fit assuming two state unfolding (Fig. 5.3b and Table 5.1). Large deviations on $C^{1/2}_{SUPREX}$ values *vs.* ΔG_f either indicate large errors associated with the determination of $C^{1/2}_{SUPREX}$ values or unfolding of groEL does not exhibit two-state unfolding behaviour. The deuterium level of the pretransition baseline is between ~112 and 130 Da for the investigated incubation times, whereas the posttransition baseline exhibits levels between ~275-300 Da, resulting in a deprotection of ~167 amide protons. Interestingly the SUPREX curves for 10-120 min do not exhibit uniform sigmoidal behaviour, moreover they reveal a slight increase in the deuterium level before complete denaturation occurs. This agrees with denaturation/reassembly studies of groEL conducted by Munehito *et al.* in 2003. It is reported, that groEL exhibits partial denaturation at concentrations of urea <3 M and cooperatively unfolds at concentrations >3 M [289]. As GDH is a more efficient denaturant, ESI-SUPREX denaturation experiments demonstrate partial unfold-

ing below 1 M GDH and completely unfolding between 1.0-1.5 M depending on the incubation time. These findings further indicate that ESI-SUPREX derived thermodynamic data would not be accurate as accuracy of SUPREX is based on two state unfolding behaviour. Nonetheless, a qualitative comparison between ESI-SUPREX derived data should shed some light into the PPIase-chaperonin interaction.

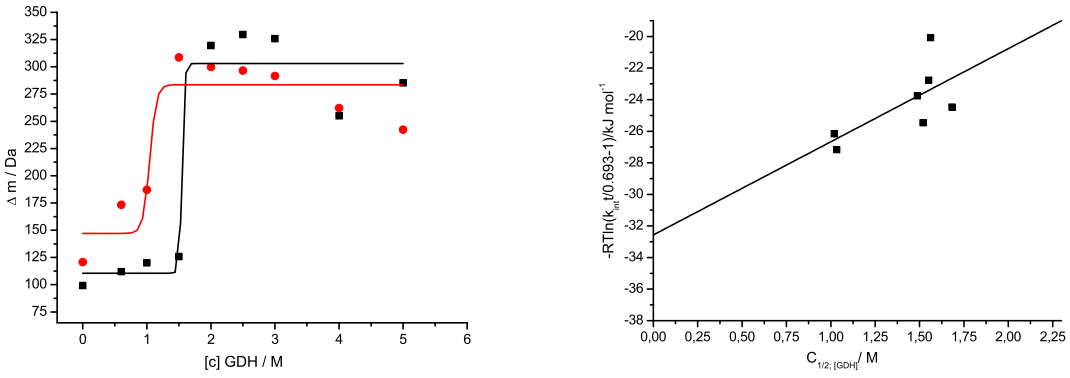

(a) (b)

Figure 5.3: Automated SUPREX data for apo groEL. (a) SUPREX curves for apo groEL for 30 (black squares) and 120 min (red circles) incubation. (b) Free energy of protein folding *vs.* $C^{1/2}_{SUPREX}$ plot, with ΔG_f -32.55 ± 4.23 kJmol^{-1} and an m value of 5.80 ± 2.94 kJmol^{-1}M^{-1}.

5.4.2 CypA-GroEL

ESI-SUPREX derived thermodynamic parameters are displayed in Table 5.1 on page 149, indicating CypA experiences a stabilisation of 0.31, 0.54, 0.49, 0.42, 0.41 and 0.39 M for incubation times 10, 30, 45, 60, 90, 120 and 180 min. For 30 min incubation the stabilisation of 0.54 M of CypA in the groEL-CypA complex is visualised in Figure 5.4a. ΔG_f is calculated to be -39.54 ± 2.26 kJmol^{-1} with a m value of 13.81 ± 2.13 kJmol^{-1}M^{-1}, resulting in a stabilisation of -7.11 ± 4.77 kJmol^{-1}. The stabilisation is similar to CypA in 18/2.3 % MeOH with -6.32 kJmol^{-1} and more than half the value of the CypA-CsA complex with -12.05 ± 4.73 kJmol^{-1} solely attributed to the interaction with groEL. On the other hand an increased m value of 13.81 ± 2.13 kJmol^{-1}M^{-1} compared to 12.38 ± 3.01 kJmol^{-1}M^{-1} in apo CypA and 7.11 ± 1.63 kJmol^{-1}M^{-1} in the CypA-CsA complex, suggests a higher degree of unfolding during the denaturation step. These findings agree with the theorem of the denaturing properties of groEL in conjunction with stabilising a highly unfolded species *via* hydrophobic interactions in the Anfinson's cage (Fig. 5.5).

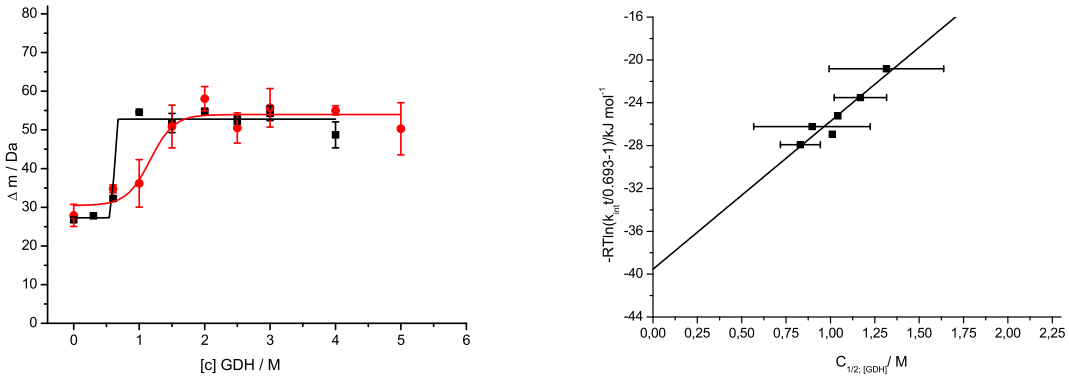

(a) (b)

Figure 5.4: Automated SUPREX data for CypA in the presence of groEL. (a) SUPREX curves of 30 min incubation of apo CypA (black squares; from Chapter 3.7.1) and in complex with groEL (red circles). (b) Free energy of protein folding *vs.* $C^{1/2}_{SUPREX}$ plot, with ΔG_f -39.54 ± 2.26 kJmol^{-1} and an m value of 13.81 ± 2.13 kJmol^{-1}M^{-1}, resulting in a -7.11 ± 4.77 kJmol^{-1} stabilisation.

Evaluation of SUPREX curves for the *E. coli* chaperonin in the presence with CypA (Appendix 12.4) reveals a stabilisation between 0.04-0.69 M for identical incubation times (Table 5.1). Figure 5.6a illustrates the stabilisation of groEL upon denaturation in the presence of the PPIase for a 120 min incubation time. The pre-transition baseline is similar for free and CypA complexed groEL and significantly decreases for the post-transition baseline of the complexed groEL. This decrease indicates an increased protection of amide protons in the groEL-CypA complex as a result of CypA being bound and stabilised in groEL's inner cavity (Fig. 5.5). These SUPREX results clearly demonstrate the stabilisation of CypA by groEL, whereas this information cannot be obtained directly from HDX labeling studies alone.
To enable a direct comparison to the apo protein the ΔG_f *vs.* $C^{1/2}_{SUPREX}$ plot was linear fitted, though two-state unfolding was questionable. The resulting ΔG_f value is extrapolated to be -35.86 ± 10.84 kJmol^{-1} with a m value of 6.49 ± 6.15 kJmol^{-1}M^{-1}, culminating in a $\Delta\Delta G_f$ of -3.10 ± 11.63 kJmol^{-1} (Fig. 5.6b). Large errors of ΔG_f and m values are associated with linear fitting of acquired SUPREX data. However, comparing the m values of groEL with and without CypA concludes a lower surface exposure of CypA-complexed groEL upon denaturation and/or a more stepwise fashion of unfolding, rather than one cooperative event. The calculated stabilisation of -3.10 ± 11.63 kJmol^{-1} is not quantitative *per se*, notwithstand-

ing a stabilisation of groEL upon CypA binding is evident as $C_{SUPREX}^{1/2}$ values are shifted to higher concentrations of GDH (Table 5.1 and Fig. 5.6).

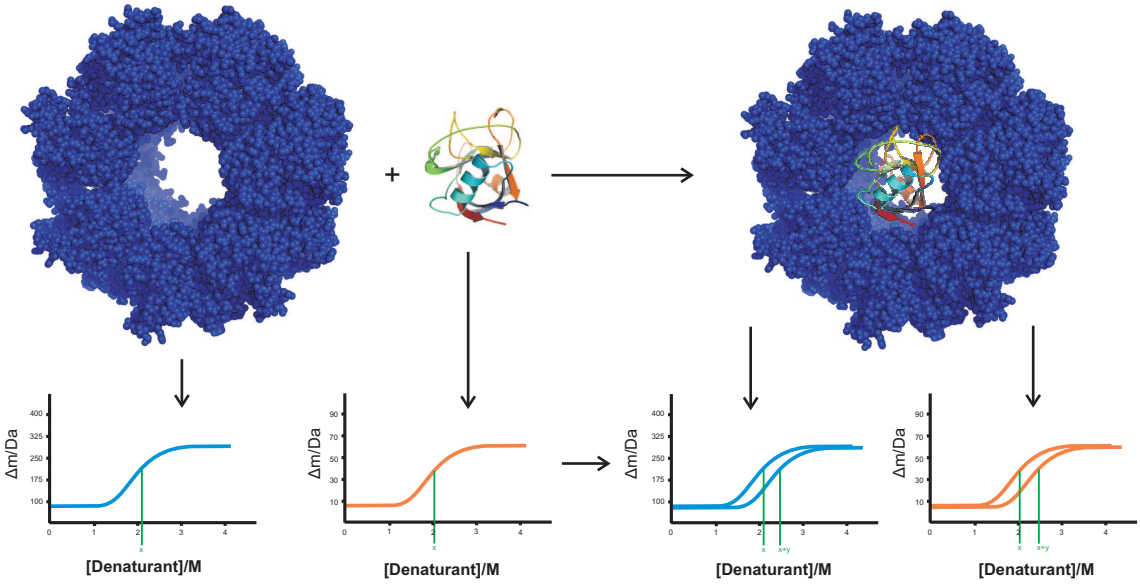

Figure 5.5: The groEL-cyclophilin A interaction. GroEL (blue) interacting with CypA (coloured) and binding of a partially unfolded CypA species in the central cavity, resulting in detectable stabilisations of both proteins in automated ESI-SUPREX experiments (pdb files 1cwa and 1oel displayed and modified with pymol (DeLano Scientific LLC - Palo Alto, USA)).

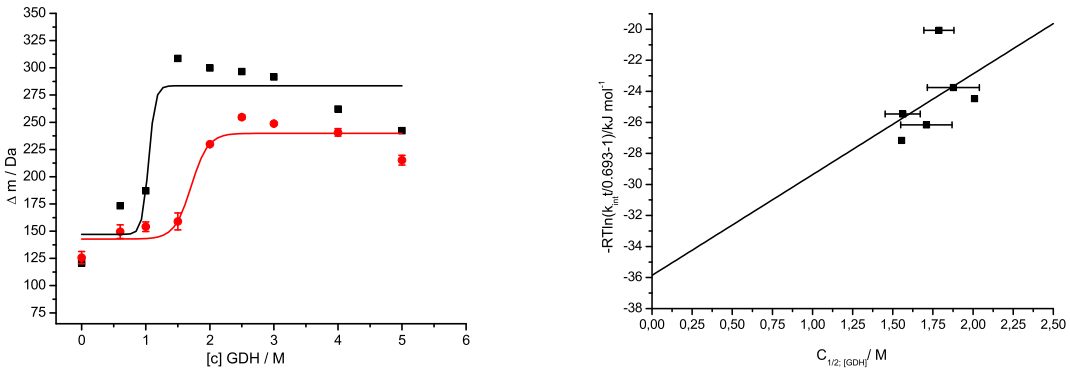

(a) (b)

Figure 5.6: Automated SUPREX data for groEL in the presence of CypA. (a) SUPREX curves of 30 min incubation of apo groEL (black squares) and in complex with CypA (red circles). (b) Free energy of protein folding *vs.* $C_{SUPREX}^{1/2}$ plot, with ΔG_f -35.86 $\pm$ 10.84 kJmol^{-1} and an m value of 6.49 $\pm$ 6.15 kJmol^{-1}M^{-1}, resulting in a -3.10 $\pm$ 11.63 kJmol^{-1} stabilisation.

5.4.3 CypA-CsA-GroEL

To probe effects of CsA on the groEL-CypA complex, automated ESI-SUPREX experiments were conducted. Samples were prepared and experiments executed according to Section 2.7.1 and 2.7.3. After 20 min CypA-CsA incubation groEL was added and further incubated for 20 min, before SUPREX buffers were added and samples subjected to the SUPREX routine. The final groEL concentration was identical to that used in previous experiments at a tenth of the CypA concentration. Four incubation times were probed from 10-90 min, resulting in SUPREX curves visualised in Appendix 12.5. For longer incubation times no SUPREX data was recovered due to degradation of the enzymes utilised.

SUPREX inflexion points for 10, 30, 60 and 90 min incubation demonstrate an increased stability compared to apo CypA (Table 5.1). When considered along with the CypA-CsA experiments described in the previous Section, a lower degree of stabilisation is observed for all investigated incubation times, ranging from -0.01 to -0.44 M (Table 5.1). This destabilisation indicates an interaction of groEL with the pre-formed CypA-CsA complex. One possibility might be direct interaction of the CypA-CsA complex with groEL, destabilising the tight CypA-CsA binding without dissociating it. $C^{1/2}_{SUPREX}$ values over 2 M GDH for incubation times between 10-60 min support the existence of the CypA-CsA complex in the presence of groEL. Thereby CypA conformation might be altered, lowering the strength of CypA-CsA interaction but still preserving the characteristics necessary for CsA binding.
The deuterium levels of the pre-transition baselines exhibit similarities to those in the apo CypA and CypA-CsA-complex, whereas the post-transition baselines are non consistent. The four incubation times show post-transition deuterium levels between 35-100 Da, increasing with incubation time from 10-60 min and decreasing for the 90 min incubation. These findings are different from those for apo CypA and CypA-CsA from Chapter 3.7, suggesting an increased degree of unfolding of CypA with prolonged incubation times followed by an event, which disables cooperative unfolding in the presence of groEL.

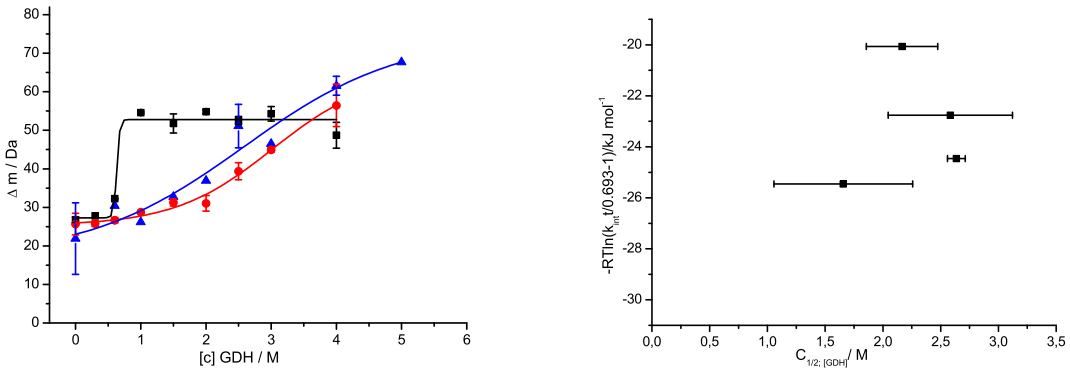

(b)

Figure 5.7: Automated SUPREX data for CypA in the presence of CsA and groEL. (a) Comparison of apo CypA (black squares), CypA-CsA (red circles) and CypA-CsA in the presence of groEL (blue triangles) at a 30 min incubation time. Apo CypA and CypA-CsA data is taken from Chapter 3.7.1. CypA is incubated with CsA for 20 min before groEL is added and incubated for further 20 min. (b) Free energy of protein folding *vs.* $C^{1/2}_{SUPREX}$ plot, complicating linear fit analysis.

ESI-SUPREX data for groEL in the presence of the CypA-CsA complex was extracted from the same experiment conducted for CypA. SUPREX parameters for groEL in the presence of the CypA-CsA complex are visualised in Table 5.1, demonstrating an inverse shift of $C^{1/2}_{SUPREX}$ values with regards to time. Comparison with the apo protein indicates that groEL gets more and more stabilised in the presence of the CypA-CsA complex upon denaturation *vs.* time as visualised in Figure 5.8a. The comparison of CypA-bound *vs.* CypA-CsA-bound groEL does exhibit on average a less stabilisation of CypA-CsA bound groEL. Nevertheless, CypA in complexed with groEL displays a similar trend at 10-60 min incubation before decreasing appropriately for incubation times over 60 min (Table 5.1). Figure 5.8b displays the resulting ΔG_f *vs.* $C^{1/2}_{SUPREX}$ plot, showing an inversed trend which impedes thermodynamical analysis. However, thermodynamic parameters are calculated (Table 5.1) but are out of context for acquired data.
These observations indicate a conformational change in the groEL protein due to the presence of the CypA-CsA complex and GDH, resulting in a more stable form. However, no evidence has been yet reported to support these findings.

The deuterium levels of the pre-transition baseline of groEL in the presence of the CypA-CsA complex are higher compared to the apo protein but similar to those obtained in the groEL-CypA ESI-SUPREX experiments. The post-transition

baseline is significantly lower compared to the apo protein and displays a similar deuterium level as in CypA-groEL experiments, leading to the conclusion that the CypA-CsA complex possesses some degree of affinity for the groEL's inner cavity, as indicated by the analysis of CypA in the CsA-complex and the presence of groEL.

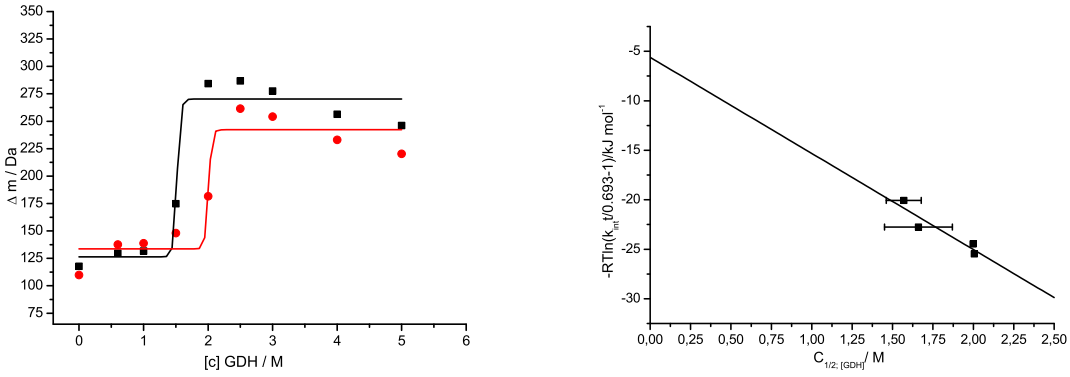

(a) (b)

Figure 5.8: Automated SUPREX data for groEL in the presence of CypA and CsA. (a) SUPREX curves for groEL in the presence of the CypA-CsA complex at a 90 min incubation. CypA and CsA are incubated for 20 min before groEL addition (red circles), whereas black squares represent apo groEL. (b) Free energy of protein folding *vs.* $C_{SUPREX}^{1/2}$ plot, with ΔG_f -5.61 $\pm$ 4.73 kJmol^{-1} and an m value of -9.71 $\pm$ 2.59 kJmol^{-1}M^{-1}, resulting in a 26.82 $\pm$ 6.36 kJmol^{-1} destabilisation, which is not comparable to other data acquired due to the inverse denaturation behaviour of the protein.

Table 5.1: Automated CypA-CsA-groEL SUPREX results ($C^{1/2}_{SUPREX}$ values are visualised for bold printed proteins).

Incubation/min	Apo CypA[a]	Apo GroEL[b]	**CypA**-CsA[c]	**CypA**-groEL[d] $C^{1/2}_{SUPREX}$/M	**groEL**-CypA[e]	**CypA**-CsA-groEL[f]	CypA-CsA-**groEL**[g]
10	1.00	1.56	2.57 (1.57)	1.31 (0.31)	1.79 (0.23)	2.16 (-0.41)	1.57 (0.01/-0.22)
15	0.68		2.39 (1.71)				
30	0.63	1.55	3.02 (2.39)	1.17 (0.54)	1.87 (0.32)	2.58 (-0.44)	1.66 (0.11/-0.21)
45	0.54	1.49	2.68 (2.14)				
60	0.55	1.68	2.64 (2.09)	1.04 (0.49)	2.00 (0.32)	2.63 (-0.01)	2.00 (0.32/±0.00)
90	0.48	1.52		0.90 (0.42)	1.56 (0.04)	1.65 (N/A)	2.00 (0.48/+0.44)
120	0.60	1.02	2.53 (1.93)	1.01 (0.41)	1.71 (0.69)		
150	0.51						
180	0.44	1.03	2.39 (1.95)	0.83 (0.39)	1.56 (0.53)		
420	0.62						
ΔG_f/kJmol^{-1}	-32.43 ± 1.88	-32.55 ± 4.23	-44.48 ± 4.35	-39.54 ± 2.26	35.86 ± 10.84		-5.61 ± 4.73*
$\Delta\Delta G_f$/kJmol^{-1}			-12.05 ± 4.73	-7.11 ± 4.77	-3.10 ± 11.63		26.82 ± 6.36*
m/kJmol^{-1}M^{-1}	12.38 ± 3.01	5.90 ± 2.94	7.11 ± 1.63	13.81 ± 2.13	6.49 ± 6.15		-9.71 ± 2.59*

[a] visualised in Section 3.7.1 Fig. 3.14 and Appendix 10.6.

[b] visualised in Section 5.4.1 Fig. 5.3 and Appendix 12.2.

[c] visualised in Section 3.7.3 Fig. 3.16 and Appendix 10.8. Values in brackets denote change of $C^{1/2}_{SUPREX}$ compared to apo protein.

[d] visualised in Section 5.4.2 Fig. 5.4 and Appendix 12.3. Values in brackets denote change of $C^{1/2}_{SUPREX}$ compared to apo protein.

[e] visualised in Section 5.4.2 Fig. 5.4 and Appendix 12.4. Values in brackets denote change of $C^{1/2}_{SUPREX}$ compared to apo protein.

[f] visualised in Section 5.4.3 Fig. 5.7 and Appendix 12.5. Values in brackets denote change of $C^{1/2}_{SUPREX}$ compared to CypA-CsA complex.

[g] visualised in Section 5.4.3 Fig. 5.8 and Appendix 12.6. Values in brackets denote change of $C^{1/2}_{SUPREX}$ compared to apo protein and in complex with CypA.

* Thermodynamic SUPREX parameters are out of context to other parameters as an inverse trend in the ΔG_f *vs.* $C^{1/2}_{SUPREX}$ plot is observed (Fig. 5.8b).

5.5 Conclusion

DI-ESI-MS analysis of expressed groEL further emphasises the success of protein expression and purification and indicates a lack of one methionine residue consistent with recent reported data.

In HDX labeling experiments cyclophilin A in complex with groEL in a 3:1 stoichiometry clearly exhibits denaturation. However the degree of denaturation is lower compared to alcohol induced denaturation with methanol and denaturation in the presence of the chemical denaturant guanidinium hydrochloride. Nevertheless, the observed denaturation properties of CypA can solely be attributed to the interaction with groEL, albeit that a globally unfolded and stabilised CypA species could not be observed.
Labeling experiments with groEL display a decreased protection of amide hydrogen atoms and therefore a higher deuterium uptake in the chaperonin in the presence of CypA, suggesting that conformational alterations occur upon CypA complexation culminating in a more solvent-accessible conformation of the *E. coli* chaperonin.

Apo ESI-SUPREX experiments demonstrate non-two state unfolding behaviour for the *E. coli* chaperonin groEL, as partial unfolding is observed for almost all incubation times utilised at guanidinium hydrochloride concentrations below 1 M. Above this concentration cooperative unfolding is observed. Non-two state conditions compromise data accuracy for ESI-SUPREX, however, a qualitative comparison is possible. The SUPREX determined thermodynamic parameters are not directly comparable *per se*, except determined K_d's.

For CypA in complex with groEL the denaturing properties and stabilisation of the denatured CypA species in the groEL-CypA-complex are confirmed by ESI-SUPREX. Thermodynamic data determined demonstrates similarities to alcohol induced denaturation with methanol, however, solely attributed to the interaction with groEL. Contextualising apo groEL SUPREX data, CypA still exhibits two state unfolding behaviour.
GroEL in complex with CypA displays the same non-two state unfolding behaviour as apo groEL indicating dynamic partial dissociation before cooperative unfolding. Moreover a stabilisation of groEL in the presence of CypA is evident, as confirmed by SUPREX curves and non-two state free energies of protein folding. Comparison of apo- and CypA-complexed groEL SUPREX curves and associated deuterium lev-

els, contradict the HDX labeling experiments performed, concluding an increased protection of amide protons and/or conformational tightening upon CypA binding.

CypA in complex with CsA in the presence of groEL exhibits a stabilisation in comparison to the apo protein, which is lower than the stabilisation in the CypA-CsA complex. GroEL alters the CypA conformation in the complex with CsA when interacting with the inner cavity of the chaperonin resulting in a partial destabilisation of the CypA-CsA complex, however, not resulting in ligand dissociation.
Results for groEL ESI-SUPREX experiments are not conclusive as data exhibits an inverse trend of stabilisation upon denaturation with guanidinium hydrochloride over time, impeding thermodynamic analysis. Qualitatively, a change in conformation of groEL upon penetration with denaturant and the presence of the CypA-CsA complex to a more stable/compact state would account for the observations reported.

6 Summary

This thesis details the advancement and development of a liquid chromatography interface for electrospray ionisation mass spectrometry to enable investigation of protein-ligand interactions. Thermodynamic properties of various protein-ligand systems can be measured in a high-throughput fashion. The method employs hydrogen-deuterium exchange and titration an adaptation of PLIMSTEX and SUPREX. The major challenge of this work was to develop a liquid chromatography setup delivering reproducible data for rapidly investigating a given protein-ligand system (Chapter 2). Initially the hardware developed was tested with the well investigated, self expressed and purified, cyclophilin A-cyclosporin A protein system and PLIMSTEX and SUPREX experiments were conducted (Chapter 3). Then a set of 'unknown' proteins and ligands were investigated with ESI-SUPREX: The potential oncogene anterior gradient 2 exhibiting binding potential to a set of hexapeptides and two modules of the complement control protein 19-20 (fH19-20), which shows great promise to bind to polyanions, such as fondaparinux (Chapter 4). For these enzyme systems the SUPREX approach was enhanced by conducting experiments at different temperatures. Finally the *E. coli* chaperonin groEL was expressed and purified and subjected ESI-SUPREX analysis in conjunction with CypA and CsA to demonstrate the chaperoning effects of groEL on the peptidyl-prolyl-isomerase (Chapter 5).

The development and progress of the manual and the automated ESI-PLIMSTEX and SUPREX approach is documented in Chapter 2 along with various optimisation steps with respect to sample handling and hydrogen deuterium exchange optimisation. PLIMSTEX and SUPREX methodologies were tested on their general applicability with insulin and myoglobin exhibiting the expected PLIMSTEX and SUPREX behaviour. The self expressed and purified proteins cyclophilin A and groEL are positively identified by biological methods and by direct infusion electrospray ionisation mass spectrometry.

Experimental HDX labeling data presented in Chapter 3 reveals lower deuterium levels of CypA in complex with CsA, KM184 and ES1234 qualitatively indicating an interaction of these ligands with CypA. Manual PLIMSTEX experiments of CypA and CsA demonstrated dissociation constants within a factor of ten of that found with biological assays [282, 252, 283, 284, 141, 145] and a factor of four to MALDI-

SUPREX data [268]. Evaluation of automated, bulk and individually incubated PLIMSTEX does not demonstrate useful binding data due to the fact that associated errors are within the margin of the deuterium uptake due to protection upon ligand binding. These findings call into question the general applicability of PLIMSTEX and emphasise the necessity of measurable amide protection. The larger this protection is the more reproducible and reliable PLIMSTEX data is acquired making PLIMSTEX highly system dependent and unsuitable for *a priori* protein-ligand high throughput screening.
Manual and automated ESI-SUPREX exhibited better data reproducibility than PLIMSTEX and dissociation constants determined for the CypA-CsA interaction were within a factor of ten and eight to K_d's determined with biological [282, 252, 283, 284, 141, 145] and MALDI-SUPREX methodologies [268], respectively. For the interaction with KM184 a dissociation constant was found that is almost identical to values determined by surface plasmon resonance [252, 141]. By contrast the CypA-ES1234 interaction either exhibits a, by a factor of four, tighter binding with respect to CsA or suggests non-two state unfolding behaviour as the dissociation constant contradicts the individual SUPREX midpoint concentrations. Again this finding throws into question the validity of high-throughput HDX-MS strategies for screening applications.
In terms of throughput, automation of the ESI-SUPREX approach doubled the number of analysed samples in a 24 hour period, compared to the manual experiment, in conjunction with elimination of errors associated with manually timing and execution.

The investigation of 'unknown' protein-ligand systems, anterior gradient 2 and factor H, with the developed ESI-SUPREX setup in Chapter 4 exhibited a dualistic trend of data acquired for AGr2. Findings suggest either a non-two state unfolding or a large experimental error associated with a two-state unfolding event. Given the preliminary nature of these findings the latter is more likely. Multiple approaches of data evaluation and fitting were discussed comprising individual hand selected data sets. However, if all the experimental data collected was subjected data analysis based on two-state unfolding and EX2 exchange conditions, an ESI-SUPREX dissociation constant (24.52 µM) close to the competition fluorescence anisotropy one was determined (25-40 µM; unpublished data) for the hendeca-tagged hexapeptide PTTIYY-Pen and the 27 amino acid long His-tagged AGr2. The interaction with PATIYY-Pen was quantified with a dissociation constant of 198.98 µM. Care

must be taken attesting quantitative binding information to the AGr2-PTTIYY interaction on grounds of both compounds comprising massive cell penetrating tags (Chapter 4), which may well affect protein-ligand interactions. However, at the beginning of investigating new protein-ligand systems these measures are necessary and often the only way to access the biological species of interest and will be refined as more information becomes available.
Temperature dependent HDX labling and ESI-SUPREX experiments demonstrated posttransition deuterium levels at all denaturant concentrations for the shortest possible SUPREX incubation time and an aggregation and precipitation of AGr2 at 50 °C.
For factor H ESI-SUPREX experiments, the limits of general SUPREX applicability were demonstrated as incubation times longer than 60 minutes exhibited no further transition upon denaturation as HDX equilibrium was already reached. These findings emphasise the solvent accessibility, in conjunction with a low difference in mass incorporation upon denaturation and the rigidness of fH19-20 due to the four disulfide bonds. ESI-SUPREX experiments with the pentasaccharose fondaparinux and the two fH variants did not yield a dissociation constant due to the lack of SUPREX midpoint denaturing concentrations of the holo system. However, HDX labeling experiments suggest a gain in solvent accessibility and conformational opening upon interaction with fondaparinux.
Meeting the criteria of two-state unfolding behaviour and following EX2 conditions as well as a decent 'protection' against complete hydrogen/deuterium exchange, seems to be guarantor for reliable and reproducible thermodynamical data and dissociation constants. When these requirements are not fulfilled or unknown, SUPREX is proposed to still deliver reliable data. The work on AGr2 and fH19-20 along with their ligands demonstrated the outcome, if one or both of these requirements were not met, the universal applicability of SUPREX for *a priori* screening of not well characterised proteins and their potential ligands is questionable. On the other hand SUPREX has been demonstrated to deliver qualitatively good thermodynamical data for K_d calculations with well investigated protein ligand-systems following the SUPREX requirements, and so we can conclude that successful SUPREX analysis is system dependent.

In Chapter 5 the experimental HDX labling data of CypA in the presence of the *E. coli* chaperonin groEL revealed the unfolding capabilities of the chaperonin and the resulting stabilisation of a partially unfolded CypA species, however, a globally

unfolded CypA was not detected under experimental conditions. ESI-SUPREX experiments on the CypA-groEL system further emphasised the stabilisation of a CypA species in complex with groEL, as SUPREX midpoint concentrations demonstrated. Apo groEL conducted automated ESI-SUPREX experiments displayed non-two state unfolding behaviour for the *E. coli* chaperonin, as partially unfolding was observed for concentrations below one molar of the chemical denaturant, whereas above this concentration cooperative unfolding was evident. In the complex with CypA, groEL also exhibited a stabilisation in comparison with the apo protein.
Cyclophilin A in complex with CsA in the presence of groEL demonstrated a destabilisation of the CypA-CsA complex without dissociation due to the interaction with groEL. On the contrary, experiments conducted with groEL in the presence of the CypA-CsA complex, interestingly, exhibited an inverse trend of the SUPREX free energy of protein folding *versus* midpoint concentrations curve, suggesting CypA in complex with CsA stabilises groEL over time despite the chemical denaturant. These findings suggest a specific interaction of the CypA-CsA complex with groEL in conjunction with the presence of guanidinium hydrochloride, altering the conformation of the chaperonin to a more stable one.

In conclusion, the utilised, modified and developed HDX methodologies are highly system dependent and *ad hoc* not applicable for general protein-ligand screening. Nevertheless, with system optimisation useful binding data may be determined but not necessarily.

7 References

1. Zhu, M. M.; Rempel, D. L.; Du, Z.; Gross, M. L., Quantification of protein-ligand interactions by mass spectrometry, titration, and h/d exchange: Plimstex. *J. Am. Chem. Soc.* **2003**, *125*, 18, 5252–5253. (Cited on pages viii, 31, 65, 78, and 80.)

2. Ghaemmaghami, S.; Fitzgerald, M. C.; Oas, T. G., A quantitative, high-throughput screen for protein stability. *PNAS* **2000**, *97*, 15, 8296–8301. (Cited on pages viii, 33, 34, 35, 67, 80, and 194.)

3. Couderc, F.; Berjeaud, J. M.; Prom, J. C.; Cooks, R. G.; Alan, L. R., Letters to the editor. *Rap. Comm. Mass Spec.* **1991**, *5*, 2, 92–93. (Cited on page 1.)

4. de Hoffmann E., S. V., *Mass Spectrometry - Principles and Applications*. John Wiley & Sons, Inc, Hoboken, **2001**. (Cited on pages 2, 3, 4, 5, and 6.)

5. Bleakney, W., A new method of positive ray analysis and its application to the measurement of ionization potentials in mercury vapor. *Phys. Rev.* **1929**, *34*, 1, 157–160. (Cited on page 2.)

6. Nier, A. O., A mass spectrometer for isotope and gas analysis. *Rev. Sci. Instrum.* **1947**, *18*, 6, 398–411. (Cited on page 2.)

7. Barber, M.; Bordoli, R. S.; Sedgwick, R. D.; Tyler, A. N., Fast atom bombardment of solids (f.a.b.): a new ion source for mass spectrometry. *J. Chem Soc. Chem. Comm.* **1981**, *15*, 7, 325–327. (Cited on page 2.)

8. Herzog, R. F. K.; Viehböck, F. P., Ion source for mass spectrography. *Phys. Rev.* **1949**, *76*, 6, 855–856. (Cited on page 2.)

9. Yamashita, M.; Fenn, J. B., Electrospray ion source. another variation on the free-jet theme. *J. Phys. Chem.* **1984**, *88*, 20, 4451–4459. (Cited on page 2.)

10. Whitehouse, C. M.; Dreyer, R. N.; Yamashita, M.; Fenn, J. B., Electrospray interface for liquid chromatographs and mass spectrometers. *Anal. Chem.* **1985**, *57*, 3, 675–679. (Cited on page 2.)

11. Dole, M.; Mack, L. L.; Hines, R. L.; Mobley, R. C.; Ferguson, L. D.; Alice, M. B., Molecular beams of macroions. *J. Chem. Phys.* **1968**, *49*, 5, 2240–2249. (Cited on pages 2 and 3.)

12. Green, M. K.; Carlito, B. L., Ion-molecule reactions as probes of gas-phase structures of peptides and proteins. *Mass Spectrom. Rev.* **1997**, *16*, 2, 53–71. (Cited on page 2.)

13. Jarrold, M. F., Peptides and proteins in the vapor phase. *Annu. Rev. Phys. Chem.* **2000**, *51*, 179–207. (Cited on page 2.)

14. Wysocki, V. H.; Resing, K. A.; Zhang, Q.; Cheng, G., Mass spectrometry of peptides and proteins. *Methods* **2005**, *35*, 3, 211–222. (Cited on page 2.)

15. Cole, R. B., editor, *Electrospray ionization mass spectrometry. Fundamentals, instumentation & application*. John Wiley & Sons, Inc, Hoboken, **1997**. (Cited on page 2.)

16. Rayleigh, L., On the equilibrium of liquid conducting masses charged with electricity. *Phil. Mag.* **1882**, *14*, 87, 184–186. (Cited on page 2.)

17. Iribarne, J. V.; Thomson, B. A., On the evaporation of small ions from charged droplets. *J. Chem. Phys.* **1976**, *64*, 6, 2287–2294. (Cited on page 3.)

18. Kebarle, P.; Peschke, M., On the mechanisms by which the charged droplets produced by electrospray lead to gas phase ions. *Analy. Chim. Acta* **2000**, *406*, 1, 11–35. (Cited on page 3.)

19. Florance, H. V., *Exploring protein confirmations with mass spectrometry.* Ph.D. thesis, University of Edinburgh, **2007**. (Cited on pages 3, 78, 79, 81, 82, and 84.)

20. Koichi, T.; Hiroaki, W.; Yutaka, I.; Satoshi, A.; Yoshikazu, Y.; Tamio, Y.; Matsuo, T., Protein and polymer analyses up to m/z 100 000 by laser ionization time-of-flight mass spectrometry. *Rapid Comm. Mass Spectrom.* **1988**, *2*, 8, 151–153. (Cited on page 3.)

21. Paul, W.; Steinwedel, H., Ein neues massenspektrometer ohne magnetfeld. *Z. Naturfor.* **1953**, *8*, 7, 448–450. (Cited on page 3.)

22. Kaltashov, I. A.; Eyles, S. J., *Mass Spectrometry in Biophysics.* John Wiley & Sons, Inc, Hoboken, **2005**. (Cited on pages 4, 5, 6, 15, and 19.)

23. Stephens, W. E., A pulsed mass spectrometer with time dispersion. *Phys. Rev.* **1946**, *69*, 11-1, 691–691. (Cited on page 5.)

24. Wiley, W. C.; McLaren, I. H., Time-of-flight mass spectrometer with improved resolution. *Rev. Sci. Instrum.* **1955**, *26*, 12, 1150–1157. (Cited on page 5.)

25. Karataev, V. I.; Mamyrin, B. A.; Smikk, D.; Zagulin, V., The mass reflection, a new nonmagnetic time of flight mass spectrometer with high resolution. *Sov. Phys. Tech. JETP* **1973**, *37*, 45. (Cited on page 5.)

26. John, F. J. T., Ion trap mass spectrometer - past, present, and future ? *Mass Spectrom. Rev.* **1991**, *10*, 1, 3–52. (Cited on page 5.)

27. Stafford, G. C.; Kelley, P. E.; Syka, J. E. P.; Reynolds, W. E.; Todd, J. F. J., Recent improvements in and analytical applications of advanced ion trap technology. *Int. J. Mass Spectrom. Ion Proc.* **1984**, *60*, 1, 85–98. (Cited on page 5.)

28. Hipple, J. A.; Sommer, H.; Thomas, H. A., A precise method of determining the faraday by magnetic resonance. *Phys. Rev.* **1949**, *76*, 12, 1877–1878. (Cited on page 5.)

29. Comisarow, M. B.; Marshall, A. G., Fourier transform ion cyclotron resonance spectroscopy. *Chem. Phys. Lett.* **1974**, *25*, 2, 282–283. (Cited on page 5.)

30. Marshall, A. G.; Hendrickson, C. L.; Jackson, G. S., Fourier transform ion cyclotron resonance mass spectrometry: A primer. *Mass Spectrom. Rev.* **1998**, *17*, 1, 1–35. (Cited on page 6.)

31. Alexandrov, M. L.; Gall, L. N.; Krasnov, N. V.; Nikolaev, V. I.; Pavlenko, V. A.; Shkurov, V. A.; Baram, G. I.; Grachev, M. A.; Knorre, V. D.; Kusner, Y. S., Direct coupling of a microlumn liquid chromatograph and a mass spectrometer. *Bioorg. Khim.* **1984**, *10*, 5, 710–712. (Cited on page 6.)

32. Romijn, E. P.; Krijgsveld, J.; Heck, A. J. R., Recent liquid chromatographic-(tandem) mass spectrometric applications in proteomics. *J. Chromatogr. A* **2003**, *1000*, 1-2, 589–608. (Cited on page 6.)

33. Tomer, K. B., Separations combined with mass spectrometry. *Chem. Rev.* **2001**, *101*, 2, 297–328. (Cited on page 7.)

34. Kennedy, R. T.; German, I.; Thompson, J. E.; Witowski, S. R., Fast analytical-scale separations by capillary electrophoresis and liquid chromatography. *Chem. Rev.* **1999**, *99*, 10, 3081–3132. (Cited on page 7.)

35. Biasi, V. d.; Haskins, N.; Organ, A.; Bateman, R.; Giles, K.; Jarvis, S., High throughput liquid chromatography/mass spectrometric analyses using a novel multiplexed electrospray interface. *Rapid Comm. Mass Spectrom.* **1999**, *13*, 12, 1165–1168. (Cited on page 7.)

36. Zweigenbaum, J.; Heinig, K.; Steinborner, S.; Wachs, T.; Henion, J., High-throughput bioanalytical lc/ms/ms determination of benzodiazepines in human urine: 1000 samples per 12 hours. *Anal. Chem.* **1999**, *71*, 13, 2294–2300. (Cited on page 7.)

37. Gelpi, E., Interfaces for coupled liquid-phase separation/mass spectrometry techniques. an update on recent developments. *J. Mass Spectrom.* **2002**, *37*, 3, 241–253. (Cited on page 7.)

38. Snyder, L. R.; Kirkland, J. J.; Glajch, J. L., *Practical HPLC method development*. John Wiley & Sons, Inc, Hoboken, **1997**. (Cited on page 7.)

39. Horwich, A. L.; Weissman, J. S., Deadly conformations-protein misfolding in prion disease. *Cell* **1997**, *89*, 4, 499–510. (Cited on pages 7 and 25.)

40. Sidransky, M. D. D.; Hollstein, P. D. M., Clinical implications of the p53 gene. *Annu. Rev. Med.* **1996**, *47*, 1, 285–301. (Cited on page 7.)

41. Initial sequencing and analysis of the human genome. *Nature* **2001**, *409*, 6822, 860–921. (Cited on page 7.)

42. Venter, J. C.; Adams, M. D.; Myers, E. W.; Li, P. W.; Mural, R. J.; Sutton, G. G.; Smith, H. O.; Yandell, M.; Evans, C. A.; Holt, R. A.; Gocayne, J. D.; Amanatides, P.; Ballew, R. M.; Huson, D. H.; Wortman, J. R.; Zhang, Q.; Kodira, C. D.; Zheng, X. H.; Chen, L.; Skupski, M.; Subramanian, G.; Thomas, P. D.; Zhang, J.; Gabor Miklos, G. L.; Nelson, C.; Broder, S.; Clark, A. G.; Nadeau, J.; McKusick, V. A.; Zinder, N.; Levine, A. J.; Roberts, R. J.; Simon, M.; Slayman, C.; Hunkapiller, M.; Bolanos, R.; Delcher, A.; Dew, I.; Fasulo, D.; Flanigan, M.; Florea, L.; Halpern, A.; Hannenhalli, S.; Kravitz, S.; Levy, S.; Mobarry, C.; Reinert, K.; Remington, K.; Abu-Threideh, J.; Beasley, E.; Biddick, K.; Bonazzi, V.; Brandon, R.; Cargill, M.; Chandramouliswaran, I.; Charlab, R.; Chaturvedi, K.; Deng, Z.; Francesco, V. D.; Dunn, P.; Eilbeck, K.; Evangelista, C.; Gabrielian, A. E.; Gan, W.; Ge, W.; Gong, F.; Gu, Z.; Guan, P.; Heiman, T. J.; Higgins, M. E.; Ji, R.-R.; Ke, Z.; Ketchum, K. A.; Lai, Z.; Lei, Y.; Li, Z.; Li, J.; Liang, Y.; Lin, X.; Lu, F.; Merkulov, G. V.; Milshina, N.; Moore, H. M.; Naik, A. K.; Narayan, V. A.; Neelam, B.; Nusskern, D.; Rusch, D. B.; Salzberg, S.; Shao, W.; Shue, B.; Sun, J.; Wang, Z. Y.; Wang, A.; Wang, X.; Wang, J.; Wei, M.-H.; Wides, R.; Xiao, C.; Yan, C.; *et al.*, The sequence of the human genome. *Science* **2001**, *291*, 5507, 1304–1351. (Cited on page 7.)

43. Fersht, A., *Structure and mechansim in protein science*. W. H. Freeman, New York, **1999**. (Cited on pages 7, 8, 9, 10, 11, 12, 13, 14, and 15.)

44. Creighton, T. E., *Proteins - Structures and molecular properties*. W. H. Freeman, New York, **1993**. (Cited on pages 8 and 10.)

45. Alberts, B.; Johnson, A.; Lewis, J.; Raff, M.; Roberst, K.; Walter, P., *Molecular Biology of the Cell*. Garland Science, New York, **2002**. (Cited on page 8.)

46. Murray, R.; Mayes, P. A.; Rodwell, V. W.; Granner, D. K., *Harper's Biochemistry, 26th Edition*. McGraw-Hill Companies, **2003**. (Cited on page 8.)

47. Atkins, P.; De Paula, J., *Atkins' Physical Chemistry*. Oxford University Press, Oxford, **2006**. (Cited on pages 8 and 9.)

48. Berg, J. M.; Tymoczko, J. L.; Stryer, L., *Biochemistry*. W. H. Freeman, New York, **2002**. (Cited on pages 8, 9, 10, 11, 12, and 75.)

49. Anfinsen, C. B., Principles that govern the folding of protein chains. *Science* **1973**, *181*, 4096, 223–230. (Cited on pages 10, 20, and 25.)

50. Branden, C.; Tooze, J., *Introduction to Protein Structure*. Garland Science, New York, **1999**. (Cited on page 10.)

51. Hesse, M.; Meier, H.; Zeeh, B., *Spektroskopische Methoden in der Organischen Chemie*. Thieme Verlag, Stuttgart, **2002**. (Cited on page 11.)

52. Wedler, G., *Lehrbuch der Physikalischen Chemie*. Wiley-VCH, Weinheim, **1997**. (Cited on pages 11 and 181.)

53. Baldwin, R. L., Energetics of protein folding. *J. Mol. Biol.* **2007**, *371*, 2, 283–301. (Cited on page 12.)

54. Brooks Iii, C. L.; Onuchic, J. N.; Wales, D. J., Statistical thermodynamics: Taking a walk on a landscape. *Science* **2001**, *293*, 5530, 612–613. (Cited on page 12.)

55. Naganathan, A. N.; Doshi, U.; Fung, A.; Sadqi, M.; Munoz, V., Dynamics, energetics, and structure in protein folding. *Biochemistry* **2006**, *45*, 28, 8466–8475. (Cited on page 12.)

56. Cheung, M. S.; Chavez, L. L.; Onuchic, J. N., The energy landscape for protein folding and possible connections to function. *Polymer* **2004**, *45*, 2, 547–555. (Cited on page 12.)

57. Huang, G. S.; Oas, T. G., Submillisecond folding of monomeric lambda repressor. *PNAS* **1995**, *92*, 15, 6878–6882. (Cited on page 12.)

58. Onuchic, J. N.; Luthey-Schulten, Z.; Wolynes, P. G., Theory of protein folding: The energy landscape perspective. *Annu. Rev. Phys. Chem.* **1997**, *48*, 1, 545–600. (Cited on pages 12 and 13.)

59. Frauenfelder, H.; Parak, F.; Young, R. D., Conformational substates in proteins. *Annu. Rev. Biophys. Biophys. Chem.* **1988**, *17*, 1, 451–479. (Cited on page 12.)

60. Frauenfelder, H.; Sligar, S. G.; Wolynes, P. G., The energy landscapes and motions of proteins. *Science* **1991**, *254*, 5038, 1598–1603. (Cited on page 12.)

61. Becker, O. M.; Karplus, M., The topology of multidimensional potential energy surfaces: Theory and application to peptide structure and kinetics. *J. Chem. Phys.* **1997**, *106*, 4, 1495–1517. (Cited on page 13.)

62. Schellman, J. A., The thermodynamics of solvent exchange. *Biopolymers* **1994**, *34*, 8, 1015–1026. (Cited on page 13.)

63. Tanford, C.; Anfinsen, C.; Edsall, J. M. L. A. J. T.; Richards, F. M., Protein denaturation. In *Adv. Prot. Chem.*, volume 23, Academic Press, **1968**, pages 121–282. (Cited on page 13.)

64. Tanford, C.; C.B. Anfinsen, J. J. T. E.; Richards, F. M., Protein denaturation: Part c. theoretical models for the mechanism of denaturation. In *Adv. Prot. Chem.*, volume 24, Academic Press, **1970**, pages 1–95. (Cited on pages 13 and 105.)

65. Greene, R. F.; Pace, C. N., Urea and guanidine hydrochloride denaturation of ribonuclease, lysozyme, -chymotrypsin, and -lactoglobulin. *J. Biol. Chem.* **1974**, *249*, 17, 5388–5393. (Cited on page 14.)

66. Myers, J. K.; Pace, C. N.; Scholtz, J. M., Denaturant m values and heat capacity changes: relation to changes in accessible surface areas of protein unfolding. *Protein Sci.* **1995**, *4*, 10, 2138–2148. (Cited on pages 14 and 105.)

67. Hummel, J. P.; Dreyer, W. J., Measurement of protein-binding phenomena by gel filtration. *Biochim. Biophys. Acta* **1962**, *63*, 3, 530–532. (Cited on page 14.)

68. Behlke, J.; Ristau, O., Analysis of interacting biopolymer systems by analytical ultracentrifugation. *Eur. Biophys. J. Biophys. Lett.* **1997**, *25*, 5, 325–332. (Cited on page 14.)

69. Yarus, M.; Berg, P., On the properties and utility of a membrane filter assay in the study of isoleucyl-trna synthetase. *Anal. Biochem.* **1970**, *35*, 2, 450–465. (Cited on page 14.)

70. Ganem, B.; Li, Y. T.; Henion, J. D., Detection of noncovalent receptor-ligand complexes by mass spectrometry. *J. Am. Chem. Soc.* **1991**, *113*, 16, 6294–6296. (Cited on page 15.)

71. Loo, J. A., Studying noncovalent protein complexes by electrospray ionization mass spectrometry. *Mass Spectrom. Rev.* **1997**, *16*, 1, 1–23. (Cited on page 15.)

72. Heck, A. J. R.; Van den Heuvel, R. H. H., Investigation of intact protein complexes by mass spectrometry. *Mass Spectrom. Rev.* **2004**, *23*, 5, 368–389. (Cited on page 15.)

73. Ganem, B.; Henion, J. D., Going gently into flight: analyzing noncovalent interactions by mass spectrometry. *Bioorg. Med. Chem.* **2003**, *11*, 3, 311–314. (Cited on page 15.)

74. Breuker, K., New mass spectrometric methods for the quantification of protein-ligand binding in solution. *Angew. Chem. Int. Ed. Engl.* **2004**, *43*, 1, 22–25. (Cited on page 15.)

75. Breuker, K., The study of protein-ligand interactions by mass spectrometry–a personal view. *Int. J. Mass Spectrom.* **2004**, *239*, 1, 33–41. (Cited on page 15.)

76. Aplin, R. T.; Robinson, C. V.; Schofield, C. J.; Westwood, N. J., Does the observation of noncovalent complexes between biomolecules by electrospray ionisation mass spectrometry necessarily reflect specific solution interactions? *J. Chem. Soc. Chem. Comm.* **1994**, 2415–2417. (Cited on page 15.)

77. Hernandez, H.; Robinson, C. V., Dynamic protein complexes: Insights from mass spectrometry. *J. Biol. Chem.* **2001**, *276*, 50, 46685–46688. (Cited on page 15.)

78. Jennings, K. R., The changing impact of the collision-induced decomposition of ions on mass spectrometry. *Int. J. Mass Spectrom.* **2000**, *200*, 1-3, 479–493. (Cited on page 16.)

79. Chen, C.-H., Review of a current role of mass spectrometry for proteome research. *Anal. Chim. Acta* **2008**, *624*, 1, 16–36. (Cited on page 16.)

80. Dongre, A. R.; Arpad, S.; Wysocki, V. H., Surface-induced dissociation: An effective tool to probe structure, energetics and fragmentation mechanisms of protonated peptides. *J. Mass Spectrom.* **1996**, *31*, 4, 339–350. (Cited on page 16.)

81. Laskin, J.; Futrell, J. H., Surface-induced dissociation of peptide ions: kinetics and dynamics. *J. Am. Soc. Mass Spectrom.* **2003**, *14*, 12, 1340–1347. (Cited on page 16.)

82. Zubarev, R. A.; Kelleher, N. L.; McLafferty, F. W., Electron capture dissociation of multiply charged protein cations. a nonergodic process. *J. Am. Chem. Soc.* **1998**, *120*, 13, 3265–3266. (Cited on page 16.)

83. Breuker, K.; McLafferty, F. W., The thermal unfolding of native cytochrome c in the transition from solution to gas phase probed by native electron capture dissociation. *Angew. Chem. Int. Ed. Engl.* **2005**, *44*, 31, 4911–4914. (Cited on page 16.)

84. Taucher, M.; Rieder, U.; Breuker, K., Minimizing base loss and internal fragmentation in collisionally activated dissociation of multiply deprotonated rna. *J. Am. Soc. Mass Spectrom.* **2009**, *Article in Press*. (Cited on page 16.)

85. Verbeck, G.; Ruotolo, B.; Sawyer, H.; Gillig, K.; Russell, D., A fundamental introduction to ion mobility mass spectrometry applied to the analysis of biomolecules. *J. Biomol. Techn.* **2002**, *13*, 2, 56–61. (Cited on page 16.)

86. Liu, D.; Wyttenbach, T.; Barran, P. E.; Bowers, M. T., Sequential hydration of small protonated peptides. *J. Am. Chem. Soc.* **2003**, *125*, 28, 8458–8464. (Cited on page 16.)

87. Faull, P. A.; Korkeila, K. E.; Kalapothakis, J. M.; Gray, A.; McCullough, B. J.; Barran, P. E., Gas-phase metalloprotein complexes interrogated by ion mobility-mass spectrometry. *Int. J. Mass Spectrom.* **2009**, *283*, 1-3, 140–148. (Cited on page 16.)

88. Sobott, F.; Robinson, C. V., Characterising electrosprayed biomolecules using tandem-ms-the noncovalent groel chaperonin assembly. *Int. J. Mass Spectrom.* **2004**, *236*, 1-3, 25–32. (Cited on page 16.)

89. Duijn, E. v.; Barendregt, A.; Synowsky, S.; Versluis, C.; Heck, A. J. R., Chaperonin complexes monitored by ion mobility mass spectrometry. *J. Am. Chem. Soc.* **2009**, *131*, 4, 1452–1459. (Cited on pages 16, 26, 27, 137, and 138.)

90. Urey, H. C.; Brickwedde, F. G.; Murphy, G. M., A hydrogen isotope of mass 2. *Phys. Rev.* **1932**, *39*, 1. (Cited on page 16.)

91. Bonhöffer, K. F.; Klar, R., Ueber den austausch von schweren wasserstoffatomen zwischen wasser und organischen verbindungen. *Naturwissenschaften* **1933**, *22*, 45. (Cited on pages 16 and 17.)

92. Hvidt, A.; Linderstrøm-Lang, K., Exchange of hydrogen atoms in insulin with deuterium atoms in aqueous solutions. *Biochim. Biophys. Acta* **1954**, *14*, 574–575. (Cited on page 16.)

93. Hvidt, A.; Linderstrøm-Lang, K., The kinetics of the deuterium exchange of insulin with d_2o. an amendment. *Biochim. Biophys. Acta* **1955**, *16*, 168–169. (Cited on page 16.)

94. Dempsey, C. E., Hydrogen exchange in peptides and proteins using nmr spectroscopy. *Prog. Nucl. Magn. Res. Spec.* **2001**, *39*, 2, 135–170. (Cited on pages 16, 17, 19, and 20.)

95. Katta, V.; Chait, B. T.; Carr, S., Conformational changes in proteins probed by hydrogen-exchange electrospray-ionization mass spectrometry. *Rapid Comm. Mass Spectrom.* **1991**, *5*, 4, 214–217. (Cited on page 16.)

96. Kaltashov, I. A.; Eyles, S. J., Studies of biomolecular conformations and conformational dynamics by mass spectrometry. *Mass Spectrom. Rev.* **2002**, *21*, 1, 37–71. (Cited on page 16.)

97. Hoofnagle, A. N.; Resing, K. A.; Ahn, N. G., Protein analysis by hydrogen exchange mass spectrometry. *Annu. Rev. Biophys. Biomol. Struct.* **2003**, *32*, 1–25. (Cited on page 16.)

98. Wales, T. E.; Engen, J. R., Hydrogen exchange mass spectrometry for the analysis of protein dynamics. *Mass Spectrom. Rev.* **2006**, *25*, 1, 158–170. (Cited on pages 16 and 18.)

99. Englander, S. W., Hydrogen exchange and mass spectrometry: A historical perspective. *J. Am. Soc. Mass Spectrom.* **2006**, *17*, 11, 1481–1489. (Cited on page 16.)

100. Englander, S. W.; Sosnick, T. R.; Englander, J. J.; Mayne, L., Mechanisms and uses of hydrogen exchange. *Curr. Op. Struc. Biol.* **1996**, *6*, 1, 18–23. (Cited on page 17.)

101. Englander, S. W.; Kallenbach, N. R., Hydrogen exchange and structural dynamics of proteins and nucleic acids. *Q. Rev. Biophys.* **1983**, *16*, 04, 521–655. (Cited on page 18.)

102. Woodward, C. K.; Hilton, B. D., Hydrogen isotope exchange kinetics of single protons in bovine pancreatic trypsin inhibitor. *Biophys. J.* **1980**, *32*, 1, 561–575. (Cited on page 18.)

103. Bai, Y.; Milne, J. S.; Mayne, L.; Englander, S. W., Protein stability parameters measured by hydrogen exchange. *Proteins* **1994**, *20*, 1, 4–14. (Cited on page 18.)

104. Hvidt, A.; Nielsen, S. O., Hydrogen exchange in proteins. *Adv. Protein Chem.* **1966**, *21*, 287–386. (Cited on page 18.)

105. Roder, H.; Wagner, G.; Wüthrich, K., Amide proton exchange in proteins by ex1 kinetics: studies of the basic pancreatic trypsin inhibitor at variable p2h and temperature. *Biochemistry* **1985**, *24*, 25, 7396–7407. (Cited on page 18.)

106. Clarke, J.; Itzhaki, L. S., Hydrogen exchange and protein folding. *Cur. Op. Struc. Biol.* **1998**, *8*, 1, 112–118. (Cited on page 18.)

107. Bai, Y.; Milne, J. S.; Mayne, L.; Englander, S. W., Primary structure effects on peptide group hydrogen exchange. *Proteins* **1993**, *17*, 1, 75–86. (Cited on pages 19, 34, and 74.)

108. Handschumacher, R. E.; Harding, M. W.; Rice, J.; Drugge, R. J.; Speicher, D. W., Cyclophilin: a specific cytosolic binding protein for cyclosporin a. *Science* **1984**, *226*, 4674, 544–547. (Cited on pages 20 and 23.)

109. Harding, M. W.; Galat, A.; Uehling, D. E.; Schreiber, S. L., A receptor for the immunosuppressant fk506 is a cis-trans peptidyl-prolyl isomerase. *Nature* **1989**, *341*, 6244, 758–760. (Cited on page 20.)

110. Siekierka, J. J.; Hung, S. H. Y.; Poe, M.; Lin, C. S.; Sigal, N. H., A cytosolic binding protein for the immunosuppressant fk506 has peptidyl-prolyl isomerase activity but is distinct from cyclophilin. *Nature* **1989**, *341*, 6244, 755–757. (Cited on page 20.)

111. Fischer, G.; Wittmann-Liebold, B.; Lang, K.; Kiefhaber, T.; Schmid, F. X., Cyclophilin and peptidyl-prolyl cis-trans isomerase are probably identical proteins. *Nature* **1989**, *337*, 6206, 476–478. (Cited on page 20.)

112. Takahashi, N.; Hayano, T.; Suzuki, M., Peptidyl-prolyl cis-trans isomerase is the cyclosporin a-binding protein cyclophilin. *Nature* **1989**, *337*, 6206, 473–475. (Cited on pages 20 and 21.)

113. Rahfeld, J. U.; Rucknagel, K. P.; Schelbert, B.; Ludwig, B.; Hacker, J.; Mann, K.; Fischer, G., Confirmation of the existence of a third family among peptidyl-prolyl cis/trans isomerases. amino acid sequence and recombinant production of parvulin. *FEBS Lett.* **1994**, *352*, 2, 180–184. (Cited on page 20.)

114. Hennig, L.; Christner, C.; Kipping, M.; Schelbert, B.; Rucknagel, K. P.; Grabley, S.; Kullertz, G.; Fischer, G., Selective inactivation of parvulin-like peptidyl-prolyl cis/trans isomerases by juglone. *Biochemistry* **1998**, *37*, 17, 5953–5960. (Cited on page 20.)

115. Vitikainen, M.; Lappalainen, I.; Seppala, R.; Antelmann, H.; Boer, H.; Taira, S.; Savilahti, H.; Hecker, M.; Vihinen, M.; Sarvas, M.; Kontinen, V. P., Structure-function analysis of prsa reveals roles for the parvulin-like and flanking n- and c-terminal domains in protein folding and secretion in bacillus subtilis. *J. Biol. Chem.* **2004**, *279*, 18, 19302–19314. (Cited on page 20.)

116. Kiefhaber, T.; Quaas, R.; Hahn, U.; Schmid, F. X., Folding of ribonuclease t1. 2. kinetic models for the folding and unfolding reactions. *Biochemistry* **1990**, *29*, 12, 3061–3070. (Cited on page 21.)

117. Kleerebezem, M.; Heutink, M.; Tommassen, J., Characterization of an escherichia coli mutant, affected in periplasmic peptidyl-prolyl cis/trans isomerase. *Mol. Microbiol.* **1995**, *18*, 02, 313–320. (Cited on page 21.)

118. Kok, R. G.; Christoffels, V. M.; Vosman, B.; Hellingwerf, K. J., A gene of acinetobacter calcoaceticus bd413 encodes a periplasmic peptidyl-prolyl cis-trans isomerase of the cyclophilin sub-class that is not essential for growth. *Biochim. Biophys. Acta - Gene Struc. Expr.* **1994**, *1219*, 3, 601–606. (Cited on page 21.)

119. Schneuwly, S.; Shortridge, R. D.; Larrivee, D. C.; Ono, T.; Ozaki, M.; Pak, W. L., Drosophila ninaa gene encodes an eye-specific cyclophilin (cyclosporine a binding protein). *PNAS* **1989**, *86*, 14, 5390–5394. (Cited on page 21.)

120. Dornan, J.; Page, A. P.; Taylor, P.; Wu, S.-y.; Winter, A. D.; Husi, H.; Walkinshaw, M. D., Biochemical and structural characterization of a divergent loop cyclophilin from caenorhabditis elegans. *J. Biol. Chem.* **1999**, *274*, 49, 34877–34883. (Cited on page 21.)

121. Bloom, B. R.; Salgame, P.; Diamond, B., Revisiting and revising suppressor t cells. *Immunol. Today* **1992**, *13*, 4, 131–136. (Cited on page 21.)

122. Clardy, J., The chemistry of signal transduction. *PNAS* **1995**, *92*, 1, 56–61. (Cited on page 21.)

123. Göthel, S. F.; Marahiel, M. A., Peptidyl-prolyl cis-trans isomerases, a superfamily of ubiquitous folding catalysts. *Cell. Mol. Life Sci.* **1999**, *55*, 3, 423–436. (Cited on page 22.)

124. Ke, H.; Zydowsky, L. D.; Liu, J.; Walsh, C. T., Crystal structure of recombinant human t-cell cyclophilin a at 2.5 resolution. *PNAS* **1991**, *88*, 21, 9483–9487. (Cited on page 22.)

125. Weber, C.; Wider, G.; Von Freyberg, B.; Traber, R.; Braun, W.; Widmer, H.; Wüthrich, K., Nmr structure of cyclosporin a bound to cyclophilin in aqueous solution. *Biochemistry* **1991**, *30*, 26, 6563–6574. (Cited on page 22.)

126. Wüthrich, K.; Spitzfaden, C.; Memmert, K.; Widmer, H.; Wider, G., Protein secondary structure determination by nmr. application with recombinant human cyclophilin. *FEBS Lett.* **1991**, *285*, 2, 237–247. (Cited on page 22.)

127. Kallen, J.; Spitzfaden, C.; Zurini, M. G.; Wider, G.; Widmer, H.; Wüthrich, K.; Walkinshaw, M. D., Structure of human cyclophilin and its binding site for cyclosporin a determined by x-ray crystallography and nmr spectroscopy. *Nature* **1991**, *353*, 6341, 276–279. (Cited on page 22.)

128. Kallen, J.; Walkinshaw, M. D., The x-ray structure of a tetrapeptide bound to the active site of human cyclophilin a. *FEBS Lett.* **1992**, *300*, 3, 286–290. (Cited on page 22.)

129. Spitzfaden, C.; Weber, H. P.; Braun, W.; Kallen, J.; Wider, G.; Widmer, H.; Walkinshaw, M. D.; Wüthrich, K., Cyclosporin a-cyclophilin complex formation. a model based on x-ray and nmr data. *FEBS Lett.* **1992**, *300*, 3, 291–300. (Cited on page 22.)

130. Spitzfaden, C.; Braun, W.; Wider, G.; Widmer, H.; Wüthrich, K., Determination of the nmr solution structure of the cyclophilin a-cyclosporin a complex. *J. Biomol. NMR* **1994**, *4*, 4, 463–482. (Cited on page 22.)

131. Braun, W.; Kallen, J.; Mikol, V.; Walkinshaw, M. D.; Wüthrich, K., Three-dimensional structure and actions of immunosuppressants and their immunophilins. *FASEB J.* **1995**, *9*, 1, 63–72. (Cited on page 22.)

132. Ottiger, M.; Zerbe, O.; Guntert, P.; Wüthrich, K., The nmr solution conformation of unligated human cyclophilin a. *J. Mol. Biol.* **1997**, *272*, 1, 64–81. (Cited on page 22.)

133. Mikol, V.; Kallen, J.; Pflgl, G.; Walkinshaw, M. D., X-ray structure of a monomeric cyclophilin a-cyclosporin a crystal complex at 2.1 resolution. *J. Mol. Biol.* **1993**, *234*, 4, 1119–1130. (Cited on page 23.)

134. Mikol, V.; Taylor, P.; Kallen, J.; Walkinshaw, M. D., Conformational differences of an immunosuppressant peptolide in a single crystal and in a crystal complex with human cyclophilin a. *J. Mol. Biol.* **1998**, *283*, 2, 451–461. (Cited on page 23.)

135. Li, Z.; Lazaridis, T., Thermodynamics of buried water clusters at a protein-ligand binding interface. *J. Phys. Chem. B* **2005**, *110*, 3, 1464–1475. (Cited on page 23.)

136. Popov, S.; Rexach, M.; Zybarth, G.; Reiling, N.; Lee, M. A.; Ratner, L.; Lane, C. M.; Moore, M. S.; Blobel, G.; Bukrinsky, M., Viral protein r regulates nuclear import of the hiv-1 pre-integration complex. *Embo J.* **1998**, *17*, 4, 909–917. (Cited on page 23.)

137. Zander, K.; Sherman, M. P.; Tessmer, U.; Bruns, K.; Wray, V.; Prechtel, A. T.; Schubert, E.; Henklein, P.; Luban, J.; Neidleman, J.; Greene, W. C.; Schubert, U., Cyclophilin a interacts with hiv-1 vpr and is required for its functional expression. *J. Biol. Chem.* **2003**, *278*, 44, 43202–43213. (Cited on page 23.)

138. Braaten, D.; Franke, E. K.; Luban, J., Cyclophilin a is required for an early step in the life cycle of human immunodeficiency virus type 1 before the initiation of reverse transcription. *J. Virol.* **1996**, *70*, 6, 3551–3560. (Cited on page 23.)

139. Braaten, D.; Luban, J., Cyclophilin a regulates hiv-1 infectivity, as demonstrated by gene targeting in human t cells. *Embo J.* **2001**, *20*, 6, 1300–1309. (Cited on page 23.)

140. Towers, G. J.; Hatziioannou, T.; Cowan, S.; Goff, S. P.; Luban, J.; Bieniasz, P. D., Cyclophilin a modulates the sensitivity of hiv-1 to host restriction factors. *Nat. Med.* **2003**, *9*, 9, 1138–1143. (Cited on page 23.)

141. Yang, Y.; Moir, E.; Kontopidis, G.; Taylor, P.; Wear, M. A.; Malone, K.; Dunsmore, C. J.; Page, A. P.; Turner, N. J.; Walkinshaw, M. D., Structure-based discovery of a family of synthetic cyclophilin inhibitors showing a cyclosporin-a phenotype in caenorhabditis elegans. *Biochem. Biophys. Res. Commun.* **2007**, *363*, 4, 1013–1019. (Cited on pages 23, 79, 82, 84, 152, and 153.)

142. Altschuh, D.; Braun, W.; Kallen, J.; Mikol, V.; Spitzfaden, C.; Thierry, J. C.; Vix, O.; Walkinshaw, M. D.; Wüthrich, K., Conformational polymorphism of cyclosporin a. *Structure* **1994**, *2*, 10, 963–972. (Cited on page 23.)

143. Wüthrich, K.; von Freyberg, B.; Weber, C.; Wider, G.; Traber, R.; Widmer, H.; Braun, W., Receptor-induced conformation change of the immunosuppressant cyclosporin a. *Science* **1991**, *254*, 5034, 953–954. (Cited on page 23.)

144. Kallen, J.; Mikol, V.; Taylor, P.; D.Walkinshaw, M., X-ray structures and analysis of 11 cyclosporin derivatives complexed with cyclophilin a. *J. Mol. Biol.* **1998**, *283*, 2, 435–449. (Cited on page 23.)

145. Wear, M. A.; Patterson, A.; Walkinshaw, M. D., A kinetically trapped intermediate of fk506 binding protein forms in vitro: chaperone machinery dominates protein folding in vivo. *Protein Expr. Purif.* **2007**, *51*, 1, 80–95. (Cited on pages 24, 82, 152, and 153.)

146. Bierer, B. E.; Mattila, P. S.; Standaert, R. F.; Herzenberg, L. A.; Burakoff, S. J.; Crabtree, G.; Schreiber, S. L., Two distinct signal transmission pathways in t lymphocytes are inhibited by complexes formed between an immunophilin and either fk506 or rapamycin. *PNAS* **1990**, *87*, 23, 9231–9235. (Cited on page 24.)

147. Sun, F.; Li, P.; Ding, Y.; Wang, L.; Bartlam, M.; Shu, C.; Shen, B.; Jiang, H.; Li, S.; Rao, Z., Design and structure-based study of new potential fkbp12 inhibitors. *Biophys. J.* **2003**, *85*, 5, 3194–3201. (Cited on page 24.)

148. Graziani, F.; Aldegheri, L.; Terstappen, G. C., High throughput scintillation proximity assay for the identification of fkbp-12 ligands. *J. Biomol. Screen.* **1999**, *4*, 1, 3–7. (Cited on page 24.)

149. Michnick, S. W.; Rosen, M. K.; Wandless, T. J.; Karplus, M.; Schreiber, S. L., Solution structure of fkbp, a rotamase enzyme and receptor for fk506 and rapamycin. *Science* **1991**, *252*, 5007, 836–839. (Cited on page 24.)

150. Van Duyne, G. D.; Standaert, R. F.; Karplus, P. A.; Schreiber, S. L.; Clardy, J., Atomic structures of the human immunophilin fkbp-12 complexes with fk506 and rapamycin. *J. Mol. Biol.* **1993**, *229*, 1, 105–124. (Cited on page 24.)

151. Burkhard, P.; Taylor, P.; Walkinshaw, M. D., X-ray structures of small ligand-fkbp complexes provide an estimate for hydrophobic interaction energies. *J. Mol. Biol.* **2000**, *295*, 4, 953–962. (Cited on page 24.)

152. Dornan, J.; Taylor, P.; Walkinshaw, M. D., Structures of immunophilins and their ligand complexes. *Curr. Top. Med. Chem.* **2003**, *3*, 1392–1409. (Cited on page 24.)

153. Denesyuk, A. I.; Denessiouk, K. A.; Zav'yalov, V. P.; Lundell, J.; Korpela, T., Analogous conformations of both binding and effector regions in cyclosporin a, fk506 and rapamycin. *Comp. Chem.* **1998**, *22*, 4, 339–344. (Cited on page 24.)

154. Kino, T.; Hatanaka, H.; Hashimoto, M.; Nishiyama, M.; Goto, T.; Okuhara, M.; Kohsaka, M.; Aoki, H.; Imanaka, H., Fk506, a novel immunosuppressant isolated from a streptomyces. i. fermentation, isolation, and physico-chemical and biological characteristics. *J. Antib.* **1987**, *40*, 9, 1249–1255. (Cited on page 25.)

155. Xiaodong, J. W.; Felicia, A. E., Peptidyl-prolyl isomerase inhibitors. *Pept. Sci.* **2006**, *84*, 2, 125–146. (Cited on page 25.)

156. Lu, K. P.; Finn, G.; Lee, T. H.; Nicholson, L. K., Prolyl cis-trans isomerization as a molecular timer. *Nat. Chem. Biol.* **2007**, *3*, 10, 619–629. (Cited on page 25.)

157. Stebbins, J. L.; Zhang, Z.; Chen, J.; Wu, B.; Emdadi, A.; Williams, M. E.; Cashman, J.; Pellecchia, M., Nuclear magnetic resonance fragment-based identification of novel fkbp12 inhibitors. *J. Med. Chem.* **2007**, *50*, 26, 6607–6617. (Cited on page 25.)

158. Ellis, R., editor, *The Chaperonins*. Academic Press, San Diego, **1996**. (Cited on page 25.)

159. Hartl, F. U., Molecular chaperones in cellular protein folding. *Nature* **1996**, *381*, 6583, 571–580. (Cited on pages 25 and 142.)

160. Xu, Z.; Horwich, A. L.; Sigler, P. B., The crystal structure of the asymmetric groel-groes-(adp)7 chaperonin complex. *Nature* **1997**, *388*, 6644, 741–750. (Cited on pages 26 and 44.)

161. Goloubinoff, P.; Christeller, J. T.; Gatenby, A. A.; Lorimer, G. H., Reconstitution of active dimeric ribulose bisphosphate carboxylase from an unfolded state depends on two chaperonin proteins and mg-atp. *Nature* **1989**, *342*, 6252, 884–889. (Cited on pages 26 and 137.)

162. Marchenkov, V. V.; Semisotnov, G. V., Groel-assisted protein folding: does it occur within the chaperonin inner cavity? *Int. J. Mol. Sci.* **2009**, *10*, 5, 2066–2083. (Cited on pages 26, 27, and 28.)

163. Braig, K.; Simon, M.; Furuya, F.; Hainfeld, J. F.; Horwich, A. L., A polypeptide bound by the chaperonin groel is localized within a central cavity. *PNAS* **1993**, *90*, 9, 3978–3982. (Cited on page 26.)

164. Chen, S.; Roseman, A. M.; Hunter, A. S.; Wood, S. P.; Burston, S. G.; Ranson, N. A.; Clarke, A. R.; Saibil, H. R., Location of a folding protein and shape changes in groel-groes complexes imaged by cryo-electron microscopy. *Nature* **1994**, *371*, 6494, 261–264. (Cited on pages 26 and 137.)

165. Fenton, W. A.; Kashi, Y.; Furtak, K.; Norwich, A. L., Residues in chaperonin groel required for polypeptide binding and release. *Nature* **1994**, *371*, 6498, 614–619. (Cited on pages 26 and 137.)

166. Ishii, N.; Taguchi, H.; Sasabe, H.; Yoshida, M., Folding intermediate binds to the bottom of bullet-shaped holo-chaperonin and is readily accessible to antibody. *J. Mol. Biol.* **1994**, *236*, 3, 691–696. (Cited on page 26.)

167. Langer, T.; Pfeifer, G.; Martin, J.; Baumeister, W.; Hartl, F. U., Chaperonin-mediated protein folding: Groes binds to one end of the groel cylinder which accomodates the protein substrate within its central cavity. *EMBO J.* **1992**, *11*, 13, 4757–4765. (Cited on page 26.)

168. Boisvert, D. C.; Wang, J.; Otwinowski, Z.; Norwich, A. L.; Sigler, P. B., The 2.4 a crystal structure of the bacterial chaperonin groel complexed with atp-gamma-s. *Nat. Struct. Mol. Biol.* **1996**, *3*, 2, 170–177. (Cited on page 26.)

169. Clare, D. K.; Bakkes, P. J.; van Heerikhuizen, H.; van der Vies, S. M.; Saibil, H. R., Chaperonin complex with a newly folded protein encapsulated in the folding chamber. *Nature* **2009**, *457*, 7225, 107–110. (Cited on page 26.)

170. van Duijn, E.; Bakkes, P. J.; Heeren, R. M. A.; van den Heuvel, R. H. H.; van Heerikhuizen, H.; van der Vies, S. M.; Heck, A. J. R., Monitoring macromolecular complexes involved in the chaperonin-assisted protein folding cycle by mass spectrometry. *Nat. Meth.* **2005**, *2*, 5, 371–376. (Cited on pages 26, 27, and 137.)

171. Ellis, R. J.; Hartl, F. U., Principles of protein folding in the cellular environment. *Curr. Opin. Struct. Biol.* **1999**, *9*, 1, 102–110. (Cited on page 27.)

172. Martin, J.; Mayhew, M.; Langer, T.; Hartl, U., The reaction cycle of groel and groes in chaperonin-assisted protein folding. *Nature* **1993**, *366*, 6452, 228–233. (Cited on page 27.)

173. Mayhew, M.; da Silva, A. C. R.; Martin, J.; Erdjument-Bromage, H.; Tempst, P.; Hartl, F. U., Protein folding in the central cavity of the groel-groes chaperonin complex. *Nature* **1996**, *379*, 6564, 420–426. (Cited on page 27.)

174. Radford, S. E., Groel: More than just a folding cage. *Cell* **2006**, *125*, 5, 831–833. (Cited on page 27.)

175. Weissman, J. S.; Rye, H. S.; Fenton, W. A.; Beechem, J. M.; Horwich, A. L., Characterization of the active intermediate of a groel groes-mediated protein folding reaction. *Cell* **1996**, *84*, 3, 481–490. (Cited on pages 27 and 137.)

176. Chaudhuri, T. K.; Farr, G. W.; Fenton, W. A.; Rospert, S.; Horwich, A. L., Groel/groes-mediated folding of a protein too large to be encapsulated. *Cell* **2001**, *107*, 2, 235–246. (Cited on page 27.)

177. Subhankar, P.; Shashikala, P.; Tapan, K. C., Chaperone-assisted refolding of escherichia coli maltodextrin glucosidase. *FEBS J.* **2007**, *274*, 22, 6000–6010. (Cited on pages 27 and 137.)

178. Zahn, R.; Buckle, A.; Perrett, S.; Johnson, C. M.; Corrales, F.; Golbik, R.; Fersht, A., Chaperone activity and structure of monomeric polypeptide binding domains of groel. *PNAS* **1996**, *93*, 26, 15024–15029. (Cited on pages 27 and 137.)

179. Nieba-Axmann, S. E.; Ottiger, M.; Wüthrich, K.; Pluckthun, A., Multiple cycles of global unfolding of groel-bound cyclophilin a evidenced by nmr. *J. Mol. Biol.* **1997**, *271*, 5, 803–818. (Cited on pages 27, 137, 138, and 140.)

180. Komiya, T.; Tanigawa, Y.; Hirohashi, S., Cloning of the gene gob-4, which is expressed in intestinal goblet cells in mice. *Biochim. Biophys. Acta - Gene Struc. Expr.* **1999**, *1444*, 3, 434–438. (Cited on page 28.)

181. Thompson, D. A.; Weigel, R. J., hag-2, the human homologue of the xenopus laevis cement gland gene xag-2, is coexpressed with estrogen receptor in breast cancer cell lines. *Biochem. and Biophys. Res. Commun.* **1998**, *251*, 1, 111–116. (Cited on page 28.)

182. Ramachandran, V.; Arumugam, T.; Wang, H.; Logsdon, C. D., Anterior gradient 2 is expressed and secreted during the development of pancreatic cancer and promotes cancer cell survival. *Cancer Res.* **2008**, *68*, 19, 7811–7818. (Cited on page 28.)

183. Aberger, F.; Weidinger, G.; Grunz, H.; Richter, K., Anterior specification of embryonic ectoderm: the role of the xenopus cement gland-specific gene xag-2. *Mech. Dev.* **1998**, *72*, 1-2, 115–130. (Cited on page 28.)

184. Liu, D.; Rudland, P. S.; Sibson, D. R.; Platt-Higgins, A.; Barraclough, R., Human homologue of cement gland protein, a novel metastasis inducer associated with breast carcinomas. *Cancer Res.* **2005**, *65*, 9, 3796–3805. (Cited on page 28.)

185. Altschul, S. F.; Madden, T. L.; Schaffer, A. A.; Zhang, J.; Zhang, Z.; Miller, W.; Lipman, D. J., Gapped blast and psi-blast: a new generation of protein database search programs. *Nucl. Acids Res.* **1997**, *25*, 17, 3389–3402. (Cited on page 28.)

186. Persson, S.; Rosenquist, M.; Knoblach, B.; Khosravi-Far, R.; Sommarin, M.; Michalak, M., Diversity of the protein disulfide isomerase family: Identification of breast tumor induced hag2 and hag3 as novel members of the protein family. *Mol. Phylogenet. Evol.* **2005**, *36*, 3, 734–740. (Cited on page 28.)

187. Sevier, C. S.; Kaiser, C. A., Formation and transfer of disulphide bonds in living cells. *Nat. Rev. Mol. Cell Biol.* **2002**, *3*, 11, 836–847. (Cited on page 28.)

188. Pohler, E.; Craig, A. L.; Cotton, J.; Lawrie, L.; Dillon, J. F.; Ross, P.; Kernohan, N.; Hupp, T. R., The barrett's antigen anterior gradient-2 silences the p53 transcriptional response to dna damage. *Mol. Cell. Proteomics* **2004**, *3*, 6, 534–547. (Cited on pages 28 and 29.)

189. Smirnov, D. A.; Zweitzig, D. R.; Foulk, B. W.; Miller, M. C.; Doyle, G. V.; Pienta, K. J.; Meropol, N. J.; Weiner, L. M.; Cohen, S. J.; Moreno, J. G.; Connelly, M. C.; Terstappen, L. W. M. M.; O'Hara, S. M., Global gene expression profiling of circulating tumor cells. *Cancer Res.* **2005**, *65*, 12, 4993–4997. (Cited on page 28.)

190. Zweitzig, D.; Smirnov, D.; Connelly, M.; Terstappen, L.; OHara, S.; Moran, E., Physiological stress induces the metastasis marker agr2 in breast cancer cells. *Mol. Cell. Biochem.* **2007**, *306*, 1, 255–260. (Cited on page 28.)

191. Fletcher, G. C.; Patel, S.; Tyson, K.; Adam, P. J.; Schenker, M.; Loader, J. A.; Daviet, L.; Legrain, P.; Parekh, R.; Harris, A. L.; Terrett, J. A., hag-2 and hag-3, human homologues of genes involved in differentiation, are associated with oestrogen receptor-positive breast tumours and interact with metastasis gene c4.4a and dystroglycan. *Br. J. Cancer* **2003**, *88*, 4, 579–585. (Cited on page 28.)

192. Zhang, J.-S.; Gong, A.; Cheville, J. C.; Smith, D. I.; Young, C. Y. F., Agr2, an androgen-inducible secretory protein overexpressed in prostate cancer. *Genes Chrom. Cancer* **2005**, *43*, 3, 249–259. (Cited on page 28.)

193. Vivekanandan, P.; Micchelli, S. T. L.; Torbenson, M., Anterior gradient-2 is overexpressed by fibrolamellar carcinomas. *Human Pathology* **2009**, *40*, 3, 293–299. (Cited on page 28.)

194. Zhu, H.; Lam, D. C. L.; Han, K. C.; Tin, V. P. C.; Suen, W. S.; Wang, E.; Lam, W. K.; Cai, W. W.; Chung, L. P.; Wong, M. P., High resolution analysis of genomic aberrations by metaphase and array comparative genomic hybridization identifies candidate tumour genes in lung cancer cell lines. *Cancer Lett.* **2007**, *245*, 1-2, 303–314. (Cited on page 28.)

195. Reid, B. J.; Blount, P. L.; Rabinovitch, P. S., Biomarkers in barrett's esophagus. *Gastrointest. Endosc. Clin. N. Am.* **2003**, *13*, 2, 369–397. (Cited on page 29.)

196. Reid, B. J., p53 and neoplastic progression in barrett's esophagus. *Am. J. Gastroenterol.* **2001**, *96*, 5, 1321–1323. (Cited on page 29.)

197. Wang, Z.; Hao, Y.; Lowe, A. W., The adenocarcinoma-associated antigen, agr2, promotes tumor growth, cell migration, and cellular transformation. *Cancer Res.* **2008**, *68*, 2, 492–497. (Cited on page 29.)

198. Zipfel, P. F.; Hallstrm, T.; Hammerschmidt, S.; Skerka, C., The complement fitness factor h: Role in human diseases and for immune escape of pathogens, like pneumococci. *Vaccine* **2008**, *26*, Supplement 8, I67–I74. (Cited on pages 29 and 30.)

199. Morley B.J., W. M., editor, *The complement facts book*. Academic Press, San Diego, **2000**. (Cited on page 29.)

200. Huber-Lang, M.; Sarma, J. V.; Zetoune, F. S.; Rittirsch, D.; Neff, T. A.; McGuire, S. R.; Lambris, J. D.; Warner, R. L.; Flierl, M. A.; Hoesel, L. M.; Gebhard, F.; Younger, J. G.; Drouin, S. M.; Wetsel, R. A.; Ward, P. A., Generation of c5a in the absence of c3: a new complement activation pathway. *Nat. Med.* **2006**, *12*, 6, 682–687. (Cited on page 29.)

201. Walport, M. J., Complement - first of two parts. *N. Engl. J. Med.* **2001**, *344*, 14, 1058–1066. (Cited on page 29.)

202. Zipfel, P. F.; Heinen, S.; Jzsi, M.; Skerka, C., Complement and diseases: Defective alternative pathway control results in kidney and eye diseases. *Mol. Immunol.* **2006**, *43*, 1-2, 97–106. (Cited on pages 29 and 30.)

203. Gros, P.; Milder, F. J.; Janssen, B. J. C., Complement driven by conformational changes. *Nat. Rev. Immunol.* **2008**, *8*, 1, 48–58. (Cited on page 29.)

204. Nilsson, U. R.; Müller-Eberhard, H. J., Isolation of β1f-globulin from human serum and its characterization as the fifth component of complement. *J. Exp. Med.* **1965**, *122*, 2, 277–298. (Cited on page 29.)

205. Morgan, B., editor, *Complement methods and protocols*. Human Press, Totowa, **2000**. (Cited on page 30.)

206. Noris, M.; Remuzzi, G., Hemolytic uremic syndrome. *J. Am. Soc. Nephrol.* **2005**, *16*, 4, 1035–1050. (Cited on page 30.)

207. Atkinson, J. P.; Goodship, T. H. J., Complement factor h and the hemolytic uremic syndrome. *J. Exp. Med.* **2007**, *204*, 6, 1245–1248. (Cited on page 30.)

208. Smith, R. J. H.; Alexander, J.; Barlow, P. N.; Botto, M.; Cassavant, T. L.; Cook, H. T.; de Cordoba, S. R.; Hageman, G. S.; Jokiranta, T. S.; Kimberling, W. J.; Lambris, J. D.; Lanning, L. D.; Levidiotis, V.; Licht, C.; Lutz, H. U.; Meri, S.; Pickering, M. C.; Quigg, R. J.; Rops, A. L.; Salant, D. J.; Sethi, S.; Thurman, J. M.; Tully, H. F.; Tully, S. P.; van der Vlag, J.; Walker, P. D.; Wurzner, R.; Zipfel, P. F.; Dense Deposit Disease Focus, G., New approaches to the treatment of dense deposit disease. *J. Am. Soc. Nephrol.* **2007**, *18*, 9, 2447–2456. (Cited on page 30.)

209. Appel, G. B.; Cook, H. T.; Hageman, G.; Jennette, J. C.; Kashgarian, M.; Kirschfink, M.; Lambris, J. D.; Lanning, L.; Lutz, H. U.; Meri, S.; Rose, N. R.; Salant, D. J.; Sethi, S.; Smith, R. J. H.; Smoyer, W.; Tully, H. F.; Tully, S. P.; Walker, P.; Welsh, M.; Wurzner, R.; Zipfel, P. F., Membranoproliferative glomerulonephritis type ii (dense deposit disease): an update. *J. Am. Soc. Nephrol.* **2005**, *16*, 5, 1392–1403. (Cited on page 30.)

210. Klein, R. J.; Zeiss, C.; Chew, E. Y.; Tsai, J.-Y.; Sackler, R. S.; Haynes, C.; Henning, A. K.; SanGiovanni, J. P.; Mane, S. M.; Mayne, S. T.; Bracken, M. B.; Ferris, F. L.; Ott, J.; Barnstable, C.; Hoh, J., Complement factor h polymorphism in age related macular degeneration. *Science* **2005**, *308*, 5720, 385–389. (Cited on page 30.)

211. Hageman, G. S.; Anderson, D. H.; Johnson, L. V.; Hancox, L. S.; Taiber, A. J.; Hardisty, L. I.; Hageman, J. L.; Stockman, H. A.; Borchardt, J. D.; Gehrs, K. M.; Smith, R. J. H.; Silvestri, G.; Russell, S. R.; Klaver, C. C. W.; Barbazetto, I.; Chang, S.; Yannuzzi, L. A.; Barile, G. R.; Merriam, J. C.; Smith, R. T.; Olsh, A. K.; Bergeron, J.; Zernant, J.; Merriam, J. E.; Gold, B.; Dean, M.; Allikmets, R., A common haplotype in the complement regulatory gene factor h (hf1/cfh) predisposes individuals to age-related macular degeneration. *PNAS* **2005**, *102*, 20, 7227–7232. (Cited on page 30.)

212. DiScipio, R. G., Ultrastructures and interactions of complement factors h and i. *J. Immunol.* **1992**, *149*, 8, 2592–2599. (Cited on page 30.)

213. Moore, M. D.; DiScipio, R. G.; Cooper, N. R.; Nemerow, G. R., Hydrodynamic, electron microscopic, and ligand-binding analysis of the epstein-barr virus/c3dg receptor (cr2). *J. Biol. Chem.* **1989**, *264*, 34, 20576–20582. (Cited on page 30.)

214. Alsenz, J.; Lambris, J. D.; Schulz, T. F.; Dierich, M. P., Localization of the complement-component-c3b-binding site and the cofactor activity for factor i in the 38kda tryptic fragment of factor h. *Biochem. J.* **1984**, *224*, 2, 389–398. (Cited on page 30.)

215. Gordon, D. L.; Kaufman, R. M.; Blackmore, T. K.; Kwong, J.; Lublin, D. M., Identification of complement regulatory domains in human factor h. *J. Immunol.* **1995**, *155*, 1, 348–356. (Cited on page 30.)

216. Kühn, S.; Zipfel, P. F., Mapping of the domains required for decay acceleration activity of the human factor h-like protein 1 and factor h. *Eur. J. Immunol.* **1996**, *26*, 10, 2383–2387. (Cited on page 30.)

217. Kühn, S.; Skerka, C.; Zipfel, P. F., Mapping of the complement regulatory domains in the human factor h-like protein 1 and in factor h1. *J. Immunol.* **1995**, *155*, 12. (Cited on page 30.)

218. Jokiranta, T. S.; Hellwage, J.; Koistinen, V.; Zipfel, P. F.; Meri, S., Each of the three binding sites on complement factor h interacts with a distinct site on c3b. *J. Biol. Chem.* **2000**, *275*, 36, 27657–27662. (Cited on page 30.)

219. Sharma, A. K.; Pangburn, M. K., Identification of three physically and functionally distinct binding sites for c3b in human complement factor h by deletion mutagenesis. *PNAS* **1996**, *93*, 20, 10996–11001. (Cited on page 30.)

220. Blackmore, T. K.; Sadlon, T. A.; Ward, H. M.; Lublin, D. M.; Gordon, D. L., Identification of a heparin binding domain in the seventh short consensus repeat of complement factor h. *J. Immunol.* **1996**, *157*, 12, 5422–5427. (Cited on page 30.)

221. Blackmore, T. K.; Hellwage, J.; Sadlon, T. A.; Higgs, N.; Zipfel, P. F.; Ward, H. M.; Gordon, D. L., Identification of the second heparin-binding domain in human complement factor h. *J. Immunol.* **1998**, *160*, 7, 3342–3348. (Cited on page 30.)

222. Pangburn, M. K.; Atkinson, M. A.; Meri, S., Localization of the heparin-binding site on complement factor h. *J. Biol. Chem.* **1991**, *266*, 25, 16847–16853. (Cited on pages 30 and 112.)

223. Prodinger, W. M.; Hellwage, J.; Spruth, M.; Dierich, M. P.; Zipfel, P. F., The c-terminus of factor h: monoclonal antibodies inhibit heparin binding and identify epitopes common to factor h and factor h-related proteins. *Biochem. J.* **1998**, *331*, 1, 41–47. (Cited on page 30.)

224. Ram, S.; Sharma, A. K.; Simpson, S. D.; Gulati, S.; McQuillen, D. P.; Pangburn, M. K.; Rice, P. A., A novel sialic acid binding site on factor h mediates serum resistance of sialylated neisseria gonorrhoeae. *J. Exp. Med.* **1998**, *187*, 5, 743–752. (Cited on page 30.)

225. Schmidt, C. Q.; Herbert, A. P.; Kavanagh, D.; Gandy, C.; Fenton, C. J.; Blaum, B. S.; Lyon, M.; Uhrin, D.; Barlow, P. N., A new map of glycosaminoglycan and c3b binding sites on factor h. *J. Immunol.* **2008**, *181*, 4, 2610–2619. (Cited on page 30.)

226. Prosser, B. E.; Johnson, S.; Roversi, P.; Herbert, A. P.; Blaum, B. S.; Tyrrell, J.; Jowitt, T. A.; Clark, S. J.; Tarelli, E.; Uhrin, D.; Barlow, P. N.; Sim, R. B.; Day, A. J.; Lea, S. M., Structural basis for complement factor h linked age-related macular degeneration. *J. Exp. Med.* **2007**, *204*, 10, 2277–2283. (Cited on page 30.)

227. Ferreira, V. P.; Herbert, A. P.; Cortes, C.; McKee, K. A.; Blaum, B. S.; Esswein, S. T.; Uhrin, D.; Barlow, P. N.; Pangburn, M. K.; Kavanagh, D., The binding of factor h to a complex of physiological polyanions and c3b on cells is impaired in atypical hemolytic uremic syndrome. *J. Immunol.* **2009**, *182*, 11, 7009–7018. (Cited on pages 30 and 112.)

228. Shea, M. A.; Sorensen, B. R.; Pedigo, S.; Verhoeven, A. S.; Michael, L. J.; Ackers, G. K., Proteolytic footprinting titrations for estimating ligand-binding constants and detecting pathways of conformational switching of calmodulin. In *Meth. Enzym.*, volume 323, Academic Press, **2000**, pages 254–301. (Cited on page 31.)

229. Zhu, M. M.; Chitta, R.; Gross, M. L., Plimstex: a novel mass spectrometric method for the quantification of protein-ligand interactions in solution. *Int. J. Mass Spectrom.* **2005**, *240*, 3, 213–220. (Cited on pages 31, 32, 65, and 80.)

230. Zhu, M. M.; Rempel, D. L.; Gross, M. L., Modeling data from titration, amide h/d exchange, and mass spectrometry to obtain protein-ligand binding constants. *J. Am. Soc. Mass Spectrom.* **2004**, *15*, 3, 388–397. (Cited on pages 32, 65, and 80.)

231. Zhu, M. M.; Rempel, D. L.; Zhao, J.; Giblin, D. E.; Gross, M. L., Probing ca2+-induced conformational changes in porcine calmodulin by h/d exchange and esi-ms: effect of cations and ionic strength. *Biochemistry* **2003**, *42*, 51, 15388–15397. (Cited on pages 32 and 80.)

232. Chitta, R. K.; Rempel, D. L.; Grayson, M. A.; Remsen, E. E.; Gross, M. L., Application of simstex to oligomerization of insulin analogs and mutants. *J. Am. Soc. Mass Spectrom.* **2006**, *17*, 11, 1526–1534. (Cited on pages 32, 33, 66, and 80.)

233. Chitta, R. K.; Rempel, D. L.; Gross, M. L., Determination of affinity constants and response factors of the noncovalent dimer of gramicidin by electrospray ionization mass spectrometry and mathematical modeling. *J. Am. Soc. Mass Spectrom.* **2005**, *16*, 7, 1031–1038. (Cited on page 32.)

234. Dobson, C. M., Protein misfolding, evolution and disease. *Trends Biochem. Sci.* **1999**, *24*, 9, 329–32. (Cited on page 33.)

235. Schellman, J. A., Macromolecular binding. *Biopolymers* **1975**, *14*, 5, 999–1018. (Cited on pages 33, 34, 81, and 194.)

236. Powell, K. D.; Ghaemmaghami, S.; Wang, M. Z.; Ma, L.; Oas, T. G.; Fitzgerald, M. C., A general mass spectrometry-based assay for the quantitation of protein-ligand binding interactions in solution. *J. Am. Chem. Soc.* **2002**, *124*, 35, 10256–10257. (Cited on pages 33 and 80.)

237. Powell, K. D.; Fitzgerald, M. C., Accuracy and precision of a new h/d exchange- and mass spectrometry-based technique for measuring the thermodynamic properties of protein-peptide complexes. *Biochemistry* **2003**, *42*, 17, 4962–4970. (Cited on pages 33, 34, and 80.)

238. Mathur, S.; Badertscher, M.; Scott, M.; Zenobi, R., Critical evaluation of mass spectrometric measurement of dissociation constants: accuracy and cross-validation against surface plasmon resonance and circular dichroism for the calmodulin-melittin system. *Phys. Chem. Chem. Phys.* **2007**, *9*, 47, 6187–6198. (Cited on pages 33 and 80.)

239. Powell, K. D.; Fitzgerald, M. C., Measurements of protein stability by h/d exchange and matrix-assisted laser desorption/ionization mass spectrometry using picomoles of material. *Anal. Chem.* **2001**, *73*, 14, 3300–3304. (Cited on pages 33 and 80.)

240. Ghaemmaghami, S.; Oas, T. G., Quantitative protein stability measurement in vivo. *Nat. Struct. Biol.* **2001**, *8*, 10, 879–882. (Cited on pages 33 and 80.)

241. Powell, K. D.; Wales, T. E.; Fitzgerald, M. C., Thermodynamic stability measurements on multimeric proteins using a new h/d exchange- and matrix-assisted laser desorption/ionization (maldi) mass spectrometry-based method. *Protein Sci.* **2002**, *11*, 4, 841–851. (Cited on pages 33, 34, and 80.)

242. Ma, L.; Fitzgerald, M. C., A new h/d exchange- and mass spectrometry-based method for thermodynamic analysis of protein-dna interactions. *Chem. Biol.* **2003**, *10*, 12, 1205–1213. (Cited on pages 33 and 80.)

243. Tang, L.; Roulhac, P. L.; Fitzgerald, M. C., H/d exchange and mass spectrometry-based method for biophysical analysis of multidomain proteins at the domain level. *Anal. Chem.* **2007**, *79*, 22, 8728–8739. (Cited on pages 33 and 80.)

244. Powell, K. D.; Fitzgerald, M. C., High-throughput screening assay for the tunable selection of protein ligands. *J. Comb. Chem.* **2004**, *6*, 2, 262–269. (Cited on pages 33, 36, and 80.)

245. Hopper, E. D.; Roulhac, P. L.; Campa, M. J.; Patz, J., E. F.; Fitzgerald, M. C., Throughput and efficiency of a mass spectrometry-based screening assay for protein-ligand binding detection. *J. Am. Soc. Mass Spectrom.* **2008**, *19*, 9, 1303–1311. (Cited on pages 33, 36, 78, and 80.)

246. Zhang, Y.-Z., *Protein and peptide structure and interactions studied by hydrogen exchange and NMR*. Ph.D. thesis, University of Pennsylvania, **1995**. (Cited on page 34.)

247. Powell, K. D.; Wang, M. Z.; Silinski, P.; Ma, L.; Wales, T. E.; Dai, S. Y.; Warner, A. H.; Yang, X.; Fitzgerald, M. C., The accuracy and precision of a new h/d exchange- and mass spectrometry-based technique for measuring the thermodynamic stability of proteins. *Anal. Chim. Acta* **2003**, *496*, 1-2, 225–232. (Cited on pages 35 and 80.)

248. Dai, S. Y.; Fitzgerald, M. C., Accuracy of suprex (stability of unpurified proteins from rates of h/d exchange) and maldi mass spectrometry-derived protein unfolding free energies determined under non-ex2 exchange conditions. *J. Am. Soc. Mass Spectrom.* **2006**, *17*, 11, 1535–1542. (Cited on pages 35 and 80.)

249. Sivaraman, T.; Arrington, C. B.; Robertson, A. D., Kinetics of unfolding and folding from amide hydrogen exchange in native ubiquitin. *Nat. Struct. Mol. Biol.* **2001**, *8*, 4, 331–333. (Cited on page 35.)

250. Fitzgerald, M. C.; West, G. M., Painting proteins with covalent labels: What's in the picture? *J. Am. Soc. Mass Spectrom.* **2009**, *20*, 6, 1193–1206. (Cited on page 36.)

251. Hanahan, D., Studies on transformation of escherichia coli with plasmids. *J. Mol. Biol.* **1983**, *166*, 4, 557–580. (Cited on page 37.)

252. Wear, M. A.; Patterson, A.; Malone, K.; Dunsmore, C.; Turner, N. J.; Walkinshaw, M. D., A surface plasmon resonance-based assay for small molecule inhibitors of human cyclophilin a. *Anal. Biochem.* **2005**, *345*, 2, 214–226. (Cited on pages 41, 43, 82, 152, and 153.)

253. Bradford, M. M., A rapid and sensitive method for the quantitation of microgram quantities of protein utilizing the principle of protein-dye binding. *Anal. Biochem.* **1976**, *72*, 248–254. (Cited on page 48.)

254. Glasoe, P. K.; Long, F. A., Use of glass electrodes to measure acidities in deuterium oxide. *J. Phys. Chem.* **1960**, *64*, 1, 188–190. (Cited on page 51.)

255. Ludvigsen, S.; Olsen, H. B.; Kaarsholm, N. C., A structural switch in a mutant insulin exposes key residues for receptor binding. *J. Mol. Biol.* **1998**, *279*, 1, 1–7. (Cited on page 66.)

256. Chang, X.; Jorgensen, A. M. M.; Bardrum, P.; Led, J. J., Solution structures of the r6 human insulin hexamer. *Biochemistry* **1997**, *36*, 31, 9409–9422. (Cited on page 66.)

257. DeFelippis MR, F. B., Chance RE, Crit rev ther drug carrier syst. *Crit. Rev. Ther. Drug Carrier Syst.* **2001**, *18*, 2, 201–264. (Cited on page 66.)

258. Brange, J.; Vlund, A., Insulin analogs with improved pharmacokinetic profiles. *Adv. Drug Deliv. Rev.* **1999**, *35*, 2-3, 307–335. (Cited on page 66.)

259. Creighton, T. E., editor, *Protein structure: a practical approach*. Oxford University Press, Oxford, **1997**. (Cited on pages 67 and 68.)

260. Feng, R.; Konishi, Y., Stepwise refolding of acid-denatured myoglobin: evidence from electrospray mass spectrometry. *J. Am. Soc. Mass Spectrom.* **1993**, *4*, 8, 638–645. (Cited on page 75.)

261. Sogbein, O. O.; Simmons, D. A.; Konermann, L., Effects of ph on the kinetic reaction mechanism of myoglobin unfolding studied by time-resolved electrospray ionization mass spectrometry. *J. Am. Soc. Mass Spectrom.* **2000**, *11*, 4, 312–319. (Cited on page 75.)

262. Dai, S. Y.; Fitzgerald, M. C., A mass spectrometry-based probe of equilibrium intermediates in protein-folding reactions. *Biochemistry* **2006**, *45*, 42, 12890–12897. (Cited on pages 76 and 80.)

263. Pace, C. N.; Vanderburg, K. E., Determining globular protein stability: guanidine hydrochloride denaturation of myoglobin. *Biochemistry* **1979**, *18*, 2, 288–292. (Cited on page 76.)

264. Ahmad, F.; Yadav, S.; Taneja, S., Determining stability of proteins from guanidinium chloride transition curves. *Biochem. J.* **1992**, *287*, 2, 481–485. (Cited on page 76.)

265. Daniel, J. M.; Friess, S. D.; Rajagopalan, S.; Wendt, S.; Zenobi, R., Quantitative determination of noncovalent binding interactions using soft ionization mass spectrometry. *Int. J. Mass Spectrom.* **2002**, *216*, 1, 1–27. (Cited on page 78.)

266. Sannes-Lowery, K. A.; Griffey, R. H.; Hofstadler, S. A., Measuring dissociation constants of rna and aminoglycoside antibiotics by electrospray ionization mass spectrometry. *Anal. Biochem.* **2000**, *280*, 2, 264–271. (Cited on page 78.)

267. Gao, H.; Yu, Y.; Leary, J. A., Mechanism and kinetics of metalloenzyme phosphomannose isomerase: Measurement of dissociation constants and effect of zinc binding using esi-fticr mass spectrometry. *Anal. Chem.* **2005**, *77*, 17, 5596–5603. (Cited on page 78.)

268. Wang, M. Z.; Shetty, J. T.; Howard, B. A.; Campa, M. J.; Patz, J., E. F.; Fitzgerald, M. C., Thermodynamic analysis of cyclosporin a binding to cyclophilin a in a lung tumor tissue lysate. *Anal. Chem.* **2004**, *76*, 15, 4343–4348. (Cited on pages 78, 80, 100, 102, and 153.)

269. West, G. M.; Tang, L.; Fitzgerald, M. C., Thermodynamic analysis of protein stability and ligand binding using a chemical modification- and mass spectrometry-based strategy. *Anal. Chem.* **2008**, *80*, 11, 4175–4185. (Cited on pages 78, 80, and 100.)

270. Yan-Hong, S.; Dong-Hai, L.; Jian-Ying, H.; Xu, S., Study of structural stability of cyclophilin a by nmr and circular dichroism spectra. *Chin. J. Chem.* **2006**, *24*, 7, 973–979. (Cited on pages 78 and 137.)

271. Sperry, J. B.; Shi, X.; Rempel, D. L.; Nishimura, Y.; Akashi, S.; Gross, M. L., A mass spectrometric approach to the study of dna-binding proteins: interaction of human trf2 with telomeric dna. *Biochemistry* **2008**, *47*, 6, 1797–1807. (Cited on page 80.)

272. Reid, C. W.; Brewer, D.; Clarke, A. J., Substrate binding affinity of pseudomonas aeruginosa membrane-bound lytic transglycosylase b by hydrogen-deuterium exchange maldi ms. *Biochemistry* **2004**, *43*, 35, 11275–11282. (Cited on page 80.)

273. Roulhac, P. L.; Powell, K. D.; Dhungana, S.; Weaver, K. D.; Mietzner, T. A.; Crumbliss, A. L.; Fitzgerald, M. C., Suprex (stability of unpurified proteins from rates of h/d exchange) analysis of the thermodynamics of synergistic anion binding by ferric-binding protein (fbpa), a bacterial transferrin. *Biochemistry* **2004**, *43*, 50, 15767–15774. (Cited on page 80.)

274. Dai, S. Y.; Gardner, M. W.; Fitzgerald, M. C., Protocol for the thermodynamic analysis of some proteins using an h/d exchange- and mass spectrometry-based technique. *Anal. Chem.* **2005**, *77*, 2, 693–697. (Cited on page 80.)

275. Tong, Y.; Wuebbens, M. M.; Rajagopalan, K. V.; Fitzgerald, M. C., Thermodynamic analysis of subunit interactions in escherichia coli molybdopterin synthase. *Biochemistry* **2005**, *44*, 7, 2595–2601. (Cited on page 80.)

276. Reid, C. W.; Blackburn, N. T.; Clarke, A. J., Role of arginine residues in the active site of the membrane-bound lytic transglycosylase b from pseudomonas aeruginosa. *Biochemistry* **2006**, *45*, 7, 2129–2138. (Cited on page 80.)

277. Frego, L.; Gautschi, E.; Martin, L.; Davidson, W., The determination of high-affinity protein/inhibitor binding constants by electrospray ionization hydrogen/deuterium exchange mass spectrometry. *Rapid Commun. Mass Spectrom.* **2006**, *20*, 16, 2478–2482. (Cited on page 80.)

278. Frankel, B. A.; Tong, Y.; Bentley, M. L.; Fitzgerald, M. C.; McCafferty, D. G., Mutational analysis of active site residues in the staphylococcus aureus transpeptidase srta. *Biochemistry* **2007**, *46*, 24, 7269–7278. (Cited on page 80.)

279. Tang, L.; Hopper, E. D.; Tong, Y.; Sadowsky, J. D.; Peterson, K. J.; Gellman, S. H.; Fitzgerald, M. C., H/d exchange- and mass spectrometry-based strategy for the thermodynamic analysis of protein-ligand binding. *Anal. Chem.* **2007**, *79*, 15, 5869–5877. (Cited on page 80.)

280. Roulhac, P. L.; Weaver, K. D.; Adhikari, P.; Anderson, D. S.; DeArmond, P. D.; Mietzner, T. A.; Crumbliss, A. L.; Fitzgerald, M. C., Ex vivo analysis of synergistic anion binding to fbpa in gram-negative bacteria. *Biochemistry* **2008**, *47*, 14, 4298–4305. (Cited on page 80.)

281. Weaver, K. D.; Heymann, J. J.; Mehta, A.; Roulhac, P. L.; Anderson, D. S.; Nowalk, A. J.; Adhikari, P.; Mietzner, T. A.; Fitzgerald, M. C.; Crumbliss, A. L., Ga3+ as a mechanistic probe in fe3+ transport: characterization of ga3+ interaction with fbpa. *J. Biol. Inorg. Chem.* **2008**, *13*, 6, 887–898. (Cited on page 80.)

282. Zeder-Lutz, G.; Wenger, R.; Van Regenmortel, M. H. V.; Altschuh, D., Interaction of cyclosporin a with an fab fragment or cyclophilin affinity measurements and time-dependent changes in binding. *FEBS Lett.* **1993**, *326*, 1-3, 153–157. (Cited on pages 82, 152, and 153.)

283. Fanghänel, J.; Fischer, G., Thermodynamic characterization of the interaction of human cyclophilin 18 with cyclosporin a. *Biophys. Chem.* **2003**, *100*, 1-3, 351–366. (Cited on pages 82, 152, and 153.)

284. Seebach, D.; Bossler, H. G.; Flowers, R.; Arnett, E. M., Calorimetric measurements of the complexation of cyclosporin a, ascomycin, fujimycin, and rapamycin with lithium chloride and with an immunophilin. *Helv. Chim. Acta* **1994**, *77*, 1, 291–305. (Cited on pages 82, 152, and 153.)

285. Myung, J. K.; Frischer, T.; Afjehi-Sadat, L.; Pollak, A.; Lubec, G., Mass spectrometrical analysis of the processed metastasis-inducing anterior gradient protein 2 homolog reveals 100**2008**, *35*, 2, 485–494. (Cited on page 111.)

286. Murray, E.; McKenna, E. O.; Burch, L. R.; Dillon, J.; Langridge-Smith, P.; Kolch, W.; Pitt, A.; Hupp, T. R., Microarray-formatted clinical biomarker assay development using peptide aptamers to anterior gradient-2. *Biochemistry* **2007**, *46*, 48, 13742–13751. (Cited on page 111.)

287. Herbert, A. P.; Uhrin, D.; Lyon, M.; Pangburn, M. K.; Barlow, P. N., Disease-associated sequence variations congregate in a polyanion recognition patch on human factor h revealed in three-dimensional structure. *J. Biol. Chem.* **2006**, *281*, 24, 16512–16520. (Cited on pages 112 and 118.)

288. Cereghino, J. L.; Cregg, J. M., Heterologous protein expression in the methylotrophic yeast *Pichia pastoris*. *FEMS Microbiol. Rev.* **2000**, *24*, 1, 45–66. (Cited on page 114.)

289. Munehito, A.; Tomonao, I.; Kosuke, M.; Teikichi, I.; Hiroshi, K.; Yoshiyuki, A.; Kunihiro, K., Denaturation and reassembly of chaperonin groel studied by solution x-ray scattering. *Prot. Sci.* **2003**, *12*, 4, 672–680. (Cited on pages 137 and 142.)

290. Robinson, C. V.; Grosz, M.; Eyles, S. J.; Ewbank, J. J.; Mayhew, M.; Hartl, F. U.; Dobson, C. M.; Radford, S. E., Conformation of groel-bound α-lactalbumin probed by mass spectrometry. *Nature* **1994**, *372*, 6507, 646–651. (Cited on page 137.)

291. Miranker, A.; Robinson, C. V.; Radford, S. E.; Dobson, C. M., Investigation of protein folding by mass spectrometry. *FASEB J.* **1996**, *10*, 1, 93–101. (Cited on page 137.)

292. Gross, M.; Robinson, C. V.; Mayhew, M.; Hartl, F. U.; Radford, S. E., Significant hydrogen exchange protection in groel-bound dhfr is maintained during iterative rounds of substrate cycling. *Protein Sci.* **1996**, *5*, 12, 2506–2513. (Cited on page 137.)

293. Robinson, C. V.; Gross, M.; Radford, S. E.; George, H. L.; Baldwin, T. O., Probing conformations of groel-bound substrate proteins by mass spectrometry. In *Meth. Enzymol.*, volume 290, Academic Press, **1998**, pages 296–313. (Cited on page 137.)

294. Coyle, J. E.; Texter, F. L.; Ashcroft, A. E.; Masselos, D.; Robinson, C. V.; Radford, S. E., Groel accelerates the refolding of hen lysozyme without changing its folding mechanism. *Nat. Struct. Mol. Biol.* **1999**, *6*, 7, 683–690. (Cited on page 137.)

295. Ashcroft, A. E.; Brinker, A.; Coyle, J. E.; Weber, F.; Kaiser, M.; Moroder, L.; Parsons, M. R.; Jager, J.; Hartl, U. F.; Hayer-Hartl, M.; Radford, S. E., Structural plasticity and noncovalent substrate binding in the groel apical domain. *J. Biol. Chem.* **2002**, *277*, 36, 33115–33126. (Cited on page 137.)

296. van Duijn, E.; Simmons, D. A.; van den Heuvel, R. H. H.; Bakkes, P. J.; van Heerikhuizen, H.; Heeren, R. M. A.; Robinson, C. V.; van der Vies, S. M.; Heck, A. J. R., Tandem mass spectrometry of intact groel substrate complexes reveals substrate-specific conformational changes in the trans ring. *J. Am. Chem. Soc.* **2006**, *128*, 14, 4694–4702. (Cited on page 137.)

297. Ohtsu, I.; Nakanisi, T.; Furuta, M.; Ando, E.; Nishimura, O., Direct matrix-assisted laser desorption/ionization time-of-flight mass spectrometric identification of proteins on membrane detected by western blotting and lectin blotting. *J. Proteome Res.* **2005**, *4*, 4, 1391–1396. (Cited on page 137.)

298. Zahn, R.; Spitzfaden, C.; Ottiger, M.; Wüthrich, K.; Pluckthun, A., Destabilization of the complete protein secondary structure on binding to the chaperone groel. *Nature* **1994**, *368*, 6468, 261–265. (Cited on page 137.)

299. Pace, C. N.; Timasheff, C. H. W. H.; N., S., Determination and analysis of urea and guanidine hydrochloride denaturation curves. *Methods Enzymol.* **1986**, *131*, 266–280. (Cited on page 194.)

8 Appendix 1

8.1 Amino Acid Table

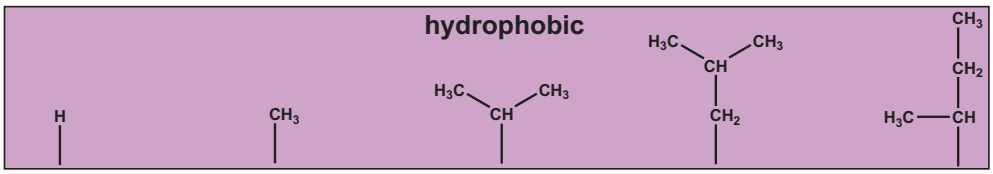

	Gly (G)	Ala (A)	Val (V)	Leu (L)	Ile (I)
average mass	57.052	71.079	99.133	113.160	113.160
exchangeable H's	1	1	1	1	1

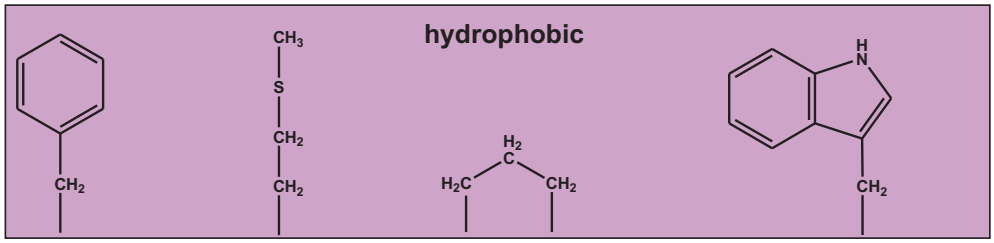

Phe (F)	Met (M)	Pro (P)	Trp (W)
147.177	131.199	97.117	186.213
1	1	0	2

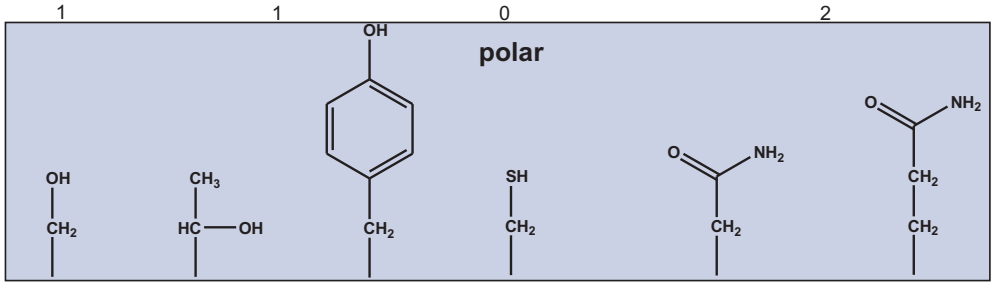

Ser (S)	Thr (T)	Tyr (Y)	Cys (C)	Asn (N)	Gln (Q)
87.078	101.105	163.176	103.145	114.104	128.131
2	2	2	2	3	3

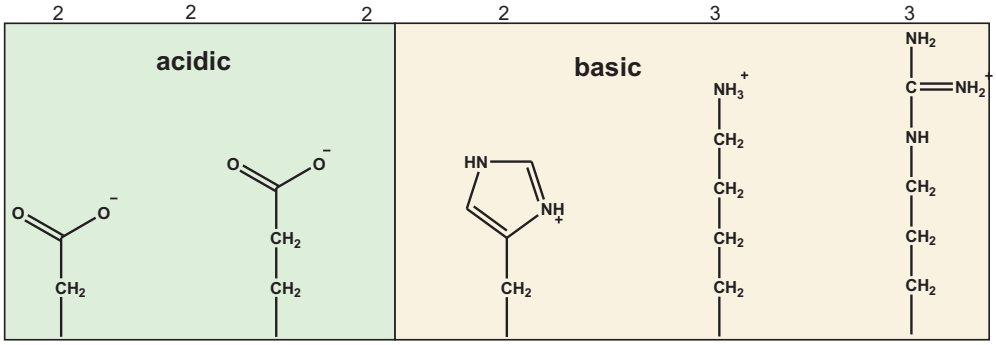

Asp (D)	Glu (E)	His (H)	Lys (K)	Arg (R)
115.089	129.116	137.141	128.174	156.188
2	2	2	3	5

8.2 Thermodynamics

The Internal Energy and Enthalpy

Due to the first law of thermodynamics the internal energy of a system is governed by volume work and heat.

$$dU = \delta W + \delta Q \tag{24}$$

The internal energy U is

$$U = f(T, V, n_i) \tag{25}$$

defining volume work as:

$$W = -\int_{V_1}^{V_2} p dV \tag{26}$$

resulting in:

$$dU = \delta Q - p dV \tag{27}$$

assuming a closed system and isobar conditions:

$$dU = \delta Q - p dV \quad \Rightarrow \quad U_{II} - U_I = Q - p(V_{II} - V_I) \tag{28}$$

Solving for the exchanged heat:

$$Q = U_{II} - U_I + p(V_{II} - V_I) = U + pV \tag{29}$$

The enthalpy H is a state function $f(T, p, n_i)$:

$$H = U + pV \tag{30}$$

The enthalpy for isobaric systems equals the amount of heat exchanged with the surrounding:

$$(H_{II} - H_I)_p = Q_p \tag{31}$$

Heat Capacities

The heat needed to warm a system is proportional to the temperature difference and the number of moles n:

$$Q = C(T_2 - T_1) = c \cdot n(T_2 - T_1) \tag{32}$$

Hereby the proportionality factor C is termed the heat capacity, and c the molar heat capacity ($c = C/n$).

The partial differentials of U and T with respect to T delivers the heat capacities. According to

the first law of thermodynamics (eq. 27) and writing the total differentials for U and I:

$$dU = \delta W + \delta Q = \delta Q - pdV = \left(\frac{\partial U}{\partial T}\right)_V dT + \left(\frac{\partial U}{\partial V}\right)_T dV \tag{33}$$

$$dH = d(U + pV) = dU + pdV + Vdp = \delta Q + Vdp = \left(\frac{\partial H}{\partial T}\right)_p dT + \left(\frac{\partial H}{\partial p}\right)_T dp \tag{34}$$

solving for δQ:

$$\delta Q = \left(\frac{\partial U}{\partial T}\right)_V dT + \left[\left(\frac{\partial U}{\partial V}\right)_T + p\right] dV \tag{35}$$

$$\delta Q = \left(\frac{\partial H}{\partial T}\right)_p dT + \left[\left(\frac{\partial H}{\partial p}\right)_T - V\right] dp \tag{36}$$

Now one can add δQ to the system by either keeping pressure or volume constant.

$$\delta Q_V = \left(\frac{\partial U}{\partial T}\right)_V dT \qquad \delta Q_p = \left(\frac{\partial H}{\partial T}\right)_V dT \tag{37}$$

The heat capacity results by inserting eq 37 into 32 and is defined as the heat needed to warm up a system by one degree centigrade:

$$C_V = \left(\frac{\partial Q}{\partial T}\right)_V = \left(\frac{\partial U}{\partial T}\right)_V \tag{38}$$

$$C_p = \left(\frac{\partial Q}{\partial T}\right)_p = \left(\frac{\partial H}{\partial T}\right)_p \tag{39}$$

Entropy, Free Enthalpy and Energy

According to the second law of thermodynamics the entropy (S) is constant in an isolated system for reversible processes, and increases for irreversible ones.

$$(S_2 - S_1)_{U,V} \geq 0 \tag{40}$$

An assumption that a system is in contact with a big thermostat enables the usage of the thermodynamic basic equations and resolves the duality of the driving forces of entropy increase and energy decrease.

$$dS(isolatedsystem) = dS(system) + dS(thermostat) \geq 0 \tag{41}$$

$$dS(system) - \frac{dQ(system)}{T} \geq 0 \tag{42}$$

$$dS(system) - \frac{dU}{T} \geq 0 \quad (V, T\ const) \qquad dS(system) - \frac{dH}{T} \geq 0 \quad (p, T\ const) \tag{43}$$

The free energy A (Helmholtz) is defined as:

$$A = U - T \cdot S \tag{44}$$

and the free enthalpy G (Gibbs):

$$G = H - T \cdot S \tag{45}$$

with equation 43 the criteria for spontaneous processes become:

$$dA_{V,T} \leq 0 \qquad dG_{p,T} \leq 0 \tag{46}$$

All equations and derivations adapted from [52].

9 Appendix 2

9.1 Bradford Assay for Cyclophilin A

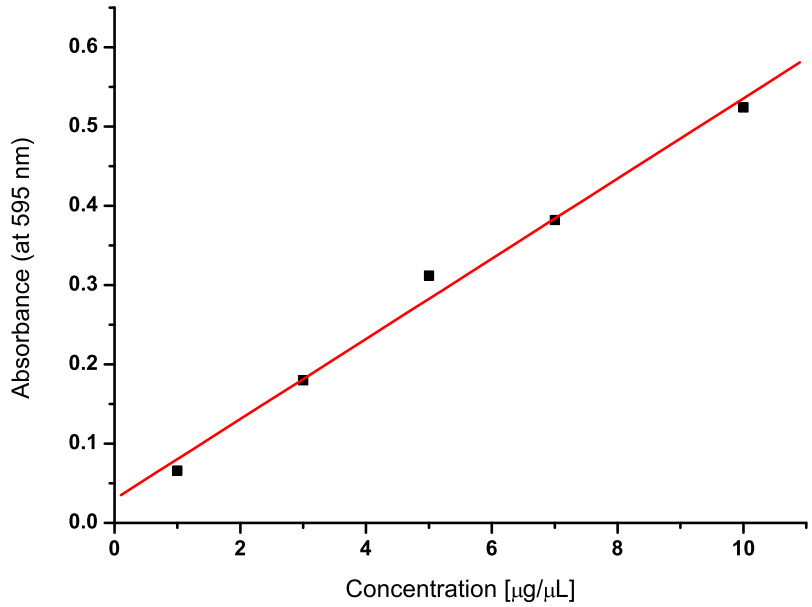

9.2 Direct Infusion Chromatogram

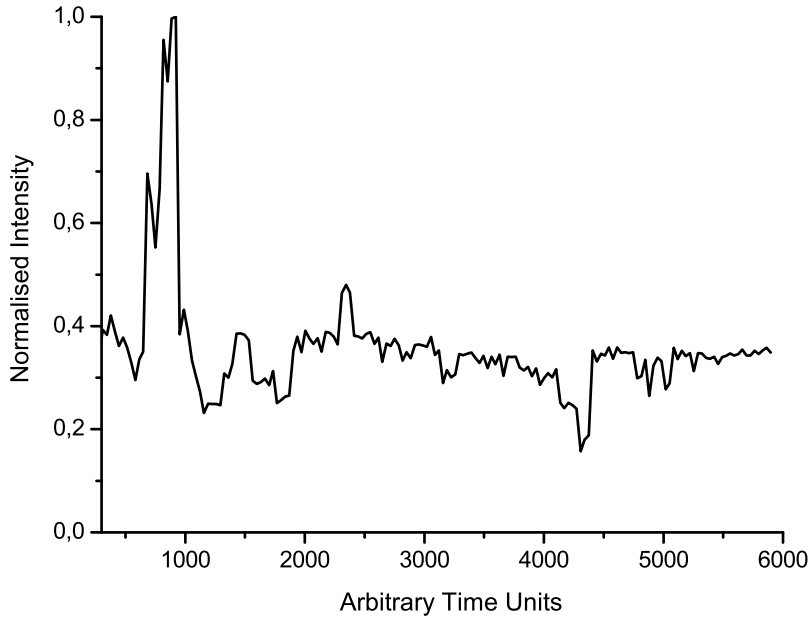

9.3 HPLC-MS Elution Chromatogram

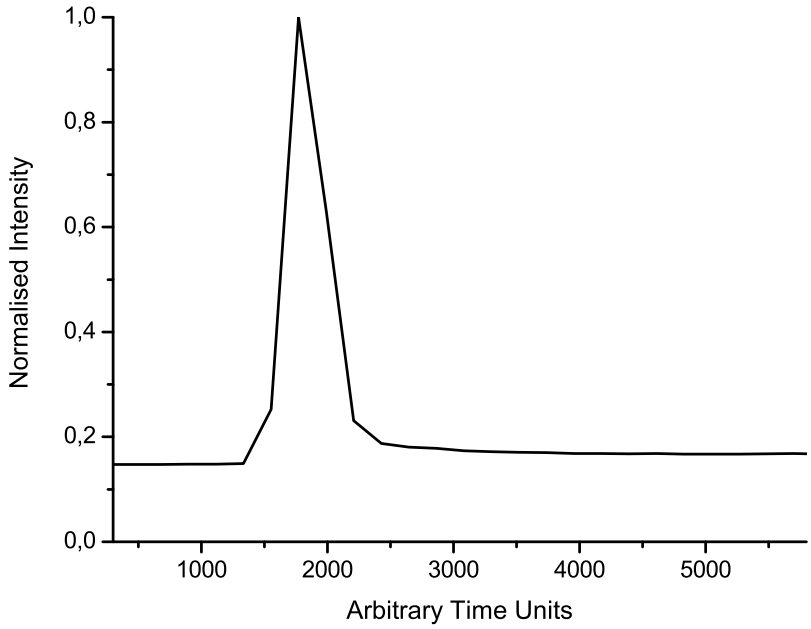

9.4 Manual PLIMSTEX CypA Mass Spectrum

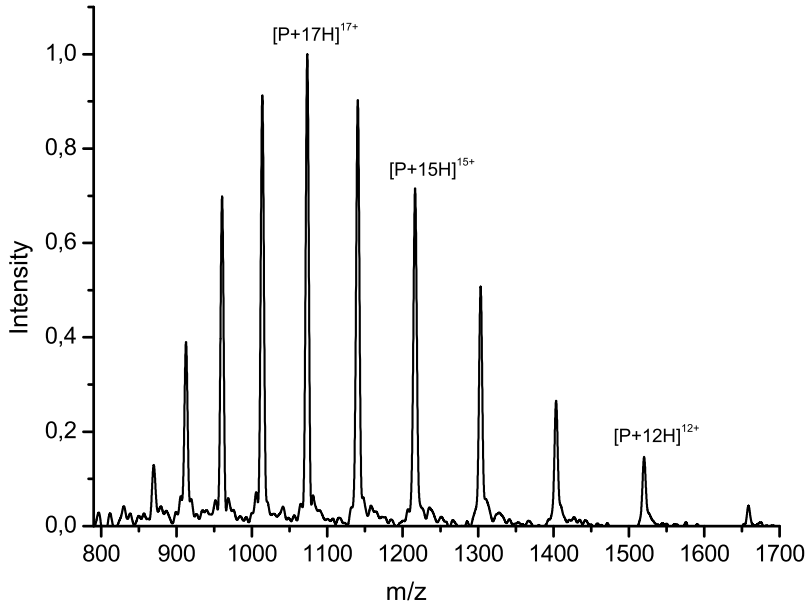

9.5 LC Program for HDX Labeling

TempCtrl =	On	
	Temperature.Nominal =	20.0 [°C]
	Temperature.LowerLimit =	5.0 [°C]
	Temperature.UpperLimit =	85.0 [°C]
	EquilibrationTime =	0.5 [min]
	ReadyTempDelta =	5.0 [°C]
	Pressure.LowerLimit =	2 [bar]
	Pressure.UpperLimit =	300 [bar]
	MaximumFlowRampDown =	300000 [µl/min²]
	MaximumFlowRampUp =	300000 [µl/min²]
	%A.Equate =	"Wash Buffer"
	%B.Equate =	"Elution Buffer"
	%C.Equate =	"%C"
	InjectMode =	UserProg
	ReagentAVial=	1
	ReagentBVial=	2
	ReagentCVial=	3
	ReagentDVial=	4
	PrepVial=	F8
	SyringeValve	Position=Needle
	InjectValve	Position=Load
	Draw	From=SampleVial, Volume=25.0,
SyringeSpeed=Normal, SampleHeight=3		
	InjectMarker	
	MixWait	Duration=20
	Draw	From=SampleVial, Volume=0.0,
SyringeSpeed=1, SampleHeight=3		
	InjectValve	Position=Inject
	SyringeValve	Position=Waste
	MoveSyringeHome	
	SyringeValve	Position=Needle
	MixNeedleWash	Volume=100
	Pump_Pressure.Step =	Auto
	Pump_Pressure.Average =	On
0.000	Flow =	30 [µl/min]
	%B =	0.0 [%]
	%C =	0.0 [%]
	Curve =	5
	Wait	UV.Ready and ColumnOven.Ready and
Sampler.Ready		
	Inject	
	Pump_Pressure.AcqOn	
	Flow =	30 [µl/min]
	%B =	0.0 [%]
	%C =	0.0 [%]
	Curve =	5
0.100	MS_Start.State	On
0.200	MS_Start.State	Off
8.000	Flow =	30 [µl/min]
	%B =	0.0 [%]
	%C =	0.0 [%]
	Curve =	5
1.010	Flow =	30 [µl/min]
	%B =	100.0 [%]
	%C =	0.0 [%]
	Curve =	5
8.000	Flow =	30 [µl/min]
	%B =	100.0 [%]
	%C =	0.0 [%]
	Curve =	5
8.010	Flow =	30 [µl/min]
	%B =	0.0 [%]
	%C =	0.0 [%]
	Curve =	5
10.000	Flow =	30 [µl/min]
	%B =	0.0 [%]
	%C =	0.0 [%]
	Curve =	5
10.100	Pump_Pressure.AcqOff	
	End	

9.6 LC Program for Bulk PLIMSTEX

```
                TempCtrl                        =       On
                Temperature.Nominal     =       20.0 [°C]
                Temperature.LowerLimit  =       5.0 [°C]
                Temperature.UpperLimit  =       85.0 [°C]
                EquilibrationTime               =       0.5 [min]
                ReadyTempDelta                  =       5.0 [°C]
                Pressure.LowerLimit     =       2 [bar]
                Pressure.UpperLimit     =       400 [bar]
                MaximumFlowRampDown=    300000 [µl/min²]
                MaximumFlowRampUp       =       300000 [µl/min²]
                %A.Equate                       =       "%A"
                %B.Equate                       =       "%B"
                %C.Equate                       =       "%C"
                InjectMode                      =       UserProg
                ReagentAVial            =       1
                ReagentBVial            =       2
                ReagentCVial            =       3
                ReagentDVial            =       4
                PrepVial                =       A1
                SyringeValve    Position =Needle
                InjectValve     Position =Load
        Draw    From    =       PrepVial, Volume=60, SyringeSpeed=3, SampleHeight=3
        MixWait         Duration=10
        Draw    From    =       PrepVial, Volume=0.0, SyringeSpeed=3, SampleHeight=3
        InjectMarker
        InjectValve     Position        =Inject
        SyringeValve    Position        =Waste
        MoveSyringeHome
        SyringeValve    Position        =Needle
        MixNeedleWash   Volume  =600
        Pump_Pressure.Step              =Auto
        Pump_Pressure.Average           =On

0.000   Flow            =       30 [µl/min]
        %B              =       0.0 [%]
        %C              =       0.0 [%]
        Curve           =       5
        Wait    UV.Ready and ColumnOven.Ready and Sampler.Ready
        Inject
        Pump_Pressure.AcqOn
        Flow            =       30 [µl/min]
        %B              =       0.0 [%]
        %C              =       0.0 [%]
        Curve           =       5
0.100   MS_Start.State  On
0.200   MS_Start.State  Off
0.490   Flow            =       30 [µl/min]
        %B              =       0.0 [%]
        %C              =       0.0 [%]
        Curve           =       5
0.500   Flow            =       30 [µl/min]
        %B              =       100.0 [%]
        %C              =       0.0 [%]
        Curve           =       5
15.500  Flow            =       30 [µl/min]
        %B              =       100.0 [%]
        %C              =       0.0 [%]
        Curve           =       5
15.510  Flow            =       30 [µl/min]
        %B              =       0.0 [%]
        %C              =       0.0 [%]
        Curve           =       5
25.500  Pump_Pressure.AcqOff
        Flow            =       30 [µl/min]
        %B              =       0.0 [%]
        %C              =       0.0 [%]
        Curve           =       5
        End
```

9.7 LC Program for Individual PLIMSTEX

```
TempCtrl = On
Temperature.Nominal = 20.0 [°C]
Temperature.LowerLimit = 5.0 [°C]
Temperature.UpperLimit = 85.0 [°C]
EquilibrationTime = 0.5 [min]
ReadyTempDelta = 5.0 [°C]
Pressure.LowerLimit = 2 [bar]
Pressure.UpperLimit = 400 [bar]
MaximumFlowRampDown = 300000 [µl/min²]
MaximumFlowRampUp = 300000 [µl/min²]
%A.Equate = "%A"
%B.Equate = "%B"
%C.Equate = "%C"
InjectMode = UserProg
ReagentAVial=1
ReagentBVial=2
ReagentCVial=3
ReagentDVial=4
PrepVial=F8
SyringeValvePosition=Needle
InjectValvePosition=Load
DrawFrom=PrepVial, Volume=1.0, SyringeSpeed=1,
SampleHeight=3
MixWaitDuration=6
DrawFrom=PrepVial, Volume=0.0, SyringeSpeed=1,
SampleHeight=3
DispenseTo=SampleVial, Volume=1.0, SyringeSpeed=High,
SampleHeight=3
DrawFrom=SampleVial, Volume=3.0, SyringeSpeed=Low,
SampleHeight=3
DispenseTo=SampleVial, Volume=3.0, SyringeSpeed=High,
SampleHeight=3
MixNeedleWashVolume=150
MixWaitDuration=1020
DrawFrom=ReagentCVial, Volume=25.0, SyringeSpeed=Normal,
SampleHeight=3
MixWaitDuration=25
DrawFrom=ReagentCVial, Volume=0.0, SyringeSpeed=Normal,
SampleHeight=3
DispenseTo=SampleVial, Volume=25.0, SyringeSpeed=7,
SampleHeight=3
DrawFrom=ReagentCVial, Volume=17.5, SyringeSpeed=Normal,
SampleHeight=3
MixWaitDuration=25
DrawFrom=ReagentCVial, Volume=0.0, SyringeSpeed=Normal,
SampleHeight=3
DispenseTo=SampleVial, Volume=17.5, SyringeSpeed=7,
SampleHeight=3
DrawFrom=SampleVial, Volume=25.0, SyringeSpeed=3,
SampleHeight=3
MixWaitDuration=10
DispenseTo=SampleVial, Volume=25.0, SyringeSpeed=7,
SampleHeight=3
 MixNeedleWashVolume=150
 MixWaitDuration=2280
 MixWaitDuration=2280
DrawFrom=ReagentAVial, Volume=1.0, SyringeSpeed=3,
SampleHeight=3
DispenseTo=SampleVial, Volume=1.0, SyringeSpeed=6,
SampleHeight=3
DrawFrom=SampleVial, Volume=20.0, SyringeSpeed=Normal,
SampleHeight=3
DispenseTo=SampleVial, Volume=20.0, SyringeSpeed=7,
SampleHeight=3
DrawFrom=SampleVial, Volume=25.0, SyringeSpeed=Normal,
SampleHeight=3
MixWaitDuration=25
DrawFrom=SampleVial, Volume=0.0, SyringeSpeed=Normal,
SampleHeight=3
SyringeValvePosition=Waste
MoveSyringeHome
SyringeValvePosition=Needle
```

DrawFrom=SampleVial, Volume=22.0, SyringeSpeed=Normal,
SampleHeight=3
MixWaitDuration=25
DrawFrom=SampleVial, Volume=0.0, SyringeSpeed=Normal,
SampleHeight=3
InjectMarker
InjectValvePosition=Inject
SyringeValvePosition=Waste
MoveSyringeHome
SyringeValvePosition=Needle
MixNeedleWashVolume=150

Pump_Pressure.Step = Auto
Pump_Pressure.Average = On
Data_Collection_Rate = 2 [Hz]
Response = 0.1 [s]
UV_VIS_1.Wavelength = 214 [nm]
UV_VIS_1.Step = 0.50 [s]
UV_VIS_1.Average = On

0.000Autozero
Flow = 30 [µl/min]
%B = 0.0 [%]
%C = 0.0 [%]
Curve = 5
WaitUV.Ready and ColumnOven.Ready and Sampler.Ready
Inject
Pump_Pressure.AcqOn
UV_VIS_1.AcqOn
Flow = 30 [µl/min]
%B = 0.0 [%]
%C = 0.0 [%]
Curve = 5

0.100MS_Start.StateOn

0.200MS_Start.StateOff

0.490Flow = 30 [µl/min]
%B = 0.0 [%]
%C = 0.0 [%]
Curve = 5

0.500Flow = 30 [µl/min]
%B = 100.0 [%]
%C = 0.0 [%]
Curve = 5

15.500Flow = 30 [µl/min]
%B = 100.0 [%]
%C = 0.0 [%]
Curve = 5

15.510Flow = 30 [µl/min]
%B = 0.0 [%]
%C = 0.0 [%]
Curve = 5

16.500Pump_Pressure.AcqOff
UV_VIS_1.AcqOff
Flow = 30 [µl/min]
%B = 0.0 [%]
%C = 0.0 [%]
Curve = 5
End

9.8 The PLIMSTEX Modelling Procedure

Derivation of the PLIMSTEX fitting equation[8]. In the case of a 1:1 protein ligand binding equilibrium

$$P + L \rightleftharpoons PL \tag{47}$$

is P the protein, L the ligand and PL the protein-ligand complex. The equilibrium constant can be written as

$$K = \frac{[PL]c^{\theta}}{[P][L]} \tag{48}$$

where $c^{\theta} = 1$ M. [P], [L] and [PL] are subject to the two conditions

$$[P] + [PL] = [P]_0 \tag{49}$$

$$[L] + [PL] = [L]_0 \tag{50}$$

where $[P]_0$ and $[L]_0$ are the total amounts of protein and ligand, respectively. Therefore one could get

$$K = \frac{[PL]c^{\theta}}{([P]_0 - [PL])([L]_0 - [PL])}. \tag{51}$$

Now define $\Lambda = K[P]_0/c^{\theta}$, $x = [L]_0/[P]_0$ and $f = [PL]/[P]_0$, in terms of which equation (51) becomes

$$\Lambda = \frac{f}{(1-f)(x-f)}. \tag{52}$$

Where f is the fraction of protein that is complexed with the ligand, and it can be found by solving equation (52) to yield

$$f(x) = \frac{[1 + \Lambda(1+x)] - \sqrt{1 + 2\Lambda(1+x) + \Lambda^2(1-x)^2}}{2\Lambda}. \tag{53}$$

The measured experimental data is a linear combination of 'free' and 'complex' signals, and is given by

$$\Delta m(x) = \Delta m_{free}[1 - f(x)] + \Delta m_{complex} f(x). \tag{54}$$

Equations 53 and 54 define an analytical expression which was fitted to the experimental PLIMSTEX data to obtain values of Δm_{free}, $\Delta m_{complex}$ and $K = \Lambda c/[P]_0$ (Fig. 1.14, chapter 1.5). For further 1:1 protein ligand systems equation (54) was used for data analysis (2.6.5).

[8] by Dr. Phillip Camp, University of Edinburgh

9.9 Human Insulin Sequence

```
          10                                                  50
GIVEQCCTSI SSLYQLENYC NFVNQHLCGD HLVEALYLVC GERGFFYTPL

T
```

9.10 SUPREX LC Method Apo Sample List

90 min	120 min	150 min	180 min	420 min
0:00:00 1 B+PL	0:00:00 1 B+PL	0:00:00 1 B+PL	0:00:00 1 B+PL	0:00:00 1 B+PL
0:23:08	0:24:08	0:25:08	0:22:08	0:10:08
0:26:00 2 B+PL	0:27:00 2 B+PL	0:28:00 2 B+PL	0:25:00 2 B+PL	0:13:00 2 B+PL
0:23:08	0:24:08	0:25:08	0:22:08	0:10:08
0:52:00 3 B+PL	0:54:00 3 B+PL	0:56:00 3 B+PL	0:50:00 3 B+PL	0:26:00 3 B+PL
0:23:08	0:24:08	0:25:08	0:22:08	0:10:08
1:18:00 4 B+PL	1:21:00 4 B+PL	1:24:00 4 B+PL	1:15:00 4 B+PL	0:39:00 4 B+PL
0:09:08	0:24:08	0:25:08	0:22:08	0:10:08
1:30:00 1 run	1:48:00 5 B+PL	1:52:00 5 B+PL	1:40:00 5 B+PL	0:52:00 5 B+PL
1:43:00	0:09:08	0:25:08	0:22:08	0:10:08
0:01:00	2:00:00 1 run	2:20:00 6 B+PL	2:05:00 6 B+PL	1:05:00 6 B+PL
1:44:00 5 B+PL	2:13:00	0:07:08	0:22:08	0:10:08
0:09:08	0:02:00	2:30:00 1 run	2:30:00 7 B+PL	1:18:00 7 B+PL
1:56:00 2 run	2:15:00 6 B+PL	2:43:00	0:22:08	0:10:08
2:09:00	0:09:08	0:05:00	2:55:00 8 B+PL	1:31:00 8 B+PL
0:01:00	2:27:00 2 run	2:48:00 7 B+PL	0:02:08	0:10:08
2:10:00 6 B+PL	2:40:00	0:07:08	3:00:00 1 run	1:44:00 9 B+PL
0:09:08	0:02:00	2:58:00 2 run	3:13:00	0:10:08
2:22:00 3 run	2:42:00 7 B+PL	3:11:00	0:07:00	1:57:00 10 B+PL
2:35:00	0:09:08	0:05:00	3:20:00 9 B+PL	0:10:08
0:01:00	2:54:00 3 run	3:16:00 8 B+PL	0:02:08	2:10:00 11 B+PL
2:36:00 7 B+PL	3:07:00	0:07:08	3:25:00 2 run	0:10:08
0:09:08	0:02:00	3:26:00 3 run	3:38:00	2:23:00 12 B+PL
2:48:00 4 run	3:09:00 8 B+PL	3:39:00	0:07:00	0:10:08
3:01:00	0:09:08	0:05:00	3:45:00 10 B+PL	2:36:00 13 B+PL
0:01:00	3:21:00 4 run	3:44:00 9 B+PL	0:02:08	0:10:08
3:02:00 8 B+PL	3:34:00	0:07:08	3:50:00 3 run	2:49:00 14 B+PL
0:09:08	0:02:00	3:54:00 4 run	4:03:00	0:10:08
3:14:00 5 run	3:36:00 9 B+PL	4:07:00	0:12:00	3:02:00 15 B+PL
3:27:00	0:09:08	0:05:00	4:15:00 4 run	0:10:08
0:01:00	3:48:00 5 run	4:12:00 10 B+PL	4:28:00	3:15:00 16 B+PL
3:28:00 9 B+PL	4:01:00	0:07:08	0:12:00	0:10:08
0:09:08	0:02:00	4:22:00 5 run	4:40:00 5 run	3:28:00 17 B+PL
3:40:00 6 run	4:03:00 10 B+PL	4:35:00	4:53:00	0:10:08
3:53:00	0:09:08	0:15:00	0:12:00	3:41:00 18 B+PL
0:01:00	4:15:00 6 run	4:50:00 6 run	5:05:00 6 run	3:16:08
3:54:00 10 B+PL	4:28:00	5:03:00	5:18:00	7:00:00 1 run
0:09:08	0:14:00	0:15:00	0:12:00	7:13:00
4:06:00 7 run	4:42:00 7 run	5:18:00 7 run	5:30:00 7 run	7:13:00 2 run
4:19:00	4:55:00	5:31:00	5:43:00	7:26:00
0:13:00	0:14:00	0:15:00	0:12:00	7:26:00 3 run
4:32:00 8 run	5:09:00 8 run	5:46:00 8 run	5:55:00 8 run	7:39:00
4:45:00	5:22:00	5:59:00	6:08:00	7:39:00 4 run
0:13:00	0:14:00	0:15:00	0:12:00	7:52:00
4:58:00 9 run	5:36:00 9 run	6:14:00 9 run	6:20:00 9 run	7:52:00 5 run
5:11:00	5:49:00	6:27:00	6:33:00	8:05:00
0:13:00	0:14:00	0:15:00	0:12:00	8:05:00 6 run
5:24:00 10 run	6:03:00 10 run	6:42:00 10 run	6:45:00 10 run	8:18:00
5:37:00	6:16:00	6:55:00	6:58:00	8:18:00 7 run
				8:31:00
				8:31:00 8 run
				8:44:00
				8:44:00 9 run
				8:57:00
				8:57:00 10 run
				9:10:00
				9:10:00 11 run
				9:23:00
				9:23:00 12 run
				9:36:00
				9:36:00 13 run
				9:49:00
				9:49:00 14 run
				10:02:00
				10:02:00 15 run
				10:15:00
				10:15:00 16 run
				10:28:00
				10:28:00 17 run
				10:41:00
				10:41:00 18 run
				10:54:00

	0:22:08
	0:02:08
	0:07:00
	0:12:00
	0:24:08
	0:09:08
	0:02:00
	0:14:00
	0:23:08
	0:25:08
	0:01:00
	0:13:00
	0:07:08
	0:05:00
	0:15:00
	0:10:08
	3:16:08

9.11 SUPREX LC Method Holo Sample List (Even)

60 min	120 min	180 min	240 min
0:00:00 1 P+L	0:00:00 1 P+L	0:00:00 1 P+L	0:00:00 1 P+L
0:17:04	0:17:04	0:17:04	0:17:04
0:20:00 1 B+PL	0:20:00 1 B+PL	0:20:00 1 B+PL	0:20:00 1 B+PL
0:37:08	0:37:08	0:37:08	0:37:08
1:00:00 2 P+L	1:00:00 2 P+L	1:00:00 2 P+L	1:00:00 2 P+L
0:14:12	0:14:12	0:14:12	0:14:12
1:20:00 2 B+PL	1:20:00 2 B+PL	1:20:00 2 B+PL	1:20:00 2 B+PL
1:20:00 1 run	0:37:08	0:37:08	0:37:08
1:33:00	2:00:00 3 P+L	2:00:00 3 P+L	2:00:00 3 P+L
0:27:00	0:14:12	0:14:12	0:14:12
2:00:00 3 P+L	2:20:00 3 B+PL	2:20:00 3 B+PL	2:20:00 3 B+PL
0:14:12	2:20:00 1 run	0:37:08	0:37:08
2:20:00 3 B+PL	2:33:00	3:00:00 4 P+L	3:00:00 4 P+L
2:20:00 2 run	0:27:00	0:14:12	0:14:12
2:33:00	3:00:00 4 P+L	3:20:00 4 B+PL	3:20:00 4 B+PL
0:27:00	0:14:12	3:20:00 1 run	0:37:08
3:00:00 4 P+L	3:20:00 4 B+PL	3:33:00	4:00:00 5 P+L
0:14:12	3:20:00 2 run	0:27:00	0:14:12
3:20:00 4 B+PL	3:33:00	4:00:00 5 P+L	4:20:00 5 B+PL
3:20:00 3 run	0:27:00	0:14:12	4:20:00 1 run
3:33:00	4:00:00 5 P+L	4:20:00 5 B+PL	4:33:00
0:27:00	0:14:12	4:20:00 2 run	0:27:00
4:00:00 5 P+L	4:20:00 5 B+PL	4:33:00	5:00:00 6 P+L
0:14:12	4:20:00 3 run	0:27:00	0:14:12
4:20:00 5 B+PL	4:33:00	5:00:00 6 P+L	5:20:00 6 B+PL
4:20:00 4 run	0:27:00	0:14:12	5:20:00 2 run
4:33:00	5:00:00 6 P+L	5:20:00 6 B+PL	5:33:00
0:27:00	0:14:12	5:20:00 3 run	0:27:00
5:00:00 6 P+L	5:20:00 6 B+PL	5:33:00	6:00:00 7 P+L
0:14:12	5:20:00 4 run	0:27:00	0:14:12
5:20:00 6 B+PL	5:33:00	6:00:00 7 P+L	6:20:00 7 B+PL
5:20:00 5 run	0:27:00	0:14:12	6:20:00 3 run
5:33:00	6:00:00 7 P+L	6:20:00 7 B+PL	6:33:00
0:27:00	0:14:12	6:20:00 4 run	0:27:00
6:00:00 7 P+L	6:20:00 7 B+PL	6:33:00	7:00:00 8 P+L
0:14:12	6:20:00 5 run	0:27:00	0:14:12
6:20:00 7 B+PL	6:33:00	7:00:00 8 P+L	7:20:00 8 B+PL
6:20:00 6 run	0:27:00	0:14:12	7:20:00 4 run
6:33:00	7:00:00 8 P+L	7:20:00 8 B+PL	7:33:00
0:27:00	0:14:12	7:20:00 5 run	0:27:00
7:00:00 8 P+L	7:20:00 8 B+PL	7:33:00	8:00:00 9 P+L
0:14:12	7:20:00 6 run	0:27:00	0:14:12
7:20:00 8 B+PL	7:33:00	8:00:00 9 P+L	8:20:00 9 B+PL
7:20:00 7 run	0:27:00	0:14:12	8:20:00 5 run
7:33:00	8:00:00 9 P+L	8:20:00 9 B+PL	8:33:00
0:27:00	0:14:12	8:20:00 6 run	0:27:00
8:00:00 9 P+L	8:20:00 9 B+PL	8:33:00	9:00:00 10 P+L
0:14:12	8:20:00 7 run	0:27:00	0:14:12
8:20:00 9 B+PL	8:33:00	9:00:00 10 P+L	9:20:00 10 B+PL
8:20:00 8 run	0:27:00	0:14:12	9:20:00 6 run
8:33:00	9:00:00 10 P+L	9:20:00 10 B+PL	9:33:00
0:27:00	0:14:12	9:20:00 7 run	0:47:00
9:00:00 10 P+L	9:20:00 10 B+PL	9:33:00	10:20:00 7 run
0:14:12	9:20:00 8 run	0:47:00	10:33:00
9:20:00 10 B+PL	9:33:00	10:20:00 8 run	0:47:00
9:20:00 9 run	0:47:00	10:33:00	11:20:00 8 run
9:33:00	10:20:00 9 run	0:47:00	11:33:00
0:47:00	10:33:00	11:20:00 9 run	0:47:00
10:20:00 10 run	0:47:00	11:33:00	12:20:00 9 run
10:33:00	11:20:00 10 run	0:47:00	12:33:00
	11:33:00	12:20:00 10 run	0:47:00
		12:33:00	13:20:00 9 run
			13:33:00

0:17:04
0:37:08
0:14:12
0:27:00
0:47:00
0:37:08
0:27:00

9.12 SUPREX LC Method Holo Sample List (Odd)

90 min	150 min	210 min
0:00:00 1 P+L	0:00:00 1 P+L	0:00:00 1 P+L
0:17:04	0:17:04	0:17:04
0:20:00 1 B+PL	0:20:00 1 B+PL	0:20:00 1 B+PL
0:39:08	0:39:08	0:39:08
1:02:00 2 P+L	1:02:00 2 P+L	1:02:00 2 P+L
0:17:04	0:17:04	0:17:04
1:22:00 2 B+PL	1:22:00 2 B+PL	1:22:00 2 B+PL
0:25:08	0:39:08	0:39:08
1:50:00 1 run	2:04:00 3 P+L	2:04:00 3 P+L
2:03:00	0:17:04	0:17:04
0:01:00	2:24:00 3 B+PL	2:24:00 3 B+PL
2:04:00 3 P+L	0:23:08	0:39:08
0:17:04	2:50:00 1 run	3:06:00 4 P+L
2:24:00 3 B+PL	3:03:00	0:17:04
0:25:08	0:03:00	3:26:00 4 B+PL
2:52:00 2 run	3:06:00 4 P+L	0:21:08
3:05:00	0:17:04	3:50:00 1 run
0:01:00	3:26:00 4 B+PL	4:03:00
3:06:00 4 P+L	0:23:08	0:05:00
0:17:04	3:52:00 2 run	4:08:00 5 P+L
3:26:00 4 B+PL	4:05:00	0:17:04
0:25:08	0:03:00	4:28:00 5 B+PL
3:54:00 3 run	4:08:00 5 P+L	0:21:08
4:07:00	0:17:04	4:52:00 2 run
0:01:00	4:28:00 5 B+PL	5:05:00
4:08:00 5 P+L	0:23:08	0:05:00
0:17:04	4:54:00 3 run	5:10:00 6 P+L
4:28:00 5 B+PL	5:07:00	0:17:04
0:25:08	0:03:00	5:30:00 6 B+PL
4:56:00 4 run	5:10:00 6 P+L	0:21:08
5:09:00	0:17:04	5:54:00 3 run
0:01:00	5:30:00 6 B+PL	6:07:00
5:10:00 6 P+L	0:23:08	0:05:00
0:17:04	5:56:00 4 run	6:12:00 7 P+L
5:30:00 6 B+PL	6:09:00	0:17:04
0:25:08	0:03:00	6:32:00 7 B+PL
5:58:00 5 run	6:12:00 7 P+L	0:21:08
6:11:00	0:17:04	6:56:00 4 run
0:01:00	6:32:00 7 B+PL	7:09:00
6:12:00 7 P+L	0:23:08	0:05:00
0:17:04	6:58:00 5 run	7:14:00 8 P+L
6:32:00 7 B+PL	7:11:00	0:17:04
0:25:08	0:03:00	7:34:00 8 B+PL
7:00:00 6 run	7:14:00 8 P+L	0:21:08
7:13:00	0:17:04	7:58:00 5 run
0:01:00	7:34:00 8 B+PL	8:11:00
7:14:00 8 P+L	0:23:08	0:05:00
0:17:08	8:00:00 6 run	8:16:00 9 P+L
7:34:00 8 B+PL	8:13:00	0:17:04
0:25:08	0:03:00	8:36:00 9 B+PL
8:02:00 7 run	8:16:00 9 P+L	0:21:08
8:15:00	0:17:04	9:00:00 6 run
0:01:00	8:36:00 9 B+PL	9:13:00
8:16:00 9 P+L	0:23:08	0:05:00
0:17:04	9:02:00 7 run	9:18:00 10 P+L
8:36:00 9 B+PL	9:15:00	0:17:04
0:25:08	0:03:00	9:38:00 10 B+PL
9:04:00 8 run	9:18:00 10 P+L	0:21:08
9:17:00	0:17:04	10:02:00 7 run
0:01:00	9:38:00 10 B+PL	10:15:00
9:18:00 10 P+L	0:23:08	0:49:00
0:17:04	10:04:00 8 run	11:04:00 8 run
9:38:00 10 B+PL	10:17:00	11:17:00
0:25:08	0:49:00	0:49:00
10:06:00 9 run	11:06:00 9 run	12:06:00 9 run
10:19:00	11:19:00	12:19:00
0:49:00	0:49:00	0:49:00
11:08:00 10 run	12:08:00 10 run	13:08:00 10 run
11:21:00	12:21:00	13:21:00

	0:17:04
	0:39:08
	0:25:08
	0:01:00
	0:49:00
	0:23:08
	0:03:00
	0:21:08
	0:05:00

9.13 Automated SUPREX CypA Mass Spectrum

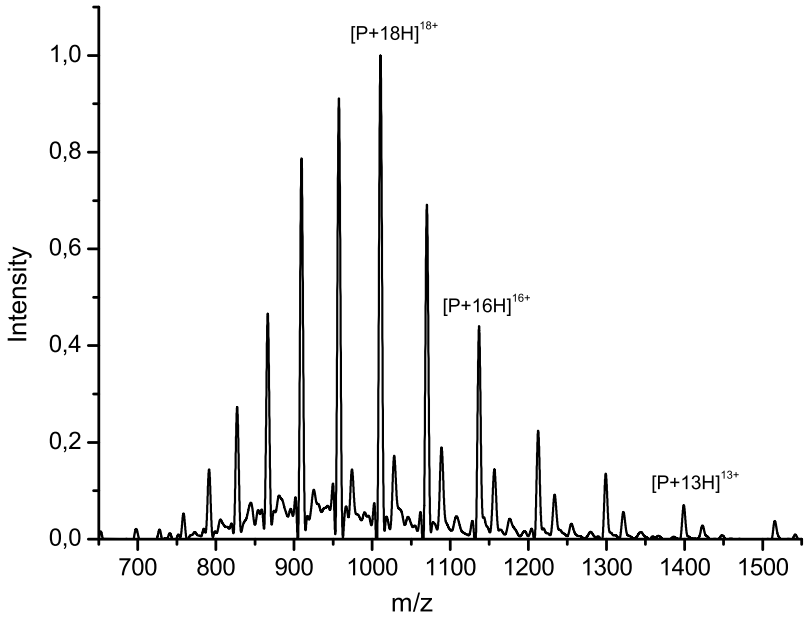

9.14 Derivation of SUPREX Equations

Derivation of the SUPREX equation based on principles of HDX (1.3.2). In case of a folded protein $K_{op} \ll 1$, k_{ex} in equation 15 (1.3.2) can be written as:

$$k_{ex} = \frac{K_{op} k_{int}}{K_{op} + 1} \tag{55}$$

For amide protons exhibiting exchange *via* a global unfolding mechanism, $1/K_{op}$ or K_{cl} (the equilibrium constant for the closing reaction) is equal to K_f, the equilibrium constant for the global folding reaction of the protein. Substitution of $1/K_{op} = 1/K_f$ in equation 55 results in:

$$k_{ex} = \frac{k_{int}}{K_f + 1} \tag{56}$$

Solving eq 56 for K_f yields:

$$K_f = \frac{k_{int}}{k_{ex}} - 1 \tag{57}$$

Which is an expression of the equilibrium rate constant for a protein's folding reaction in terms of k_{int} and k_{ex}

$$k_{ex} = \frac{0.693}{t} \tag{58}$$

At the inflection point of a SUPREX curve the HDX has progressed to one half-life. Equation 58 describes the relation between HDX time, t, and k_{ex}. Substitution of eq 58 in 57 yields:

$$K_f = \frac{\langle k_{int}\rangle t}{0.693} - 1 \tag{59}$$

Assuming all k_{int} values for global exchanging hydrogen atoms can be approximated by $\langle k_{int}\rangle t$. The most common method to analyse traditional solvent-induced denaturation curves is the linear extrapolation method (LEM, [2], [299]) based on equation 60:

$$-RT\ln K_f = m[\text{Denaturant}] + \Delta G_f \tag{60}$$

With R, gas constant, T is the temperature in Kelvin, K_f the apparent equilibrium folding constant, m is $\delta\Delta G_f/\delta$[Denaturant] with [Denaturant] the molar concentration of the denaturant and ΔG_f the free energy of protein folding in the absence of the denaturant. At this point it is worth pointing out that equation 60 is only valid for a two-state unfolding process. Substitution of [Denaturant] in eq 60 with $C^{1/2}_{SUPREX}$ the midpoint denaturing concentration of a SUPREX curve. Again SUPREX $C^{1/2}_{SUPREX}$ are not equal to classical midpoints of denaturing curves $C^{1/2}_{den}$ (1.6.1).

$$-RT\ln\left(\frac{\langle k_{int}\rangle t}{0.693} - 1\right) = mC^{1/2}_{SUPREX} + \Delta G_f \tag{61}$$

Equation 61 describes SUPREX behaviour of monomeric proteins, whereas eq 62 is valid for multimeric proteins.

$$-RT\left[\ln\frac{\left(\frac{\langle k_{int}\rangle t}{0.693} - 1\right)}{\left(\frac{n^n}{2n^{n-1}} - [P]^{n-1}\right)}\right] = mC^{1/2}_{SUPREX} + \Delta G_f \tag{62}$$

Dissociation constants (K_d's) were determined using equation 63 according to [235].

$$K_d = \left(\frac{[L]}{e^{-\frac{\Delta\Delta G_f}{nRT}} - 1}\right) \tag{63}$$

Hereby [L] is the molar concentration of the ligand, n the number of independent binding sites and $\Delta\Delta G_f$ the change in folding free energy upon ligand binding.

9.15 HHM Sequence

10 **50**
MGLSDGEWQQ VLNVWGKVEA DIAGHGQEVL IRLFTGHPET LEKFDKFKHL

60 **100**
KTEAEMKASE DLKKHGTVVL TALGGILKKK GHHEAELKPL AQSHATKHKI

110 **150**
PIKYLEFISD AIIHVLHSKH PGDFGADAQG AMTKALELFR NDIAAKYKEL

GFQG

9.16 Automated Myoglobin SUPREX Curves

10 min

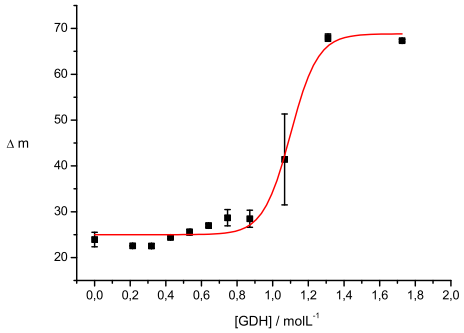

15 min

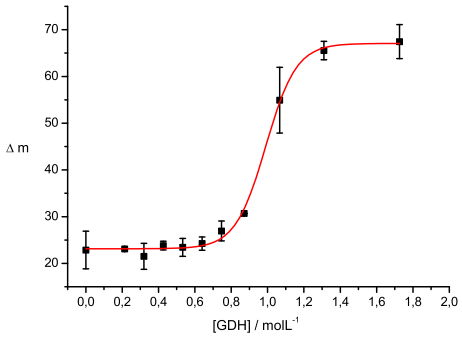

20 min

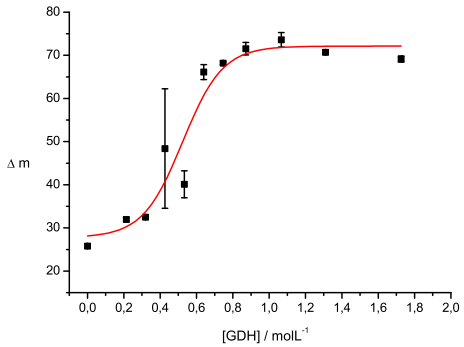

25 min

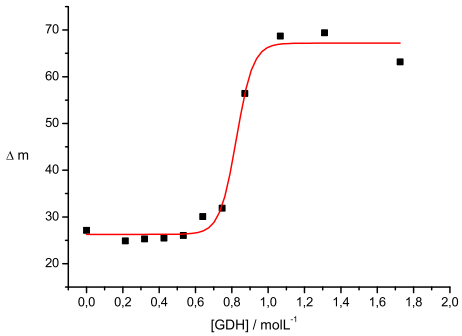

40 min

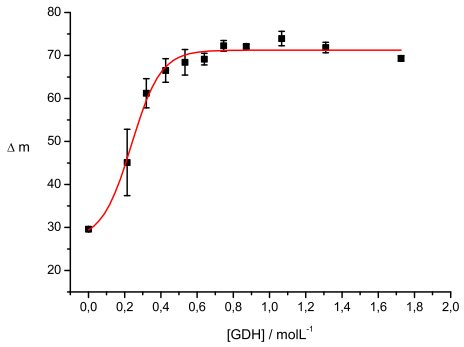

60 min

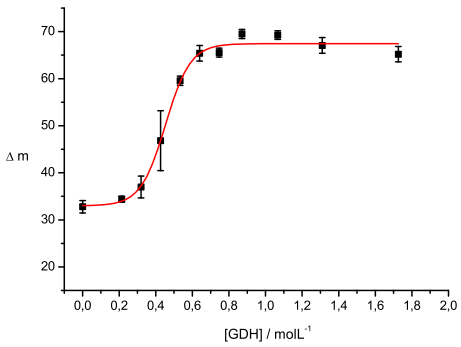

90 min

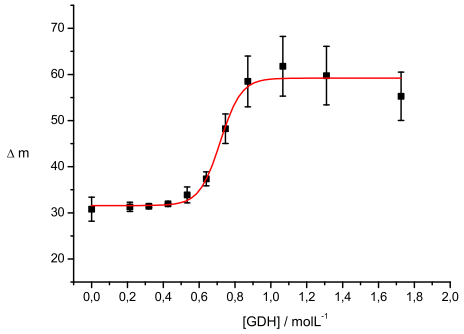

120 min

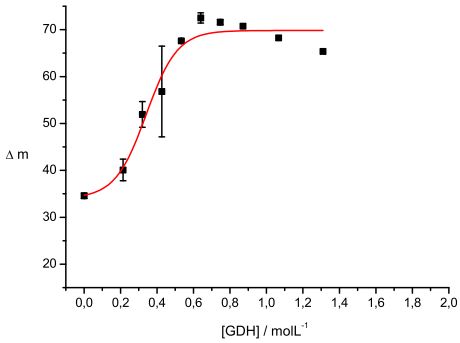

180 min

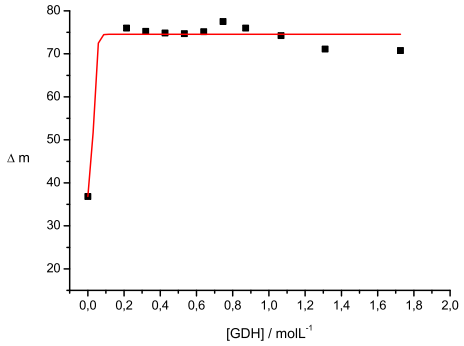

10 Appendix 3

10.1 Cyclophilin A Sequence

Additional N-terminal methionine illustrated in red.

```
          10                                                  50
MMVNPTVFFD IADVGEPLGR VSFELFADKV PKTAENFRAL STGEKGFGYK
          60                                                  100
GSCFHRIIPG FMCQGGDFTR HNGTGGKSIY GEKFEDENFI LKHTGPGILS
          110                                                 150
MANAGPNTNG SQFFICTAKT EWLDGKHVVF GKVKEGMNIV EAMERFGSRN
          160
GKTSKKITIA DCGQLE
```

10.2 FKBP12 Sequence

His-Tag-sequence illustrated in red.

```
          10                                                  50
MRGSHHHHHH HGSMMGVEIE TISPGDGRTF PKKGQTCVVH YTGMLQNGKK
          60                                                  100
FDSSRDRNKP FKFRIGKQEV IKGFEEGAAQ MSLGQRAKLT CTPDVAYGAT
          110
GHPGVIPPNA TLIFDVELLN LE
```

10.3 CypA Manual SUPREX Curves

10 min **40 min**

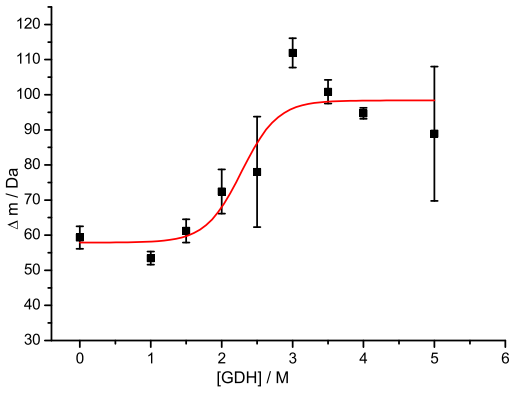

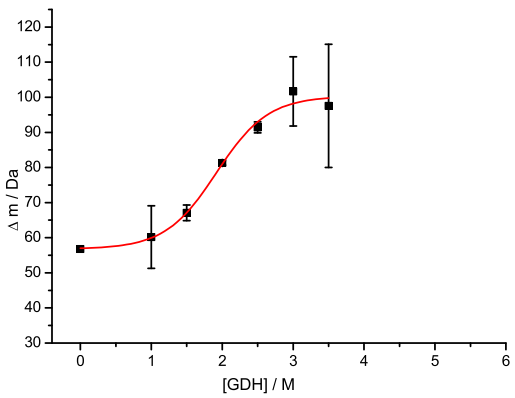

60 min **120 min**

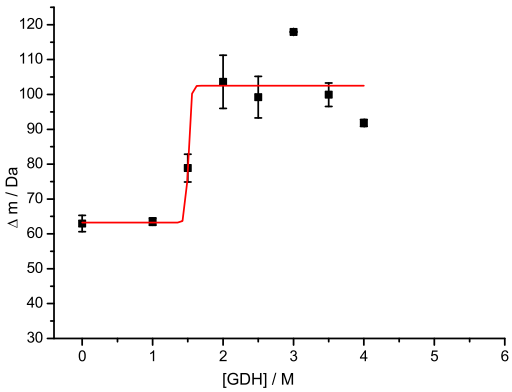

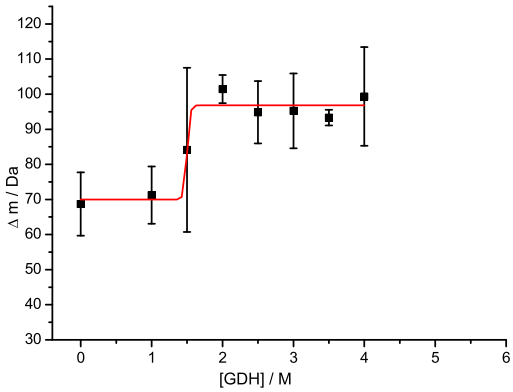

10.4 CypA-CsA Manual SUPREX Curves

10 min **40 min**

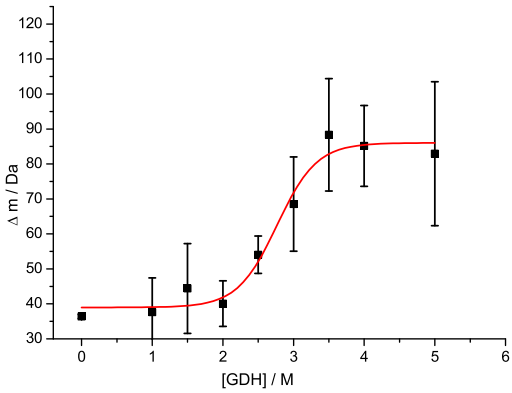

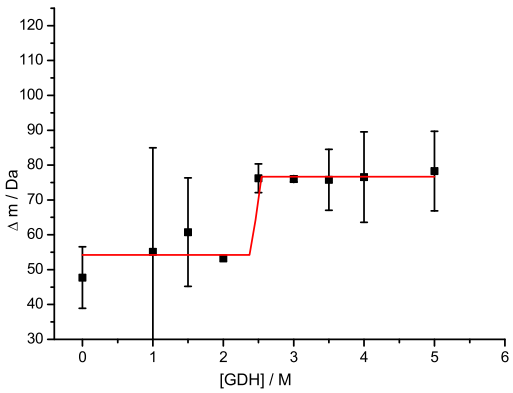

60 min **120 min**

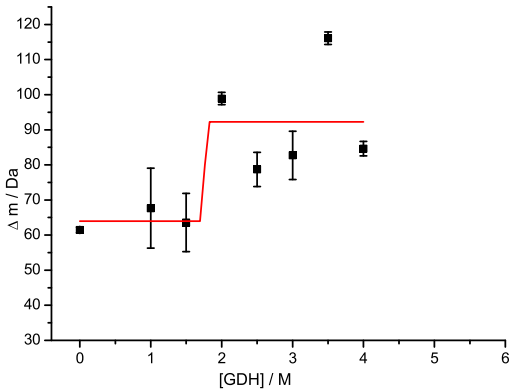

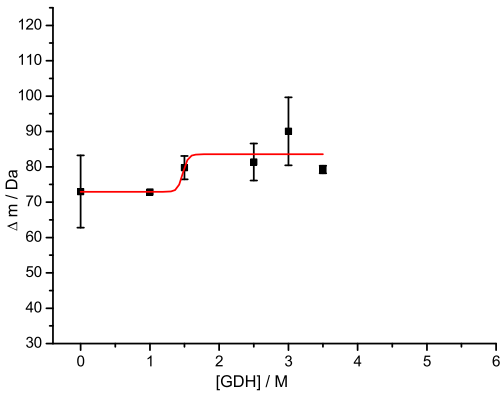

10.5 CypA-ES1234 Manual SUPREX Curves

10 min

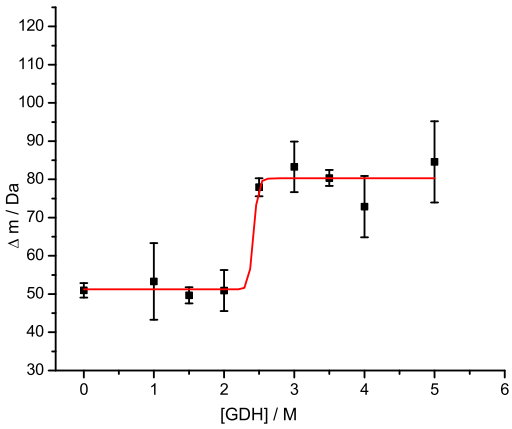

40 min

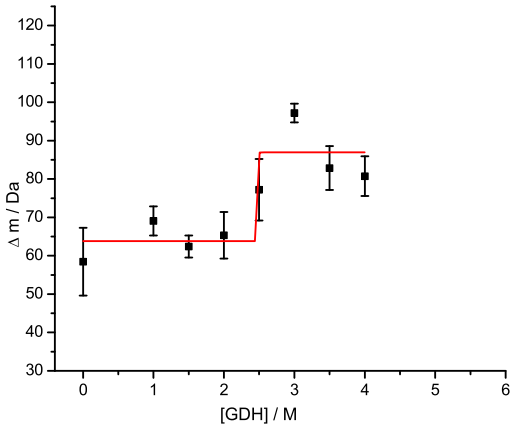

60 min

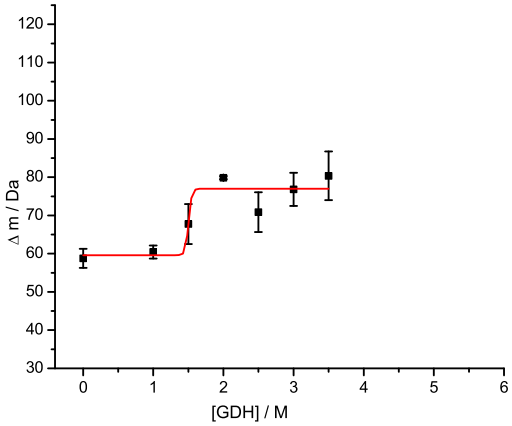

120 min

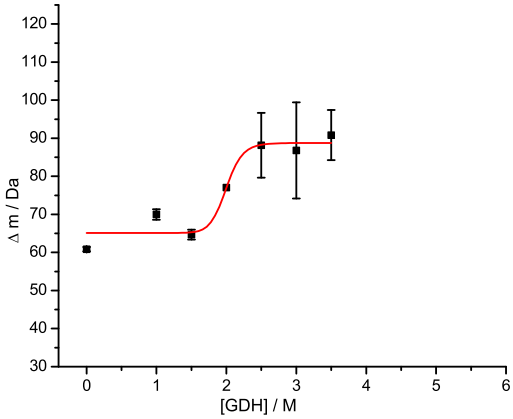

10.6 Apo CypA Automated SUPREX Curves

10 min

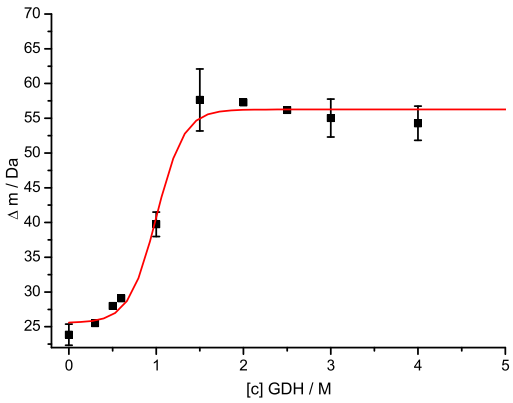

15 min

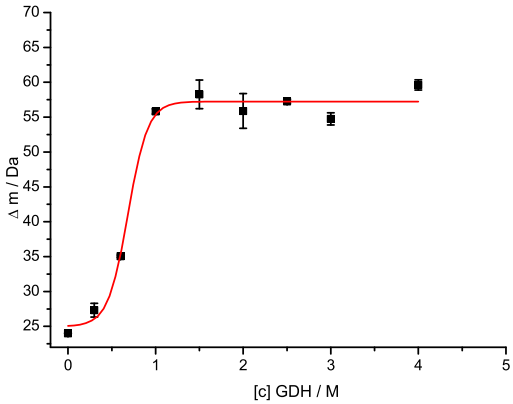

30 min

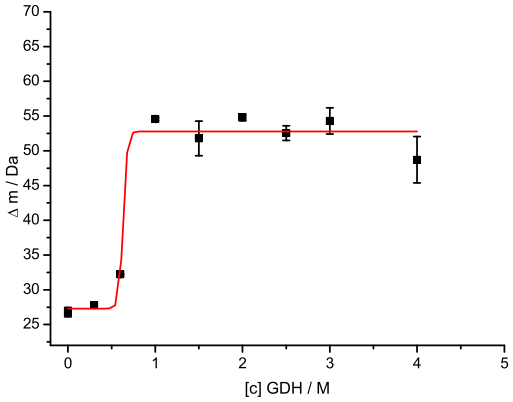

45 min

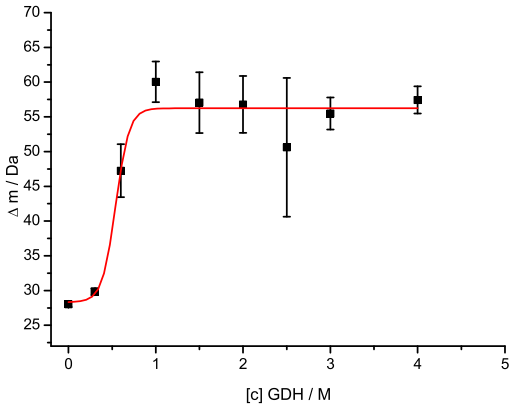

60 min

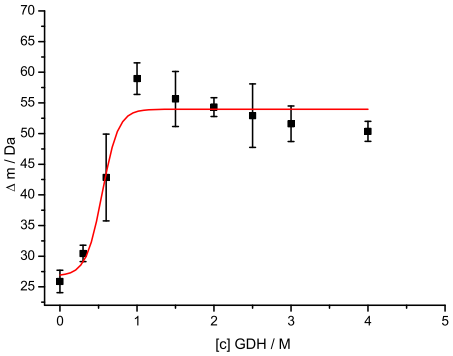

90 min

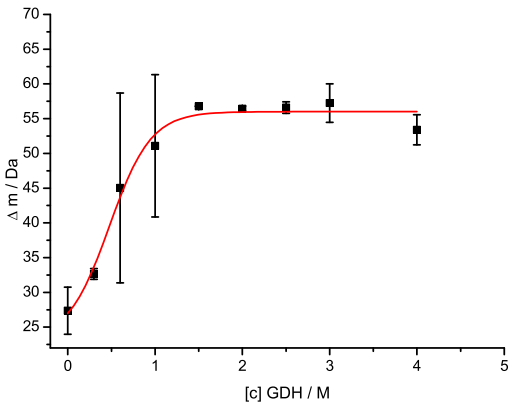

120 min

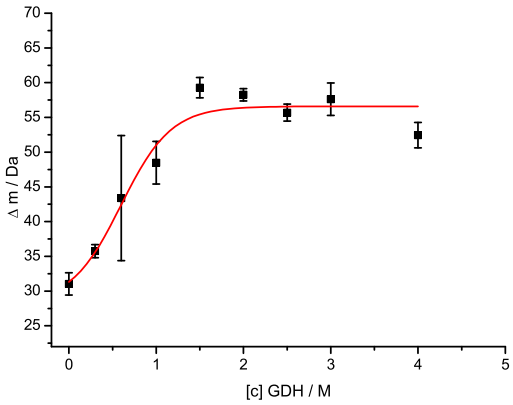

150 min

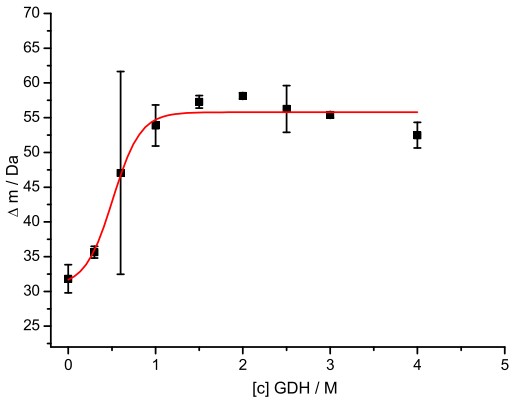

180 min

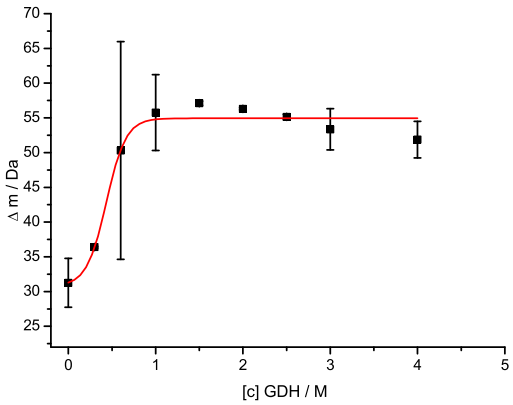

420 min

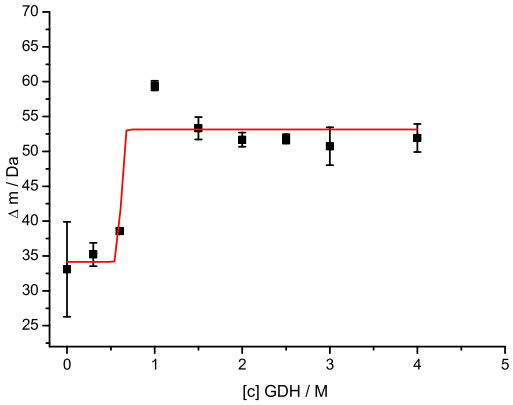

10.7 CypA-36.88 % MeOH Automated SUPREX Curves

10 min

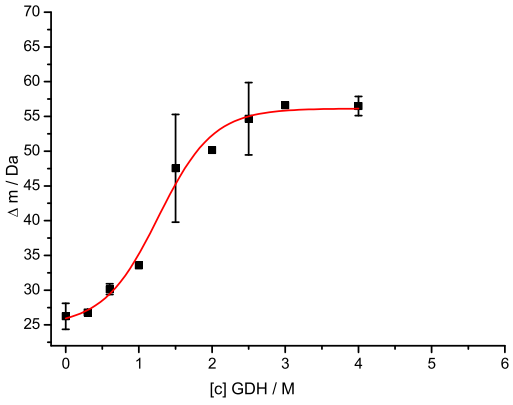

30 min

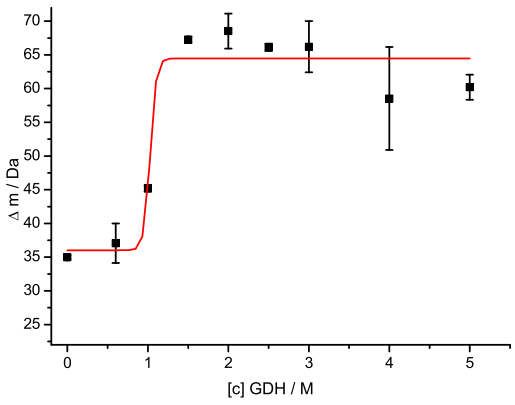

60 min **120 min**

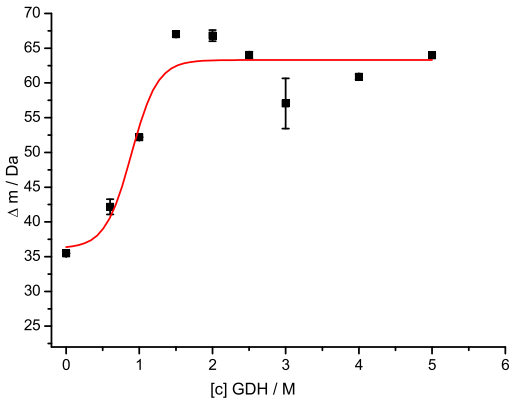

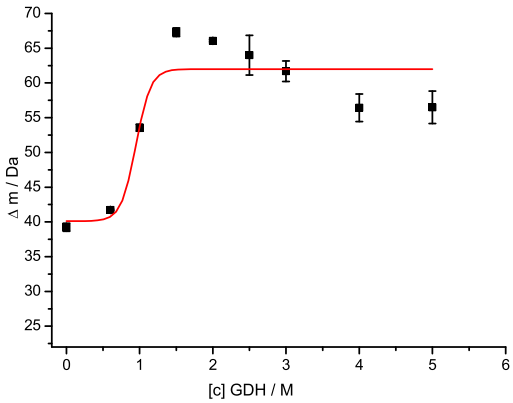

10.8 CypA-CsA Automated SUPREX Curves

10 min **15 min**

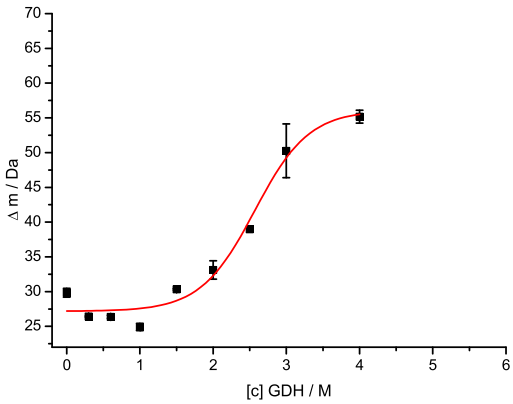

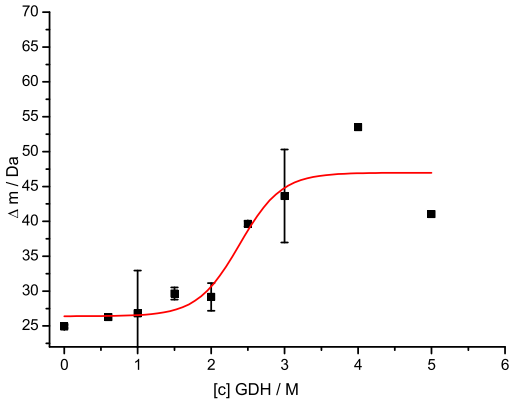

30 min **45 min**

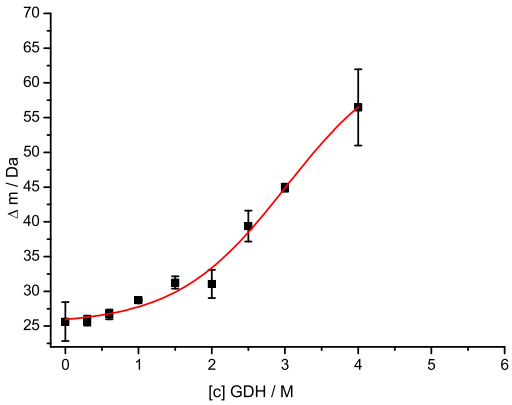

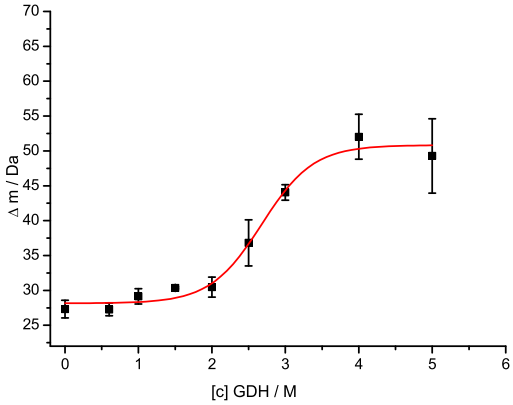

60 min

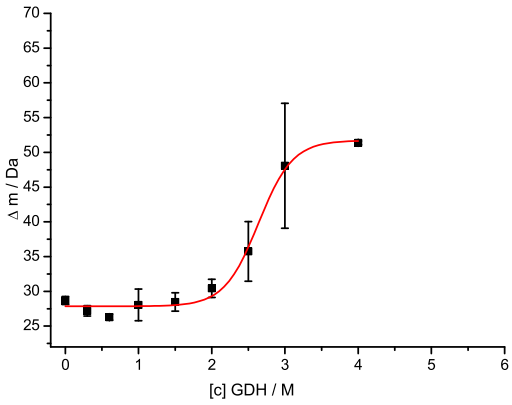

120 min

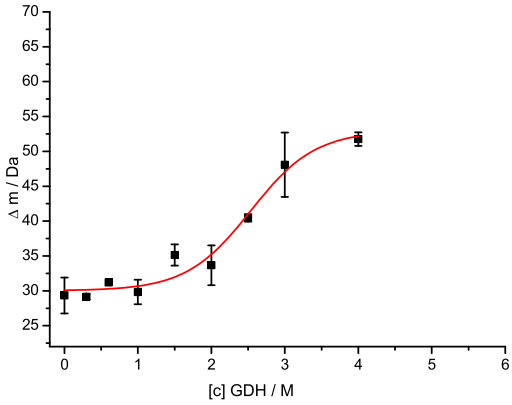

180 min

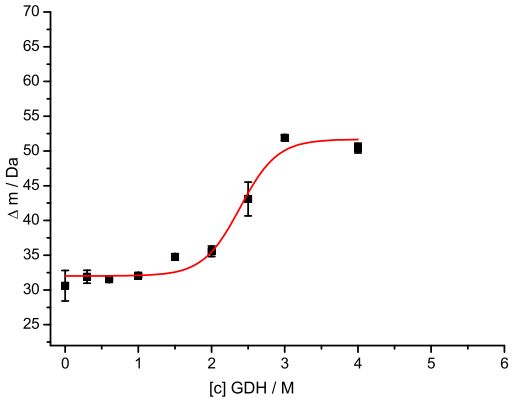

10.9 CypA-KM184 Automated SUPREX Curves

10 min

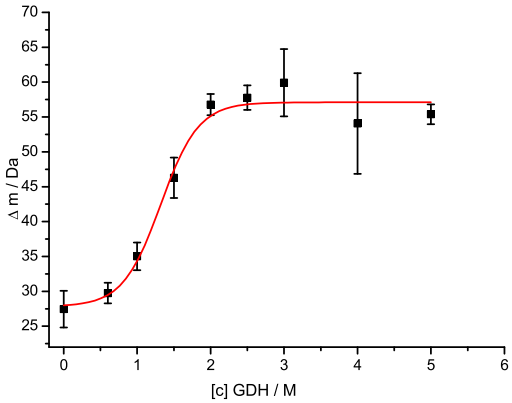

15 min

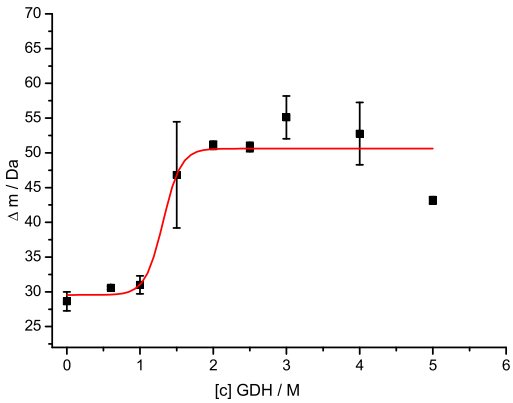

30 min

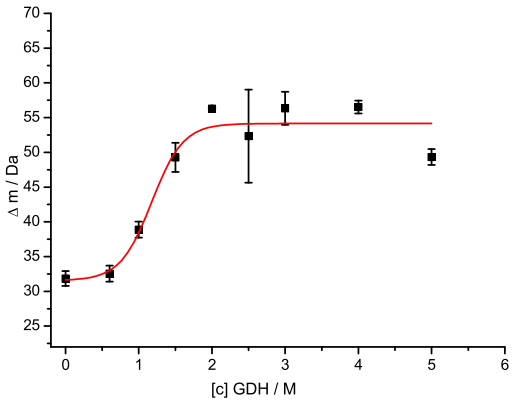

45 min

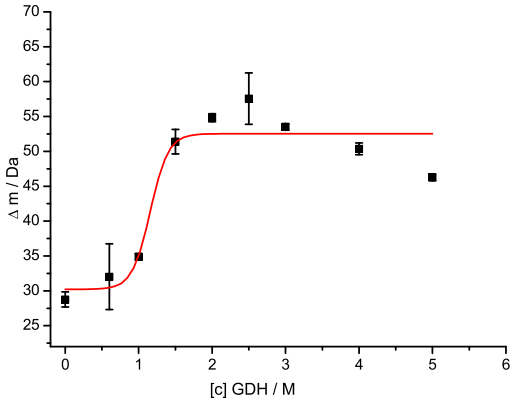

60 min

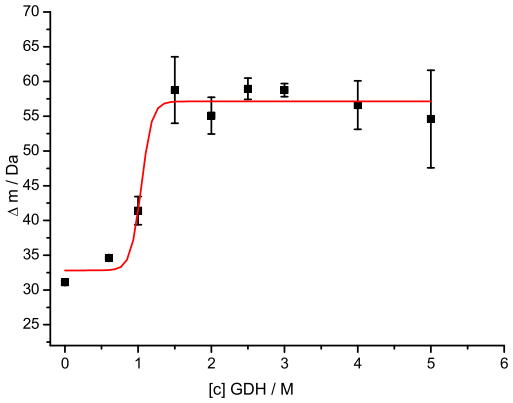

90 min

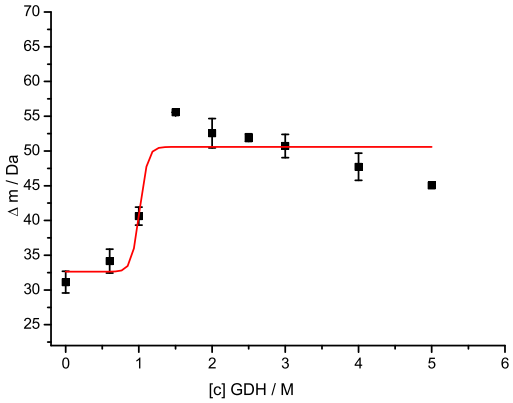

120 min

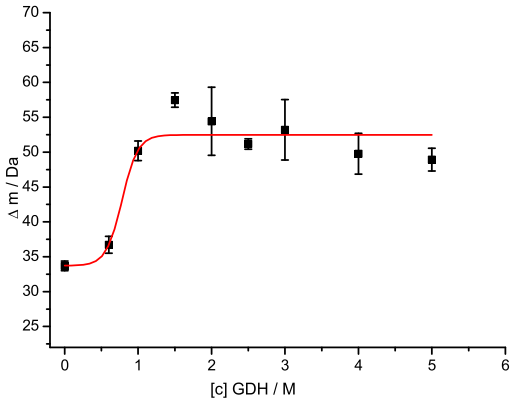

180 min

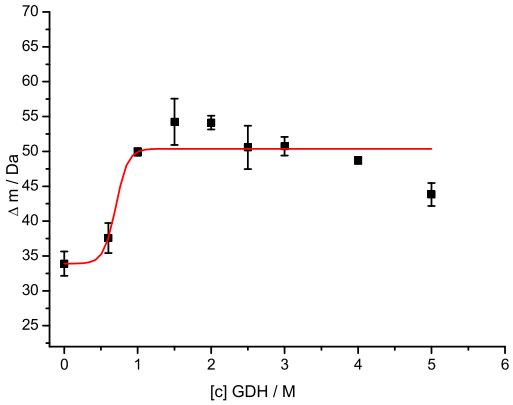

10.10 CypA-ES1234 Automated SUPREX Curves

10 min

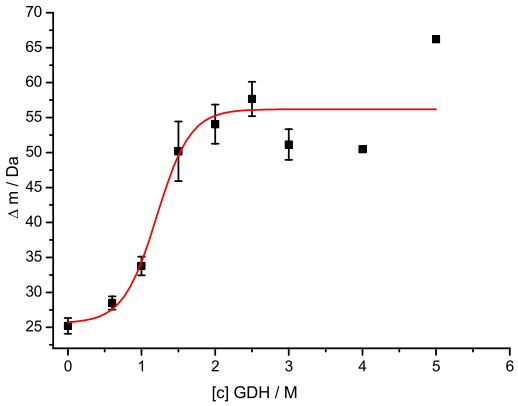

15 min

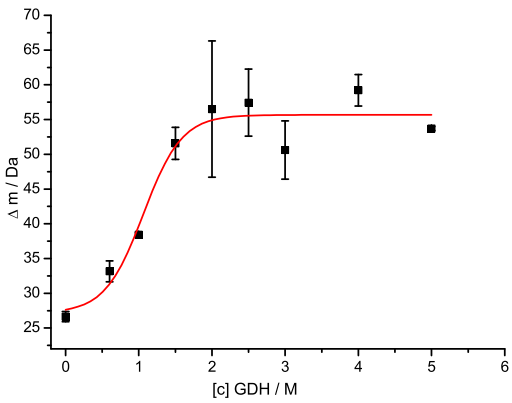

30 min

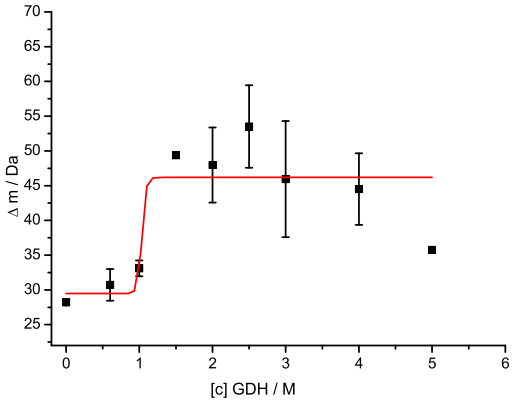

45 min

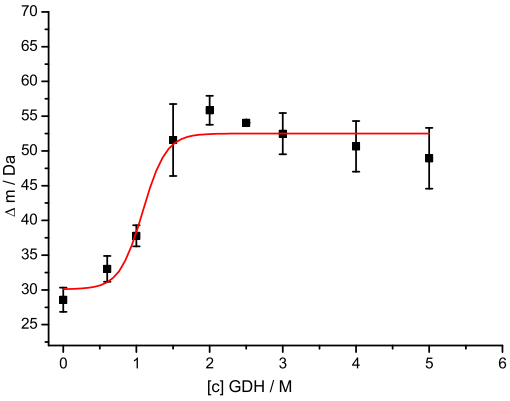

60 min

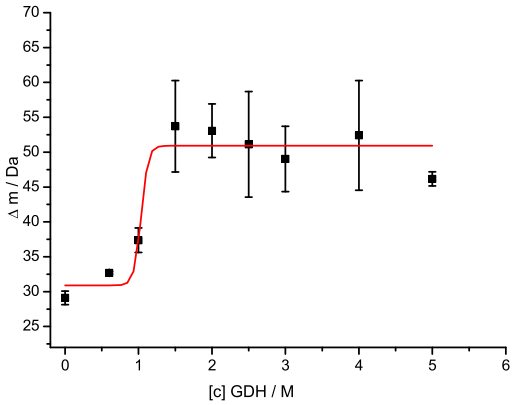

90 min

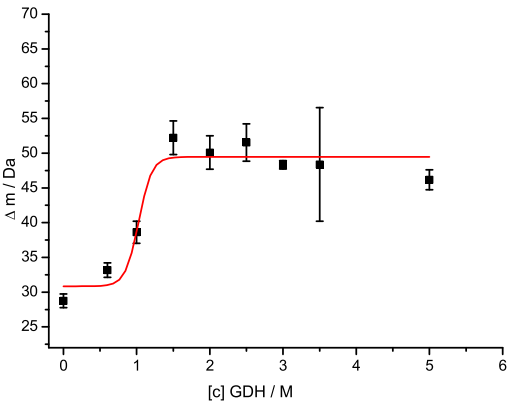

11 Appendix 4

11.1 Anterior Gradient 2 Sequence

His tag is visualised in red.

```
          10                                                  50
MSYYHHHHHH LESTSLYKKA GFEGDRTMRD TTVKPGAKKD TKDSRPKLPQ
          60                                                  100
TLSRGWGDQL IWTQTYEEAL YKSKTSSKPL MIIHHLDECP HSQALKKVFA
          110                                                 150
ENKEIQKLAE QFVLLNLVYE TTDKHLSPDG QYVPRIMFVD PSLTVRADIT
          160
GRYSNRLYAY EPADTALLLD NMKKALKLLK TEL
```

11.2 FH19-20 Sequence

```
          10                                                  50
EAEFGKCGPP PPIDNGDITS FPLSVYAPAS SVEYQCQNLY QLEGNKRITC
          60                                                  100
RNGQWSEPPK CLHPCVISRE IMENYNIALR WTAKQKLYSR TGESVEFVCK
          110
RGYRLSSRSH TLRTTCWDGK LEYPTCAKR
```

11.3 Apo AGr2^{Nicholson} Manual SUPREX Curves

10 min **40 min**

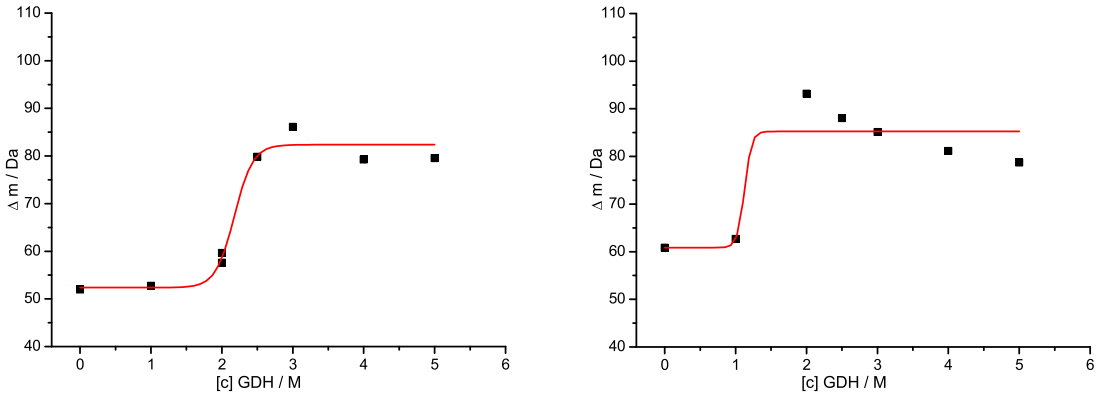

60 min

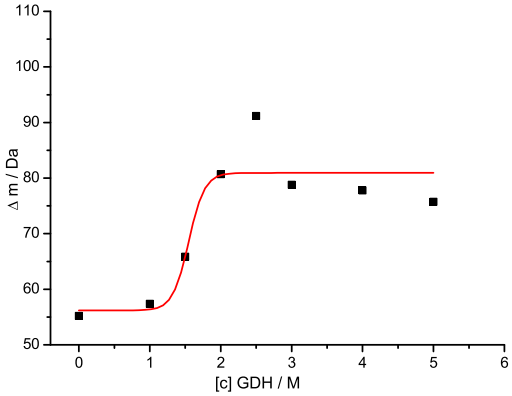

180 min

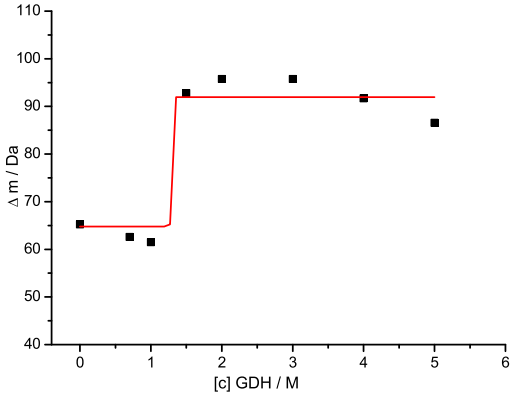

11.4 AGr2^{Nicholson}-PTTIYY-Pen Manual SUPREX Curves

10 min

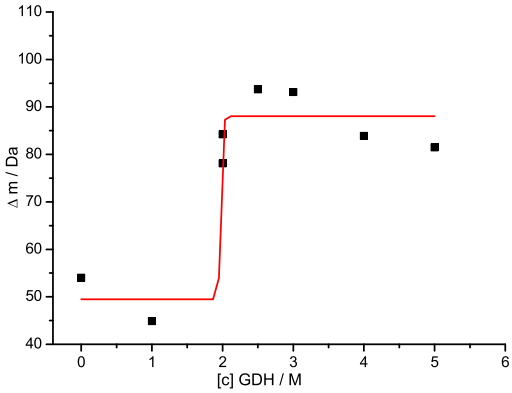

60 min

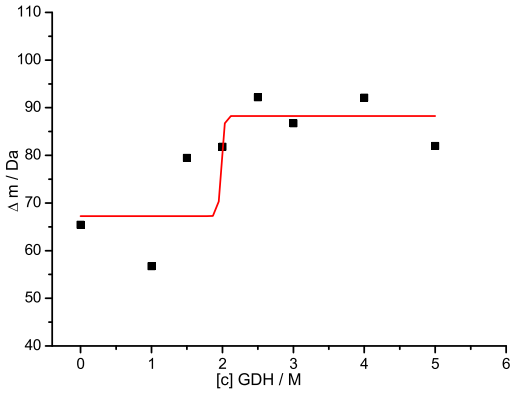

120 min

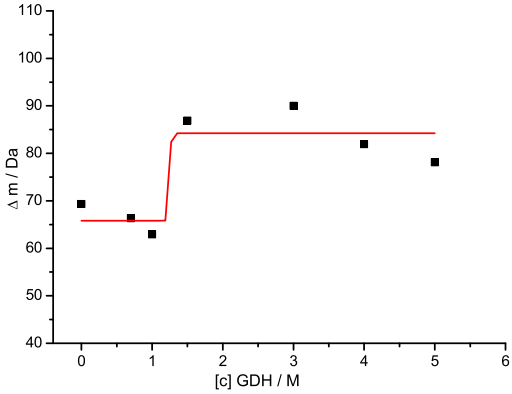

11.5 Apo AGr2^{Florance} Automated SUPREX Curves

10 min

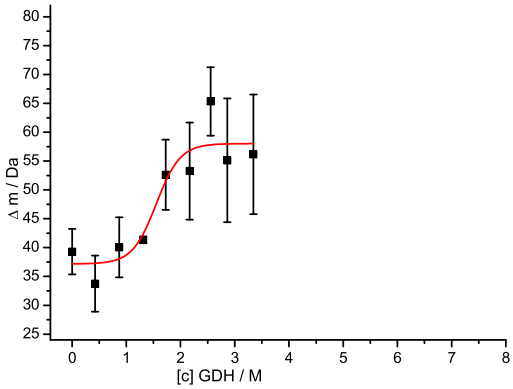

15 min

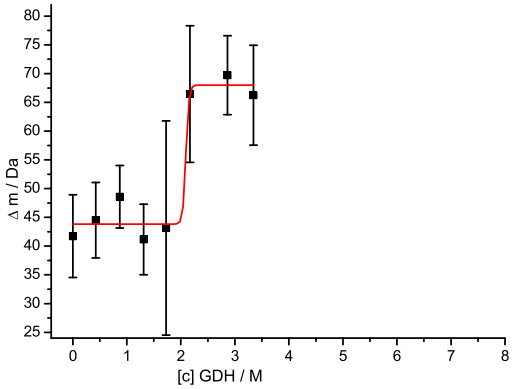

25 min

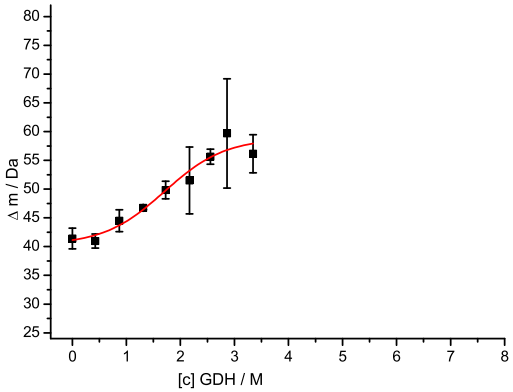

60 min

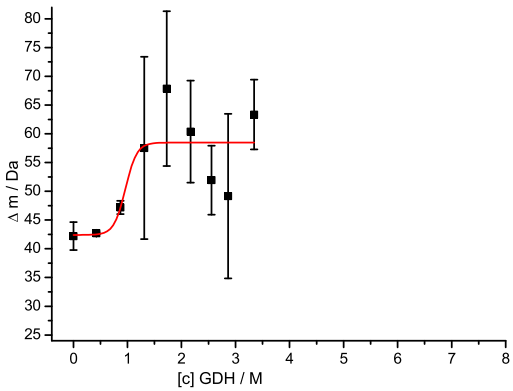

90 min

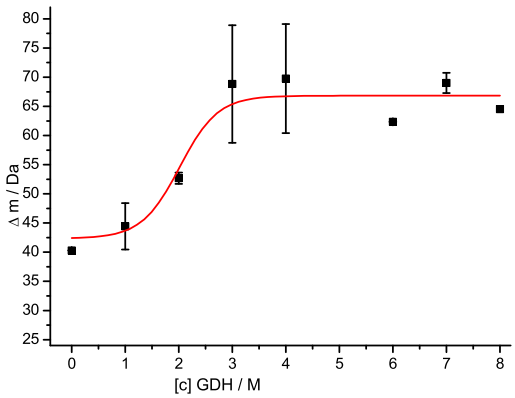

120 min

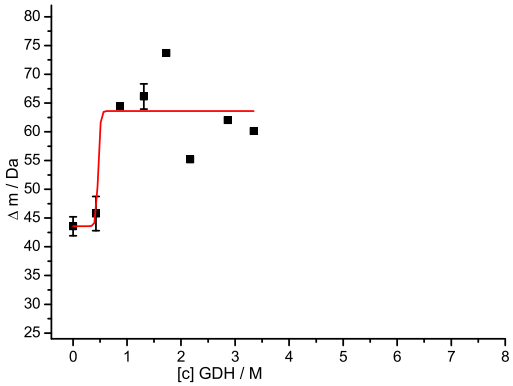

11.6 Apo AGr2^{Nicholson} Automated SUPREX Curves

10 min

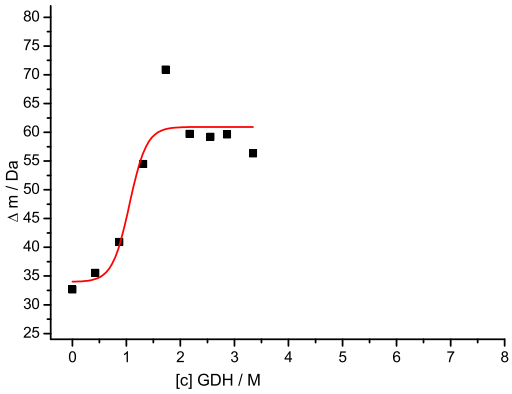

15 min

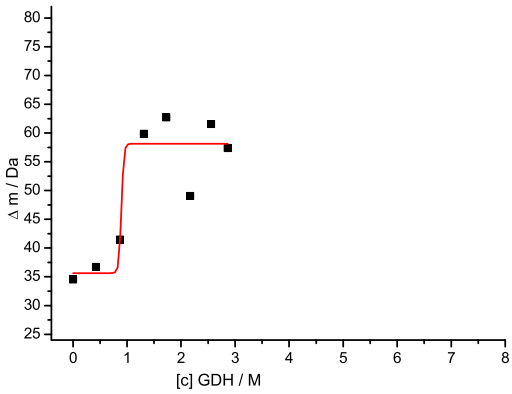

30 min

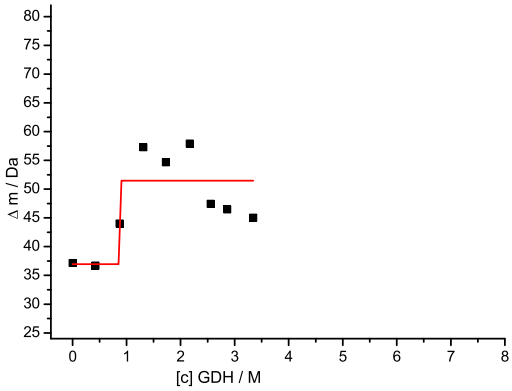

60 min

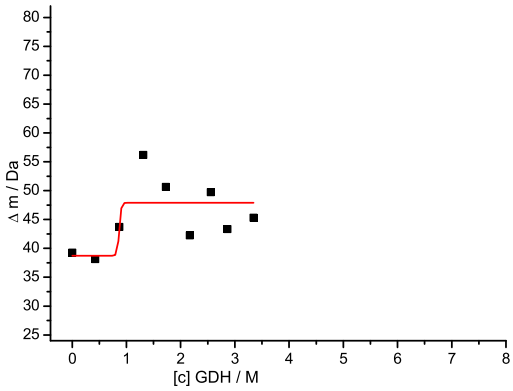

90 min

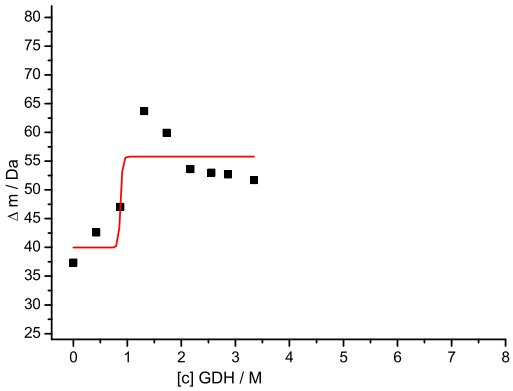

120 min

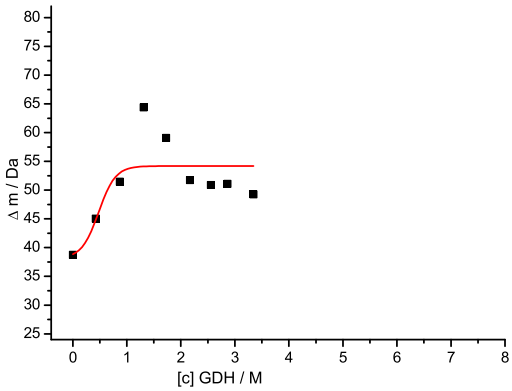

180 min

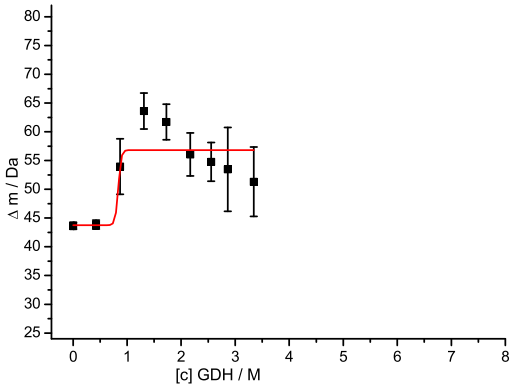

11.7 AGr2^{Nicholson}-PTTIYY-Pen Automated SUPREX Curves

10 min

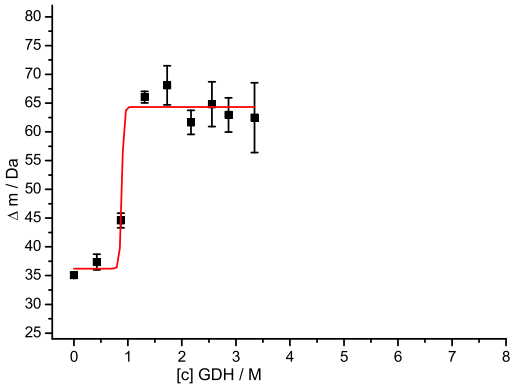

15 min

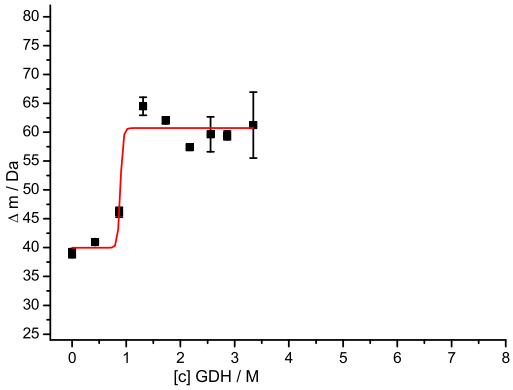

60 min

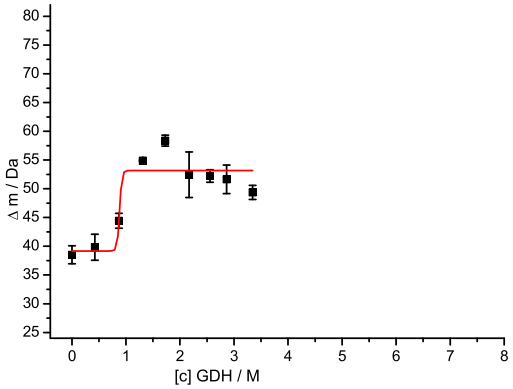

90 min

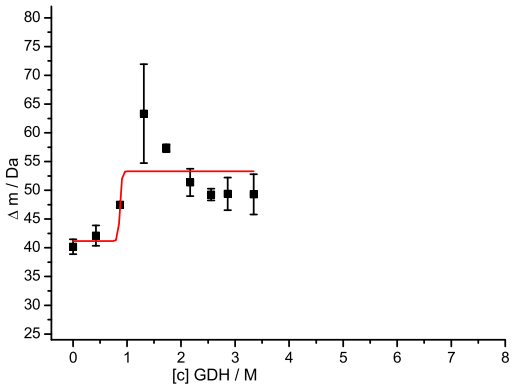

120 min

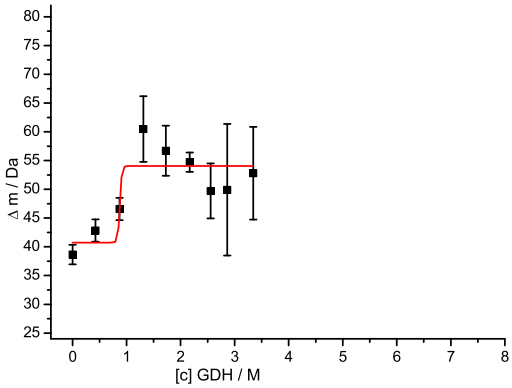

180 min

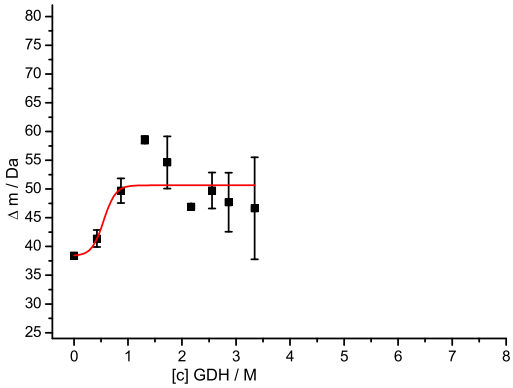

11.8 AGr2^{Nicholson}-PATIAA-Pen Automated SUPREX Curves

10 min

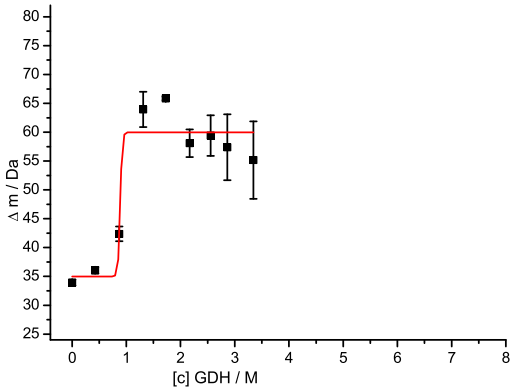

15 min

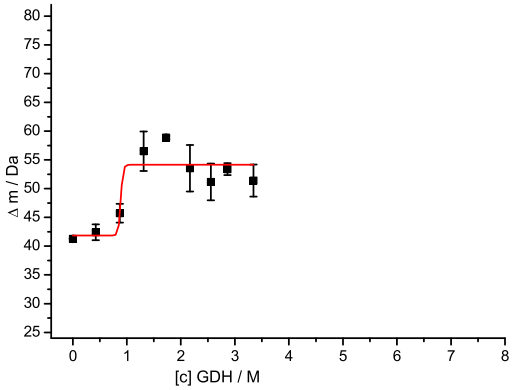

60 min

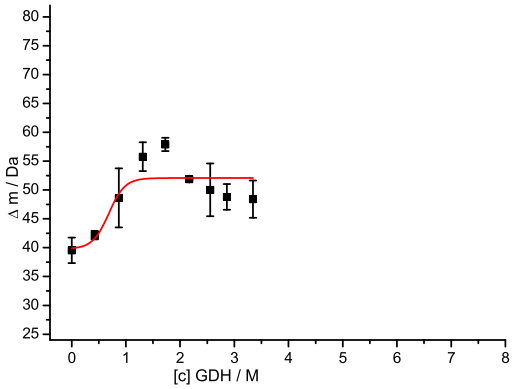

90 min

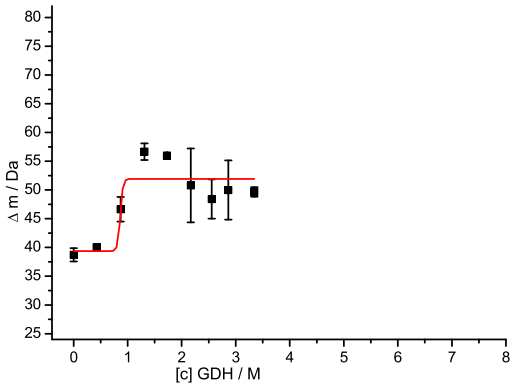

120 min **180 min**

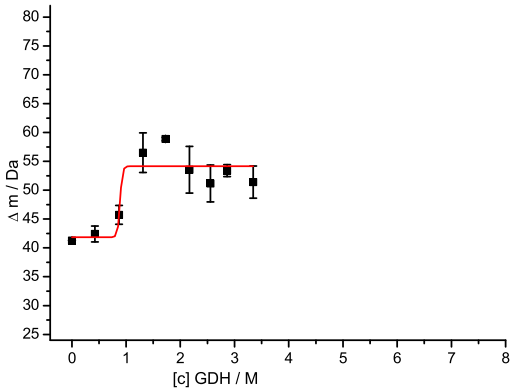

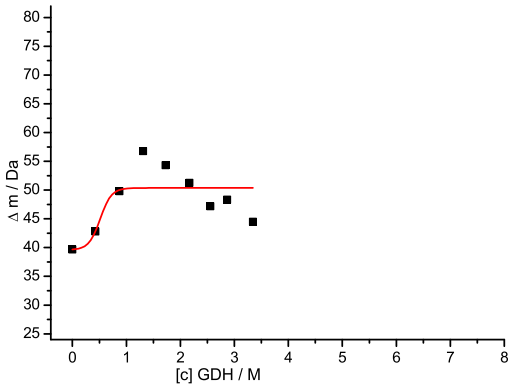

11.9 Apo FH19-20 Automated SUPREX Curves

10 min **30 min**

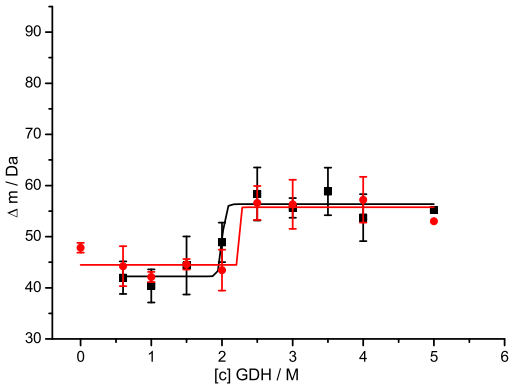

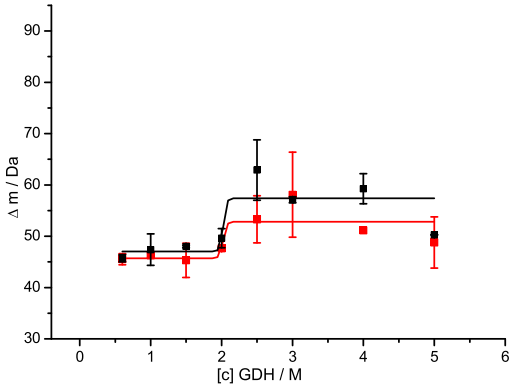

60 min **120 min**

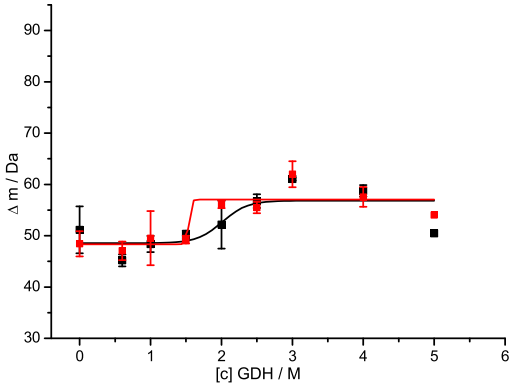

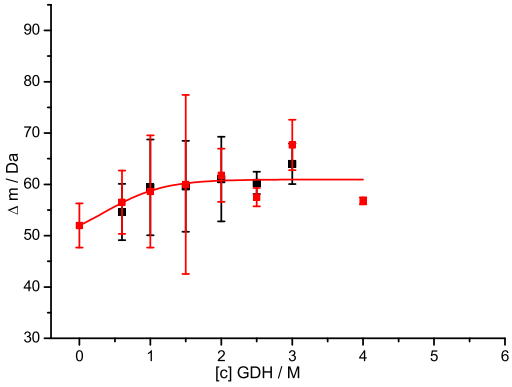

180 min

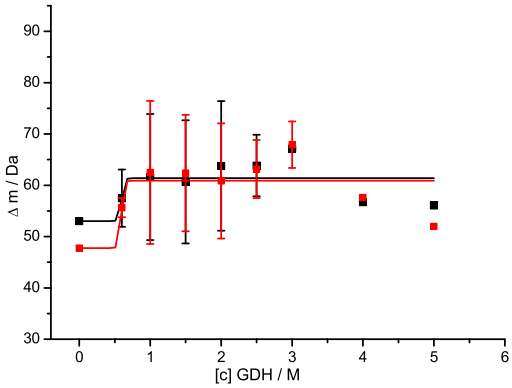

11.10 FH19-20-Fondaparinux Automated SUPREX Curves

10 min

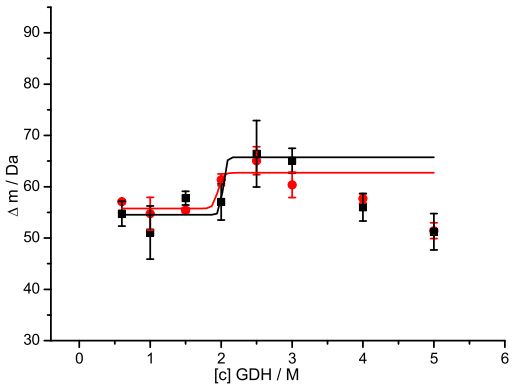

30 min

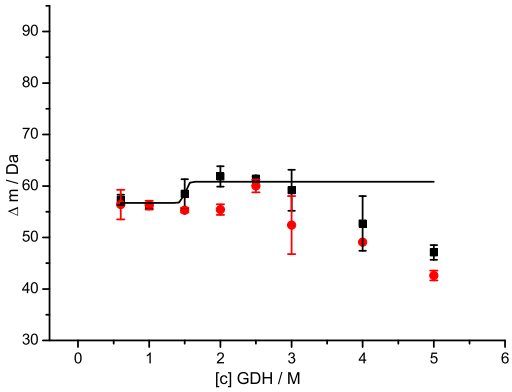

60 min

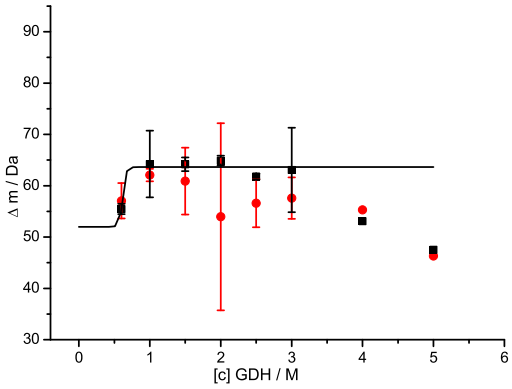

120 min

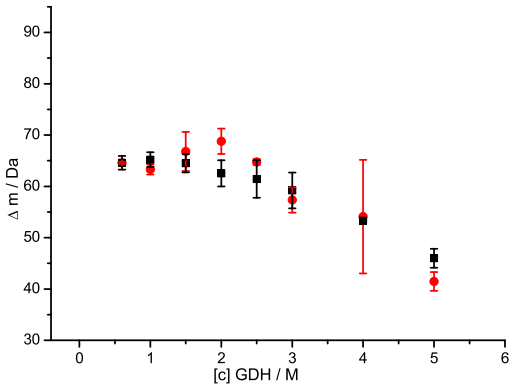

180 min

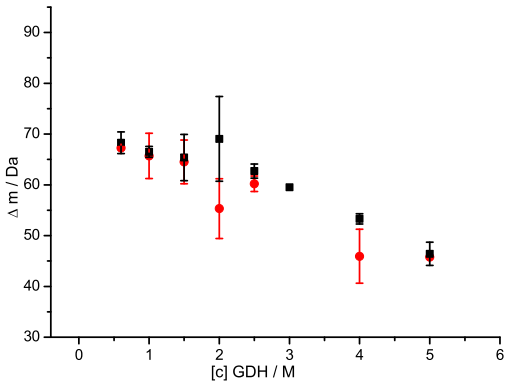

12 Appendix 5

12.1 GroEL Sequence

10 **50**
MAAKDVKFGN DARVKMLRGV NVLADAVKVT LGPKGRNVVL DKSFGAPTIT

60 **100**
KDGVSVAREI ELEDKFENMG AQMVKEVASK ANDAAGDGTT TATVLAQAII

110 **150**
TEGLKAVAAG MNPMDLKRGI DKAVTAAVEE LKALSVPCSD SKAIAQVGTI

160 **200**
SANSDETVGK LIAEAMDKVG KEGVITVEDG TGLQDELDVV EGMQFDRGYL

210 **250**
SPYFINKPET GAVELESPFI LLADKKISNI REMLPVLEAV AKAGKPLLII

260 **300**
AEDVEGEALA TLVVNTMRGI VKVAAVKAPG FGDRRKAMLQ DIATLTGGTV

310 **350**
ISEEIGMELE KATLEDLGQA KRVVINKDTT TIIDGVGEEA AIQGRVAQIR

360 **400**
QQIEEATSDY DREKLQERVA KLAGGVAVIK VGAATEVEMK EKKARVEDAL

410 **450**
HATRAAVEEG VVAGGGVALI RVASKLADLR GQNEDQNVGI KVALRAMEAP

460 **500**
LRQIVLNCGE EPSVVANTVK GGDGNYGYNA ATEEYGNMID MGILDPTKVT

510
RSALQYAASV AGLMITTECM VTDLPKNDAA DLGAAGGMGG MGGMGGMM

12.2 Automated Apo GroEL SUPREX Curves

10 min

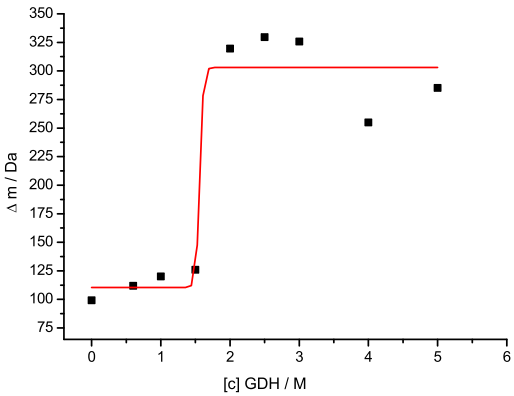

30 min

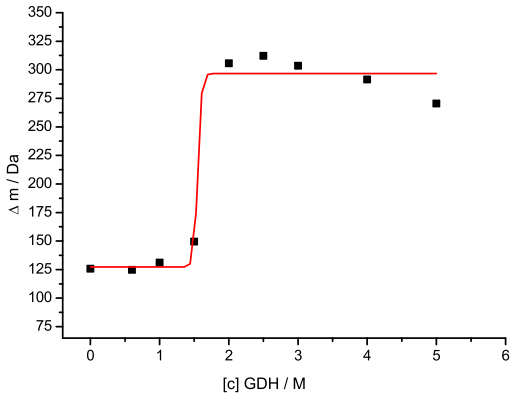

45 min

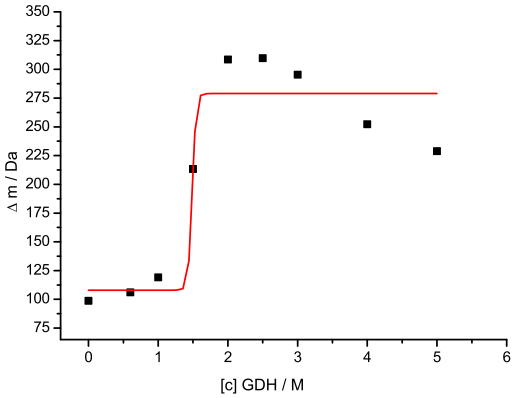

60 min

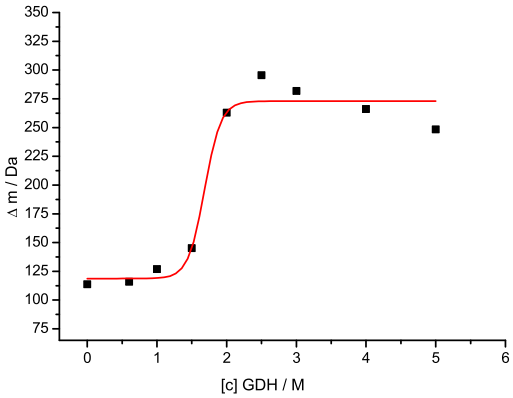

90 min

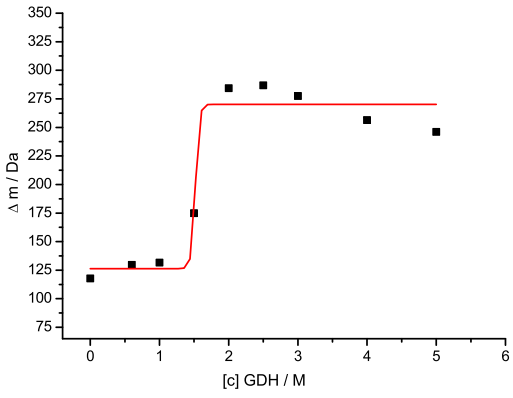

120 min

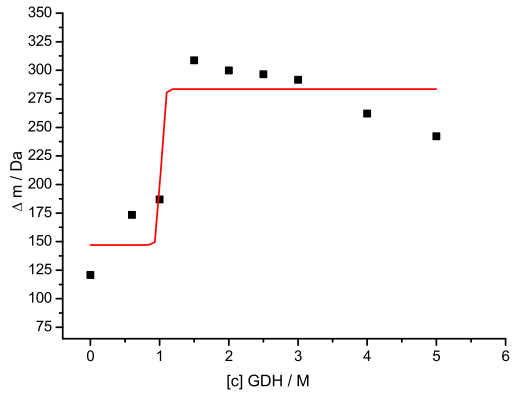

180 min

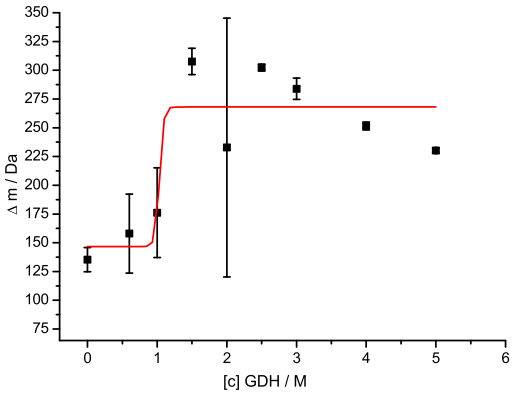

12.3 CypA-GroEL Automated SUPREX Curves for CypA

10 min

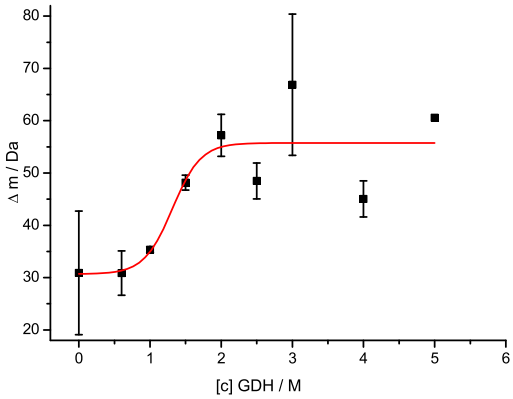

30 min

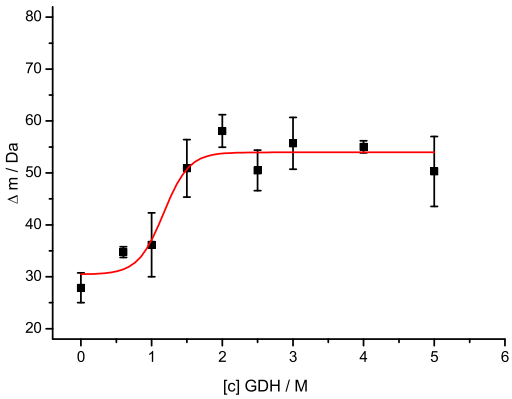

60 min

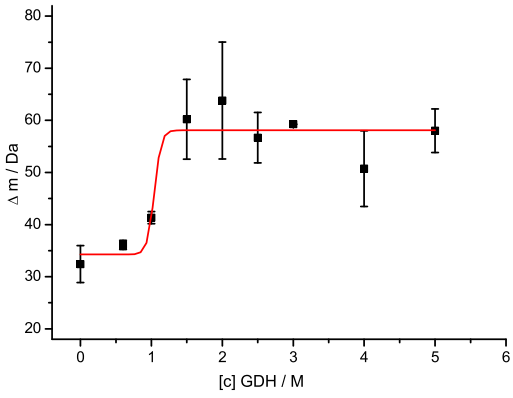

90 min

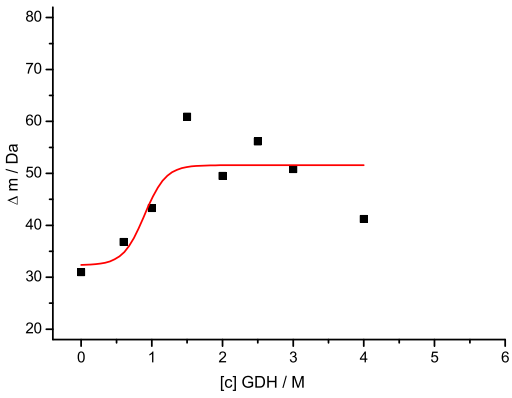

120 min

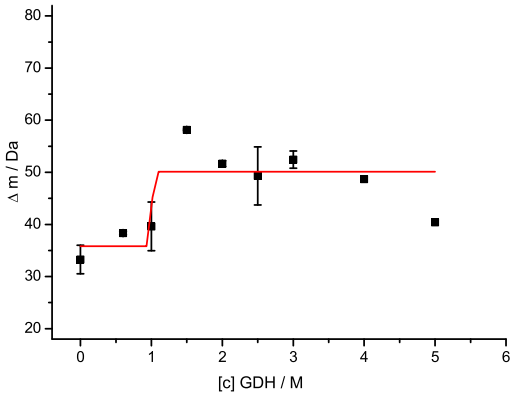

180 min

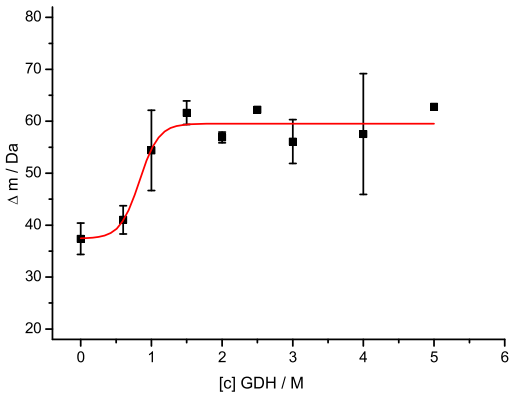

12.4 CypA-GroEL Automated SUPREX Curves for GroEL

10 min

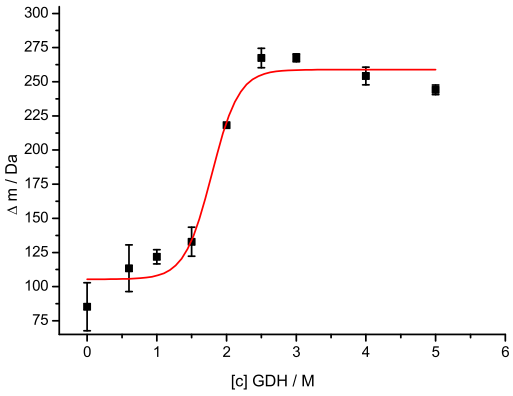

30 min

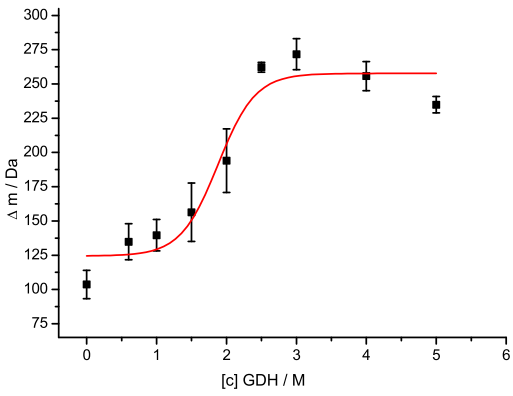

60 min

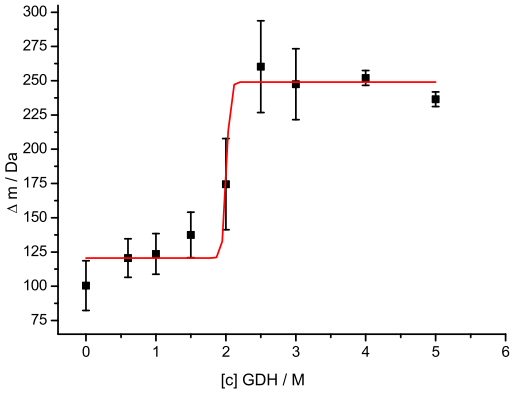

90 min

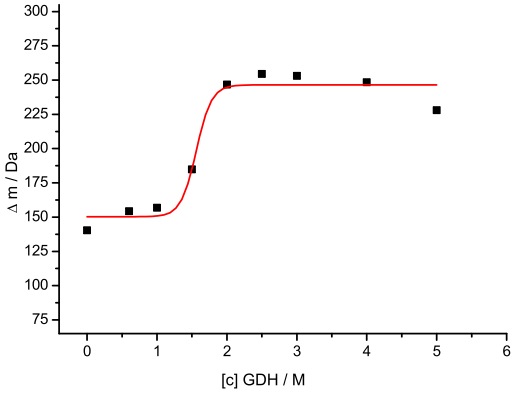

120 min **180 min**

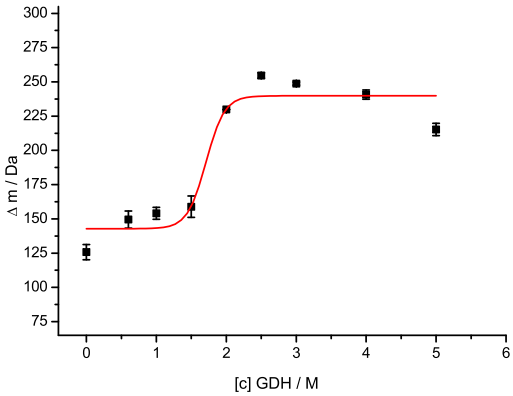

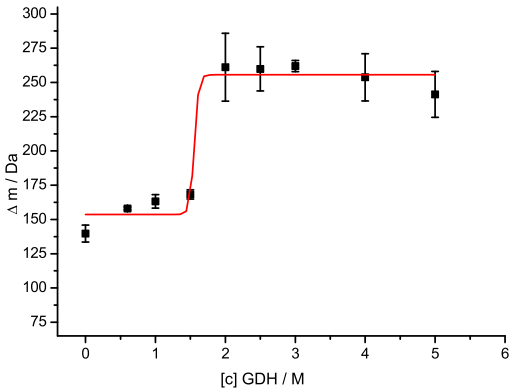

12.5 CypA-CsA-GroEL Automated SUPREX Curves for CypA

10 min **30 min**

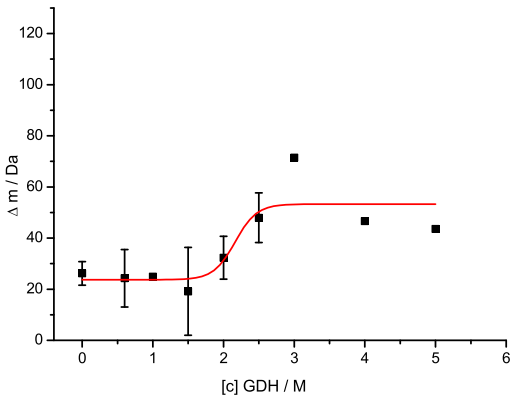

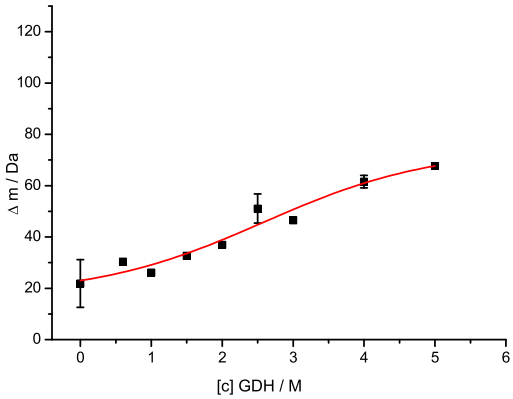

60 min **90 min**

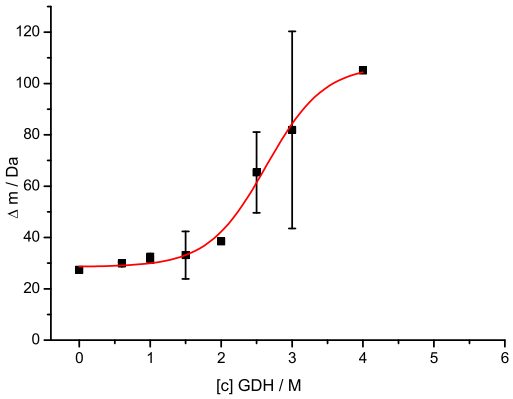

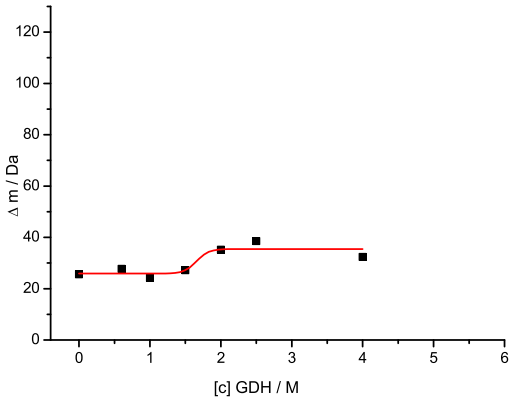

12.6 CypA-CsA-GroEL Automated SUPREX Curves for GroEL

10 min

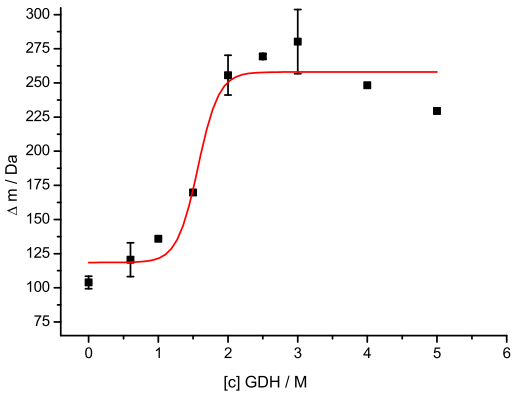

30 min

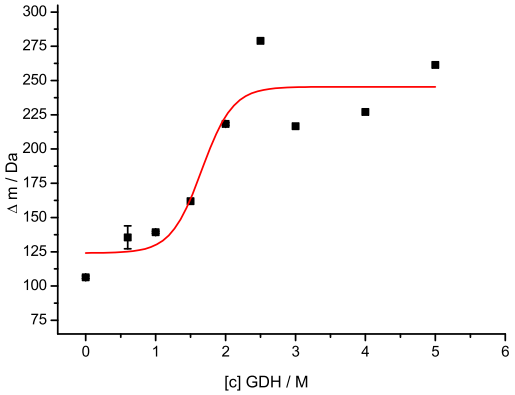

60 min

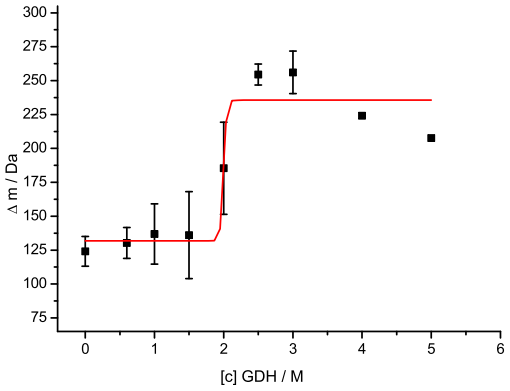

90 min